



UNIVERSIDAD DE LA RIOJA

TESIS DOCTORAL

Título
Synthesis and applications of new biomimetic molecular switches
Autor/es
Marina Blanco Lomas
Director/es
Pedro José Campos García y Diego Sampedro Ruiz
Facultad
Titulación
Departamento
Química
Curso Académico
2011-2012



Synthesis and applications of new biomimetic molecular switches, tesis doctoral de Marina Blanco Lomas, dirigida por Pedro José Campos García y Diego Sampedro Ruiz (publicada por la Universidad de La Rioja), se difunde bajo una Licencia Creative Commons Reconocimiento-NoComercial-SinObraDerivada 3.0 Unported. Permisos que vayan más allá de lo cubierto por esta licencia pueden solicitarse a los titulares del copyright.

© El autor
© Universidad de La Rioja, Servicio de Publicaciones, 2013
publicaciones.unirioja.es
E-mail: publicaciones@unirioja.es



Facultad de Ciencias, Estudios Agroalimentarios e Informática

Departamento de Química
Área de Química Orgánica

Grupo de Fotoquímica Orgánica

TESIS DOCTORAL

**SYNTHESIS AND APPLICATIONS OF NEW
BIOMIMETIC MOLECULAR SWITCHES**

Memoria presentada en la Universidad de La Rioja para
optar al grado de Doctor en Química por:

Marina Blanco Lomas
Mayo 2012

Facultad de Ciencias, Estudios Agroalimentarios e Informática

Departamento de Química
Área de Química Orgánica

Grupo de Fotoquímica Orgánica

D. PEDRO JOSÉ CAMPOS GARCÍA, Catedrático de Química Orgánica del Departamento de Química de la Universidad de La Rioja,

y D. DIEGO SAMPEDRO RUIZ, Profesor titular de Química Orgánica del Departamento de Química de la Universidad de La Rioja,

CERTIFICAN:

Que la presente memoria, titulada “Synthesis and applications of new biomimetic molecular switches”, ha sido realizada en el Departamento de Química de La Universidad de La Rioja bajo su dirección por la Licenciada en Química Dña. MARINA BLANCO LOMAS y autorizan su presentación para que sea calificada como Tesis Doctoral.

Logroño, Mayo de 2012



Fdo. Pedro J. Campos García



Fdo. Diego Sampedro Ruiz

INDEX

Abstract	vii
Resumen	ix
Abbreviations and acronyms	xi
1. Introduction	1
2. Background	11
2.1. Molecular machines and devices: Concept and features.	
2.1.1. Differences between molecular machines and devices.	
2.1.2. Main features of molecular machines.	
2.1.3. Power supply required to perform work.	
2.2. Light activated molecular switches.	
2.2.1. Differences between a molecular switch, rotor and motor.	
2.3. Natural molecular switches and motors.	
2.3.1. Natural metal ion channels.	
2.3.2. ATP-synthase, a natural rotary motor.	
2.3.3. Natural molecular motors that perform a linear-like movement.	
2.3.4. The importance of the protonated Schiff base (PSB) of the retinal chromophore as a molecular motor.	
2.3.5. Green fluorescent protein (GFP) chromophore.	
2.4. Artificial molecular machines.	
2.5. Molecular motors based on overcrowded alkenes.	
2.6. Biomimetic molecular switches based on PSB retinal.	
2.6.1. Theoretical and experimental study of a PSB retinal-based biomimetic molecular switch.	
2.6.2. <i>N</i>- Alkylated Indanylidene-pyrrolines (NAIPs).	
2.6.3. <i>N</i>- Alkylated Fluorenylidene-pyrrolines (NAFPs).	

3. Objectives	61
4. Synthesis of biomimetic molecular switches	65
4.1. Synthesis of molecular switches with structure based on the protonated Schiff base of retinal (PSB-retinal) chromophore.	
4.1.1. Synthesis of neutral photoswitches with structure based on the PSB-retinal chromophore.	
4.1.2. Synthesis of methylated photoswitches with structure based on the PSB-retinal chromophore.	
4.1.3. Synthesis of metallated photoswitches with structure based on the PSB-retinal chromophore.	
4.2. Synthesis of molecular switches with structure based on the green fluorescent protein (GFP) chromophore.	
4.2.1. Synthesis of photoswitches with structure based on the GFP chromophore.	
4.2.2. Stability of the GFP-based photoswitches in different solvents.	
4.2.3. Synthesis of methylated photoswitches with structure based on the GFP chromophore.	
4.2.4. Synthesis of photoswitches using an alkyl aldehyde as starting material.	
4.2.5. Synthesis of metallated photoswitches with structure based on the GFP chromophore.	
5. Photochemical study	91
5.1. Introduction.	
5.1.1. Absorption spectra.	
5.2. Photochemical study of photoswitches with structure based on the PSB-retinal chromophore.	
5.2.1. Photochemical study of neutral photoswitches with structure based on the PSB-retinal chromophore.	
5.2.1.1. Photochemical and thermal stability of the photoswitches with structure based on the PSB-retinal chromophore.	
5.2.2. Photochemical aspects of the mechanism of the isomerization reaction of photoswitches with structure based on the PSB-retinal chromophore.	

- 5.2.2.1. Excited state multiplicity.
 - 5.2.2.2. Isomerization quantum yield.
 - 5.2.2.3. Luminescence.
 - 5.2.2.1. Sensibilization tests.
 - 5.2.3. Photochemical study of methylated photoswitches with structure based on the PSB-retinal chromophore.
 - 5.2.4. Photochemical study of metallated photoswitches with structure based on the PSB-retinal chromophore.
- 5.3.** Photochemical study of photoswitches with structure based on the GFP chromophore.
- 5.3.1. Photochemical study of photoswitches with structure based on the GFP chromophore.
 - 5.3.1.1. Selective irradiation of the two isomers (*Z* and *E*) of the photoswitches with structure based on the GFP chromophore.
 - 5.3.1.2. Irradiation in a photoreactor of the photoswitches with structure based on the GFP chromophore.
 - 5.3.1.3. Solvent dependence of the isomerization reaction of photoswitches with structure based on the GFP chromophore.
 - 5.3.1.4. Photochemical and thermal stability of photoswitches with structure based on the GFP chromophore.
 - 5.3.1.5. Irradiation of photoswitches with structure based on the GFP chromophore in solid state.
 - 5.3.2. Photochemical aspects of the mechanism of the isomerization reaction of photoswitches with structure based on the PSB-retinal chromophore.
 - 5.3.2.1. Excited state multiplicity.
 - 5.3.2.2. Isomerization quantum yield.
 - 5.3.2.3. Luminescence.
 - 5.3.2.1. Sensibilization tests.
 - 5.3.3. Study of the azolactone ring opening process with solvents in GFP based photoswitches.
- 5.4.** Theoretical study of photoswitches with structure based on the PSB-retinal and the GFP chromophore.
- 5.4.1. Theoretical calculations of the photoswitches with structure based on the PSB-retinal chromophore.

5.4.2. Theoretical calculations on the thermal and photochemical isomerization of the photoswitches with structure based on the GFP chromophore.

5.4.2.1. Computational details.

5.4.2.2. Thermal isomerization.

5.4.2.3. Absorption spectrum.

5.4.2.4. Photoisomerization.

5.4.2.4. Comparison with the GFP chromophore.

6. Practical applications

197

6.1. Introduction.

6.2. Applications of photoswitches with structure based on the GFP chromophore.

6.2.1. Synthesis of the appropriate GFP-based photoswitches for the linkage to more complex biomolecules.

6.2.1. Linkage of the synthesized GFP-based photoswitches to model peptides.

6.3. Applications of photoswitches with structure based on the PSB-retinal chromophore.

6.3.1. Synthesis of the appropriate PSB-retinal based photoswitches for the linkage to more complex biomolecules.

6.3.1.1. Computational study of the synthesized photoswitch **5r** for the linkage to more complex systems.

6.3.1.2. Experimental study of the synthesized photoswitches **5p** and **5r** for the linkage to more complex systems.

6.3.2. Linkage of the synthesized PSB-retinal based photoswitch **5r** to a model peptide.

6.3.2.1. Selection and synthesis of the adequate model peptide for the linkage to **5r**.

6.3.2.2. Cross-linking reaction of peptide SS-11 to photoswitch **5r**.

6.3.3. Photochemical study of the cross-linked peptide.

6.3.3.1. Photochemical study of the cross-linked peptide dissolved in sodium phosphate buffer at pH 7.

6.3.3.2. Photochemical study of the cross-linked peptide dissolved in sodium phosphate buffer at different pHs.

7. Conclusions	243
8. Experimental section	247
8.1. General comments.	
8.2. Synthesis of biomimetic molecular switches.	
8.2.1. Synthesis of neutral photoswitches with structure based on the protonated Schiff base of the retinal (PSB-retinal) chromophore.	
8.2.2. Synthesis of methylated photoswitches with structure based on the PSB-retinal chromophore.	
8.2.3. Synthesis of the metallated photoswitches with structure based on the PSB-retinal chromophore.	
8.2.4. Synthesis of molecular switches with structure based on the green fluorescent protein (GFP) chromophore.	
8.2.5. Stability of the GFP based photoswitches in different solvents.	
8.3. Photochemical study	
8.3.1. Irradiation of neutral and methylated photoswitches with structure based on the PSB-retinal.	
8.3.2. Irradiation photoswitches with structure based on the GFP chromophore.	
8.3.3. Photochemical aspects of the mechanism of the isomerization reaction.	
8.4. Applications of photoswitches with structure based on the PSB-retinal.	
8.4.1. Synthesis of the appropriate PSB-retinal based photoswitches for the linkage to more complex biomolecules.	
8.4.2. Linkage of the synthesized PSB-retinal based photoswitch 5r to a model peptide.	
8.4.3. Photochemical study of the cross-linked peptide.	
Appendix A. Selected NMR spectra	I
Appendix B. X-Ray Diffraction data	XVII
Appendix C. Computational study data	XI

ABSTRACT

This doctoral thesis is focused on the synthesis, photochemical study and applications of two novel families of molecular switches, which are respectively based on the protonated Schiff base of the retinal chromophore (benzylidene pyrrolines) and the green fluorescent protein chromophore (alkylidene oxazolones).

The objectives are described (Chapter 3) after a brief introduction and a literature overview in Chapters 1 and 2.

In Chapter 4, the synthetic methodology employed to prepare these two kinds of compounds is described. Moreover, the studies performed to fully characterize these structures are discussed. Finally, the reactivity of these compounds over metallic salts is briefly reviewed.

Chapter 5 explains the study carried out in order to photochemically and photophysically characterize the synthesized molecular switches. Moreover, the efficiency of the photoisomerization reaction undergone by these two families of switches is analyzed. Furthermore, the possibility of performing the isomerization reaction under sensitized conditions is checked. Finally, the experimental results are contrasted with theoretical calculations.

Finally, in Chapter 6, the practical applications of this kind of photoswitches are outlined. In the case of the photoswitches with structure based on the PSB-retinal chromophore, the possibility of linkage to more complex systems such as peptides is reported. In addition to this, the photochemical study of the target cross-linked peptide is performed so as to check the potential ability of these switches to photocontrol other biomolecules.

Resumen

Durante esta tesis doctoral se desarrolla la síntesis, el estudio fotoquímico y las aplicaciones de dos nuevas familias de interruptores moleculares, las cuales se basan respectivamente en el cromóforo de la base de Schiff protonada del retinal (benziliden-pirrolinas) y el cromóforo de la proteína verde fluorescente (alquiliden-oxazolonas).

Tras una breve introducción (Capítulo 1), el análisis de los antecedentes bibliográficos (Capítulo 2) permite fijar unos objetivos a alcanzar (Capítulo 3).

En el Capítulo 4, se describe la metodología sintética seguida para llevar a cabo la preparación de estos dos tipos de compuestos. Asimismo, se discuten los estudios realizados para caracterizar de forma completa estas estructuras. Finalmente, se resume brevemente la reactividad de estos compuestos frente a sales metálicas.

En el Capítulo 5 se trata el estudio elaborado para caracterizar fotoquímica y fotofísicamente los interruptores moleculares sintetizados. De la misma manera, se analiza la eficiencia del proceso de isomerización fotoinducido que sufren estas dos familias de compuestos. Además, se comprueba la posibilidad de realizar la reacción de isomerización bajo condiciones de sensibilización. Finalmente, se contrastan los resultados experimentales con los de los cálculos teóricos.

Para terminar, en el Capítulo 6, se explican las aplicaciones prácticas de ambas familias de fotointerruptores. En el caso de los interruptores moleculares con estructura basada en la base de Schiff protonada del retinal se presenta la posibilidad de unión de estos compuestos a sistemas más complejos, como por ejemplo péptidos. Además, se realiza el estudio fotoquímico del interruptor una vez unido al péptido para comprobar la habilidad potencial de estos interruptores de fotocontrolar otras biomoléculas.

ABBREVIATIONS AND ACRONYMS

Å	angstrom
ADN/ARN	desoxyribonucleic acid/ribonucleic acid
approx.	approximately
ATP	adenosine triphosphate
atm.	atmosphere
Boc	<i>tert</i> -butyloxycarbonyl
BP	benzylidene pyrroline
Bu	butyl
^t Bu	<i>tert</i> -butyl
¹³ C RMN	carbon nuclear magnetic resonance
ca.	approximately
CASSCF	complete active space-self-consistent field
CASPT2	complete active space-perturbation theory of second order
CD	circular dichroism
CIS	intersystem crossing
col.	collaborators
conc.	concentration
D	Debye

d	doublet (in NMR spectroscopy)
dd	doublet of doublets (in NMR spectroscopy)
DFT	density functional theory
DIEA	diisopropyl ethyl amine
DMF	dimethylformamide
E	energy
EM	mass spectrometry
Ep	moles of fotons absorbed x cm^{-2} x s^{-1}
ES	electrospray
ES(+)	electrospray in positive ion mode
ES(-)	electrospray in negative ino mode
Et	ethyl
etc.	<i>et cetera</i> , and so on
eV	electron volt
F(λ)	F factor
FC	Frank-Condon
FP	fluorenylidene-pyrroline
fs	femtosecond
GC/MS	gas chromatograpy/mass spectrometry
GFP	green fluorescent protein

^1H NMR	proton nuclear magnetic resonance
HF	Hartree-Fock
Hz	hertz
h ν	light, photons, irradiation
I	intermediate
IBX	2-iodoxybenzoic acid
<i>i.e.</i>	for example
IP	indanylidene-pyrroline
J	joule
<i>J</i>	coupling constant (expressed in Hz, in NMR spectroscopy)
<i>Jr.</i>	junior
kJ	kilojoules
M	molarity
m	multiplet (in NMR spectroscopy)
Me	methyl
MEP	minimum energy path
min.	minute
MP	Møller-Plesset
ms	millisecond
NAP	<i>N</i> -alkylated arylidene-pyrroline

Abbreviations and acronyms

NABP	<i>N</i> -alkylated benzylidene-pyrroline
NAIP	<i>N</i> -alkylated indanylidene-pyrroline
NAFP	<i>N</i> -alkylated fluorenylidene pyrroline
nm	nanometer (10^{-9} meters)
NMR	nuclear magnetic resonance
NOE	nuclear Overhauser effect
NOESY	nuclear Overhauser effect spectroscopy
Ph	phenyl
pN	picoNewton
ppm	parts-per-million
PSB	protonated Schiff base
PSS	photostationary state
q	quatriplet (in NMR spectroscopy)
r.p.m.	revolutions per minute
s	singlet (in NMR spectroscopy), second
S_0	ground state
S_n	singlet excited state
t	triplet (in NMR spectroscopy); time
T_n	triplet excited state
TBTU	<i>O</i> -(Benzotriazol-1-yl)- <i>N,N,N',N'</i> -tetramethyluronium tetrafluoroborate

TCEP	tris(2-carboxyethyl)phosphine
td	triplet of doublets (in NMR spectroscopy)
THF	tetrahydrofuran
TLC	thin layer chromatography
TMS	trimethylsilane
Tris (buffer)	tris(hydroxymethyl)aminomethane
TS	transition state
W	watts
wt	weight
UV-VIS	ultraviolet-visible
Δ	heat; increase
ΔG	Gibbs free energy
δ	chemical shift
ϵ	molar extinction coefficient, molar absorptivity
λ	wavelength
Φ	quantum yield
μm	micrometer (10^{-6} meters)

CHAPTER 1

Introduction

Ancient civilizations highlighted the importance of light for the maintenance and sustenance of life on earth. In particular, the sun, which is considered the ultimate source of light as it provides the energy that drives life, has been an object of veneration in many cultures throughout human history. For example, worship of the sun was essential for civilizations such as the Inca of South America or the Aztecs from Central America.

Sunlight is directly or indirectly involved (by providing food and fuel) in most chemical transformations in biota.¹ For instance, photosynthesis (Figure 1.1) is the source of food for plants, algae, and many species of bacteria (except archaea), and has played an important role in the origin of life.²

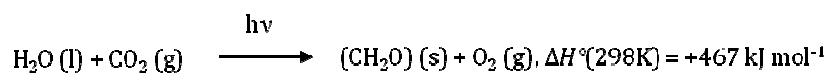


Figure 1.1. Scheme of the photochemical reaction involved in photosynthesis.

However, careful research on the connection between the absorption of light by matter and its chemical and physical consequences was not found in the scientific literature until the last decades of the past century. At that moment, systematic efforts revealed that exposure of matter to sunlight led to a rich range of transformations, which are nowadays known as photochemical reactions. Over the last century a great number of photochemical reactions have been unveiled. In modern times, these kinds of reactions are used in organic synthesis and industrially, as complex organic products can be easily obtained.

In this context, Giacomo Luigi Ciamician (1857-1922)³ foresaw a hundred years ago the impact of photochemistry on the future of mankind. In particular, he

¹ Klán, P.; Wirz, J. *Photochemistry of Organic Compounds. From Concepts to Practice*. Wiley: Chichester, **2009**.

² For instance, the evolution of oxygenic photosynthesis by bacteria, which were the dominant form of life in the early stages of the Earth, eventually led to oxygenation of the atmosphere. This altered environment ultimately resulted in the evolution of animal and plant species.

³ (a) Ciamician, G. *Science*, **1912**, *36*, 385. (b) Albini, A.; Fagnoni, M. *ChemSusChem* **2008**, *1*, 63.

proposed at the 8th International Congress on Applied Chemistry in 1912 that the future world would use clean energy supplied by solar power:

"On the arid lands there will spring up industrial colonies without smoke and without smokestacks; forests of glass tubes will extend over the plains and glass buildings will rise everywhere; inside of these will take place the photochemical processes that hitherto have been the guarded secret of the plants, but that will have been mastered by human industry which will know how to make them bear even more abundant fruit than nature, for nature is not in a hurry and mankind is. And if in a distant future the supply of coal becomes completely exhausted, civilization will not be checked by that, for life and civilization will continue as long as the sun shines!"

On the other hand, the first attempts to relate the colour of organic compounds to their molecular structure date back to the mid-19th century, when synthetic dyes became one of the chemical industry's most important products. In 1876, the terms *chromophore* (a molecular group that carries the potential for generating colour) and *auxochrome* (polar substituents that increase the depth of colour) were introduced by Otto N. Witt. However, these colour theories had to remain empirical and rather mystical until the appearance of molecular quantum mechanics after 1930.

Later on, in the early 1940s, staggering experimental evidence allowed confirming the theoretical concept of the triplet state of organic molecules. Furthermore, simple molecular orbital theories such as Platt's free electron model (FEMO), E. Hückel molecular orbital theory (HMO) and R. Pariser, R. Parr and J. Pople's configuration interaction model (PPP SCF CI) were settled around 1950. Thanks to these theories, correlations were made between the spectroscopic properties of molecules and the orbital configurations of electronically excited state, as they provided clear and satisfying models for the interpretation of electronic spectra of conjugated molecules.

Afterwards, the general lines of thought on how to understand the reactivity of electronically excited molecules were developed. Several scientists, among which T. Förster,⁴ M. Kasha,⁵ G. Porter,⁶ E. Havinga,⁷ G. S. Hammond,⁸ H. E.

⁴ Förster, T. *Discuss. Faraday Soc.*, **1959**, 27, 7.

⁵ R. Hochstrasser, J. Saltiel. Research Career of Michael Kasha. *J. Phys. Chem. A*, **2003**, 107, 3161.

Zimmerman,⁹ and N. J. Turro¹⁰ were included, uncovered the basic concepts for structure-reactivity correlations in photochemistry.

Between the 1960s and 1970s, a great number of new photoreactions were discovered, whose mechanisms were studied with a many powerful novel spectroscopic techniques and theories. During this period, the power of mechanistic research was proven, and the field of molecular photochemistry became a truly new and emerging discipline. The fast development of commercially available lasers and electronic equipment permitted the real-time detection of primary transient intermediates by flash photolysis. By that time, photochemistry was considered the principal branch science for the general study of organic reaction mechanisms. This was due to the fact that it could be used to generate the intermediates that were involved in chemical reactions.

However, it was only in the 1980 that photochemistry became an integral part of organic, inorganic and biological chemistry. This development led photochemists to import concepts from other disciplines and develop these ideas into what is nowadays known as supramolecular photochemistry.¹¹ This latter is the part of chemistry that goes beyond the molecules and focuses on the chemical systems made up of a discrete number of assembled molecular subunits or components.

In the present ages, photochemistry has become an integral part of all branches of science, such as chemistry, biochemistry, medicine,¹² biophysics, material science, or analytical chemistry.¹³ Photochemists have increasingly

⁶ Phillips, D. Obituary: George Porter (1920-2002) *Nature* **2002**, 419, 578.

⁷ Havinga, E.; de Jongh, R. O.; Dorst, W. *Rec. Trav. Chim.* **1956**, 76, 378.

⁸ Hammond, G. S.; Saltiel, J.; Lamola, A. A.; Turro, N. J.; Bradshaw, J. S.; Cowan, D. O.; Counsell, R. C.; Vogt, V.; Dalton, C. *J. Am. Chem. Soc.* **1964**, 86, 3197.

⁹ Zimmerman, H. E. *Quantum mechanics for organic chemists*. Academic Press: New York, **1975**,

¹⁰ Turro Photochemistry Laboratory, <http://turroserver.chem.columbia.edu/> (web page visited on February 25th, 2012)

¹¹ *Supramolecular Photochemistry. Controlling Photochemical Processes*. Ramamurthy, V.; Inoue, Y. (eds.) Wiley: New Jersey, **2011**.

¹² Gorostiza, P.; Isacoff, E. Y. *Science* **2008**, 322, 395.

¹³ *Optical Sensors and Switches*. Ramamurthy, V.; Schanze, K. S. (eds.) Marcel Dekker, Inc.: New York, **2001**.

focused on the development of photochemical systems and materials that respond in a controllable manner to chemical and/or optical stimuli. Moreover, photoresponsive systems and materials are really advantageous. This is illustrated by the fact that they are included in a variety of technologically relevant processes and products, such as chemical sensors, photochromic optical elements, optical data storage media, photoresists, organic light emitting diodes, optical limiters, photoconductors for use in xerography, and molecular systems for photodynamic therapy.

Although many useful photoresponsive systems are based on basic molecular photochemistry (*i.e.* photochromic azobenzene and spiropyrans, which are used in optical data storage media,¹⁴ and ruthenium and platinum complexes, which are useful optical oxygen sensors) alternatives to many high-technology applications of current interest involve complex supramolecular assemblies to achieve the desired photoresponsive function.

This way, inspiration from and aspiration to mimic the highly effective function of biological systems have been a driving force for the development of supramolecular photochemistry.

It is known that light represents a unique stimulus for nearly all organisms, triggering and driving diverse biological processes, among which visual perception in higher organisms (which will be later described in section 2.3.4),¹⁵ photosynthesis in plants, algae and several examples of bacteria (mentioned above),¹⁶ and photomovement responses¹⁷ are included. The fundamental concept behind such diverse photoreactivities is localized on photoresponsible proteins, which regulate biological activity in many living beings by sensing light.¹⁸ The common feature that these proteins present, which allows them to absorb visible-light, and therefore interact with light, is usually a small light-absorbing ligand

¹⁴ Bossi, M. L.; Aramendía, P. F. J. *Photochem. Photobio. C* **2011**, *12*, 154.

¹⁵ Bruce, V.; Green, P. R.; Georgeson, M. A. *Visual Perception: Physiology, Psychology and Ecology*, 4th ed. Psychology: Hove, **2003**.

¹⁶ Hall, K. K. R. *Photosynthesis (Studies in Biology)*, Vol 6. Cambridge University Press, Cambridge: **1999**.

¹⁷ Häder, D.-P.; Lebert, M. *Photomovement*. Elsevier, Amsterdam: **2001**.

¹⁸ Krauss, U.; Drepper, T.; Jaeger, K.-E. *Chem. Eur. J.* **2011**, *17*, 2552.

bound within the protein. This unit is known as the *chromophore*.¹⁹ Due to their electronic properties, chromophoric molecules can absorb light of a defined wavelength depending on the structure of the respective chromophore. Thus, biological photocontrol is the result of the photoexcitation process and subsequent photochemical reactions undergone by the chromophore. It will be later discussed that in certain cases these reactions are linked to a conformational change in the protein structure.

As said before, the chromophore, which is in the ground state, captures a photon resulting in the formation of an electronic excited state, from which subsequent photochemical reaction products are formed (Figure 1.2).²⁰ Different photochemical processes can occur after photoexcitation of the chromophore, such as:

- A) bond cleavage (photouncaging);²¹
- B) isomerization of a double bond within the chromophore;²² or
- C) bond formation with a nearby reactive molecule.²³

The two most widely used approaches in order to make a biomolecule light sensitive are the “caging approach” and the use of photoswitches.

¹⁹ In this case, the definition of *chromophore* is different from the aforementioned one. For instance, in biological molecules that are able to capture or detect light energy, the *chromophore* is the moiety that causes a conformational change of the molecule when hit by light.

²⁰ See ref. 18.

²¹ Kaplan, J. H.; Forbush III, B.; Hoffman, J. F. *Biochemistry* **1978**, *17*, 1929.

²² Dugave, C.; Demange, L. *Chem. Rev.* **2003**, *103*, 2475.

²³ Losi, A.; Gartner, W. *Photochem. Photobiol. Sci.* **2008**, *7*, 1168.

1. Introduction

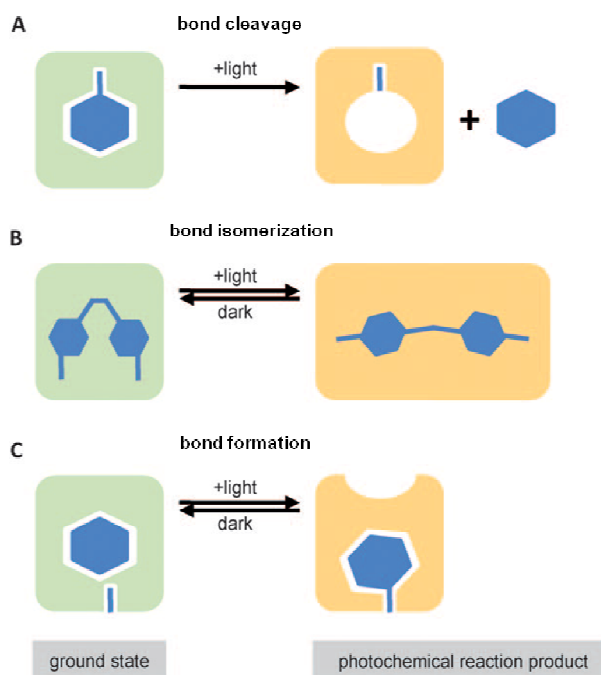


Figure 1.2. Examples of photochemical processes that may happen after photoexcitation of a chromophore (see ref. 18).

Once these photochemical transformations take place, the structural change provoked in the chromophore is then transferred to the protein, which undergoes a change in its conformation or structure. This structural change is either followed by a change of the protein reactivity (*i.e.*, modulation or induction of catalytic turnover, or of ion conductance),²⁴ is transduced to coupled (non-light absorbing) protein domains to influence their activity,²⁵ or results in a structural rearrangement that allows for different protein-protein interactions to occur at the cellular level.²⁶ As said before, these principles are already accomplished by different natural photoreceptor protein families.

²⁴ a) Gärtner, W. *Angew. Chem.* **2009**, *121*, 4552; *Angew. Chem. Int. Ed.* **2009**, *48*, 4484. b) Müller, M.; Carell, T. *Curr. Opin. Struct. Biol.* **2009**, *19*, 277. c) Nagel, G.; Szellas, T.; Kateriya, S.; Adeishvili, N.; Hegemann, P.; Bamberg, E. *Biochem. Soc. Trans.* **2005**, *33*, 863.

²⁵ See ref. 22.

²⁶ a) Corrochano, L. M. *Photochem. Photobiol. Sci.* **2007**, *6*, 725. b) Demarsy, E.; Frankhauser, C. *Curr. Opin. Plant Biol.* **2009**, *12*, 69.

It is understandable that this topic has been really appealing for researchers since the beginning of science.²⁷ The advances in modern biochemistry and biophysics have provided substantial information about many of these processes, being the significance of this research acknowledged by a Nobel Prize in 1988.²⁸ Notwithstanding, as this is a complex matter, experimental studies on the molecular level have been impeded and therefore only a full theoretical treatment has been possible up to date. Thus, in contrast to previous research, which can be considered to have been a top-down strategy that has tried to zoom in even closer on molecular details, chemists are lately trying to establish a bottom up approach, which starts from small, tractable systems (these concepts will be more extensively explained in chapter 2). Emulating the rapid, close coupling changes in conformation to changes in function is a challenging goal for photochemists, but it would mean a great advance of novel devices and biological tools. The ultimate aim is to use these fundamental photochemical principles experienced by natural biomolecules for the creation of photoswitchable biological systems that permit spatiotemporal control of defined biological activities.

To sum up, the use of light to control the activity of biomolecules, as well as to mimic their function, is an attractive strategy for probing interactions in complex living systems. Photosensitive biomolecules can be introduced into cell and manipulated noninvasively with a high degree of spatial and temporal control.²⁹ Two main strategies may be used in order to design photosensitive biomolecules.

The first one involves the introduction of caged compounds, in which a light flash is used to produce a step increase in the concentration of a bioactive species. This methodology has facilitated studies of muscle contraction, intracellular signaling, and neurotransmission.³⁰ However, synthetic caged compounds present the drawback that they undergo an essentially irreversible photochemical reaction.

²⁷ Renner, C.; Moroder, L. *ChemBioChem* **2006**, *7*, 868.

²⁸ In 1988, the Nobel Prize of Chemistry was assigned to three researchers: Johann Deisenhofer, Rober Huber and Hartmut Michel, for the determination of the three dimensional structure of a photosynthetic reaction centre.

²⁹ (a) Adams, S. R.; Tsien, R. Y. *Annu. Rev. Physiol.* **1993**, *55*, 755. (b) Curley, K.; Lawrence, D. *S. Curr. Opin. Chem. Biol.* **1999**, *3*, 84.

³⁰ (a) Thompson, S. M., Kao, J. P., Kramer, R. H., Poskanzer, K. E., Silver, R. A., Digregorio, D., and Wang, S. S. *J. Neurosci.* **2005**, *25*, 10358. (b) Shigeri, Y., Tatsu, Y., and Yumoto, N. *Pharmacol. Ther.* **2001**, *91*, 85.

Thus, once uncaged, the biomolecule remains active until it is removed in some other manner.

In contrast, “photoswitches” are a class of chemical compounds that undergo reversible photochemistry so that many rounds of active/inactive states may be produced. In addition to this, it is possible to find a wide range of molecules that experience a photoswitchable behavior.³¹

In this dissertation, we will describe the synthesis and photochemical study of two different families of photoswitches whose structure is based on that of natural chromophores (the protonated Schiff base of the retinal chromophore and the green fluorescent protein chromophore), and the properties that make them attractive for the photo-control of biomolecules will be outlined.

³¹ See ref. 13.

CHAPTER 2

Background

Nanoscience constitutes a scientific field whose research is directed towards controlling and manipulating matter of dimensions smaller than 100 nm or 1000 nm, depending on authors. The research and development within this field leads to a general scientific progress, in which material science and engineering are involved. In the last 50 years, the advances achieved by nanoscience have been greatly remarkable.

In this process, it must be ensured that all the components of a desired machine present a nanometric size at least in one dimension, so miniaturization of its components has to be done. This involves shrinking the original size in such way that at the end it only occupies around a hundred of nanometers.¹

One of the most advanced current fabrication methods, the “top-down” approach to miniaturization in the semiconductor industry, is nearing its limits in scaling.² This strategy, which is mainly used by physicists and engineers, consists of manipulating progressively smaller pieces of macroscopic matter by using photolithography and related techniques³ to reach an equivalent microscopic entity. It is thought that the inherent limitations of this strategy would lead to a dead end in the next few years, due to the fact that in some applications no dimensions smaller than 100 nm can be achieved.⁴ For instance, silicon’s band structure disappears when silicon layers are just a few atoms thick. Photolithography and other related techniques, also used for microelectromechanical systems (MEMS) fabrication, are limited by the wavelengths at which they operate.

On the other hand, miniaturization can be pushed further beyond the limit set by the current “top-down” approach by using the “bottom-up” approach, which starts from molecules to construct nanostructures. This strategy is put into practice by chemists. By the nature of their discipline, chemists are already at the bottom, so they are able to build up nanoscale devices from molecules (the smaller entities of matter with different shapes and properties) (Figure 2.1)

¹ (a) Ballardini, R.; Ceroni, P.; Credi, A.; Gandolfi, M. T.; Maestri, M.; Semararo, M.; Venturi, M.; Balzani, V. *Adv.Funct.Mater.*, **2007**,17,740. (b) Balzani, V. *Photochem. Photobiol. Sci.*, **2003**, 2, 459.

² (a) James, D. K.; Tour, J. M. *Aldrichimica Acta*, **2006**, 39, 47; (b) James, D. K.; Tour, J. M. *Top. Curr. Chem.*, **2005**, 257, 33.

³ (a) Kawata, S.; Sun, H.-B.; Tanaka, T.; Takada, K. *Nature*, **2001**, 412, 697. (b) Li, B.; Yu, H.; Sharon, A.; Zhang, X.; *Appl. Phys. Lett.*, **2004**, 85, 2426.

⁴ Keyes, R. W. *Proc. IEEE*, **2001**, 89, 227.

2. Background

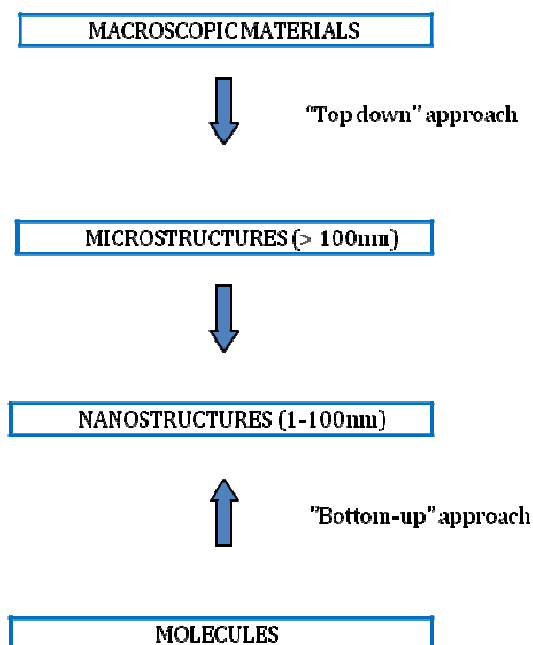


Figure 2.1. Top-down and bottom-up approaches to miniaturization.

In a "bottom-up" process, simple building blocks interact with each other in a coordinated way to form large and more complex supramolecular assemblies.⁵ Processes of molecular recognition and self-assembly direct the way in which relatively simple building blocks recognize each other, associate, and form ordered one-dimensional, two-dimensional, and three dimensional nanostructures and macroscopic objects with nano-scale order. The organization of the building blocks into ordered structures is based on specific recognition that is facilitated by a combination of many different non-covalent interactions. Among these interactions, it is possible to find electrostatic interactions, hydrogen bonds, hydrophobic interactions, London interactions, and aromatic stacking interactions. The overall coordinated combination of the various molecular forces, which are quite weak individually, results in the process of self-organization from simple building blocks into elaborate and ordered structures (Figure 2.2).

⁵ Gazit, E. *Chem. Soc. Rev.* **2007**, *36*, 1263.

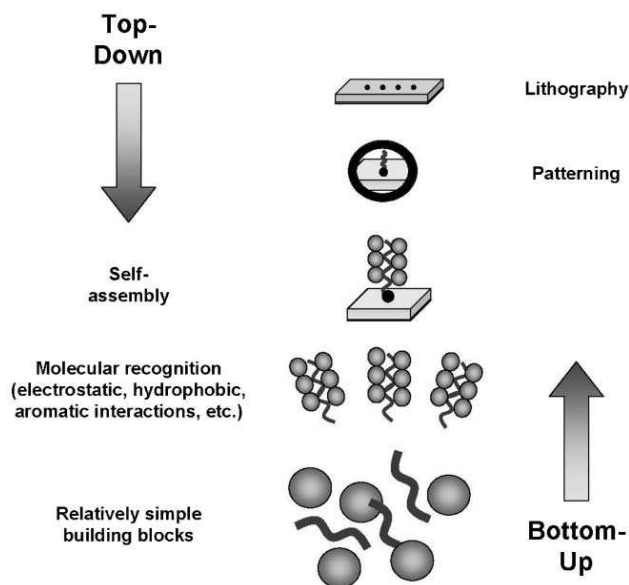


Figure 2.2. The process of “top-down” as compared to “bottom-up” self assembly.

Nanotechnology in its “bottom-up” and self-assembly facets stems directly from earlier studies on self-association and self-organization. The concept of “supramolecular chemistry”, the chemistry of complex non-covalent structures at the nano-scale, began with the study of various organic polymers and sophisticated host-guest chemistry that was based on advanced organic chemistry. The term “supramolecular chemistry” was coined by the pioneering work of Jean-Marie Lehn, whose work was directed towards the engineering of molecular cryptand cages with a desired shape by which only a certain type of molecule was allowed to be lodged in the cage.⁶ Lehn shared the 1987 Nobel Prize in Chemistry with Donald Cram and Charles Pedersen, two other eminent chemists who initiated the development of crown ethers capable of recognizing and selectively binding ions of certain metal elements.

There are multiple kinds of building blocks for nanotechnology, including both organic and inorganic species. Classical nanotechnology emerged with the use

⁶ (a) Berl, V.; Huc, I.; Khoury, R. G.; Krische, M. J.; Lehn, J. M. *Nature*, **2000**, *407*, 720. (b) Ramstrom, O.; Bunyapaiboonsri, T.; Lohmann, S.; Lehn, J. M. *Biochim. Biophys. Acta*, **2002**, *1572*, 178.

of pure carbon structures of the buckminsterfullerene and carbon nanotubes, or modified analogs of these carbon structures.⁷ This was later followed by the study of inorganic nanostructures, such as silicone nanowires,⁸ and inorganic nanotubes and fullerene-like structures from layered materials, such as WS₂, MoS₂, and NbS₂.⁹ Other efforts in nanotechnology were directed towards the development of organic nanostructures, due to the fact that a great deal of modern materials science is based on organic chemistry. In the broadest sense, nanochemistry employs the tools of synthetic and materials chemistry to make nanomaterials with size, shape and surface properties that are designed to evoke a specific function, and orchestrated to target a particular end use.¹⁰ These building blocks of nanochemistry may either have value on their own (*i.e.* a nanocrystal single-electron transistor), or be a part of self-assembled structures and patterns that accomplish a function and utility, such as a semiconductor nanowire electronic circuit.

On the other hand,¹¹ in current computers, information processing takes place at logic gates, which consists of a series of devices whose switches are initiated by input and output signals, following Boolean logic. Data manipulation relies on the binary digital (bit) nature of these signals. In relation to electronics, in the last few years, the “bottom-up” strategy described above has been used in order to miniaturize electronic components. This way, miniaturized electric circuits that are even smaller than the micrometer-scale digital logic circuits fabricated on conventional solid-state semiconductor chips have been described. These studies belong to a new research field called molecular electronics. Moreover, many investigations on electrical conductivity and electrical-switching properties of molecules and supramolecular systems have been performed in order to obtain logic gates based on molecular diodes that could be a million times smaller in area than the corresponding logic gates that are currently constructed in a semiconductor chip.

⁷ (a) Kroto, H. W.; Heath, J. R.; O’Brien, S. C.; Curl, R. F.; Smalley, R. E. *Nature*, **1985**, *318*, 162. (b) Iijima, S. *Nature*, **1991**, *354*, 56.

⁸ (a) Yang, C.; Zhong, Z.; Lieber, C. M. *Science*, **2005**, *310*, 1304. (b) Hannon, J. B.; Kodambaka, S.; Ross, F. M.; Tromp, R. M. *Nature*, **2006**, *440*, 69.

⁹ Tenne, R.; Rao, C. N. *Philos. Trans. R. Soc. London, Ser. A*, **2004**, *362*, 2099.

¹⁰ Ozin, G. A.; Cademartiri, L. *Small* **2009**, *5*, 1240.

¹¹ See ref. 1(a).

In addition to molecular electronics, if photons are used instead of electric signals to make the nanoscale system work, we find ourselves in the field of molecular photonics, and when using chemical reactions, in the field of chemionics.

Therefore, the “bottom-up” approach opens up a wide variety of possibilities for the design of new materials and structures presenting nanometric size. As expected, these studies are not only directed towards the construction of components of molecular machines, but also to build molecular machines in a broad way. In the following epigraphs, some features and examples of molecular machines and devices will be reviewed.

2.1. MOLECULAR MACHINES AND DEVICES: CONCEPT AND FEATURES

2.1.1. Differences between molecular machines and devices.

The definitions of machine and device are often mistaken. A macroscopic machine is any combination of mechanisms for utilizing, modifying, applying, or transmitting energy, either simple or complex. The movements of the mobile parts of a macroscopic machine can be described by Newton’s equations of motion, which determine the coordinates and speed of each part of the machine relative to a given origin. However, a macroscopic device is something designed for a specific purpose. Machines are constituted by a combination of components (devices) that, even though when they work separately they perform simple actions, altogether they execute more complex functions as a whole, which are inherent of that machine or appliance.

In order to understand better the aforementioned definitions, the operation of a hair dryer may be used as an example (Figure 2.3). The function of producing hot air is the result of the action performed by a switch, a resistance, a fan, and several electric wires connected in an appropriate way.¹²

¹² Balzani, V.; Credi, A.; Venturi, M. *Molecular devices and Machines – Concepts and Perspectives for the Nanoworld*. Wiley-VCH, Weinheim, **2008**.

2. Background

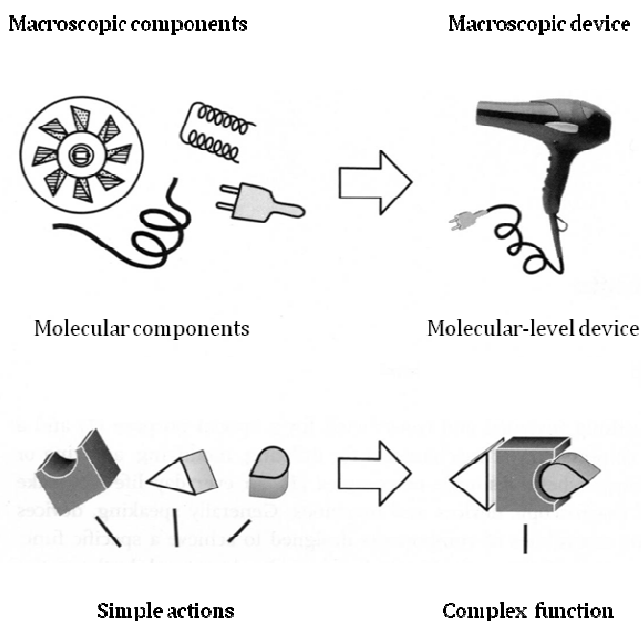


Figure 2.3. The concept of a macroscopic device extended to a molecular level.

The concept of a macroscopic machine or device can be extended to the molecular level by designing and synthesizing (supra)-molecular species capable of performing specific functions. Therefore, a molecular machine can be regarded as a discrete combination of molecular devices that perform a specific function. Each molecular device executes a simple action, while the entire supramolecular assembly carries out a more complex function, which results from the cooperation of all the molecular components. The idea of constructing artificial molecular-level machines is quite recent. The first time the topic was seriously contemplated was in 1959 by Richard Feynman,¹³ Nobel Laureate in Physics, in his historic address “There is Plenty of Room at the Bottom”, to the American Physical Society in December of that year. The extension of the concept of a machine or device to the molecular level is of interest, not only for basic research, but also for the growth of nanoscience and the development of nanotechnology. They are thought to be used in information storage, display, processing and, eventually, the construction of molecular-based (chemical) computers.

¹³ (a) Feynman, R. P. *Eng. Sci.* **1960**, *23*, 22. (b) Feynman, R. P. *Saturday Rev.* **1960**, *43*, 45. (c) <http://www.its.caltech.edu/~feynman/plenty.html> (web page visited on March 1st, 2012).

2.1.2. Main features of molecular machines.

As it has been mentioned above, a molecular machine can be defined as an assembly of a discrete number of molecular components designed to perform mechanical-like movements (output) as a consequence of appropriate external stimuli (input). Although there are many chemical compounds whose constitutions and/or shapes can be modified by an external stimulus, the term molecular-level machine is only used for systems whose component parts undergo movements with relative large amplitudes, leading to real translocation of some components of the system.¹⁴ Furthermore, systems in which the molecular movements are not controlled by some easily identifiable and well-characterized external stimulus will not be considered to be molecular-level machines.

Moreover, particularly interesting nuclear motions from the point of view of artificial molecular machines are those related to:

- isomerization reactions involving -N=N-, -C=N-, and -C=C- double bonds in covalent supramolecular structures;
- metal-ligand reactions causing the formation or disruption of coordinating bonds; and
- acid-base or redox reactions causing the making/breaking of intermolecular bonds, (including hydrogen bonds).

This is due to the fact that they allow the synthetic design of a wide variety of molecular devices, which undergo the proper chemical reactions in order to produce the aforementioned nuclear movements.

In common with their macroscopic counterparts, a molecular machine is characterized by:

- the kind of energy input supplied to make it work (which will be later described in section 2.1.3.);
- the nature of the movements of its component parts;

¹⁴ Balzani, V.; Credi, A.; Venturi, M. *Pure Appl. Chem.* **2003**, *75*, 541.

- the way in which its operation can be monitored and controlled;
- the ability to make it repeat its operation in a cyclic fashion;
- the timescale needed to complete a full cycle of movements; and
- the purpose of its operation.

On the other hand, one of the most important parts of a molecular machine is its motor, which means a molecular device capable of transforming the energy supplied to the system (either chemical energy, electric or photochemical) into mechanical energy so that it is possible to perform work. A molecular motor consists of a mobile and a stationary part, so that an external operator should be able to induce the displacement of the movable component from the stationary one. The definition and features of a molecular motor will be further analyzed in the following sections. Apart from a motor, a molecular machine might contain other components that are equivalent to those of the macroscopic machines, such as brakes, fasteners, gears, and so on.

2.1.3. Power supply required to perform work.

Machines need power supply for them to undergo mechanical movements and consequently do work.¹⁵ Just as macroscopic machines require macroscopic energy sources, natural and artificial molecular machinery need nanoscale power supplies to undergo direct molecular motions.

However, while macroscopic machines don't move until energy is supplied to the system for a specific function, nanoscale machines down at the molecular level are in perpetual relentless thermal (Brownian) motion at ambient temperatures.¹⁶ So then, in order to operate in such turbulent world, the molecular systems must either exploit Brownian motion or overcome it. Nature harnesses Brownian motion in a manner referred to as the Brownian ratchet in linear and rotary

¹⁵ Saha, S.; Stoddart, J. F. *Chem. Soc. Rev.* **2007**, *36*, 77.

¹⁶ (a) Brown, R. *Philos. Mag.* **1828**, *4*, 171. (b) Rozenbaum, V. M.; Yang, D.-Y.; Lin, S. H.; Tsong, T. Y. *J. Phys. Chem. B* **2004**, *108*, 15880. (c) Whitesides, G. M. *Sci. Am.* **2001**, *285*, 78. (d) Astumian, R. D. *Science* **1997**, *276*, 917.

protein motors where the energy input restrains random Brownian motion.¹⁷ The design of artificial molecular motors requires that specific directional mechanical motion is controlled and that the stimuli-induced motion of a motor component can be detected and distinguished above the Brownian motion, because it makes the detection of stimuli-induced, relative movements of their components a nontrivial phenomenon, as compared to the easily detectable motions performed by macroscopic machines. Achieving a biased change in motion at the molecular level is not trivial at all, and it should be realized that in both biological and synthetic molecular motors conformational mobility is crucial to their function.¹⁸

Three types of external stimuli: chemical, electrochemical and photochemical have been employed to induce well-defined mechanical movements within molecular machines. Several spectroscopic and electrochemical techniques have been used to distinguish the stimuli-induced nanomechanical motions from the random Brownian ones.

In addition to this, it is convenient that the selected kind of energy to make a molecular machine work doesn't create waste products, so the problem of finding and eliminating them at the end of the cycle doesn't need to be faced.¹⁹

Presumably, the best energy inputs to make molecular machines work are photons or electrons. Indeed, with appropriately chosen photochemically and electrochemically driven reactions, it is possible to design and synthesize molecular machines that do work. Moreover, the dramatic increase in our fundamental understanding of self-assembly and self-organizational process in chemical synthesis has aided and promoted the construction of artificial molecular machines through the development of new methods of noncovalent synthesis and the emergence of supramolecular assistance to covalent synthesis as a uniquely powerful synthetic tool.

¹⁷ (a) Goodsell, D. S. *Our Molecular Nature. The Body's Motors, Machines and Messages*. Springer-Verlag: New York, **1996**. (b) Schliwa, M. (Ed.) *Molecular Motors*. Wiley: Weinheim, Germany, **2003**. (c) Astumian, R. D. *Sci. Am.* **2001**, *285*, 45.

¹⁸ (a) Browne, W. R.; Feringa, B. L. *Nat. Nanotechnol.* **2006**, *1*, 25. (b) Kay, E. R.; Leigh, D. A.; Zerbetto, F. *Angew. Chem., Int. Ed.* **2007**, *46*, 72. (c) Stoddart, J. F. *Acc. Chem. Res.* **2001**, *34*, 410. (d) See ref 12. (e) Sauvage, J. P., Ed. *Molecular Machines and Motors*; Springer: Berlin, **2001**. (f) Harada, A. *Acc. Chem. Res.* **2001**, *34*, 456.

¹⁹ (a) See ref. 14. (b) Balzani, V.; Credi, A.; Venturi, M. *Nano Today* **2007**, *2*, 18.

However, compared to chemical and electrical energy inputs, photochemical energy shows several advantages over the previous ones, apart from not generating waste products:

- light can be switched on/off easily and rapidly;
- lasers provide the opportunity of working in very small space and very short time domains;
- photons, besides supplying the energy needed to make a machine work, can also be useful to “read” the state of the system, and therefore to control and monitor the operation of the machine; and
- if the kind of light used is solar light, it constitutes a renewable and clean kind of energy.

Light energy is able to produce photochemical reactions, such as photoisomerizations of $-C=C-$, $-C=N-$, and $-N=N-$ double bonds. These reactions are used as basic principles for the design of multiple examples of molecular machines and devices, as we will see along this thesis.

2.2. LIGHT-ACTIVATED MOLECULAR SWITCHES

2.2.1. Differences between a molecular switch, rotor and motor.

A molecular switch is a molecular device that can be reversibly interchanged between two different states (which means that it has two positions: on and off) by means of an external stimulus. In general terms, it is considered a bistable system (Figure 2.4).²⁰ If each one of the states can be “read” in a non-destructive way, the molecule can function, in principle, as a memory element in a digital system.

²⁰ (a) See ref. 18.

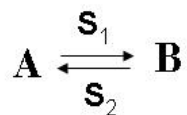


Figure 2.4. Schematic representation of a bistable molecular switch. A and B exemplify the two different states reached by molecular switches, and S₁ and S₂ the different stimuli required for the interchange.

When irradiation is used to stimulate the molecular switch, a photoisomerization of -C=C-, -C=N- and -N=N- double bonds can take place.

Throughout this thesis, the synthesis, characterization and photochemical study of different molecular switches whose movement is activated with light will be reviewed.

On the other hand, a molecular rotor is a device capable of rotating in several directions with a continuous movement. In section 2.3.2, an example of a natural molecular rotor (ATP-synthase) will be reviewed.

Finally, if the continuous rotational movement of a molecular rotor is controlled in a way that involves unidirectional rotation, that particular molecular device can be considered to be a molecular motor. In order to design new prototypes of molecular motors three basic requirements need to be fulfilled:²¹

- repetitive 360° rotary motion;
- consumption of energy for executing the movement; and
- control of the rotational direction, which can be done by introducing in the motor skeleton different chemical factors, such as the presence of chiral centers in the molecule, which favor the rotation in a certain direction due to asymmetry.

Different examples of natural and artificial molecular motors will be described in sections 2.3, 2.5 and 2.6.

²¹ (a) ter Wiel, M. K. J.; Van Delden, R. A.; Meetsma, A.; Feringa, B. L. *J. Am. Chem. Soc.* **2005**, *127*, 14208. (b) Kline, T. R.; Paxton, W. F.; Mallouk, T. E.; Sen, A. *Angew. Chem. Int. Ed.* **2005**, *44*, 744.

2.3. NATURAL MOLECULAR SWITCHES AND MOTORS

As it has been already mentioned in the previous epigraphs, different examples of nanoscale machinery can be found in Nature. Specifically, cells house hundreds of different molecular machines and motors, each of them specialized for a particular function. These natural nanomachines, which are primarily composed of proteins, nucleic acids and other organic molecules, require energy in order to perform their functions, so they convert the chemical energy stored in cells into mechanical energy. When comparing conventional technologies with natural molecular machines, it is obvious that these last kind of systems display tremendous abilities.²² The molecular machinery of green plants, for example, converts more energy and synthesizes a greater tonnage of organic compounds than does humanity's entire chemical industry, in a really clean way and using cheap raw materials. Therefore, the design of new nanosystems could be directed in a way that mimics Nature's efficient machines.

The following paragraphs reveal how these molecular machines and motors are present in a multitude of essential biological processes, such as transport of cations, synthesis of ATP, muscle contraction and vision.

2.3.1. Natural metal ion channels.

Cells require the passage of cations, such as Na^+ , Ca^{2+} and K^+ , across their membranes, so they can be distributed to their components. However, this process is prevented by the existence of membranes that protect the contents of cells. Therefore, different transport mechanisms are required so that cations are able to reach the inside of cells. Firstly, carriers are hosts molecules that are embedded in cell membranes and help cations to go through the membrane by means of complexation. However, the rate of this transport mechanism is relatively slow because it is limited by diffusion. On the other hand, ion channels are membrane proteins that form aqueous ion-conduction pathways through the center of the protein and expand the cell membrane for ions to move across. These protein channels transport ions faster than carriers.

²² Drexler, K. E. *Trends Biotechnol.* **1999**, *17*, 5.

As an example of a natural ion channel, the mechanism of bacteriorhodopsin, a small and robust membrane protein of the halophilic microorganism *Halobacterium salinarum*, which acts as a light-activated proton pump, is described below (Figure 2.5).²³

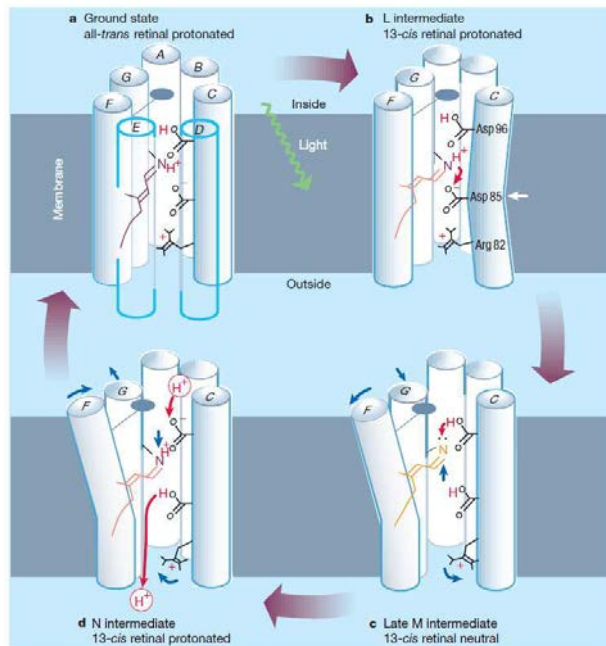


Figure 2.5. A natural molecular machine: bacteriorhodopsin acting as a proton pump.

Bacteriorhodopsin consists of seven membrane-spanning helical structures linked by short loops on either side of the cell membrane (Figure 2.5(a), from A to G). It also contains one molecule of a linear pigment called retinal, which is covalently attached to the nitrogen atom of the lysine residue of helix G through a protonated Schiff base. The retinal chromophore, which will be further studied in section 2.3.4., suffers an isomerization when irradiated with light from all-*trans* to 13-*cis*, through several intermediates named K, L, M, N and O (intermediates L, M and N are shown in Figure 2.5). This structural change is used by the Schiff base to

²³ (a) Subramaniam, S.; Henderson, R. *Nature*, **2000**, *406*, 653. (b) Kühlbrandt, W. *Nature*, **2000**, *406*, 569.

push a single proton through the seven-helix bundle, from the inside of the cell to the extracellular medium, being subsequently re protonated from the cytoplasm.

Therefore, in this particular movement, the retinal chromophore acts as a valve inside of the cell membrane of this organism.

2.3.2. ATP-synthase, a natural rotary motor.

As stated before, energy is required for molecular machines and motors to work, so they are usually fueled by the energy stored in cells. Regarding the synthesis of ATP, carried out by the enzyme ATP synthase, the two most common energy repositories of cells are used: the energy stored in the phosphate bonds of nucleotides, generally ATP (adenosine triphosphate), and in transmembrane electrochemical gradients.²⁴ The ATP synthase protein (Figure 2.6) is a natural rotary motor that consists of two units attached to a common shaft: a hydrophobic proton channel (F_0) embedded in the mitochondrial membrane and a hydrophilic catalytic unit (F_1) protruding into the mitochondria. The complex can be thought of as two rotary motor units coupled together. The F_1 motor uses free energy of ATP hydrolysis to rotate in one direction whereas the F_0 motor uses the energy stored in a transmembrane electrochemical gradient to turn in the opposite direction. The F_1F_0 -ATP synthase complex is reversible because it may synthesize or hydrolyze ATP depending on the driven force of the movement. When F_0 takes over, which is the normal situation, it drives the F_1 motor in reverse producing the synthesis of ATP from ADP and inorganic phosphate, Pi. However, when F_1 controls the rotation, it drives the F_0 motor in reverse, becoming an ion pump that moves ions across the membrane against the electrochemical gradient. Rotation of F_1 was demonstrated recently by directly observing the motion of a fluorescent actin filament specifically bound to the rotor element.²⁵ Yasuda *et al.*²⁶ observed discrete 120° rotations under low ATP concentrations by using actin filaments of variable length. Moreover, they estimated that the work required to rotate an actin filament against a viscous load was 80 pN nm, which is approximately the free energy liberated by a single ATP hydrolysis under physiological conditions. Therefore, they concluded that the F_1 -ATPase could couple nearly 100% of its ATP-derived energy into mechanical work, being considered a really efficient motor.

²⁴ Metha, A. D.; Rief, M.; Spudich, J. A.; Smith, D. A.; Simmons, R. M. *Science*, **1999**, *283*, 1689.

²⁵ Noji, H.; Yasuda, R.; Yoshida, M.; Kinosita Jr., K. *Science*, **1997**, *386*, 299.

²⁶ Yasuda, R.; Noji, H.; Kinosita Jr., K.; Yoshida, M. *Cell*, **1998**, *93*, 1117.

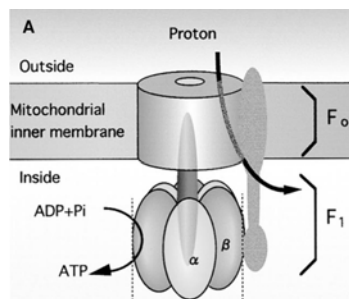


Figure 2.6. A natural rotary motor: ATP synthase.

2.3.3. Natural molecular motors that perform a linear-like movement.

Among the different types of biomolecular motors, those that move in a linear fashion along a track of some kind are considered greatly relevant because they are involved in crucial processes, such as intracellular trafficking, cell division and muscle contraction.²⁷

Eukaryotic cells require efficient systems that enable intracellular transport in order to supply their cellular organelles. Among these systems are found the microtubule motor proteins, like kinesin (Figure 2.7).²⁸

²⁷ (a) Ozin, G. A.; Arsenault, A. C. *Nanochemistry. A chemical approach to nanomaterials*. RCS publishing, Cambridge, UK, **2005**. (b) See ref. 17(a). (c) Vale, R. D.; Milligan, R. A. *Science*, **2000**, *288*, 88. (d) Howard, J. *Mechanics of Motor Proteins and Cytoskeleton*. Sinauer Associates, Sunderland, **2001**. (e) Frey, E. *ChemPhysChem*, **2002**, *3*, 270.

²⁸ (a) Block, S. M. *Cell*, **1998**, *93*, 5. (b) Limberis, L.; Stewart, R. J. *Nanotechnology*, **2000**, *11*, 47. (c) Hirokawa, N. *Science*, **1998**, *279*, 519. (d) Goldstein, L. S. B. *Proc. Natl. Acad. Sci.*, **2001**, *98*, 6999. (e) Schliwa, M.; Woehlke, G. *Nature*, **2001**, *411*, 424. (f) Svoboda, K.; Schmidt, C. F.; Schanapp, B. J.; Block, S. M. *Nature*, **1993**, *365*, 721. (g) Coy, D. L.; Wagenbach, M.; Howard, J. *J. Biol. Chem.*, **1999**, *274*, 3667.

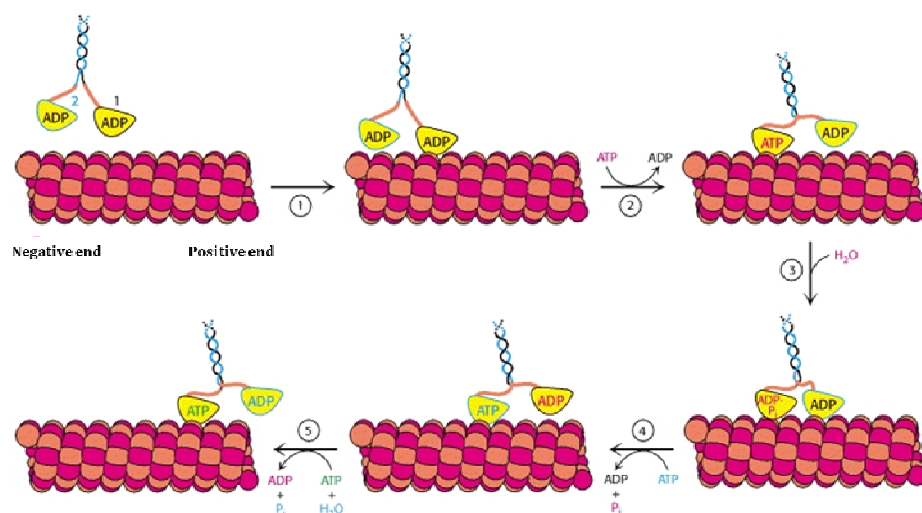


Figure 2.7. A natural linear motor: kinesin.

Conventional kinesin is a protein assembly whose total size is approximately 80 nm. It is composed of two larger protein chains, which are involved in microtubule binding and mobility, ATP hydrolysis required for the movement, and protein dimerization, as well as two smaller protein chains, which regulate heavy chain activity and binding to cargo. Kinesin transports cargo along microtubules, which are composed of self assembled tubular proteins in a cylindrical way with a 24 nm diameter. The dimensions of these tubular proteins induce the structural lattice to present periodic subunits of 8 nm. Surprisingly, for each ATP molecule hydrolyzed during the movement, kinesin performs a walking-like motion with 8 nm steps. Moreover, it moves with a high speed of about $1.8 \mu\text{m s}^{-1}$, and can move against loads of 6 pN. Another important feature of microtubule structure is polarity, so one of the ends of the microtubule is considered as positive and the other as negative. Kinesin moves towards the positive end of microtubules. However, the dynein family, which also moves along microtubules in a linear fashion, is directed towards the negative end of microtubules, which is usually anchored to the centrosome of the cell.²⁹

Among cellular division processes are also found several molecular motors that perform a linear-like movement, such as RNA polymerase, which synthesizes

²⁹ Taylor, H. C.; Holwill, E. J. *Nanotechnology*, **1999**, *10*, 237.

new RNA from a single strand RNA template,³⁰ and DNA helicase, which translates along and unwinds DNA in preparation for new DNA synthesis.³¹

2.3.4. The importance of the protonated Schiff base of the retinal chromophore as a molecular motor.

One of the most remarkable examples in Nature of a molecular motor is the retinal chromophore of rhodopsin, which suffers a *cis-trans* photoisomerization during the process of vision.³² In vertebrates, vision is initiated by rods and cones, which are photoreceptor cells located in the retina of the eye. The photosensitive entities of these cells are visual pigments that consist of the appropriate apoprotein, called opsin, and a chromophore, known as 11-*cis*-retinal, which is embedded inside the opsin (Figure 2.8).³³

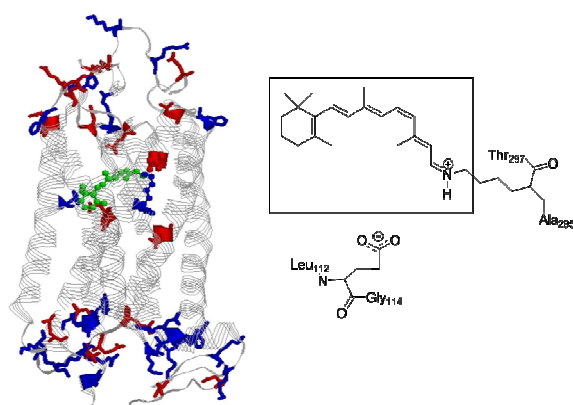


Figure 2.8. Rhodopsin and its chromophore (a protonated Schiff base of retinal).

Rhodopsin (rod opsin) belongs to the G-protein coupled receptor family and is composed of 7-transmembrane helices.³⁴ The 11-*cis* retinal is linked to a lysine residue of the 7th helix (Lys₂₉₆ in the case of bovine rhodopsin) through a protonated Schiff base (PSB), which is protonated and stabilized by a negatively

³⁰ Gelles, J.; Landick, R. *Cell*, **1998**, *93*, 13.

³¹ Lohman, T. M.; Thorn, K.; Vale, R. D. *Cell*, **1998**, *93*, 9.

³² Kandori, H.; Shichida, Y.; Yoshizawa, T. *Biochem. (Moscow)*, **2001**, *66*, 1197.

³³ Baylor, D. *Proc. Natl. Acad. Sci. USA*, **1996**, *93*, 560.

³⁴ Teller, D. C.; Okada, T.; Behnke, C. A.; Palczewski, K.; Stenkamp, R. E. *Biochemistry*, **2001**, *40*, 7761.

2. Background

charged carboxylate (Glu₁₁₃ in the case of bovine rhodopsin). Moreover, the β -ionone ring of retinal is coupled with the hydrophobic region of opsin through hydrophobic interactions.³⁵ Thus, the retinal chromophore is fixed by three kinds of chemical bonds in the retinal binding pocket of rhodopsin.

The role of rhodopsin in the signal transduction cascade of vision is to activate transducin, a heterotrimeric G protein, upon absorption of light.³⁶ In the absence of visible light, retinal presents a *cis* conformation between its carbons 11 and 12. However, when 11-*cis*-retinal absorbs visible light (λ between 400-600 nm), a selective and rapid (200 fs) photoisomerization of this double bond takes place via evolution of a single $\pi \rightarrow \pi^*$ excited state (S_1) that decays to the all-*trans* ground state (S_0) product (Figure 2.9). Picosecond time-resolved spectroscopy of 11-*cis* locked rhodopsin analogs reveals that the *cis-trans* isomerization of the retinal chromophore is the primary reaction in the process of vision, and it is followed by a conformational change in the rhodopsin protein, which activates transducin in order to initiate the process of vision.³⁷

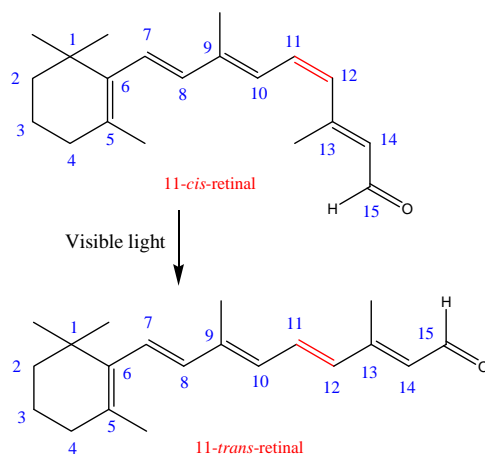


Figure 2.9. Photo-induced isomerization reaction of retinal.

³⁵ Matsumoto, H.; Yoshizawa, T. *Nature*, **1975**, 258, 523.

³⁶ (a) Khorana, H. G. *J. Biol. Chem.*, **1992**, 267, 1. (b) Hofmann, K. P.; Helmreich, E. J. M. *Biochim. Biophys. Acta*, **1996**, 1286, 285. (c) Sakmar, T. P. *Prog. Nucleic Acid Res. Mol. Biol.*, **1998**, 59, 1. (d) Shichida, Y.; Imai, H. *CMLS, Cell. Mol. Life Sci.*, **1998**, 54, 1299.

³⁷ McBee, J. K.; Palczewski, K.; Baehr, W.; Pepperberg, D. R. *Prog. Retin. Eye Res.*, **2001**, 20, 469.

It is known that the *cis-trans* isomerization is highly efficient in rhodopsin, presenting an *in vivo* isomerization quantum yield (Φ_{isom}) of 0.67,³⁸ which is essential to make twilight vision highly sensitive. In fact, a human rod cell can respond to a single photon absorption. Such an efficient photoisomerization of the retinal chromophore is characteristic in the protein environment of rhodopsin, being in contrast to the rhodopsin chromophore in solution. Due to the high efficiency of the isomerization process of retinal *in vivo*, it has been widely studied and used as a pattern for the design of new prototypes of molecular switches and motors activated by light. As it is known that the protein environment facilitates the isomerization process of retinal, the aim of these studies is the design of synthetic compounds that reproduce in solution the features of the chromophore inside the protein. Therefore, molecular switches and motors that work efficiently could be obtained.

2.3.5. Green fluorescent protein (GFP) chromophore.

Another example of biomolecules that undergo photo-induced *Z/E* isomerizations is the chromophore of the green fluorescent protein (shortened as GFP) (Figure 2.10), from *Aequorea victoria* jellyfish (Figure 2.11). GFPs are intrinsically fluorescent molecules whose optical properties are determined by a photoexcitable green-light emitter chromophore autocatalytically generated by the posttranslational modification of a 3-amino acid sequence (Ser65-Tyr66-Gly67).³⁹ GFP takes advantage of the presence of a chromophore, (*Z*)-4-(4-hydroxybenzylidene)-1,2-dimethyl-1*H*-imidazol-5(4*H*)-one (*p*-HBDI), which consists of the hydroxybenzyl side chain of Tyr66 (phenolic ring) and the imidazolidinone ring formed by cyclization of the tripeptide (heterocyclic ring). It is positioned in a cavity containing a number of neighboring polar and aromatic residues. These are important in establishing a hydrogen-bond network around the chromophore involving also some water molecules. GFP fluorescence and absorption critically depend on this network and perturbation of the latter can induce marked variation in GFP photophysics. The chromophore is the responsible for the fluorescence of this protein when it undergoes excited-state proton transfer

³⁸ (a) Dartnall, H. J. A. *Vision Res.*, **1967**, *8*, 339. (b) Mathies, R. A.; Lugtenburg, J. In *Handbook of Biological Physics*; Stavenga, D. G., de Grip, W. J., Pugh, E. N. (eds.) Elsevier: Amsterdam, **2000**; Vol. 3, p 56.

³⁹ Heim, R.; Prasher, D. C.; Tsien, R. Y. *Proc. Natl. Acad. Sci. U.S.A.* **1994**, *91*, 12501.

2. Background

(ESPT)⁴⁰ via the proton relay of the water network and/or some residues to a remote residue such as E222,⁴¹ within a picoseconds time scale,⁴² resulting in very intense anion fluorescence.

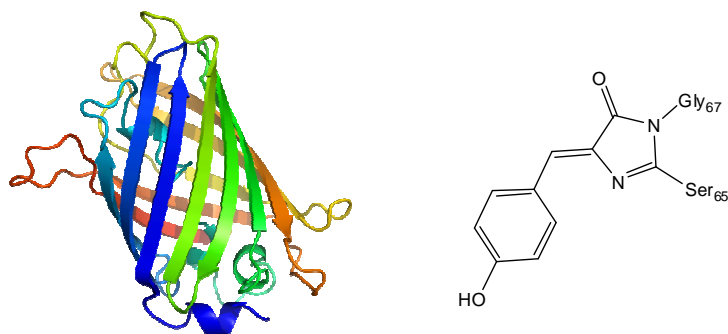


Figure 2.10. Green fluorescent protein (GFP) and its chromophore (*p*-HBDI).



Figure 2.11. *Aequorea victoria* jellyfish.

However, several studies have revealed that *p*-HBDI also undergoes nonradiative processes when irradiated with light, such as a *Z/E*

⁴⁰ (a) Agmon, N. *Biophys. J.* **2005**, *88*, 2452. (b) Stoner-Ma, D.; Jaye, A. A.; Matousek, P.; Towrie, M.; Meech, S. R.; Tonge, P. J. *J. Am. Chem. Soc.* **2005**, *127*, 2864. (c) Hosoi, H.; Mizuno, H.; Miyawaki, A.; Tahara, T. *J. Phys. Chem. B* **2006**, *110*, 22853.

⁴¹ (a) Stoner-Ma, D.; Melief, E. H.; Nappa, J.; Ronayne, K. L.; Tonge, P. J.; Meech, S. R. *J. Phys. Chem. B* **2006**, *110*, 22009. (b) Abbyad, P.; Childs, W.; Shi, X.; Boxer, S. G. *Proc. Natl. Acad. Sci. U.S.A.* **2007**, *104*, 20189. (c) Stoner-Ma, D.; Jaye, A. A.; Ronayne, K. L.; Nappa, J.; Meech, S. R.; Tonge, P. J. *J. Am. Chem. Soc.* **2008**, *130*, 1227. (d) Fang, C.; Frontiera, R. R.; Tran, R.; Mathies, R. A. *Nature* **2009**, *462*, 200.

⁴² Chatteraj, M.; King, B. A.; Bublitz, G. U.; Boxer, S. G. *Proc. Natl. Acad. Sci. U.S.A.* **1996**, *93*, 8362.

photoisomerization,⁴³ which contributes to reduce the luminescence quantum yield (Figure 2.12).

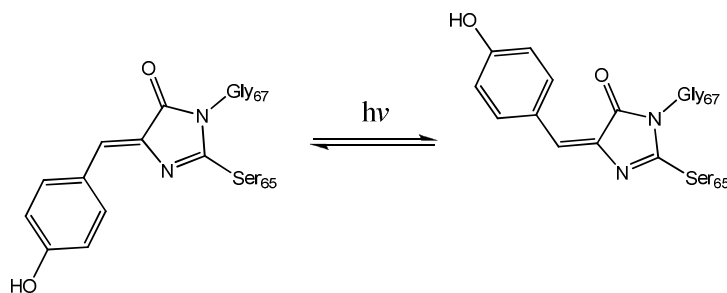


Figure 2.12. Z/E photoisomerization of the GFP chromophore.

Due to its attractive emission of fluorescence, GFP has emerged in recent years as a unique fluorescent marker in molecular and cellular biology (Figure 2.13).⁴⁴ Thus, intracellular dynamics of selected molecules can be followed by activating the fluorescent proteins to their fluorescent state.⁴⁵ This means that they

⁴³ (a) Nifosì, R.; Ferrari, A.; Arcangeli, C.; Tozzini, V.; Pellegrini, V.; Beltram, F. *J. Phys. Chem. B* **2003**, *107*, 1679. (b) Voliani, V.; Bizzarri, R.; Nifosì, R.; Abbruzzetti, S.; Grandi, E.; Viappiani, C.; Beltram, F. *J. Phys. Chem. B* **2008**, *112*, 10714. (c) Rafiq, S.; Rajbongshi, B. K.; Nair, N. N.; Sen, P.; Ramanathan, G. *J. Phys. Chem. A* **2011**, *115*, 13733.

⁴⁴ (a) Sullivan, K. F.; Kay, S. A. *Green Fluorescent Proteins*. Academic Press: San Diego, CA, **1999**. (b) Chalfie, M.; Tu, Y.; Euskirchen, G.; Ward, W. W.; Prasher, D. C. *Science* **1994**, *263*, 802. (c) Lippincott-Schwartz, J.; Patterson, G. H. *Science* **2003**, *300*, 87. (d) Ormo, M.; Cubitt, A. B.; Kallio, K.; Gross, L. A.; Tsien, R. Y.; Remington, S. J. *Science* **1996**, *273*, 1392. (e) Zimmer, M. *Chem. Rev.* **2002**, *102*, 759. (f) Tsien, R. Y. *Annu. Rev. Biochem.* **1998**, *67*, 509. (g) Matz, M. V.; Fradkov, A. F.; Labas, Y. A.; Savitsky, A. P.; Zaraisky, A. G.; Markelov, M. L.; Lukyanov, S. A. *Nat. Biotechnol.* **1999**, *17*, 969. (h) Hastings, J. W.; Morin, J. G., In *Green Fluorescent Protein*. Chalfie, M., Kain, S. (Eds.) Wiley-Liss: New York, **1998**; pp 17–41. (i) Chalfie, M. *Green Fluorescent Proteins, Properties, Applications and Protocols*. Wiley-Liss: New York, **1998**.

⁴⁵ (a) Patterson, G. H.; Lippincott-Schwartz, J. *Science* **2002**, *297*, 1873. (b) Ando, R.; Hama, H.; Yamamoto-Hino, M.; Mizuno, H.; Miyawaki, A. *Proc. Natl. Acad. Sci. USA* **2002**, *99*, 12651. (c) Chudakov, D. M.; Belousov, V. V.; Zaraisky, A. G.; Novoselov, V. V.; Staroverov, D. B.; Zorov, D. B.; Lukyanov, S.; Lukyanov, K. A. *Nat. Biotechnol.* **2003**, *21*, 191. (d) Chudakov, D. M.; Verkhusha, V. V.; Staroverov, D. B.; Souslova, E. A.; Lukyanov, S.; Lukyanov, K. A. *Nat. Biotechnol.* **2004**, *22*, 1435. (e) Wiedenmann, J.; Ivanchenko, S.; Oswald, F.; Schmitt, F.; Röcker, C.; Salih, A.; Spindler, K.-D.; Nienhaus, G. U. *Proc. Natl. Acad. Sci. USA* **2004**, *101*, 15905.

2. Background

can follow processes inside individual cells, such as illuminating growing cancer tumors, and showing the development of Alzheimer's disease in the brain or the growth of pathogenic bacteria. Thanks to molecular engineering a wide variety of GFP mutants have been designed with different spectral characteristics, enhanced brightness, photostability, quantum yield, and other properties related to different applications.

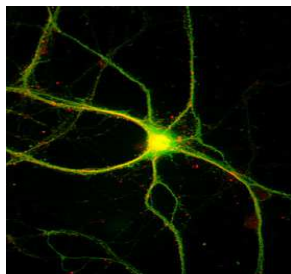


Figure 2.13. Neuron expressing GFP

In 2008, as a result of the great relevance of the luminescence of GFP, the Nobel Prize of Chemistry was assigned to three researchers that had worked in the discovery and development of the green fluorescent protein: Osamu Shimomura (Figure 2.14a), Martin Chalfie (Figure 2.14b) and Roger Y. Tsien (Figure 2.14c).⁴⁶

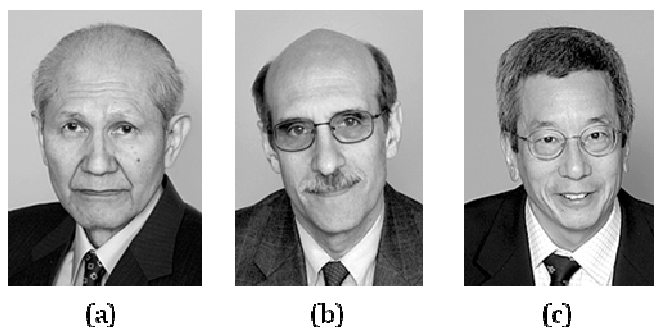


Figure 2.14. (a) Osamu Shimomura (b) Martin Chalfie (c) Roger Y. Tsien

⁴⁶ (a) Shimomura, O. (Nobel lecture) *Angew Chem. Int. Ed.*, **2009**, 48, 5590. (b) Chalfie, M. (Nobel lecture) *Angew Chem. Int. Ed.*, **2009**, 48, 5603. (c) Tsien, R.Y. (Nobel lecture) *Angew Chem. Int. Ed.*, **2009**, 48, 5612.

2.4. ARTIFICIAL MOLECULAR MACHINES

In approaches toward artificial machinery that mimic the dynamic behavior of Nature's molecular machines, several molecular systems have been designed in which translational or rotary motion is controlled by means of chemical, electrochemical, photochemical, or thermal input. Among these systems are molecular propellers,⁴⁷ rotors,⁴⁸ motors,⁴⁹ brakes,⁵⁰ switches,⁵¹ turnstiles,⁵² ratchets,⁵³ shuttles,⁵⁴ elevators,⁵⁵ muscles,⁵⁶ scissors,⁵⁷ processive artificial enzymes,⁵⁸ and catalytic self-propelled micro- and nano-rods.⁵⁹

⁴⁷ Iwamura, H.; Mislow, K. *Acc. Chem. Res.* **1988**, *21*, 175.

⁴⁸ (a) Schoevaars, A. M.; Kruizinga, W.; Zijlstra, R. W. J.; Veldman, N.; Spek, A. L.; Feringa, B. L. *J. Org. Chem.* **1997**, *62*, 4943. (b) Dominguez, Z.; Dang, H.; Strouse, M. J.; Garcia-Garibay, M. A. *J. Am. Chem. Soc.* **2002**, *124*, 2398. (c) Godlinez, C. E.; Zepeda, G.; Garcia-Garibay, M. A. *J. Am. Chem. Soc.* **2002**, *124*, 4701. (d) Dominguez, Z.; Dang, H.; Strouse, M. J.; Garcia-Garibay, M. A. *J. Am. Chem. Soc.* **2002**, *124*, 7719. (e) Dominguez, Z.; Khuong, T.-A. V.; Dang, H.; Sanrame, C. N.; Nuñez, J. E.; Garcia-Garibay, M. A. *J. Am. Chem. Soc.* **2003**, *125*, 8827. (f) Kuwatani, Y.; Yamamoto, G.; Iyoda, M. *Org. Lett.* **2003**, *5*, 3371. (g) Carella, A.; Rapenne, G.; Launey, J.-P. *New J. Chem.* **2005**, *29*, 288. (h) Hawthorne, M. F.; Zink, J. I.; Skelton, J. M.; Bayer, M. J.; Liu, C.; Livshits, E.; Baer, R.; Neuhauser, D. *Science* **2004**, *303*, 1848.

⁴⁹ See ref. 21(a).

⁵⁰ Kelly, T. R.; Bowyer, M. C.; Bhaskar, K. V.; Bebbington, D.; Garcia, A.; Lang, F.; Kim, M. H.; Jette, M. P. *J. Am. Chem. Soc.* **1994**, *116*, 3657.

⁵¹ (a) *Molecular Switches*. Feringa, B. L.; Browne, W.R. (Eds.) Wiley-VCH: Weinheim, **2011**. (b) "Photochromism: Memories and Switches." Irie, M. (Ed.) Special Issue. *Chem. Rev.* **2000**, *100*, 1683. (c) See ref. 18 (c).

⁵² Bedard, T. C.; Moore, J. S. *J. Am. Chem. Soc.* **1995**, *117*, 10662.

⁵³ (a) Kelly, T. R.; Sestelo, J. P.; Tellitu, I. *J. Org. Chem.* **1998**, *63*, 3655. (b) Harrington, L. E.; Cahill, L. S.; McGlinchey, M. J. *Organometallics* **2004**, *23*, 2884.

⁵⁴ (a) Huang, T. J.; Tseng, H.-R.; Sha, L.; Lu, W.; Brough, B.; Flood, A. H.; Yu, B.-D.; Celestre, P. C.; Chang, J. P.; Stoddart, J. F.; Ho, C.-M. *Nano Lett.* **2004**, *4*, 2065. (b) Ashton, P. R.; Baldoni, V.; Balzani, V.; Credi, A.; Hoffmann, H. D. A.; Martínez-Díaz, M.-V.; Raymo, F. M.; Stoddart, J. F.; Venturi, M. *Chem.-Eur. J.* **2001**, *7*, 3482.

⁵⁵ Badjić, J. D.; Balzani, V.; Credi, A.; Silvi, S.; Stoddart, J. F. *Science* **2004**, *303*, 1845.

⁵⁶ Jiménez, M. C.; Dietrich-Buchecker, C.; Sauvage, J.-P. *Angew. Chem., Int. Ed.* **2000**, *39*, 3284.

⁵⁷ Muraoka, T.; Kinbara, K.; Kobayashi, Y.; Aida, T. *J. Am. Chem. Soc.* **2003**, *125*, 5612.

⁵⁸ Thordarson, P.; Bijsterveld, E. J. A.; Rowan, A. E.; Nolte, R. J. M. *Nature* **2003**, *424*, 915.

⁵⁹ (a) Ismagilov, R. F.; Schwartz, A.; Bowden, N.; Whitesides, G. M. *Angew. Chem., Int. Ed.* **2002**, *41*, 652. (b) Paxton, W. F.; Kistler, K. C.; Olmeda, C. C.; Sen, A.; St. Angelo, S. K.; Coa, Y.; Mallouk, T. E.; Lammert, P. E.; Crespi, V. H. *J. Am. Chem. Soc.* **2004**, *126*, 13424. (c) Kline, T. R.;

One of the ultimate goals of the bottom-up fabrication of molecular machines is the design of nanometer-sized transporters.⁶⁰ These molecular vehicles are analogous to those in the macroscopic world, and are known to perform a wheel-like rolling motion, not stick-slip or sliding translation, due to evidence including directional preference in both direct and indirect manipulation and studies of related molecular structures. Thus, different examples of the so called nanocars (molecular devices on wheels that perform translational motion, Figure 2.15) and nanotrucks (molecular devices on wheels that have a platform that might accommodate a load, Figure 2.16) have been already described.

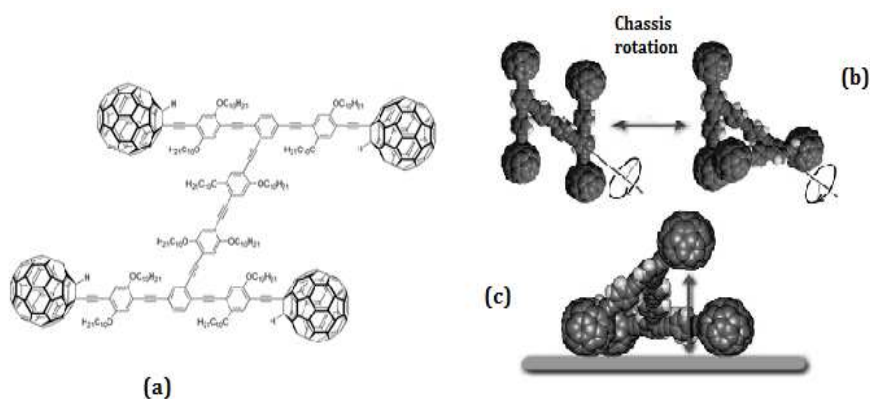


Figure 2.15. (a) Structure of a fullerene-C₆₀ wheeled nanocar (b) The triple bonds in the OPE structure are able to rotate until the fullerene wheels touch one another, which gives the nanocar flexibility orthogonal to the surface plane. (c) One fullerene wheel is lifted while the other wheels remain on the surface.

Paxton, W. F.; Mallouk, T. E.; Sen, A. *Angew. Chem., Int. Ed.* **2005**, *44*, 744. (d) Catchmark, J. M.; Subramanian, S.; Sen, A. *Small* **2005**, *1*, 202. (e) Fournier-Bidoz, S.; Arsenault, A. C.; Manners, I.; Ozin, G. A. *Chem. Commun.* **2005**, 441.

⁶⁰ (a) Shirai, Y.; Osgood, A. J.; Zhao, Y.; Kelly, K. F.; Tour, J. M. *Nano Lett.* **2005**, *5*, 2330. (b) Shirai, Y.; Osgood, A. J.; Zhao, Y.; Yao, Y.; Saudan, L.; Yang, H.; Yu-Hung, C.; Alemany, L. B.; Sasaki, T.; Morin, J. F.; Guerrero, J. M.; Kelly, K. F.; Tour, J. M. *J. Am. Chem. Soc.* **2006**, *128*, 4854. (c) Shirai, Y.; Morin, J. F.; Sasaki, T.; Guerrero, J. M.; Tour, J. M. *Chem. Soc. Rev.* **2006**, *35*, 1043.

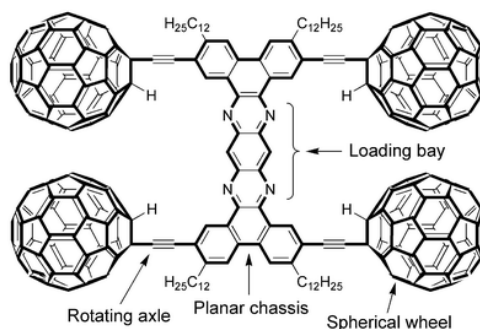


Figure 2.16. Structure of a nanotruck.

As it is shown in Figures 2.15(a) and 2.16, the basic structure of nanocars and nanotrucks is composed of:

- Fullerene- C_{60} (or *p*-carborane) wheels;
- a flexible chassis made of fused aromatic rings or oligo(phenylene ethynylene) (OPE); and
- alkyne linkers.

Although an optimal molecular structure for the movement of nanotrucks has not been synthesized yet, there have been reported different examples of nanocars capable of performing a translational and rotational movement along gold surfaces thanks to the fullerene wheels attached to the chassis and the free rotation of the axles (Figure 2.15(b)).⁶¹ The motion can be thermally (heated substrate surface) or electrically (scanning tunneling Microscopy (STM) -tip field) induced. While latent thermal energy only leads to two-dimensional Brownian motion, unidirectional motion can be achieved by consuming energy from an external source, such as electric impulses.

Using *p*-carborane wheels, and having a chassis that bears a light-powered molecular motor (which will be better described later in section 2.5.) in its central

⁶¹ Morin, J. F.; Shirai, Y.; Tour, J. M. *Org. Lett.* **2006**, *8*, 1713.

portion, a paddlewheel-like propulsion action along a substrate surface takes place resulting in motion of the vehicle (Figure 2.17).

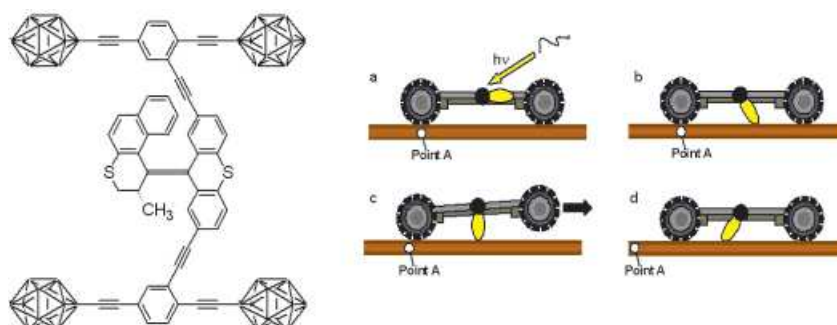


Figure 2.17. Example of a *p*-carborane nanocar.

Later on, Tour *et al.* took advantage of the energy released during a chemical reaction (specifically, a ring-opening metathesis polymerization (ROMP) reaction with Ru-based metathesis catalysts) to propel *p*-carborane-wheeled nanocars across a surface by providing the translational force required.⁶² On the other hand, synthesis of inherently highly fluorescent nanocars incorporating 4,4-difluoro-4-bora-3a,4a-diaza-s-indacene (BODIPY)-containing axles and *p*-carborane wheels has been also reported. Their quantum yields of fluorescence ($\Phi_F > 0.7$) make them excellent candidates for imaging and tracking by single-molecule fluorescence microscopy (Figure 2.18).⁶³

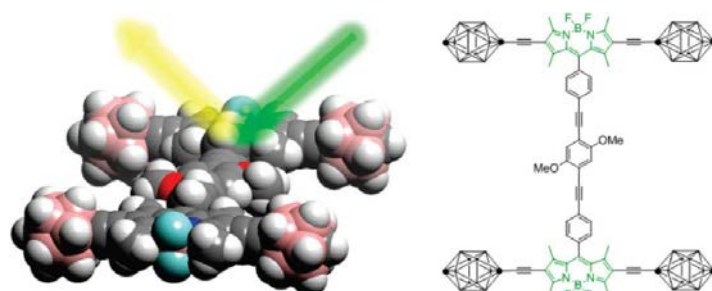


Figure 2.18. Nanocar with BODIPY axles

⁶² Godoy, J.; Vives, G.; Tour, J. M. *Nano* **2011**, 5, 85.

⁶³ Godoy, J.; Vives, G.; Tour, J. M. *Org. Lett.* **2010**, 12, 1464.

These systems are only a few examples of the molecular structures that have been obtained by bottom-up construction; however, more synthetic effort has to be done to control dynamics (*i.e.* translational and rotational motion) toward future nanoscale machines and molecular electronics.

2.5. MOLECULAR MOTORS BASED ON OVERCROWDED ALKENES.

One of the most relevant parts of a macroscopic or nano-machine is its motor, because it is the responsible of the force that drives the movement induced by the energy input.

As it has been described in section 2.3., the fascinating molecular motors present in biological systems, such as the ATP-synthase rotary motor and the kinase linear motor, are regarded as a great source of inspiration for the design of synthetic motors. Within this context, the group of prof. Ben L. Feringa at the University of Groningen, The Netherlands,⁶⁴ has strongly contributed in the design, synthesis and study of molecular devices capable of performing rotary motion by using light and heat as energy sources.

In 1991, Feringa reported the first optical molecular switches in which chirality is controlled by light.⁶⁵ This system also allowed for the first time unidirectional control of rotary motion in a molecule. These and related molecular switches were used by the Feringa group for data storage at the molecular level, control of organization in supramolecular materials and in cooperation with scientist from Applied Physics explored in a program on molecular electronics. In this way, they were able to demonstrate the modulation of electronic conductance (opto-electronic switching) at the single molecular level and in large array devices.⁶⁶

⁶⁴ The Feringa Group, www.feringa.fmns.rug.nl/ (web page visited on March 3rd, 2012).

⁶⁵ Feringa, B. L.; Jager, W. F.; De Lange, B.; Meijer, E. W. *J. Am. Chem. Soc.* **1991**, *113*, 5468.

⁶⁶ (a) Jager, W. F.; De Jong, J. C.; De Lange, B.; Huck, N. P. M.; Meetsma, A.; Feringa, B. L. *Angew. Chem., Int. Ed. Engl.* **1995**, *34*, 348. (b) Feringa, B. L.; Huck, N. P. M.; Van Doren, H. A. *J. Am. Chem. Soc.* **1995**, *117*, 9929. (c) Feringa, B. L.; Jager, W. F.; De Lange, B. *Tetrahedron* **1993**, *49*, 8267. (d) Feringa, B. L.; Huck, N. P. M.; Schoevaars, A. M. *Adv. Mater.* **1996**, *8*, 681. (e) Kudernac, T.; Katsonis, N.; Browne, W. R.; Feringa, B. L. *J. Mater. Chem.* **2009**, *19*, 7168.

2. Background

One of the first examples of a synthetic molecular motor was reported by Kelly in 1999, which comprised a helicene connected to a triptycene unit, which was able to undergo a 120° rotation with respect to each other exclusively in one direction induced by a number of chemical steps.⁶⁷ In this particular case, the source of energy consists of the formation and cleavage of urethane (Figure 2.19).

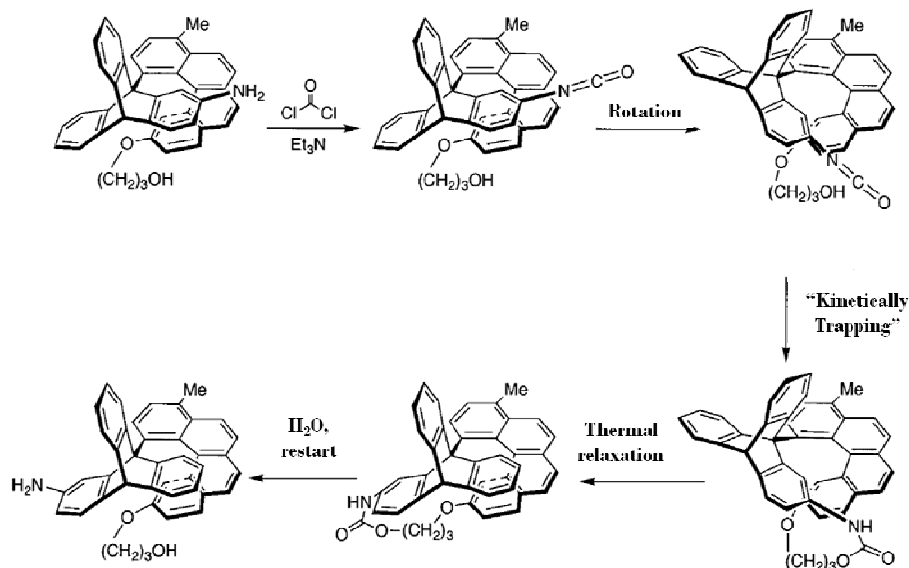


Figure 2.19. Sequence of events for the rotation of Kelly's rotor.

Later in 1999, simultaneously to Kelly's rotor,⁶⁸ Feringa and *col.* achieved the first example of a molecular motor capable of carrying out repetitive unidirectional rotary motion (360°).⁶⁹ Since then, synthetic effort has been made in order to improve this kind of system, and technological applications have been searched.

The first generation of light-driven unidirectional rotary motors is based on a chiral overcrowded alkene in which substituents R_1 and R_2 can be modified (Figure

⁶⁷ (a) Kelly, T. R.; De Silva, H.; Silva, R. A. *Nature*, **1999**, *401*, 150. (b) Kelly, T. R.; Silva, R. A.; De Silva, H.; Jasmin, S.; Zhao, Y. *J. Am. Chem. Soc.* **2000**, *122*, 6935.

⁶⁸ Kelly, T. R.; De Silva, H.; Silva, R. A. *Nature* **1999**, *401*, 150.

⁶⁹ Koumura, N.; Zijlstra, R. W. J.; Van Delden, R. A.; Harada, N.; Feringa, B. L. *Nature* **1999**, *401*, 152.

2.20).⁷⁰ They consist of two halves, one of which can be considered the stator part, and the other, the rotor part connected by a central olefinic moiety that functions as the axis of rotation.

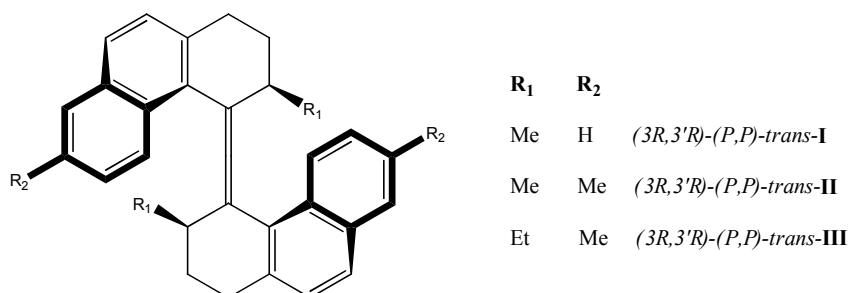


Figure 2.20. First generation of light-driven molecular motors

If the substituents R₁ are taken into account, it can be noticed that they are able to adopt two distinct orientations in the molecule: (pseudo-) axial and (pseudo-) equatorial, which results in two different *trans* conformations. The more stable form is the one in which the substituents R₁ adopt (pseudo-) axial orientations, whereas in the less stable *trans* conformation the substituents R₁ adopt (pseudo-) equatorial orientations. Therefore, the presence of the substituents R₁ in the structure forces a unidirectional rotation around the alkene axis. The clockwise or counterclockwise direction of the movement is determined by the different conformations adopted by the structure due to the chiral elements in the molecule.

The full 360° cycle of the rotor with respect to the stator part is a four-stage process involving two photochemical and two thermal isomerization steps (Figure 2.21):

⁷⁰ See ref. 21(a).

2. Background

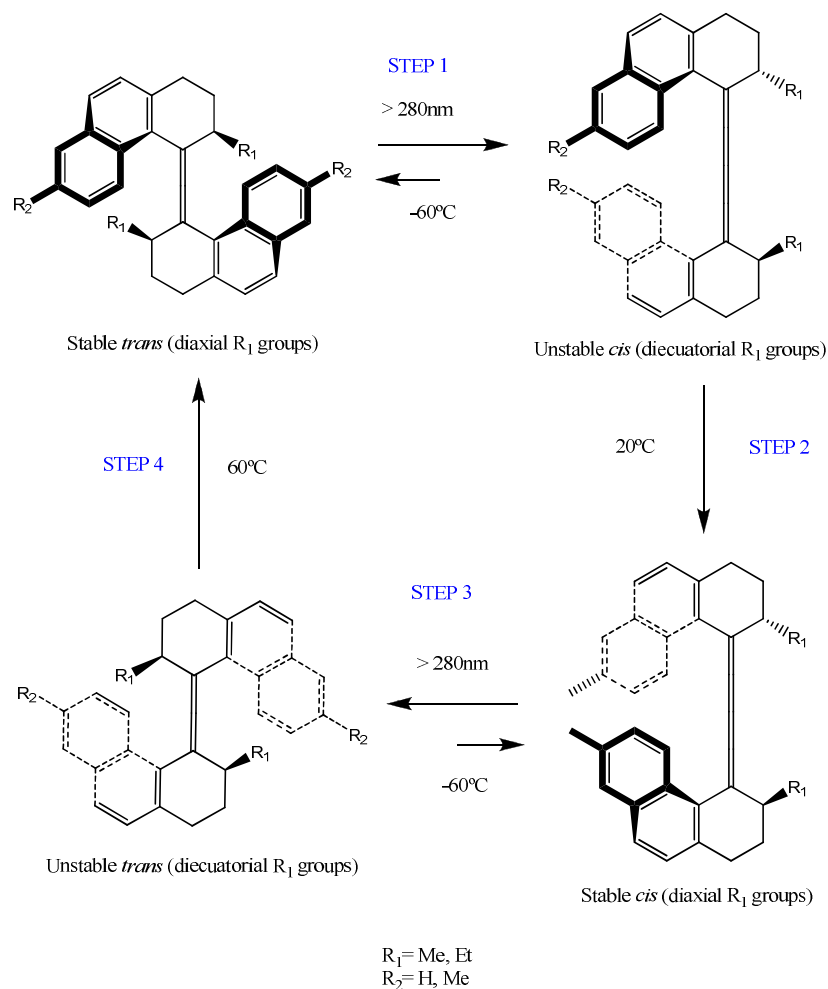


Figure 2.21. Photochemical and thermal isomerization processes during the 360° unidirectional rotary cycle of the first generation of motors.

In the first step, the stable *trans* isomer of the molecular motors, with both substituents R₁ in (pseudo-)axial orientation, is irradiated at low temperature generating the unstable *cis* isomer through a *trans/cis* photoisomerization. This is an energetically uphill process because of the higher energy of the unstable *cis* isomer that presents the substituents R₁ in (pseudo-)equatorial orientation, which produce steric constraints in the molecule. During the second step, however, a

favorable energy decrease takes place through a thermally induced helix inversion that leads to the stable *cis* isomer with both substituents R_1 in (pseudo-)axial orientation. Afterwards, in the third step, a second energetically uphill *cis-trans* isomerization induced by light occurs to yield the unstable *trans* isomer with the substituents R_1 in (pseudo-)axial orientation. Finally, the fourth step completes the cycle through a second thermal step that regenerates the initial stable *trans* isomer. Therefore, in a four-step process unidirectional rotation around a central double bond is accomplished.⁷¹ As a change in helicity takes place in each step, the directionality of the rotary motion can be readily monitored by CD spectroscopy.

The free energy for each step of the rotational cycle of the first generation of molecular motors is represented in the following diagram (Figure 2.22):

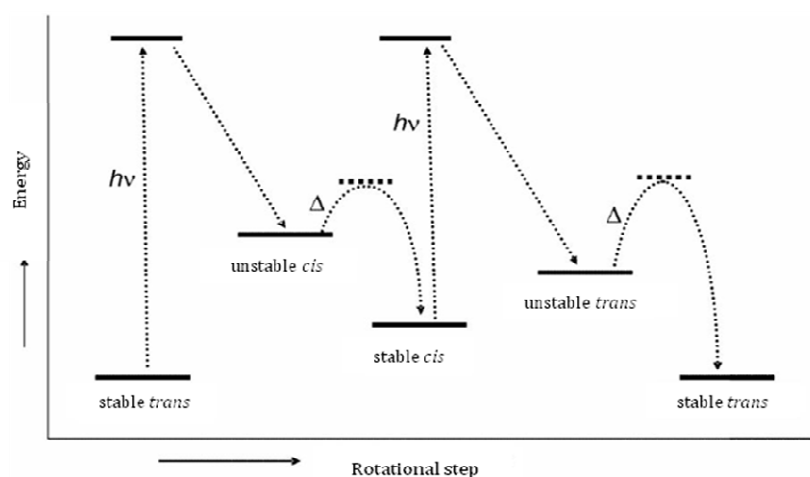


Figure 2.22. Free-energy profile of the rotary cycle of the first generation of molecular motors.

As mentioned, the thermal steps are bounded to the differences in stability between the two *cis* and *trans* isomers. For the first motor designed by Feringa in 1999 ($R_1 = \text{Me}$, $R_2 = \text{H}$), the second step has a half life of 32 minutes at 20°C in hexane and a Gibbs activation energy of 91 kJ mol⁻¹. However, the fourth step presents a half life of 439 hours at 20°C in hexane and a Gibbs activation energy of 107 kJ mol⁻¹, which requires the increase of the temperature to 60°C in order to

⁷¹ Pollard, M. M.; Klok, M.; Pijper, D.; Feringa, B. L. *Adv. Funct. Mater.* **2007**, *17*, 718.

carry out the reaction. In the other hand, the photochemical steps are really fast (<300 ps), which drives to the need of decreasing the thermal steps to improve the performance of these molecular motors. When taking a look at Nature's prototypical rotary motor, ATP-synthase (which has been described in section 2.3.2.), it is observed its capability of transforming the energy of the hydrolysis of approximately 390 molecules of ATP per second into rotational motion at a rate of 130 revolutions per second.⁷² However, as it has been mentioned above, the first light-driven motor reported by Feringa had a thermal step that took an average of 400 hours to complete it at room temperature. Therefore, modifications in the structure were required in order to mimic the natural molecular systems.

The aim of changing and increasing the speed velocity headed to the design of the second generation of light-driven molecular motors (Figure 2.23).⁷³

The main differences between the first and the second generation of molecular motors are:

- the upper and lower halves of the motor are different;
- only a single stereogenic center is sufficient to control unidirectional rotary motion; and
- the introduction of heteroatoms in the structure.

⁷² Kinoshita Jr, K.; Adachi, K.; Itoh, H. *Ann. Rev. Bioph. Biom.* **2004**, *33*, 245.

⁷³ (a) Koumura, N.; Geertsema, E. M.; Meetsma, A.; Feringa, B. L. *J. Am. Chem. Soc.* **2000**, *122*, 12005. (b) Koumura, N.; Geertsema, E. M.; Van Gelder, M. B.; Meetsma, A.; Feringa, B. L. *J. Am. Chem. Soc.* **2002**, *124*, 5037.

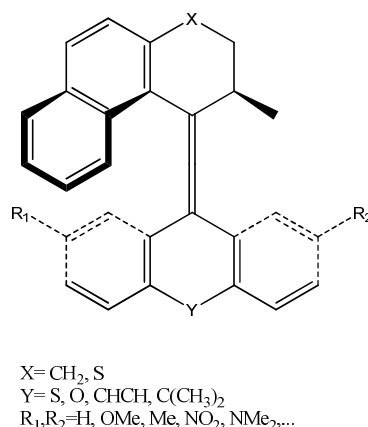


Figure 2.23. Second generation of light driven molecular motors.

This new kind of molecular motors also experience a four-step process in order to achieve a full 360° rotation around the central double bond analogous to the one showed by the first generation of molecular motors.

In these structures, the lower part is a tricyclic molecule, which makes the barriers to helix inversion for the two thermal steps in the cycle to be nearly the same. Moreover, the symmetric lower half of the second generation of molecular motors can be used for further functionalization, for instance, for the linkage of the motor to a surface where the upper half can act as a propeller.⁷⁴ In addition to this, the change in the bridging (hetero)atoms X and Y is envisaged for the lowering of the thermal isomerization barriers for helix inversion, which leads to accelerating the rotary motion without compromising unidirectionality.

For instance, a change in the structure that they performed was the contraction of the six-membered rings fused to the overcrowded central double bond (the axis of rotation) (**A**) to five-membered rings (**B**) (Figure 2.24).⁷⁵ This modification further stabilizes the stable isomers in relation to the unstable isomers, which leads to a 10⁹ fold acceleration of the process.

⁷⁴ van Delden, R. A.; ter Wiel, M. K. J.; Pollard, M. M.; Vicario, J.; Koumura, N.; Feringa, B. L. *Nature* **2005**, *437*, 1337.

⁷⁵ ter Wiel, M. K. J.; Van Delden, R. A.; Meetsma, A.; Feringa, B. L. *J. Am. Chem. Soc.* **2003**, *125*, 15076.

2. Background

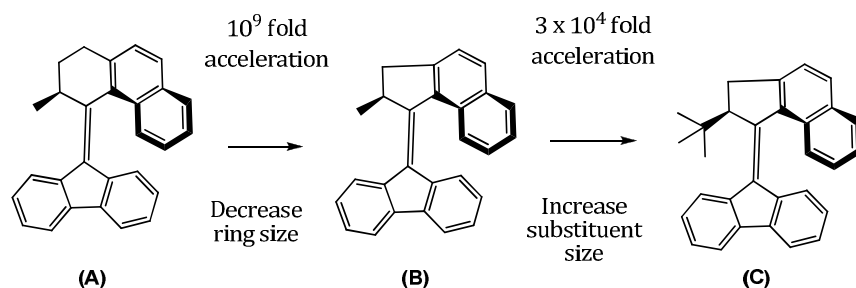


Figure 2.24. Modification of the motor structure to increase the rotational speed.

Further improvements were made by fine-tuning the size of the substituent at the stereogenic center.⁷⁶ In this way, they were able to achieve a 1.2-million fold increase in the rotation speed when having a *t*-butyl group in that position (Figure 2.24, compound (C)). This allows the propeller to rotate unidirectionally on irradiation at up to 40 revolutions per second at 20⁰C, which approaches the rotary speed of ATP-synthase (130 rotation s⁻¹). The reason for this acceleration of the thermal isomerization rate is the increased strain in the molecule due to the additional steric demand across the central overcrowded alkene.

Later on, taking advantage of changes in electronic effects, they designed a new second-generation motor (Figure 2.25) with an amine moiety in the upper half, which has a lone pair of electrons that can be delocalized by direct conjugation with a ketone functionality in the lower half of the molecule. This electronic push-pull system was anticipated to generate a large polarizing effect on the central olefinic bond evident from a resonance structure with a single bond as the central axis of the rotor. This led to an acceleration of the thermal helix inversion by elongation of the central double bond by resonance stabilization.

⁷⁶ (a) Vicario, J.; Meetsma, A.; Feringa, B. L. *Chem. Commun.* **2005**, 5910. (b) Vicario, J.; Walko, M.; Meetsma, A.; Feringa, B. L. *J. Am. Chem. Soc.* **2006**, *128*, 5127.

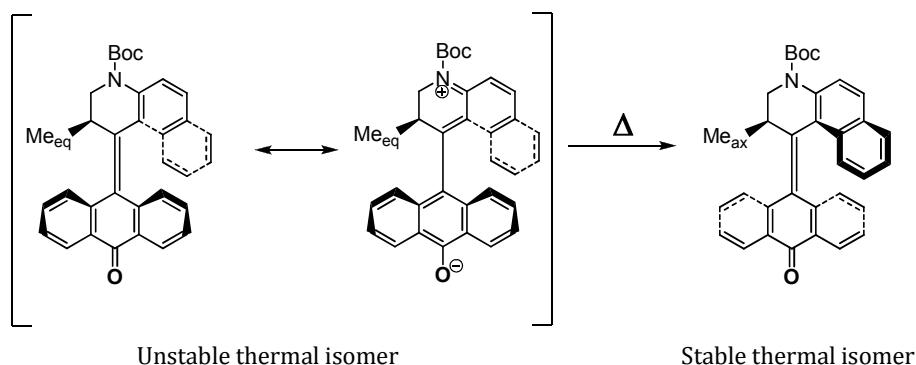


Figure 2.25. Proposed resonance contribution of the zwitterionic form, which led to partial single bond character in the central alkene facilitating thermal helix inversion.

To sum up, it should be noted that changes in the structure, nature, and position of substituents in these motor molecules can affect all of the isomerization processes; therefore, the search for synthetic molecular motors that are able of rotating at speeds similar to Nature's ATP-synthase is still required. In addition to this, anchoring molecular machines without compromising their mechanical function is critical to be able to interface them with the macroscopic world. The aforementioned motors operate in solution, but in order to overcome Brownian motion and build nanodevices, immobilization of these light-driven motors in surfaces is a crucial step. Some examples of second generation motors have been already linked to gold nanoparticles,⁷⁷ or silicon and quartz surfaces.⁷⁸ However, more work has to be done in order to improve these systems.

Moreover, recent experiments are directed towards the ability of these molecular motors to induce changes in other systems in coordination with the motor's movements, in order to find a practical application. For example, doping (1 wt.%) of motor (D) containing a phenyl group at the stereogenic center into a liquid crystal (LC) film⁷⁹ renders the film a polygonal texture, which is a

⁷⁷ See ref. 74.

⁷⁸ (a) Pollard, M. M.; Lubomska, M.; Rudolf, P.; Feringa, B. L. *Angew. Chem. Int. Ed.* **2007**, *46*, 1278. (b) London, G.; Carroll, G. T.; Fernández Landaluze, T.; Pollard, M. M.; Rudolf, P.; Feringa, B. L. *Chem. Commun.* **2009**, 1712.

⁷⁹ Eelkema, R.; Pollard, M. M.; Vicario, J.; Katsonis, N.; Ramon, B. S.; Bastiaansen, C. W. M.; Broer, D. J.; Feringa, B. L. *Nature* **2006**, *440*, 163.

2. Background

characteristic of a cholesteric LC having a helix axis parallel to the surface (Figure 2.26). Irradiation of the doped LC film with 365 nm light causes a photochemical isomerization of the C=C double bond, resulting in an inversion of helicity from the initial right-handed to the subsequent left-handed. A second inversion activated by a thermal process, followed by a second photochemical-thermal cycle, completes the full 360° rotation. This means that in the presence of light, the LC texture rotates clockwise, whereas in the dark, it moves in a counterclockwise fashion. The controlled texture reorganization of a motor-doped LC film has been used to rotate a microscopic glass rod ($5 \times 28 \mu\text{m}$) placed on the surface at an average speed of 0.67 r.p.m. clockwise photochemically and 0.22 r.p.m. counterclockwise thermally.

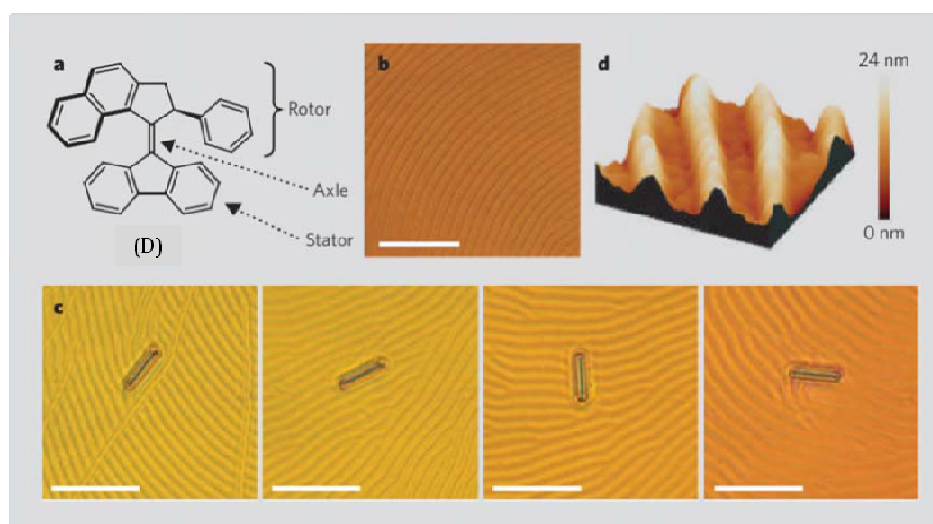


Figure 2.26. (a) Structural formula of the molecular motor (D). (b) Polygonal texture of the liquid crystal (LC) doped with 1% of compound (D). (c) Clockwise rotation (28° , 141° , 226°) of the glass rod ($5 \times 28 \mu\text{m}$) placed on the (D)-doped LC film. (d) Atomic force microscopy image ($15 \mu\text{m}^2$) of the LC film.

In conclusion, the collective unidirectional rotary motion of an ensemble of molecular motors can be harnessed to produce mechanical movement of microscopic objects.

2.6. BIOMIMETIC MOLECULAR SWITCHES BASED ON PSB RETINAL

As it has been stated before in section 2.3.4., the high efficiency shown by PSB retinal *in vivo* makes it an attractive target when designing new prototypes of switches and motors that undergo *E/Z* photoisomerization processes. In the following paragraphs, the progress that has been made up to date in this field is described.

2.6.1. Theoretical and experimental study of a PSB retinal-based biomimetic molecular switch.

One of the pathways that lead to the design of new prototypes of molecular devices, which exhibit light-induced movement, combines the use of *ab initio* quantum methods. Within this context, one of the studies carried out results really appealing due to the similarities between the compounds present in that work and the molecular switches that will be later described in this thesis. Collaboration between the group of professor Olivucci in Siena, Italy, and the photochemistry group of the University of La Rioja, Spain, headed to the fruitful design, synthesis and characterization of a new prototype of molecular switch based on the PSB retinal chromophore.⁸⁰

First of all, the design of a prototype of molecular switch took place, resulting in the structure shown in Figure 2.27(a) Furthermore, the introduction of chirality in the previous compound led to a new prototype of molecular motor (Figure 2.27(b)). Both compounds contained the penta-2,4-dieniminium unit. As preceding works⁸¹ showed that PSBs feature nearly competitive photochemical *Z/E* isomerization paths corresponding to rotary motion about the adjacent double bonds of the chromophore, which might lead to a reduction of the efficiency of the switch, the presence of penta-2,4-dieniminium unit is advantageous due to the following facts:

⁸⁰ Sampedro, D.; Migani, A.; Pepi, A.; Busi, E.; Basosi, R.; Latterini, L.; Elisei, F.; Fusi, S.; Ponticelli, F.; Zanirato, V.; Olivucci, M. *J. Am. Chem. Soc.*, **2004**, 126, 9349.

⁸¹ (a) Ben-Num, M.; Molnar, F.; Schulten, K.; Martinez, T. J. *Proc. Natl. Acad. Sci. U.S.A.* **2002**, 99, 1769. (b) Nonella, M. *J. Phys. Chem. B* **2000**, 104, 11379. (c) De Vico, L.; Page, C. S.; Garavelli, M.; Bernardi, F.; Basosi, R.; Olivucci, M. *J. Am. Chem. Soc.* **2002**, 124, 4124.

2. Background

- five member rings restrain isomerization about the $-\text{CH}=\text{NH}-$ and terminal $-\text{CH}=\text{CH}-$ double bonds of the structure;
- the possible existence of different conformers of the molecule is avoided as five member rings are conformationally rigid; and
- the two $-(\text{CH}_2)_2$ -groups present in the molecule could be functionalized, allowing to obtain a family of compounds with a common backbone .

Notice that the first property mentioned was also satisfied by the diarylene light-driven molecular motors described in section 2.5.

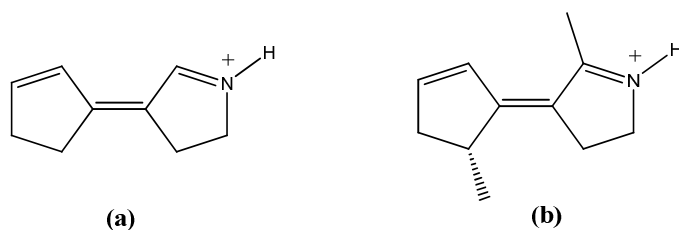
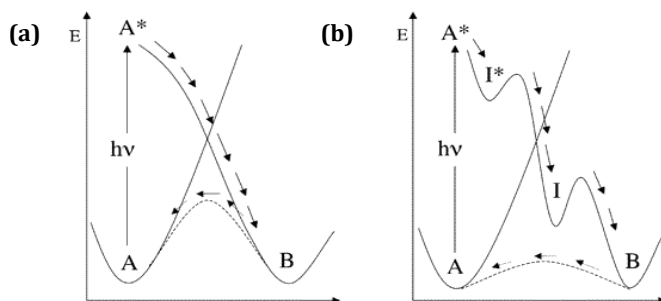


Figure 2.27. Prototypes of a molecular switch (a) and motor (b).

Thus, the pair of molecular devices shown in Figure 2.27 were studied with theoretical tools such as CASPT2//CASSCF computational calculations, being simulated the photochemical and thermal isomerization pathways for both systems. These results obtained for these calculations led to conclude that the designed prototypes satisfied the criteria for being considered an efficient switch and motor (Figure 2.28).



**Figure 2.28. (a) Reaction coordinate for an efficient molecular switch/motor.
(b) Reaction coordinate for an inefficient molecular switch/motor.**

As it is shown in Figure 2.28(a), an efficient photoisomerization takes place when the photoexcited reactant A^* , which comes from the excitation of reactant A, evolves along a barrierless excited-state path, decays to a conical intersection (CI), and finally relaxes also through a barrierless path to the energy minimum of photoproduct B. On the other hand, the diagram presented in Figure 2.28(b) corresponds to an inefficient device, which finds different excited state (I^*) and/or ground state (I) intermediates along its relaxation to photoproduct B, producing a redistribution of the photon energy. Moreover, it is also required the stability of isomers A and B with respect to thermal isomerization. Therefore, the barrier for thermal isomerization must be high enough to restrain the return of B to A by means of heat. This is relevant for efficient devices, and it is represented in Figure 2.28(a) with a dotted line.

Unfortunately, the synthesis of compounds containing the penta-2,4-dieniminium backbone (Figure 2.27) has not been reported yet.

So that the aforementioned compounds could be experimentally studied to support the theoretical predictions, it was proposed the synthesis of an analogous system shown in Figure 2.29. It corresponds to the synthetically accessible structure 4-benzylidene-3,4-dihydro-2*H*-pyrrolium where the terminal C=C double bond of the penta-2,4-dieniminium unit (Figure 2.27(a)) is replaced with a phenyl group.⁸²

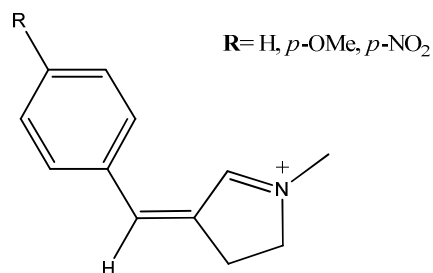


Figure 2.29. N-alkylated benzylidene-pyrroline Schiff bases (NABPs)

These new prototypes of compounds were easily achieved through the following synthetic scheme: (Figure 2.30)

⁸² See ref. 80.

2. Background

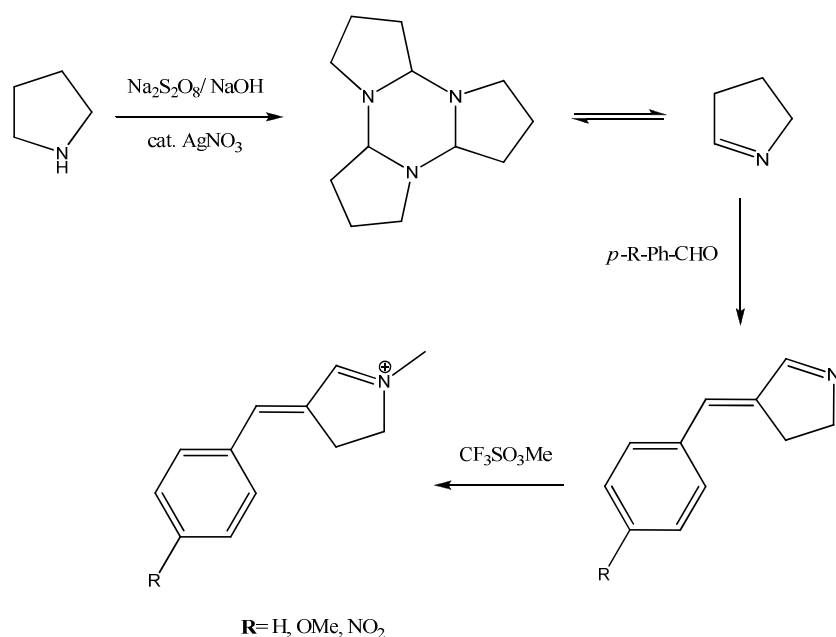


Figure 2.30. Synthetic route to yield NABPs (See ref 80.)

First of all, silver (I) catalyzed oxidation of pyrrolidine with peroxodisulfate was carried out to obtain the so called 1-pyrroline trimer.⁸³ This trimer was in equilibrium with 3,4-dihydro-2-*H*-pyrrole, which was able to react with differently substituted benzaldehydes to yield mainly the *E* isomer of the neutral compounds.⁸⁴ Methylation of these compounds with methyl triflate was enough to reach the different positively charged compounds. However, the main drawback of this synthetic path was that it was limited to the synthesis of only the three compounds represented in Figure 2.29, not allowing performing major changes in the molecule structure.

After the study of these new prototypes of molecular switches with theoretical calculations and experimentally, it was determined that although they presented some features that were desirable for having an ideal molecular switch (such as the absence of intermediates or energy barrier along the

⁸³ Ogawa, K.; Nomura, Y.; Takeuchi, Y.; Tomoda, S. *J. Chem. Soc., Perkin Trans. 1* **1982**, 3031.

⁸⁴ Nomura, Y.; Bando, T.; Takeuchi, Y.; Tomoda, S. *Bull. Chem. Soc. Jpn.* **1983**, 56, 3199.

photoisomerization pathway, the presence of a simple isomerization movement, and photostability), they couldn't be considered efficient. They showed a really low isomerization quantum yield (*ca.* 10^{-3}) due to the energy lost in the movement of other bonds capable of rotation present in the molecule. Therefore, the behavior of these molecular switches based on the PSB retinal chromophore required improvement.

2.6.2. NAIPs.

Soon after NABPs were synthesized and photochemically characterized, the synthesis of a new family of compounds based on the chromophore of the PSB retinal was accomplished (Figure 2.31).⁸⁵ These new prototypes of compounds are "chimerical" switches that incorporate into the Feringa's biarylidene skeleton a protonated or alkylated Schiff base function. This way, there is a decrease of the number of torsional degrees of freedom of the backbone of NABPs and, especially, the potential competitive rotation around the benzylic single bond that might be the responsible for the low isomerization quantum yields obtained. These kind of molecular switches are called *N*-alkylated indanylidene-pyrroline Schiff bases (NAIPs).

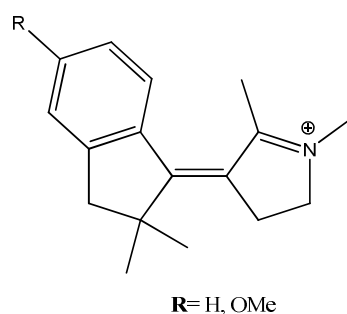


Figure 2.31. *N*-alkylated indanylidene-pyrroline Schiff bases (NAIPs)

It has been described that 4-indanylidene pyrroline derivatives (IPs) are the products of an intriguing multistep one-pot process, which has been named

⁸⁵ Lumento, F.; Zanirato, V.; Fusi, S.; Busi, E.; Latterini, L.; Elisei, F.; Sinicropi, A.; Andruniów, T.; Ferré, N.; Basosi, R.; Olivucci, M. *Angew. Chem. Int. Ed.* **2007**, *46*, 414.

“cyclopropyl ring-opening/nitrilium ion ring-closing tandem reaction”.⁸⁶ The synthetic route followed to obtain this kind of compounds is represented in Figure 2.32. The crucial step of this synthetic path takes place when the corresponding 1-cyclopropylideneols (**E**) are treated with Tf_2O in CH_3CN . Then, 1-cyclopropylidenium intermediates are formed (**F**), which react with acetonitrile to undergo homoallyl rearrangement yielding the corresponding nitrilium ions (**G**). Afterwards, the transient electrophilic species collapse onto the internal olefin generating the desired pyrroline derivatives (IPs, **H**). Methylation of these compounds with methyl triflate was again used to obtain the different positively charged compounds (NAIPs, **I**) in good yields (> 80%).

⁸⁶ Zanirato, V.; Pollini, G. P.; De Risi, C.; Valente, F.; Melloni, A.; Fusi, S.; Barbetti, J.; Olivucci, M. *Tetrahedron* **2007**, *63*, 4975.

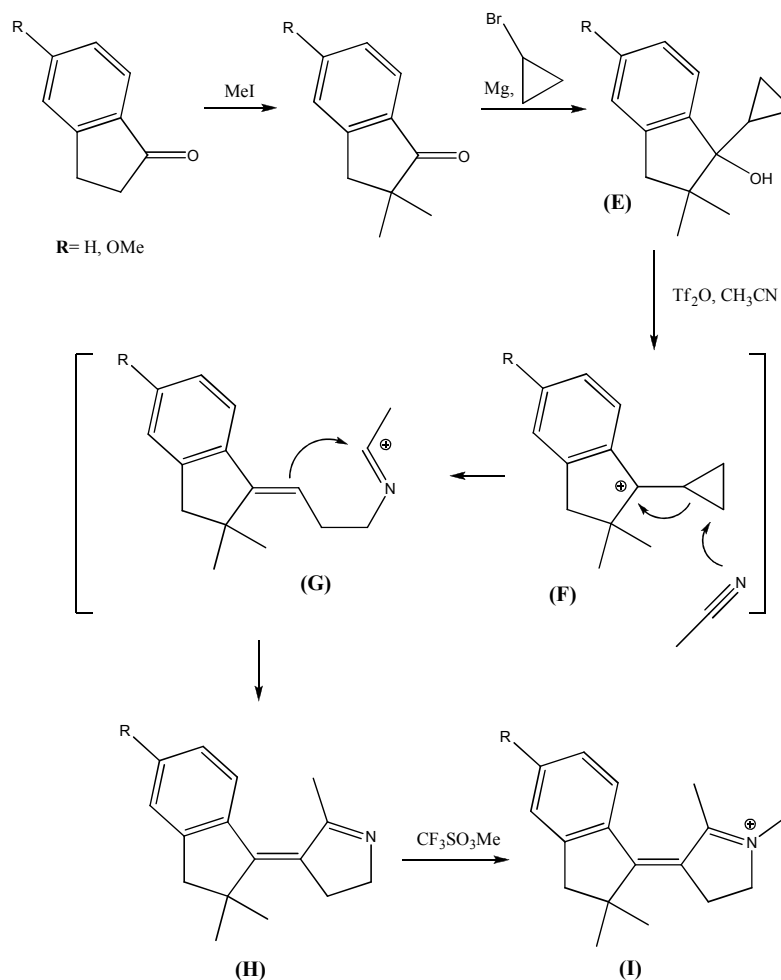


Figure 2.32. Synthetic route to obtain NAIPs (See ref 86.).

It was found that the photoinduced dynamics of these molecular switches could potentially replicate the dynamics of the PSB-retinal isomerization in rhodopsin.⁸⁷ This protein features a S_1 lifetime of ≈ 150 fs, a S_0 transient (photorhodopsin) appearance time of 180 fs, and a primary photoproduct

⁸⁷ Sinicropi, A.; Martin, E.; Ryazantsev, M.; Helbing, J.; Briand, J.; Sharma, D.; Léonard, J.; Haacke, S.; Cannizzo, A.; Chergui, M.; Zanirato, V.; Fusi, S.; Santoro, F.; Basosi, R.; Ferré, N.; Olivucci, M. *Proc. Natl. Ac. Sci. USA* **2008**, *105*, 17642.

(bathorhodopsin) appearance time of ≈ 6 ps. Moreover, the *p*-methoxy NAIP derivative is a photochromic compound completing its $Z \rightarrow E$ and $E \rightarrow Z$ photocycle in picoseconds. These time scales suggest that NAIP-based motors may complete a half-rotary cycle in less than 10 ps, which means a few orders of magnitude faster than the fastest (≈ 6 ms for half-cycle) known biarylidene.⁸⁸ In addition to this, these switches feature a higher isomerization quantum yield (*ca.* 0.3) compared to NABPs, and increased polarity with respect to azobenzene.

Despite that NAIPs show remarkable properties as molecular switches, some other features would be required to improve these systems. One of them is the possibility of presenting absorption in the visible region, so lower energies and even solar light can be used to induce the isomerization process. So far, when R= hydrogen atom, the corresponding NAIP presents an absorption maximum of 343 nm, but if R= *p*-methoxy, the band is red-shifted to 377 nm, allowing absorbance in the near-UV region. Therefore, a different change in the substitution of the molecule would be required in order to displace the band towards the visible region. Unfortunately, the other drawback presented by these systems is that the synthetic route followed was complex and hardly adaptable for switches with different substitution.

On the other hand, further modification of the substructure also allowed the preparation of a dipole moment switch (Figure 2.33).⁸⁹ It has been shown that, due to its large dipole moment, this switch may constitute the prototype of a generation of electrostatic switches achieving, at the single-molecule level, a light-induced dipole moment inversion of about 30 D. This *ca.* 30 D dipole moment change opens up a new perspective for the light-driven conformational control of macromolecular structures determined by polar interactions.

⁸⁸ See ref. 76(b).

⁸⁹ Melloni, A.; Paccani, R. R.; Donati, D.; Zanirato, V.; Sinicropi, A.; Parisi, M. L.; Martin, E.; Ryazantsev, M.; Ding, W. J.; Frutos, L. M.; Basosi, R.; Fusi, S.; Latterini, L.; Ferre, N.; Olivucci, M. *J. Am. Chem. Soc.* **2010**, *132*, 9310.

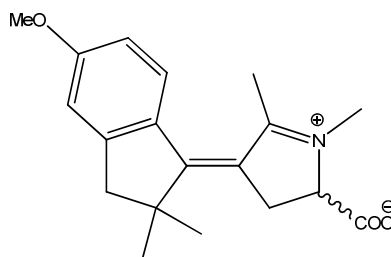


Figure 2.33. Structure of a NAIP switch featuring a stable zwitterionic head.

2.6.3. NAFPs.

Finally, a different family of molecular switches based on PSB-retinal was developed in our research group by replacing the indanylidene unit by a fluorenylidene unit.⁹⁰ The resulting compounds, named fluorenylidene-pyrrolines (FPs) and *N*-alkylated fluorenylidene-pyrrolines (NAFPs) (Figure 2.34).

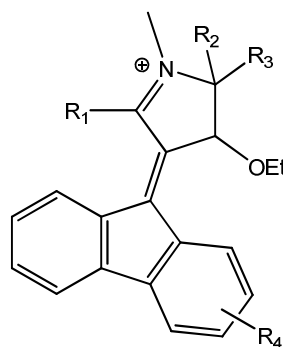


Figure 2.34. *N*-alkylated fluorenylidene-pyrrolines (NAFPs)

As shown in Figure 2.34, different substituents could be introduced with ease in almost every point of the molecule, which might allow tuning the properties of the system. The synthesis of these compounds can be carried out thanks to the

⁹⁰ (a) Rivado-Casas, L.; Sampedro, D.; Campos, P. J.; Fusi, S.; Zanirato, V.; Olivucci, M. *J. Org. Chem.* **2009**, *74*, 4666. (b) Rivado-Casas, L.; Campos, P. J.; Sampedro, D. *Organometallics* **2010**, *29*, 3117.

reaction between alkynyl Fischer carbene complexes with fluorenone imines to yield the corresponding fluorenylidene-pyrrolines (FPs) (Figure 2.35).⁹¹

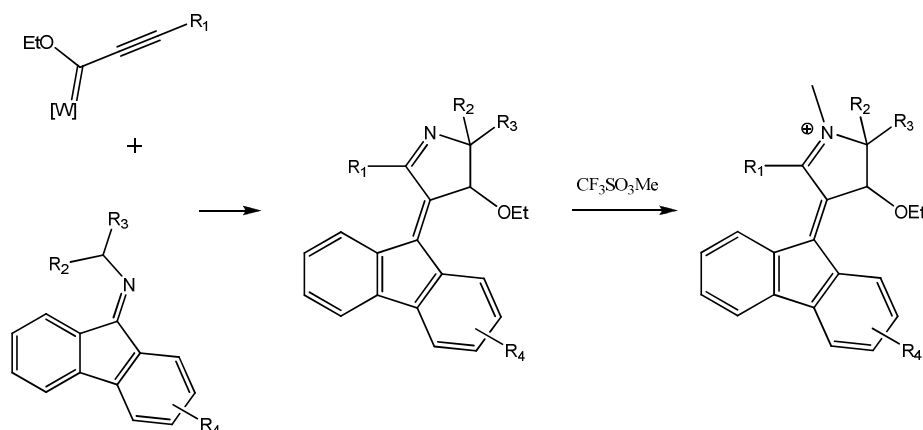


Figure 2.35. Synthesis of FPs and NAFPs.

The photochemical study and characterization of FPs and NAFPs deduce that they present really interesting features as molecular switches.⁹²

For instance, the methylated compounds suffer a bathochromic shift of the low energy band of approximately 50 nm in the UV spectra compared to the neutral compounds ($\lambda_{\text{max}} = 334$ nm), presenting absorption in the visible region ($\lambda_{\text{max}} = 401$ nm) (Figure 2.36). This allows carrying out the photoisomerization reaction with solar light, which is a clean and renewable kind of energy.

⁹¹ Aumann, R.; Yu, Z.; Fröhlich, R.; Zippel, F. *Eur. J. Inorg. Chem.* **1998**, 1623.

⁹² Rivado-Casas, L.; Blanco-Lomas, M.; Campos, P. J.; Sampedro, D. *Tetrahedron* **2011**, 67, 7570.

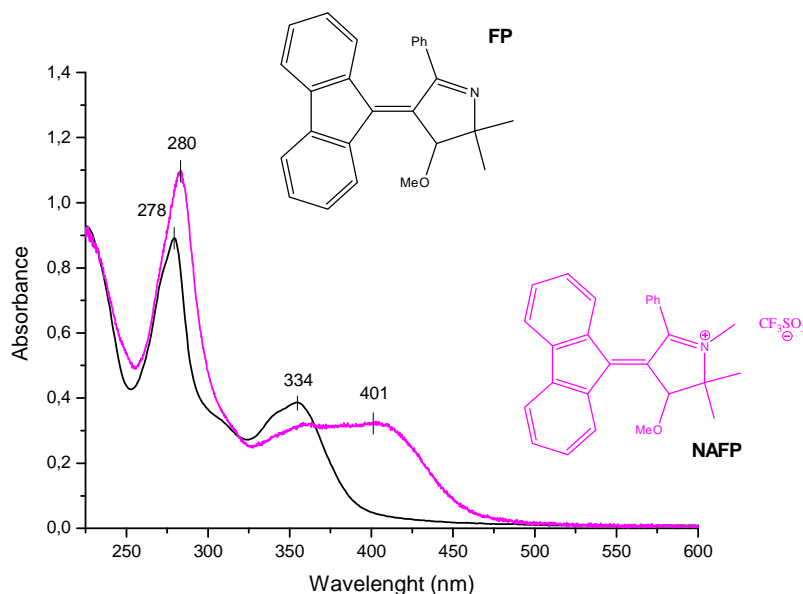


Figure 2.36. Comparison of the UV-Vis spectra of an example of a FP and a NAFP.

Furthermore, methylation also speeds up the photoisomerization process, so that the reaction is 4 times faster with NAFPs than with FPs.

In addition to this, the values of the photoisomerization quantum yields of FPs ($\Phi \approx 0.6$) and NAFPs ($\Phi \approx 0.5$) are very close to the value found for PSB-retinal *in vivo* (in rhodopsin, $\Phi \approx 0.67$), which makes these switches very efficient. Moreover, these compounds present very weak fluorescence, with a fluorescence quantum yield of 0.06. Therefore, they don't lose energy by deactivation pathways.

On the other hand, the stability of these compounds after several hours of irradiation with a 125W medium-pressure Hg lamp has been checked, realizing that these molecular switches are highly photostable, which is a good characteristic when used for technological applications.

However, these compounds present several drawbacks, such as the fact that the isomers ratio at the photostationary state is approximately 50% (*E* isomer) and 50% (*Z* isomer), due to the symmetry of the fluorenone ring. Consequently,

mixtures rich in one of the two isomers cannot be obtained by means of irradiation.

In addition to this, another great disadvantage that NAFPs share with NAIPs and previously reported NABPs is that the different ways of functionalizing the molecule haven't led to any potential application of these molecular switches, which would be useful in order to test their behaviour in other environments.

As not all of the requirements for being an efficient and ideal molecular switch have been fulfilled, the search of new prototypes of molecular switches based on PSB-retinal is still in progress. In the following chapters, the photochemical study of a new family of molecular switches based on the PSB-retinal is presented, which has been synthesized to improve some of the problems shown by the previous families of switches.

In addition to this, another type of molecular switches, whose structure is based on the green fluorescent protein chromophore, will be also described, including their synthesis, characterization and photochemical studies.

CHAPTER 3

Objectives

The objectives of this doctoral thesis are the following:

- In the first place, carrying out the synthesis of different prototypes of molecular switches with structures based on the structure of natural chromophores: the protonated Schiff base of the retinal chromophore (see section 2.3.4) and the green fluorescent protein chromophore (section 2.3.5).
- Then, tuning the photochemical and photophysical properties of the designed photoswitches by modifying the substituents present in their substructure.
- Afterwards, performing a photochemical study of the two types of prototypes of molecular switches obtained, so as to check their photochemical behavior. This study will include, among others:
 - the comparison of the photochemical properties of the less thermodynamically stable isomer with ones showed by the thermodynamically stable isomer;
 - the study of the influence of the irradiation wavelength on the photoisomerization reaction;
 - the analysis of the efficiency of the isomerization process for both kinds molecular switches; and
 - the testing of the photoisomerization reaction under sensitized conditions.
- Moreover, completing the experimental study of the photoswitches with a theoretical study.
- As soon as the photochemical study is finished, linking them to more complex systems to evaluate their adequate use in practical applications.

CHAPTER 4

Synthesis of biomimetic molecular switches

As discussed in previous chapters (2. Background, and 3. Objectives), the synthesis and characterization of different prototypes of molecular switches whose movement is induced by light, and whose structure is based on that of biomolecules, will be described in the course of this dissertation. Particularly, for the design of synthetic routes that lead to obtaining compounds that can behave as molecular switches, we will take as patterns the structures of the protonated Schiff base of retinal (PSB-retinal) chromophore and the green fluorescent protein (GFP) chromophore.

The present work will be divided in two distinct parts: one of them concerning the compounds with structure based on the PSB-retinal chromophore, and another one that includes the synthesis of the compounds with structure based on the GFP chromophore.

4.1. SYNTHESIS OF MOLECULAR SWITCHES WITH STRUCTURE BASED ON THE PROTONATED SCHIFF BASE OF RETINAL (PSB-RETINAL) CHROMOPHORE

4.1.1. Synthesis of neutral photoswitches with structure based on the PSB-retinal chromophore.

With the aim of complementing the works on molecular switches with structure based on the PSB-retinal chromophore that had been previously reported (Figure 4.1), and generating a new family of compounds that overcame the flaws that they presented, came up the idea of the design of the new prototypes of photoswitches reported in this thesis.

Despite of the promising features of the already known PSB-retinal-based molecular switches and the detailed information accumulated by both theoretical calculations and experimental data in solution of isolated molecules, little is known yet about the practical ability of these systems to act as efficient switches in real applications. In most cases, the reason behind this is the lack of available structures to be incorporated in a complex system.

Any new attempt to build a prototype of an efficient photoswitch should feature:

- an expedient and versatile synthetic route;
- a substructure that allows obtaining photostationary states (PSS) composed mainly of the less thermodynamically stable isomer;
- anchoring points adequate for linkage to other systems;
- high isomerization quantum yields; and
- low energy absorption bands compatible with complex environments.

As explained in chapter 2, the three precedent PSB-retinal-based molecular switches (Figure 4.1) were obtained through different synthetic routes; however, in all cases some experimental problems occurred and one or several of the aforementioned requisites were not fulfilled (see section 2.6).

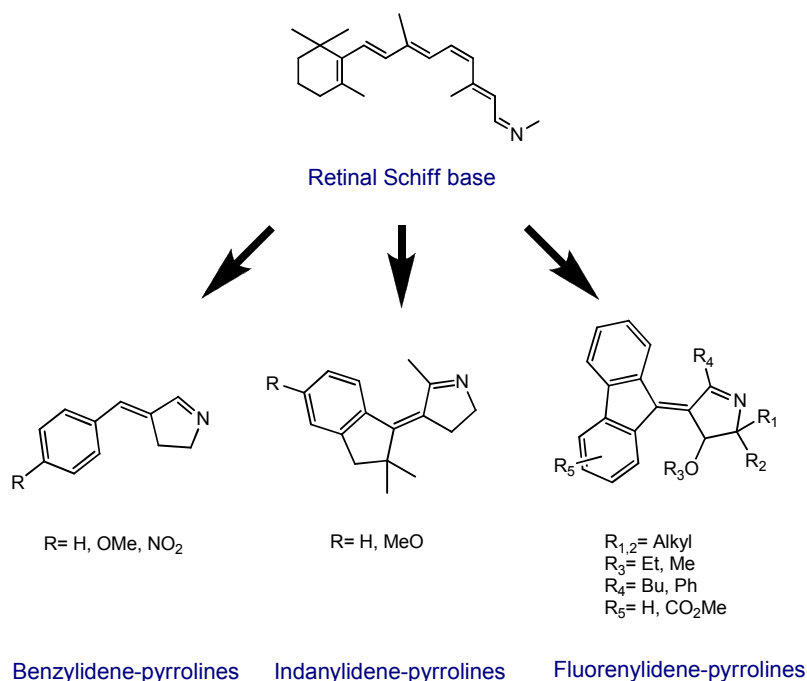


Figure 4.1. Summary of the different families of PSB-retinal-based photoswitches that have already been described, benzylidene-pyrrolines,¹ indanylidene pyrrolines² and fluorenylidene-pyrrolines³ (see sections 2.6.1, 2.6.2 and 2.6.3).

¹ Sampedro, D.; Migani, A.; Pepi, A.; Busi, E.; Basosi, R.; Latterini, L.; Elisei, F.; Fusi, S.; Ponticelli, F.; Zanirato, V.; Olivucci, M. *J. Am. Chem. Soc.* **2004**, *126*, 9349.

Therefore, we developed a new and versatile entry route to a new family of molecular PSB-retinal-based photoswitches that could improve some of the flaws of the previous compounds. These novel molecular switches based on PSB-retinal chromophore are analogous to benzylidene-pyrrolines (described in section 2.6.1), presenting a substituent R_1 in C-5 of the pyrroline ring (Figure 4.2(b)). We anticipated that a substituent in that position could affect the photoisomerization process. Moreover, a phenyl ring in that spot could substantially increase the UV-absorption and induce a bathochromic shift due to extended conjugation.

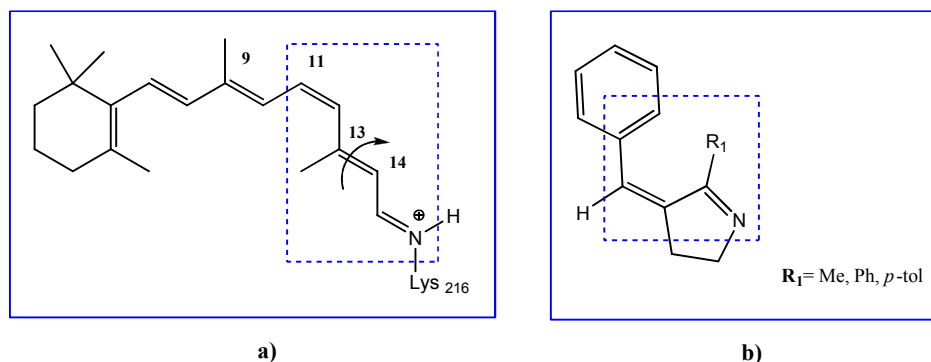


Figure 4.2. Comparison between the structures of the protonated Schiff base of retinal chromophore (a) and the new prototypes of molecular switches (b).

Although the structure of retinal has already been presented in section 2.3.4, in Figure 4.2(a) is shown the protonated Schiff base of retinal linked to an aminoacid of an opsin. Likewise, in Figure 4.2(b) appears the structure of the target compounds. If we look at the regions that are inside the dotted square, we can deduce that both PSB-retinal and our target compounds have an analogous structure in that part of the molecule. In Figure 4.2, it is visible that both structures present the following sequence of conjugated bonds: C=C-C=C-N, taking place the isomerization of the central C=C double bond when irradiating. It must be pointed out that in the compounds of Figure 4.2(b) the only possibility of rotation

² Lumento, F.; Zanirato, V.; Fusi, S.; Busi, E.; Latterini, L.; Elisei, F.; Sinicropi, A.; Andruniów, T.; Ferré, N.; Basosi, R.; Olivucci, M. *Angew. Chem. Int. Ed.* **2007**, *46*, 414.

³ Rivado-Casas, L.; Blanco-Lomas, M.; Campos, P. J.; Sampedro, D. *Tetrahedron* **2011**, *67*, 7570.

of a C=C double bond corresponds to the central C=C double bond, due to the fact that the rest of the double bonds are blocked as they belong to a ring. In the case of PSB-retinal (Figure 4.2(a)), we observe that the nitrogen atom of the imine bond (C=N) presents a positive charge. This seems relevant to the isomerization process of the PSB-retinal *in vivo*. Also, nitrogen atom quaternization provides improved features in related compounds (NAFPs, see section 2.6.3). Thus, starting from the accessible neutral compounds shown in Figure 4.2(b), the influence of the positive charge could also be explored.

We first performed a retrosynthetic analysis in order to design an accessible entry route for these compounds (Figure 4.3).

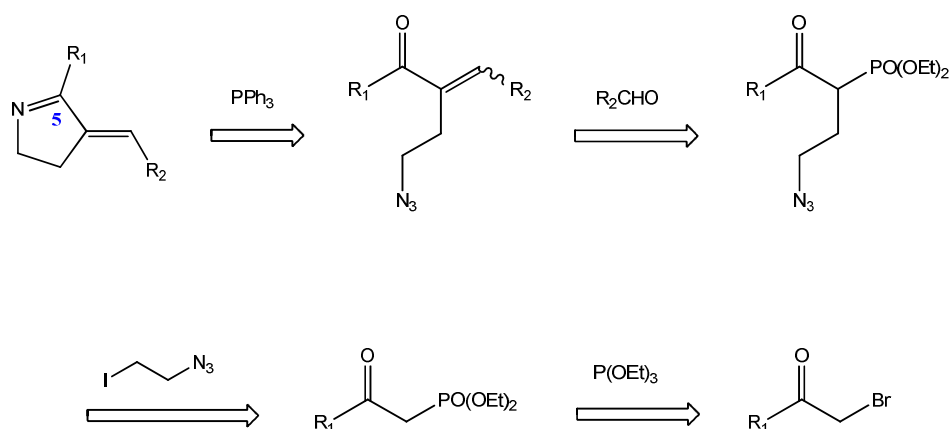


Figure 4.3. Retrosynthesis of the new prototypes of PSB-retinal-based photoswitches.

As the key step in the structure building, we decided to close the pyrrole ring in the last step. Previously, the central double bond could be formed by a Wittig-Horner reaction between an aldehyde and a conveniently synthesized phosphonate derivative. This would allow modifying the substituents in both sides of the molecular switch independently. Moreover, combination of different aldehydes and phosphonates would yield a complete family of switches with ease. A related approach has been previously reported.⁴

⁴ Snider, B. B.; Zhou, J. *J. Org. Chem.*, **2005**, *70*, 1087.

In the following paragraphs, the synthetic route to obtain the target photoswitches is broken down into each of its steps.

The first step (Figure 4.4) implies the synthesis of the phosphonate, whenever it is not commercially available. The phosphonate **2** with the adequate R_1 group ($R_1 = p\text{-tol}$) may be synthesized in an 85% yield from the corresponding 2-bromoketone **1**.

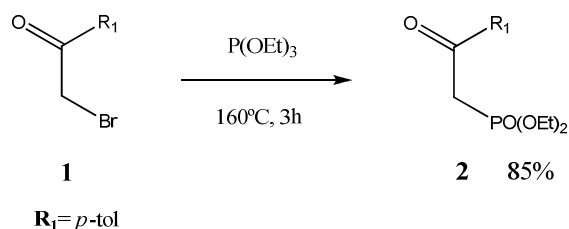


Figure 4.4. Synthesis of the phosphonate 2.

Then, the introduction in **2** of an ethyl azide side chain with 2-iodoethylazide by means of a phase-transfer procedure using tetrabutylammonium bisulfate and aqueous sodium hydroxide in CH_2Cl_2 at reflux affords the azido phosphonates **3** in 30-40% yield (Figure 4.5).

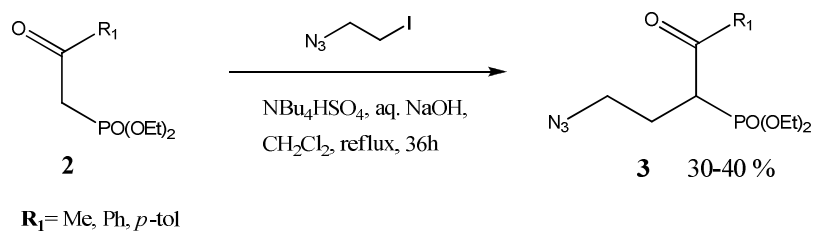


Figure 4.5. Synthesis of the azido phosphonate 3.

It should be noted that 2-iodoethylazide was synthesized prior to the reaction using the methodology previously reported in bibliography (Figure 4.6).⁵

⁵ Khoukhi, M.; Vaultier, M.; Carrié, R. *Tetrahedron Lett.* **1986**, *27*, 1031.

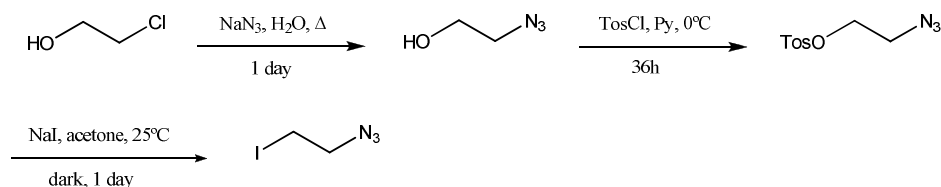


Figure 4.6. Synthesis of 2-iodoethylazide.

Afterwards, a Wittig-Horner reaction between the azido-phosphonate **3** and the aldehyde with the corresponding R_2 , using again a phase transfer procedure with aqueous K_2CO_3 and tetrabutylammonium bisulfate, leads to the formation of the azido enone **4** in 70% yield (Figure 4.7). Although a 9:1 mixture of *E* and *Z* isomers of the azido enones **4** is obtained, they can be separated by chromatography on silica gel (10:1 hexanes/EtOAc).

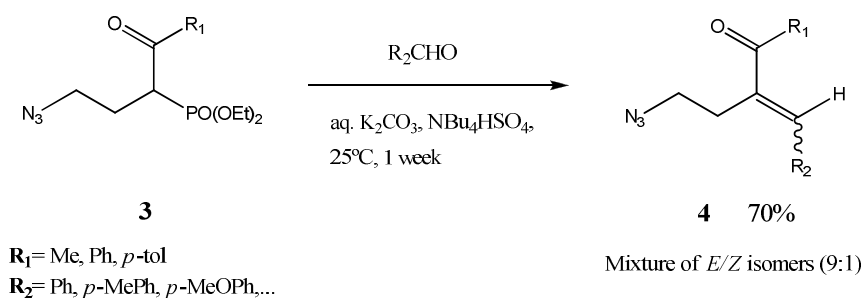
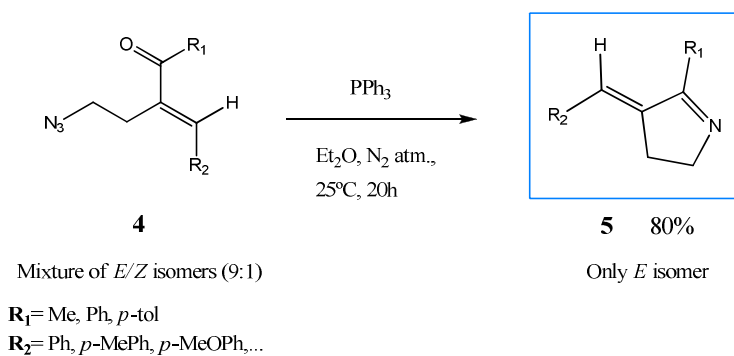


Figure 4.7. Synthesis of the azido enone **4**.

However, only the *E* isomer is found as the final product **5** in 80% yield after carrying out the intramolecular aza-Wittig reaction with triphenylphosphine (Figure 4.8). It should be noted that both isolated *E* and *Z* isomers of **4** yield the *E* isomer of **5** in the same reaction conditions. Thus, the mixture of isomers of **4** obtained in the reaction crude can be used in the last step without need of purification.

Figure 4.8. Synthesis of the photoswitches **5**.

All of the aforementioned synthetic steps are summarized in Figure 4.9:

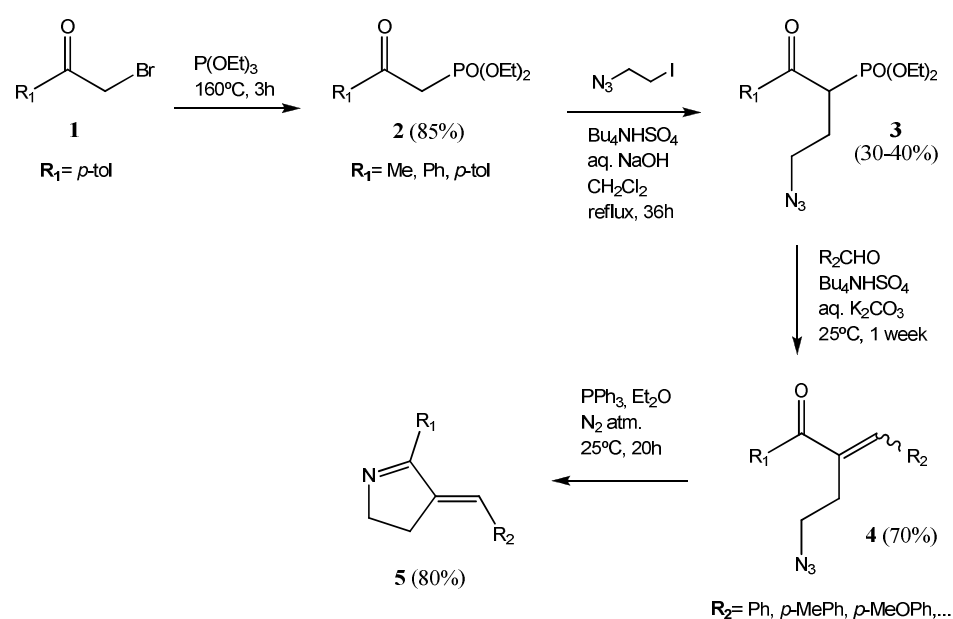


Figure 4.9. Synthetic route to afford new PSB-retinal-based photoswitches.

When comparing the aforementioned synthetic route to the one described for previously reported benzylidene-pyrrolines in section 2.6.1, we infer that even though the number of steps to yield compounds **5** is higher than the number of steps required for obtaining preceding benzylidene-pyrrolines, the synthetic route

is more versatile as it allows modifying greatly substituents R_1 and R_2 . Using the same methodology described above, a complete library of molecular switches can be obtained by changing R_1 and R_2 within the structure (Table 4.1).

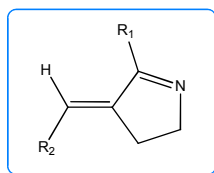


Table 4.1

Entry	R_1	R_2	Compound (<i>E</i> isomer)	Yield*
1	Me	Ph	5a	85%
2	Me	<i>p</i> -MePh	5b	82%
3	Me	<i>p</i> -MeOPh	5c	80%
4	Me	<i>o</i> -MeOPh	5d	80%
5	Me	CH ₃ (CH ₂) ₄	5e	75%
6	Ph	Ph	5f	82%
7	Ph	<i>p</i> -MePh	5g	70%
8	Ph	<i>p</i> -MeOPh	5h	83%
9	Ph	<i>o</i> -MeOPh	5i	85%
10	Ph	<i>p</i> -BrPh	5j	74%
11	Ph	<i>o</i> -BrPh	5k	77%
12	Ph	<i>p</i> -NO ₂ Ph	5l	76%
13	Ph		5m	65%
14	Ph		5n	60%
15	<i>p</i> -MePh	<i>p</i> -MePh	5o	80%

* Yield corresponding to the last step of the synthetic route

It should be highlighted that benzyl aldehydes with different electron-withdrawing and electron-donating groups may be used in the synthesis (entries 1-4, 6-12 and 15), which constitutes a major advantage over benzylidene and indanylidene pyrrolines (see sections 2.6.1 and 2.6.2). Unfortunately, the synthesis of the compounds bearing a *p*-CNPh or a *p*-CH₃CO₂Ph as R₂ groups was not possible due to the fact that the corresponding benzaldehyde derivatives were not soluble in water, so the Wittig-Horner reaction with the azido phosphonate didn't take place to give the target azido enone (see Figure 4.7).

In addition to this, hetero (switch **5m**, entry 13) and poly aromatic (switch, **5n**, entry 14) aldehydes can also be used. This fact not only contributes to enlarge the number of molecular switches showing this substructure, but also may be used to tune the switches' photophysical properties.

Moreover, the compound **5e** (entry 5) that has an alkyl chain as R₂ (Figure 4.10(b)) was obtained in order to check if the same isomerization process that takes place with its aromatic counterparts when irradiating could be also observed (This will be later discussed in section 5.2.1).

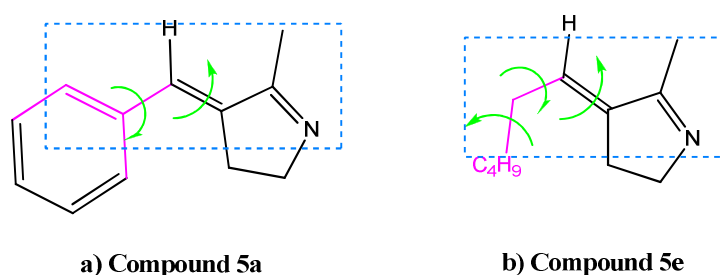


Figure 4.10. Comparison between the possible rotational movements in a molecule with a benzyl group (a) and another with an alkyl group (b).

We also checked the use of ketones with the purpose of obtaining compounds where the number of torsional degrees of freedom of the switch backbone is decreased, especially the potential competitive rotation around the allylic/benzylic single bonds. Rotation around this single bond was found to be one of the major drawbacks in previously reported benzylidene-pyrrolines (see section 2.6.1). Nevertheless, this was not possible due to the unfeasibility of carrying on the Wittig-Horner reaction under the reaction conditions described above. A raise in

reaction temperature to help the nucleophilic attack to the carbonyl of the ketone only led to decomposition of the azido phosphonate.

Finally, selecting the proper R_1 and R_2 groups it would be possible to get a photoswitch with two anchoring points for the linkage to complex structures in order to explore the practical applications of PSB-retinal based molecular switches. For example, it could be linked to a selected peptide so as to photocontrol its conformation and properties (This will be discussed extensively in section 6.3).

On the other hand, in order to confirm the *E* configuration of the final compounds **5**, 2-D NMR experiments were carried out (see Appendix A). From the NOESY spectrum of compound **5d** (Figure 4.11), it is inferred that there is NOE between the proton at the vinylic C-1' carbon and the methyl at the C-5 of the pyrroline ring, as well as between the proton at the aromatic C-3' carbon and the two protons at the C-3 of the pyrroline ring. Therefore, an *E* configuration for this isomer could be assigned. Moreover, it should be pointed out that the *o*-methoxy substituent is placed opposite to the pyrroline ring, as no NOE could be assigned between the MeO hydrogens and the two protons at the C-3 of the pyrroline ring.

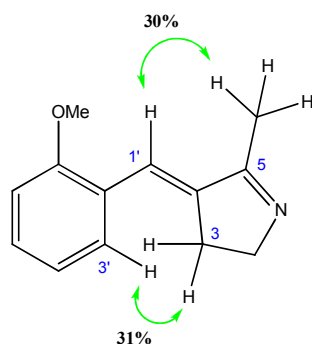


Figure 4.11. NOESY spectrum of the *E* isomer of switch **5d**.

Further stereochemical information could be obtained from the X-ray diffraction data of compound **5k** (Figure 4.12) (see Appendix B). This switch shows an *E* configuration of the central C=C double bond in agreement with the NOESY experiment. Also, X-ray diffraction data reveals that in solid state the central double bond is almost planar (torsion angle of *ca.* 6 degrees) while the phenyl group at the C-5 of the pyrroline ring is twisted *ca.* 35 degrees to avoid steric

repulsion. Furthermore, the *o*-Br substituent is placed opposite to the pyrroline ring, as the NOESY spectrum showed in the case of the methoxy substituent in **5d**.

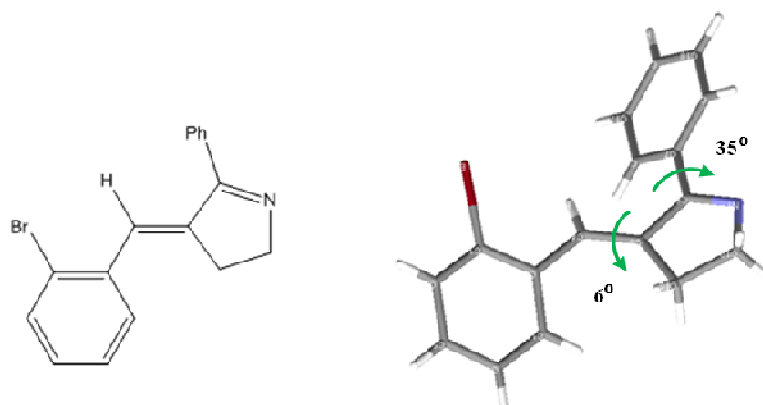


Figure 4.12. X-Ray structure of the *E* isomer of switch **5k**.

As discussed at the beginning of this section, the design of these new photoswitches was done in order to continue the study of molecular devices with structure based on the PSB-retinal chromophore. If we compare the structures of these novel compounds and the ones of the switches previously synthesized in our research group (see section 2.6.1 and 2.6.3), it is possible to distinguish the differences between them (Figure 4.13).

In Figure 4.13 we can perceive how the compounds in parts (a), (b) and (c) present an analogous structure in the area delimited by the dotted squares. Thus, due to the fact that the three types of compound share the same common backbone in the rotational region of the switch, it will be possible to compare their photochemical behavior. However, a few differences between these structures are noticeable.

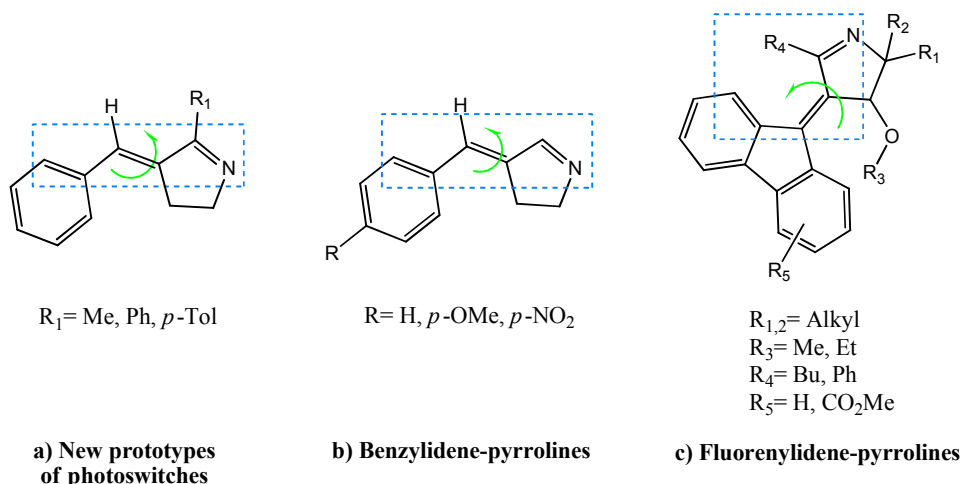


Figure 4.13. Comparison between the structures of the novel photoswitches (a), benzylidene-pyrrolines (b), and fluorenylidene-pyrrolines (c).

In the first place, the compounds in part (a) present a substituent R_1 in α position to the imine bond, while the compounds in part (b) have a hydrogen atom in that position. This fact implies that in the compounds of part (a) there is a greater steric hindrance in the rotational region of the molecule, which may provoke that the E/Z isomers ratio resulting from the photoisomerization of the switches of part (a) to be different from the one obtained for the compounds in part (b). Another difference that can be noticed is that in the new photoswitches there is the possibility of having substituents in *ortho* and *para* positions of the aromatic ring in R_2 , whilst in previously reported benzylidene-pyrrolines it is only possible to have substitution in *para* position. Taking a look at the structure of the compounds in part (a) it is remarkable that substituents in *ortho* position can considerably affect the rotation during the photoisomerization process. We expect that these differences have an influence in the photoisomerization process, and that the new molecular switches work in a more efficient way than the previously studied benzylidene-pyrrolines (see section 5.2.1).

Moreover, as we have talked about earlier in section 2.6.3, compounds in part (c) can be considered efficient. However, one of their main drawbacks is that the E/Z isomers ratio achieved after irradiation is approximately 1:1, due to the fact that the part of the molecule of the fluorenone ring is almost symmetric. In

contrast, in the new photoswitches as the corresponding part of the molecule is asymmetric, it may be possible to obtain *E/Z* isomers ratios different from 1:1.

These issues will be later reviewed in the corresponding section of Chapter 5.

4.1.2. Synthesis of methylated photoswitches with structure based on the PSB-retinal chromophore.

Once the neutral molecular switches have been synthesized, the following step towards the achievement of structures based on NAPs (*N*-alkylated arylidene-pyrrolines) that mimic the PSB-retinal structure is the quaternization of the nitrogen atom of the imine bond. As discussed in section 2.6.3, the quaternization of the nitrogen atom in that position considerably improves the photochemical and photophysical properties. Particularly, methylation of diverse compounds with substituents of the aromatic ring with different electronic properties was carried out by adding one equivalent of methyl triflate (MeSO_3CF_3) in dry toluene. Under these conditions, the iminium salt precipitates and can be easily isolated from the filtrate. Thanks to methylation, a new family of *N*-alkylated benzylidene-pyrrolines was obtained (NABPs) (Table 4.2).

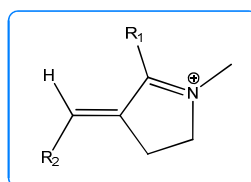


Table 4.2

Entry	Starting compound	R ₁	R ₂	Compound (<i>E</i> isomer)	Yield
1	5f	Ph	Ph	5f-met	95%
2	5h	Ph	<i>p</i> -MeOPh	5h-met	90%
3	5l	Ph	<i>p</i> -NO ₂ Ph	5l-met	97%
4	5n	Ph		5n-met	85%

The photochemical behavior of these methylated compounds will be also studied in Chapter 5.

4.1.3. Synthesis of metallated photoswitches with structure based on the PSB-retinal chromophore.

We also tested the reactivity of the molecular switches based on the PSB-retinal with metallic cations. Specifically, metallation of compound **5f** was performed by adding 0.5 equivalents of silver triflate (AgSO_3CF_3) in dry THF. The mixture was stirred overnight at room temperature to achieve a silver (I) complex, called **5f-Ag**, whose tentative structure is shown in Figure 4.14, after removing the solvent. We deduced that a new species had been formed as it was characterized by ESI+, and a displacement of the ^1H and ^{13}C signals of the initial compound **5f** was observed.

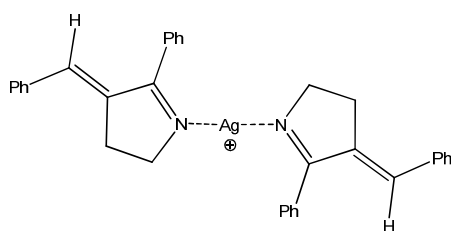


Figure 4.14. Tentative structure of compound **5f-Ag**.

A brief review of the photochemical study of the metallated photoswitches based on the PSB-retinal chromophore will be presented in section 5.2.4.

4.2. SYNTHESIS OF MOLECULAR SWITCHES WITH STRUCTURE BASED ON THE GREEN FLUORESCENT PROTEIN (GFP) CHROMOPHORE

4.2.1. Synthesis of photoswitches with structure based on the GFP chromophore.

The main goal of the design of molecular switches with structure based on the green fluorescent protein (GFP) chromophore is obtaining a new family of prototypes of molecular switches that work efficiently. For this purpose, we try to mimic the photoisomerization observed in the natural GFP chromophore. This new family of compounds has a certain structural analogy with the compounds previously reported in our research group (as they were based on the structure of the protonated Schiff base of retinal, PSB-retinal, as it has been discussed in section 4.1). The structure of the GFP chromophore is shown in Figure 4.15(a).

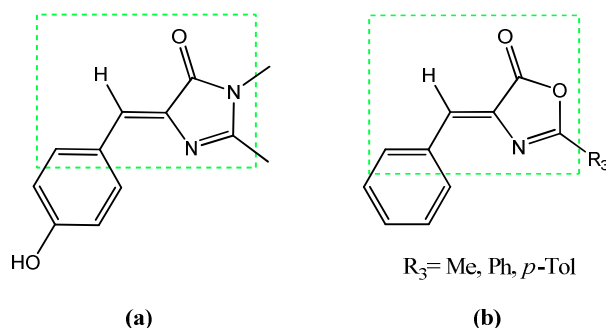


Figure 4.15. Comparison between the structures of the GFP chromophore (a) and the GFP-based photoswitches.

If we compare the structure of the GFP chromophore in Figure 4.15(a) with the structures in Figure 4.2 (Figure 4.2(a), structure of the PSB-retinal chromophore; and Figure 4.2(b), structure of the new photoswitches based on the PSB-retinal chromophore), we can infer that there is an important difference between them related to the position of the nitrogen atom of the imine bond. In the case of the GFP chromophore, the bond sequence is $-C=C-N=C-$, while in PSB-retinal, the sequence is $-C=C-C=N-$. This modification may be relevant when the

rotation of the central double bond of the designed switches takes place, due to the change in the electronegativity of the neighbouring atom of that double bond.

Another structural difference is the presence of heteroatoms in the five-membered ring, apart from the nitrogen atom of the imine bond, specifically the ones that belong to the amide function. The oxygen atom directly bonded to the imine moiety can affect the electronic properties of the whole chromophore. Besides, the carbonyl group may also affect the rotation, as it is spatially close to the region of rotation of the C=C double bond.

On the other hand, the compounds that we have synthesized present the structure shown in Figure 4.15(b). When contrasting the structure of the GFP chromophore (Figure 4.15(a)) with the one of the new photoswitches (Figure 4.15(b)), we deduce that the compounds described along this dissertation aren't exactly analogous to the GFP chromophore. The main difference between them is that the GFP chromophore and its derivatives present an amide function in the five-membered ring (dihydroimidazolone), while the compounds that we have studied have an ester function instead (5(4*H*)-oxazolones). However, it is not complicated to reach the structure of the GFP chromophore from the synthesized structures (Figure 4.15(b)), as a single reaction step would lead us to obtain the compounds with structure shown in Figure 4.15(a).⁶ Thus, in the near future, we would be able to have a large battery of compounds able to undergo *Z/E* photoisomerizations in the same way as the GFP chromophore: those belonging to the family of compounds with structure represented in part (a), and those that are related to the structure represented in part (b).

The synthesis of the new photoswitches with structure based on the GFP chromophore takes place under the classical conditions for the formation of azalactones,⁷ which is represented in Figure 4.16.

⁶ (a) Voliani, V.; Bizzarri, R.; Nifosì, R.; Abbruzzetti, S.; Grandi, E.; Viappiani, C.; Beltram, F. *J. Phys. Chem. B* **2008**, *112*, 10714. (b) Andresen, M.; Stiel, A. C.; Trowitzsch, S.; Weber, G.; Eggeling, C.; Wahl, M. C.; Hell, S. W.; Jakobs, S. *Proc. Natl. Ac. Sci. USA* **2007**, *104*, 13005.

⁷ Audia, J. E.; Droste, J. J.; Nissen, J. S.; Murdoch, G. L.; Evrard, D. A. *J. Org. Chem.* **1996**, *61*, 7937.

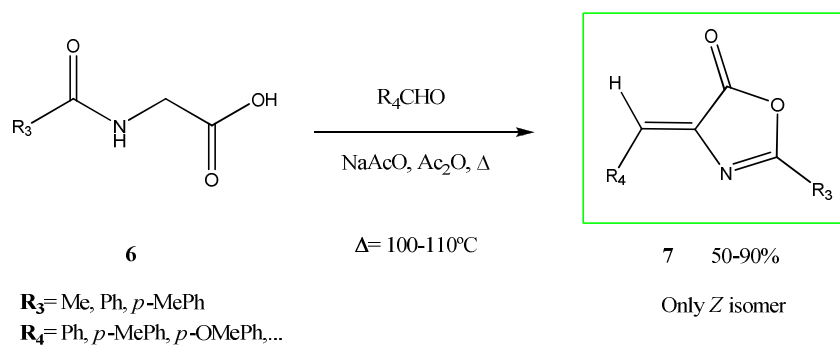


Figure 4.16. Synthetic route to achieve the GFP-based photoswitches **7**.

It should be pointed out that compounds **6** with $\text{R}_3 = \text{Me}$ and Ph are commercially available. However, when $\text{R}_3 = p\text{-MePh}$, the corresponding compound **6** has to be synthesized from glycine and p -toluic acid, which will be discussed extensively in section 6.2.1.

Through this synthetic reaction, a great number of molecular switches can be obtained by changing R_3 and R_4 within the general structure (Table 4.3).

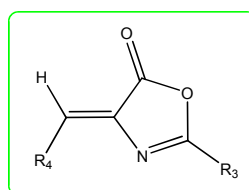
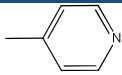
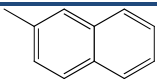
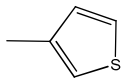
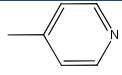


Table 4.3

Entry	R_3	R_4	Compound (Z isomer)	Yield
1	Ph	Ph	7a	85%
2	Ph	$p\text{-MePh}$	7b	85%
3	Ph	$p\text{-MeOPh}$	7c	60%
4	Ph	$o\text{-MeOPh}$	7d	87%
5	Ph	$p\text{-BrPh}$	7e	72%

6	Ph	<i>o</i> -BrPh	7f	85%
7	Ph		7g	*
8	Me	Ph	7h	80%
9	Me	<i>p</i> -MePh	7i	75%
10	Me	<i>p</i> -MeOPh	7j	65%
11	Me	<i>o</i> -MeOPh	7k	82%
12	Me	<i>p</i> -NO ₂ Ph	7l	90%
13	Me	<i>p</i> -CNPh	7m	80%
14	Me	<i>p</i> -CO ₂ MePh	7n	60%
15	Me	<i>p</i> -BrPh	7o	72%
16	Me		7p	61%
17	Me		7q	74%
18	Me		7r	*
19	<i>p</i> -MePh	<i>p</i> -MePh	7s	80%

* Couldn't be recrystallized from the crude.

The mechanism of this reaction is shown in Figure 4.17.

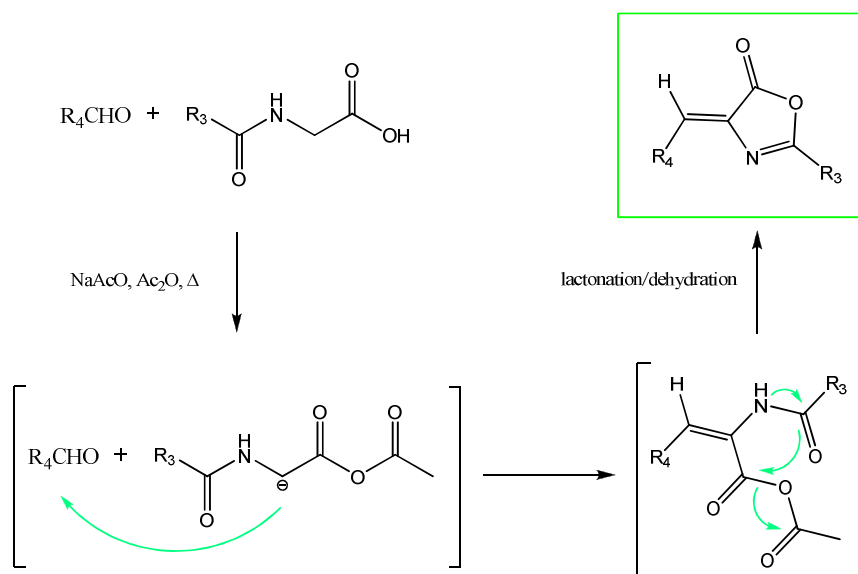


Figure 4.17. Mechanism of the synthesis of GFP-based photoswitches.

Unfortunately, the use of certain benzaldehyde derivatives, such as 2-carboxybenzaldehyde or 2-cyanobenzaldehyde, and most of ketones (*i.e.* acetophenone, benzophenone, 2-hexanone, 1-indanone, 9-oxo-9*H*-fluorene-4-carboxylic acid and methyl 9-oxo-9*H*-fluorene-4-carboxylate), didn't lead to the final product.

On the other hand, when carrying out the reaction shown in Figure 4.16 with hippuric acid (compound **6**, $R_3=Ph$) and 9*H*-fluoren-9-one, the target compound (**7t**) was achieved as it could be detected in the ESI+ spectrum (Figure 4.18).

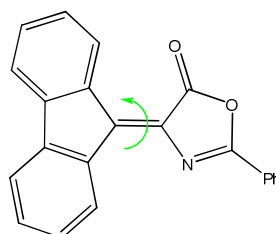


Figure 4.18. Compound 7t.

The fact that the synthetic reaction has only worked with 9*H*-fluoren-9-one, and no other ketones in which the carbonyl group is a part of a 5-membered ring, is a drawback because it would allow restraining the rotation around single bonds of the molecule (Figure 4.19).

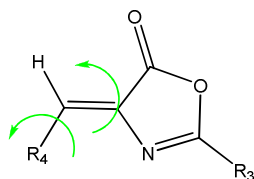


Figure 4.19. Possible rotational movements around single and double bonds in the molecule when irradiating.

This problem could be avoided in the case of compound **7t** in which alternate rotations are hampered. However, in this case, the fluorenone ring is symmetric, so no difference in the NMR spectra can be found when irradiating.

Therefore, to avoid competitive rotations it should be necessary to find an asymmetric ketone where the carbonyl group is a part of a 5-membered ring, and that could react with the appropriate α aminoacid (compounds **6**) to yield a product with the suitable structure that minimizes the rotation around single bonds.

On the other hand, stereochemical information could be obtained from the X-ray diffraction data of compound **7k** (see Appendix B). From Figure 4.20 it can be inferred that this switch shows a *Z* configuration of the central C=C double bond. Also, from the view rotated 90° (Figure 4.20(c)) it can be elucidated that in solid state the central C=C double bond is planar. Furthermore, the *o*-methoxy substituent is placed opposite to the azolactone ring, as it happened with the compounds based on the PSB-retinal.

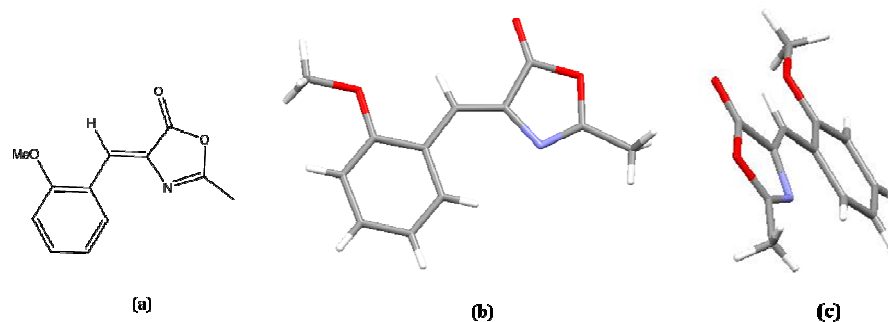


Figure 4.20. X-Ray structure of the *Z* isomer of switch 7k. (a) ChemDraw sketch, (b) flat view of the X-Ray structure, and (c) view rotated 90° of the X-Ray structure of the *Z* isomer of switch 7k.

4.2.2. Stability of the GFP-based photoswitches in different solvents.

As not all the compounds weren't achieved when trying to perform the reaction between the different α aminoacids (compounds **6**) and benzaldehyde derivatives, we decided to perform a study of the stability of these compounds in diverse solvents. It had been previously reported by Herbst *et al.* that related compounds feature a hydrolysis reaction in boiling water and acetone for 4 hours (Figure 4.21), obtaining the acetylaminoacid **8**:⁸

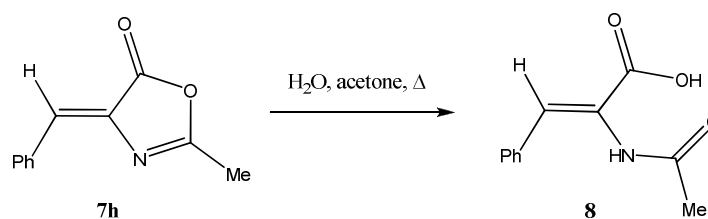


Figure 4.21. Hydrolysis of **7h** when treated with boiling water and acetone for 4 hours.

To test the stability of these compounds under different reaction conditions, we dissolved the compound **7h** in several flasks in different solvents, such as dichloromethane, acetonitrile, methanol, and aqueous sodium hydroxide (1M

⁸ Herbst, R.M.; Shemin, D. *Org. Syn.*, **1939**, *19*, 1; **1943**, *Coll. Vol. 2*, 1.

solution). **7h** is not soluble in water. All the solutions were stirred at room temperature for two weeks. In the flasks with dichloromethane and acetonitrile, **7h** was recovered unchanged. However, in the flasks with methanol and sodium hydroxide, there was a new product instead of the starting compound **7h**. In the case of the aqueous sodium hydroxide solution, hydrolysis of **7h** to give the acetylaminoacid shown in Figure 4.21 took place. On the other hand, when having methanol as solvent, it reacted with compound **7h** to give the acetamidoacetate **9** that is represented in Figure 4.22. This new compound was characterized by ESI+, and ¹H and ¹³C NMR (see the experimental section for details).

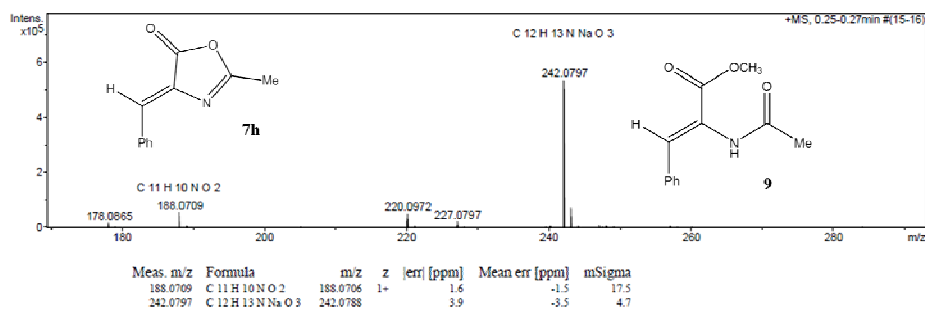


Figure 4.22. Hydrolysis of 7h in methanol to give the acetamidoacetate 9.

This means that we have to be careful when selecting the solvent of the reaction, in case that hydrolysis of the molecule takes place instead of the target reaction. This could cause some difficulties in the reaction conditions available for practical applications.

4.2.3. Synthesis of methylated photoswitches with structure based on the GFP chromophore.

Once the neutral molecular switches have been synthesized, we proceed to the quaternization of the nitrogen atom of the imine bond in order to get the methylated compounds. This could be used to compare the properties of the neutral vs. the methylated compounds as shown in the previous section for PSB-retinal photoswitches. For this purpose, methylation of diverse representative compounds (such as **7h** or **7j**) was carried out by adding one equivalent of methyl triflate (MeSO_3CF_3) in dry toluene. Under these conditions, the iminium salt should precipitate and could be easily isolated from the filtrate. However, in this case, the

methylated compounds weren't obtained as a result. Instead, the opening of the lactone ring by a molecule of water competed with methylation to achieve the opened products, which presented a molecular weight corresponding to the starting compounds plus eighteen units (+ H₂O). In Figure 4.23 there is an example of the ESI+ spectrum of the final compound **8** obtained when trying to methylate compound **7h**.

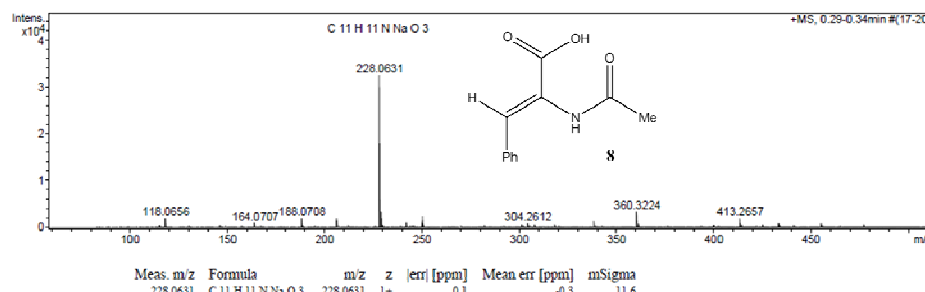


Figure 4.23. ESI+ spectrum of the final compound **8** obtained when methylating **7h**.

In the near future, other methodologies for quaternizing the photoswitches with structure based on the GFP chromophore will be explored in order to achieve the quaternized compounds.

For the time being, quaternization of the compounds with structure based on the GFP chromophore hasn't been possible, so only the photochemical behavior of the neutral compounds will be studied in the following chapter (see section 5.3).

4.2.4. Synthesis of photoswitches using an alkyl aldehyde as starting material.

As it had been previously done with the compounds based on the PSB-retinal, the achievement of a GFP-based compound in which R₄ was an alkyl chain was thought to increase the number of torsional degrees of freedom of the switch backbone, in order to check its behavior. However, the reaction between *N*-acetyl glycine (α aminoacid where R₃= Me) and *n*-hexanal afforded the final opened compound **10**. A strategy to recover the azalactone **7u** consisted on heating the opened compound in dry toluene, at reflux, and with a Dean Stark, so the water

formed in the reaction could be displaced (Figure 4.24). This approach is still under study.

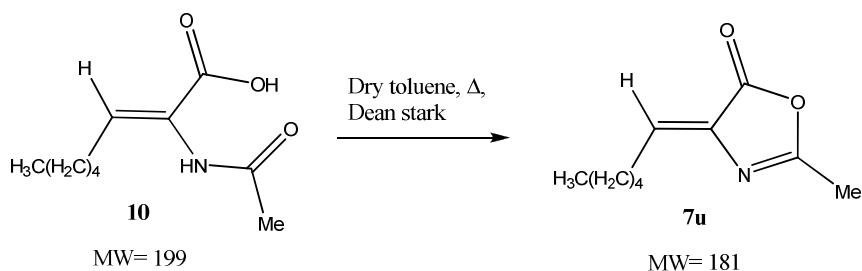


Figure 4.24. Ring cyclization to recover the azalactone **7u**.

4.2.5. Synthesis of metallated photoswitches with structure based on the GFP chromophore.

As we had previously done with the PSB-retinal based compounds (see section 4.1.3), we also checked the reactivity of the molecular switches based on the GFP with metallic cations. For this purpose, we tried the metallation of compound **7h** by adding 0.5 equivalents of silver triflate (AgSO_3CF_3) in dry THF. The mixture was stirred overnight at room temperature, but the silver (I) complex was not obtained in this case.

To sum up, we have synthesized several families of photoswitches with structure based on the PSB-retinal chromophore and the GFP chromophore, with the aim of characterizing them in the first place, and performing a photochemical study afterwards. In the following chapters, the photochemical behavior of the designed molecular switches will be reviewed.

CHAPTER 5

Photochemical study

Once the synthesis and characterization of the compounds based on the PSB-retinal and the GFP chromophores have been carried out, the following step is to perform the photochemical study of the different structures to test their capability of functioning as molecular photoswitches. The basis of a molecular switch is the ability of being reversibly interconverted between two different states by means of an external stimulus, as it has already been discussed in chapter 2 (see section 2.2). In this particular kind of systems, the two states are the *Z* and *E* isomers of the molecule, and the basic photochemical process that they undergo is a *Z/E* photoisomerization of the central C=C double bond of the molecule. Thus, after irradiating, mixtures with different ratios of *Z* and *E* isomers for each compound will be found at the photostationary state (PSS). Afterwards, the thermodynamically more stable isomer must be recovered by heating or irradiation with light of a different wavelength.

As it has been done in the section concerning the synthesis of biomimetic molecular switches (see Chapter 4), this chapter will be divided into two distinct subsections, one concerning the photochemical study of the compounds with structure based on the protonated Schiff base (PSB) of the retinal chromophore, and another that includes the photochemical study of the prototypes based on the green fluorescent protein (GFP) chromophore. In this chapter, we will go over diverse factors that might affect the photoisomerization, as well as the study of the kinetics of the reaction and the efficiency of the process.

5.1. INTRODUCTION

The electronic absorption and emission spectra of a molecule provide relevant information about the energetic and dynamic structure of the excited electronic states. This information is useful for understanding and explaining the photochemical reactivity and the photophysical properties (such as color or luminescence phenomena).¹

The absorption of ultraviolet or visible light by an organic molecule causes the excitation of an electron from an initially occupied, low energy orbital to a high energy, previously unoccupied orbital. The energy of the absorbed photon is used to energize an electron and cause it to go up to a higher energy orbital. Two excited electronic states derive from the electronic orbital configuration produced by light absorption (Figure 5.1). In one state, the electron spins are paired (antiparallel) and in the other state the electron spins are unpaired (parallel). The state with paired spins has no resultant spin magnetic moment, but the state with unpaired spins has a net spin magnetic moment.

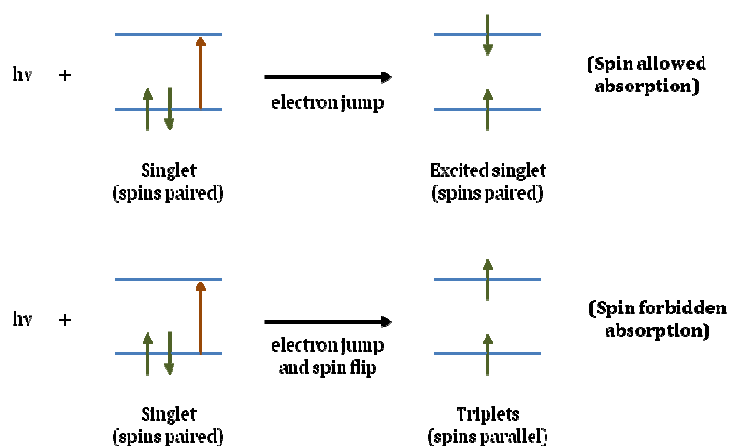


Figure 5.1. Orbital energy description of absorption. The arrows intersected by the levels represent electrons. The direction of the arrow represents the orientation of the electron spin.

¹ (a) Turro, N. J. *Modern Molecular Photochemistry*. University Science Books: Sausalito, CA, 1991. (b) Turro, N. J.; Ramamurthy, V.; Scaiano, J. C. *Principles of Molecular Photochemistry. An Introduction*. University Science Books: Sausalito, CA, 2009.

A state with paired spins remains a single state in the presence of a magnetic field, and is named as *singlet state*. On the other hand, a state with unpaired spins interacts with a magnetic field and splits into three quantized states, being called *triplet state*. Therefore, the notation to describe the states involved in organic photoreactions that will be used throughout this dissertation is the following:

- S_0 = ground, singlet state
- S_n = energy excited singlet state (where $n = 1, 2, 3, \dots$)
- T_n = triplet state (where $n = 1, 2, 3, \dots$)

The paths that can be followed by a molecule in its excited state can be divided into two kinds of processes: photochemical and photophysical.

- *Photochemical processes*: they can be defined as transitions from an electronically excited state to give structures with different constitution or configuration than the ground state (S_0).
- *Photophysical processes*: they are transitions which interconvert excited states with each other or excited states with the ground state. They can be classified as radiative or radiationless processes.

The typical photophysical radiative processes are:

- *(Photon) Absorption*: it is characterized by an extinction coefficient, ϵ , even if it is spin-allowed (singlet-singlet absorption, $S_0 + h\nu \rightarrow S_1$) or spin-forbidden (singlet-triplet absorption, $S_0 + h\nu \rightarrow T_1$).
- *Fluorescence*: it is a spin-allowed emission (singlet-singlet emission, $S_1 + h\nu \rightarrow S_0$).
- *Phosphorescence*: it is a spin-forbidden emission (triplet-singlet emission, $T_1 + h\nu \rightarrow S_0$).

Fluorescence and phosphorescence are grouped under the general term of *luminescence*.

On the other hand, the photophysical radiationless processes are:

- *Internal conversion (IC)*: they are isoenergetic and spin-allowed transitions between two electronic states of the same spin (*i.e.* $S_n \rightarrow S_{n-1}$).

5. Photochemical study

- *Intersystem crossing (ISC)*: they are isoenergetic and spin-forbidden transitions between excited electronic states of different spin (*i.e.* $S_1 \rightarrow T_1$), which may lead to subsequent phosphorescence, or between triplet states and the ground state (*i.e.* $T_1 \rightarrow S_0$).
- *Vibrational relaxation (VR)*: it is the transmission of the excess of energy from an excited vibrational level to a vibrational level with lower energy.

All of these processes are represented in the modified Jablonski diagram (Figure 5.2).²

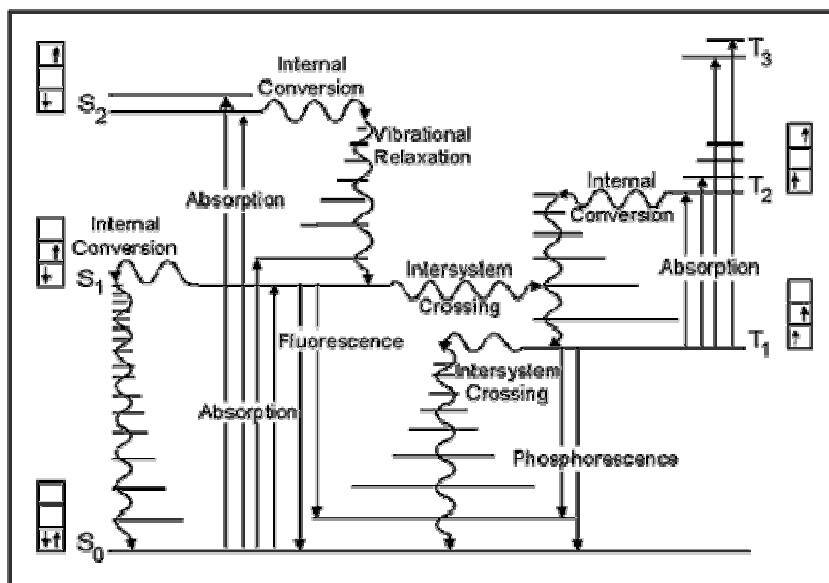


Figure 5.2. Modified Jablonski diagram.

² Originally, it was a diagram that showed the relationship between the fluorescent and phosphorescent (luminescence) states. Nowadays, modified Jablonsky diagrams are frequently used, which are actually state energy diagrams. Bourdelande, J. L.; Nonell, S.; Acuña, A. U.; Sastre, R. *Glosario de términos usados en fotoquímica. 2ª ed.*, Servei de Publicacions, Universitat Autònoma de Barcelona: Bellaterra, Barcelona, **1999**.

5.1.1. Absorption spectra.

When a species absorbs electromagnetic radiation in the ultraviolet-visible (UV-Vis) region, it becomes electronically excited. The energy of the radiation is able to produce transitions between different electronic levels to give excited electronic states (see Figure 5.2). In the absorption spectra, the absorption intensity is represented as a function of the energy applied, generally expressed as wavelength, λ . Bands are obtained instead of lines due to the vibrational levels of each electronic state. It is known as a *chromophore* the atom or group of atoms in which is located the electronic transition responsible for a given spectral band. These bands indicate transitions between the ground state and the different excited states, as well as they give the energy value of the leap. The nature of the excited states involved in a photochemical reaction can be inferred from the values of λ and ϵ of the absorption spectrum, along with the study of the influence of the polarity of the solvent. Therefore, the most appropriate wavelength for the irradiation has to be selected in order to obtain a higher absorption of light or eliminate unwanted bands that may produce undesirable side reactions.

5.2. PHOTOCHEMICAL STUDY OF PHOTOSWITCHES WITH STRUCTURE BASED ON THE PSB-RETINAL CHROMOPHORE.

5.2.1. Photochemical study of neutral photoswitches with structure based on the PSB-retinal chromophore.

When the molecular switches based on the PSB-retinal are irradiated, the induced movement generated is shown in Figure 5.3 with blue arrows, which consists of the rotation around the C=C double bond to achieve the corresponding *E* or *Z* isomers. This photoisomerization process is analogous to the one that takes place in the PSB-retinal chromophore, which has been described in section 2.3.4.

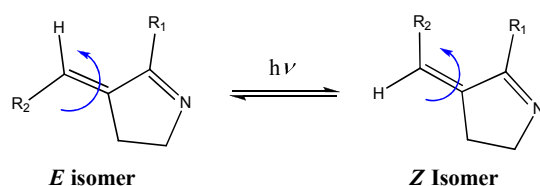


Figure 5.3. *E/Z* photoisomerization process undergone by the molecular switches with structure based on the PSB-retinal chromophore.

Before initiating the irradiation process, the UV-Vis spectra for all the synthesized compounds were recorded. The values for the maximum wavelengths and the extinction coefficients of the bands found for each compound in acetonitrile are shown in Table 5.1. In most cases, a spectrum featuring similar absorptions was obtained. It can be observed that there is a slight change in the values of the maximum wavelength for absorption when changing R_1 from a methyl to a phenyl or a *p*-tolyl group (see, for instance entries 1 and 6, 2 and 7, 3 and 8). Also, when $R_1 = \text{Ph}$ and R_2 varies from Ph (switch **5f**, entry 6) to *p*-MeOPh (switch **5h**, entry 8) or *p*-NO₂Ph (switch **5l**, entry 12), there is a bathochromic shift of the absorption band. Finally, a red-shift is also observed when maintaining $R_1 = \text{Ph}$ and changing R_2 from a phenyl to a 2-naphtyl (switch **5n**, entry 14) group (see UV-Vis of compound **5n**, Figure 5.4) due to the increase of the conjugation when adding another aromatic ring. This absorption at lower energies (**5n** features an absorption band beyond 360nm) could be relevant for technological applications which require the use of non-damaging wavelengths. Thus, a modification of the substructure of compound **5n** (*i.e.* the methylation of the nitrogen atom of the imine group, which will be later reviewed in section 5.2.3)

may lead to absorption in the visible region, which is an important feature due to the possibility of irradiating with low energy and solar light.

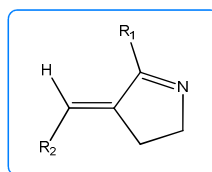
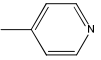
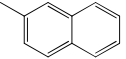


Table 5.1

Entry	R ₁	R ₂	compound	$\lambda_{\text{max}}(\text{nm})/\epsilon (\text{M}^{-1}\text{cm}^{-1})$ in CH ₃ CN
1	Me	Ph	5a	288 / 8681
2	Me	<i>p</i> -MePh	5b	287 / 7345
3	Me	<i>p</i> -MeOPh	5c	296 / 26636
4	Me	<i>o</i> -MeOPh	5d	275 / 8938
5	Me	CH ₃ (CH ₂) ₄	5e	232 / 15000
6	Ph	Ph	5f	289 / 22232
7	Ph	<i>p</i> -MePh	5g	296 / 24808
8	Ph	<i>p</i> -MeOPh	5h	304 / 24934
9	Ph	<i>o</i> -MeOPh	5i	281 / 15225 317 / 14189
10	Ph	<i>p</i> -BrPh	5j	282 / 47716
11	Ph	<i>o</i> -BrPh	5k	282 / 18182
12	Ph	<i>p</i> -NO ₂ Ph	5l	335 / 13684
13	Ph		5m	284 / 19304
14	Ph		5n	275 / 34853 311 / 28368
15	<i>p</i> -MePh	<i>p</i> -MePh	5o	294 / 20118

5. Photochemical study

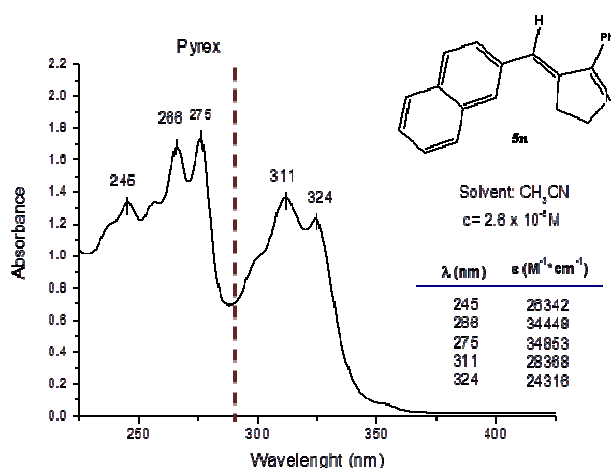


Figure 5.4. UV-Vis absorption spectrum of compound **5n** in acetonitrile.

However, when $R_1 = Ph$ and R_2 is modified from a phenyl (switch **5f**, entry 6) to a heterocycle (switch **5m**, entry 13), there is no notable change in the absorption properties.

On the other hand, when R_1 remains as a methyl group, but R_2 is changed from an aromatic to an aliphatic group (see UV-Vis of compound **5e**, Figure 5.5), the band is displaced to higher energies, being the maximum wavelength of absorption *ca.* 232 nm. This way, we proved the fact that having an aromatic ring in that position of the molecule allows irradiating with light of lower energies.

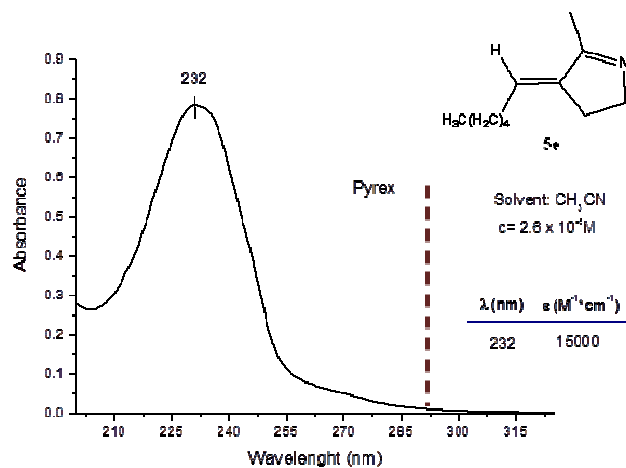
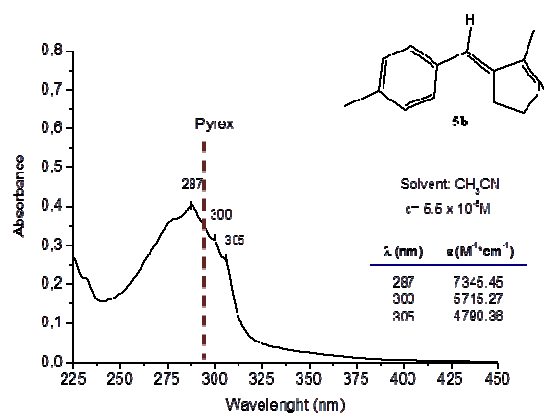


Figure 5.5. UV-Vis absorption spectrum of compound 5e in acetonitrile.

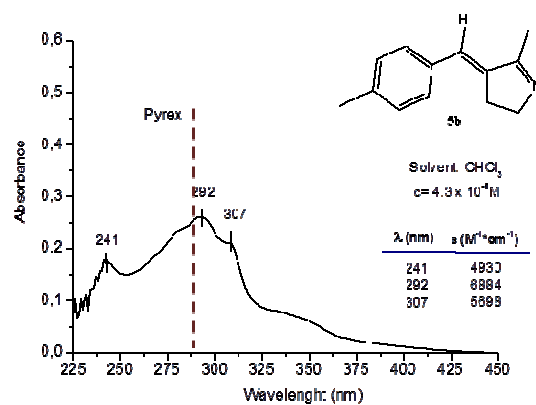
Furthermore, the UV-Vis spectra of the compounds shown in Table 5.1 were measured in diverse solvents with different polarity:³ acetonitrile (polarity 0.460) and chloroform (polarity 0.259), in order to test if there was any solvent effect. To illustrate this, the UV-Vis spectra of compounds **5b** and **5f** in acetonitrile and chloroform are shown respectively in Figures 5.6 and 5.7.

³ Normalized parameters based on empiric data of solvent polarity (E_T^N). For further info, see: Reichardt, C. *Solvents and solvent effects in organic chemistry 3rd ed.*, Wiley-VCH, Weinheim, **2003**, page 418.

5. Photochemical study

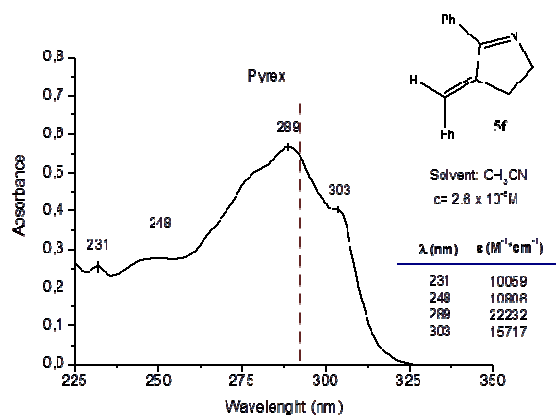


(a)

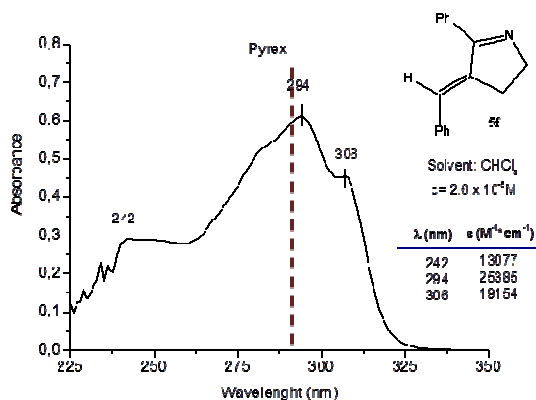


(b)

Figure 5.6. UV-Vis absorption spectrum of compound 5b in (a) acetonitrile and (b) chloroform.



(a)



(b)

Figure 5.7. UV-Vis absorption spectrum of compound 5f in (a) acetonitrile and (b) chloroform.

As can be seen, the UV spectra of both compounds remains almost the same when carried out in polar (acetonitrile) and non-polar (chloroform) solvents. Thus, photophysical properties, isomerization kinetics and photostationary state composition could be quite similar in both types of solvents, so we can use them indistinctly. Moreover, this fact could allow applications of these compounds in both polar and non-polar media, which in turn provides a wide field of action.

After analyzing the UV-Vis spectra, we infer that a Pyrex filter⁴ can be used in order to avoid radiation below 290 nm for irradiating the different compounds, except for compound **5e**, (see Figures 5.4, 5.6 and 5.7). High energy light could cause side reactions different from the isomerization process and decomposition. However, in the case of compound **5e**, as it is shown in Figure 5.5, there is almost no absorption at wavelengths longer than 290 nm, so a quartz filter has to be used instead, as it allows the passage of radiation of wavelengths longer than 220 nm. In all cases, a 125-W medium-pressure Hg lamp was used for irradiation. The results found for the different photoswitches based on the PSB-retinal are shown in Table 5.2. The irradiation process of each compound was followed by ¹H NMR, at different time intervals, until the photostationary state (PSS) was reached, since *E* and *Z* isomers have distinctive ¹H NMR signals (see as an example the ¹H NMR spectra for the isomerization process of compound **5j** at different irradiation times in Figure 5.8). Integration of the ¹H NMR signals corresponding to each isomer allowed us to know the isomers ratio at a given irradiation time.

On the other hand, various types of irradiation conditions were used:

- Type A: A 0.1M solution of the compound in CDCl₃, directly in a Pyrex NMR tube, with a Pyrex filter. These conditions were used whenever the amount of compound available wasn't enough for irradiating in an immersion reactor.
- Type B: A 0.01 M solution in CH₃CN, in an immersion well reactor, with a Pyrex filter. These are the normal conditions for performing the irradiation.
- Type C: a 0.1 M solution in CDCl₃, directly in a Quartz NMR tube, with a Quartz filter. It was only used for the irradiation of **5e**.

The conditions used for the irradiation of each compound are also displayed in Table 5.2. As it has been previously discussed, since the UV spectra of the compounds remains almost the same when carried out in acetonitrile or chloroform, both solvents could be used indistinctly. However, irradiating directly in an NMR tube was more convenient, as there was no need of any work-up prior to recording the NMR spectrum. Depending on the absorption coefficient, the irradiated mixture took from 1 to 4 hours to reach the PSS.

⁴ Pyrex glass is a type of commercial glass composed of approx. 80% of SiO₂, 13% of B₂O₃, 4% of Na₂O, 2% of Al₂O₃, and small amounts of iron, calcium and magnesium oxides and chlorine.

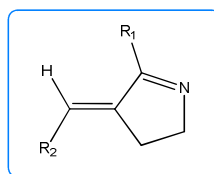
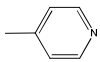
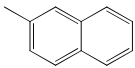


Table 5.2

Entry	R ₁	R ₂	compound	irradiation conditions	ratio at PSS*	
					%E	%Z
1	Me	Ph	5a	A	56	44
2	Me	<i>p</i> -MePh	5b	A	43	57
3	Me	<i>p</i> -MeOPh	5c	B	47	53
4	Me	<i>o</i> -MeOPh	5d	A	30	70
5	Me	CH ₃ (CH ₂) ₄	5e	C	85	15
6	Ph	Ph	5f	B	76	24
7	Ph	<i>p</i> -MePh	5g	B	72	28
8	Ph	<i>p</i> -MeOPh	5h	B	75	25
9	Ph	<i>o</i> -MeOPh	5i	B	44	56
10	Ph	<i>p</i> -BrPh	5j	B	40	60
11	Ph	<i>o</i> -BrPh	5k	B	41	59
12	Ph	<i>p</i> -NO ₂ Ph	5l	B	30	70
13	Ph		5m	A	80	20
14	Ph		5n	A	60	40
15	<i>p</i> -MePh	<i>p</i> -MePh	5o	B	76	24

* Isomers ratio at the PSS.

5. Photochemical study

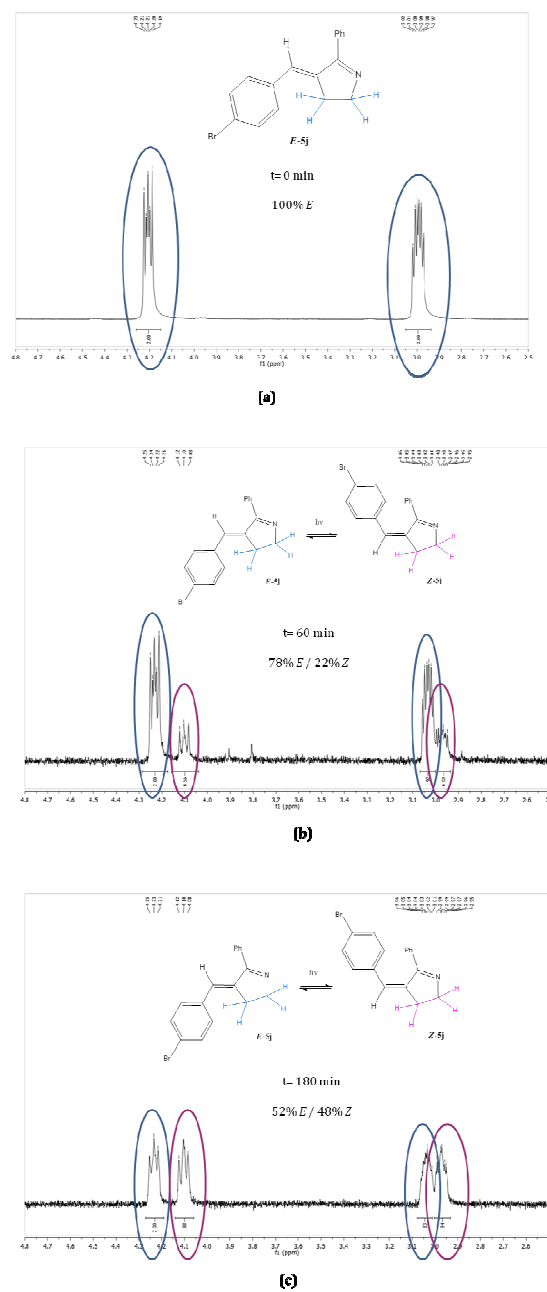


Figure 5.8. ^1H NMR spectra for the isomerization process of compound **5j** at (a) $t = 0$ min, (b) $t = 60$ min, and (c) $t = 180$ min.

From the results of the isomers ratio at the PSS for every compound shown in Table 5.2, some trends can be highlighted. When changing the R_1 group from a methyl group (*i.e.* switch **5a**, entry 1) to a phenyl group (*i.e.* switch **5f**, entry 6) and R_2 remains the same, the percentage of the *Z* isomer obtained at the PSS decreases. This could be due only to steric reasons. On the other hand, when having the same R_1 and R_2 groups, but the substituent in the phenyl group of R_2 is located in *ortho* (*i.e.* switch **5i**, entry 9) instead of *para* (*i.e.* switch **5h**, entry 8), the percentage of isomer *Z* increases. The relative absorption for both isomers together with dynamic factors in the PSS could explain these results. Finally, maintaining R_1 but modifying R_2 from a phenyl (*i.e.* switch **5f**, entry 6) to a phenyl substituted with an electron withdrawing group in *para*, such as nitro (*i.e.* switch **5l**, entry 12), the percentage of *Z* isomer increases a lot. Again the different absorption of the isomers in the reaction conditions could explain this fact.

Moreover, there is very little effect on the isomers ratio at the PSS when having a heterocycle as R_2 (switch **5m**, entry 13) instead of a phenyl group (switch **5f**, entry 6). However, the addition of another aromatic ring (switch **5n**, entry 14) increases the percentage of *Z* isomer at the PSS when compared to having only a phenyl group (switch **5f**, entry 6). Finally, we checked if having an alkyl group as R_2 (switch **5e**, entry 5) leads to a similar isomerization process than the experienced by the rest of compounds and the results confirmed that an *E/Z* isomerization was occurring in despite of the presence of multiple single bonds capable of rotation (see Figure 4.10 in section 4.1.1).

This way, we conclude that the value of isomers ratio at the photostationary state can be modified depending on the structure substitution, which constitutes a great advantage over fluorenylidene-pyrroline switches (see section 2.6.3).

Once the isomers ratio at the photostationary state has been determined, the next step is trying to separate the two isomers (*E* and *Z*) in order to individually characterize and study them. For this purpose, we irradiated a 0.01 M solution of compound **5o** (100% *E* isomer at $t=0$ min) in acetonitrile in an immersion well reactor with a 125-W medium-pressure Hg lamp, and a Pyrex filter, until the PSS was reached. Afterwards, we separated the resulting mixture of isomers by flash chromatography on silica gel, using hexane/ ethyl acetate (1:2) as eluent. This way, we could have the two isomers (*E* and *Z*) separately, so we could record the NMR

and UV-Vis spectra of the *Z* isomer (see experimental section and appendix A) and compare it with the thermodynamically more stable isomer (*E*).

In order to exemplify this, the UV-Vis spectra of solutions of the same concentration in acetonitrile of the two isomers of compound **5o** are plotted in the same axes (Figure 5.9). As it can be inferred from the figure, both isomers show only slightly differences in the absorption bands. However, these differences could be used to tune the switch behavior under irradiation using light with the adequate wavelength. Furthermore, the *E* isomer absorbs preferentially at 295 nm while the *Z* isomer features stronger absorption bands at 260 and 330 nm. Therefore, varying the wavelength of the incident light from 260 to 295 nm the main isomer in the reaction mixture would change. This fact has also some interesting implications as the average position of the switch could be modified by adjusting only the wavelength of irradiation. A similar case will be later reviewed in section 5.3.1.1, so this concept will be further discussed.

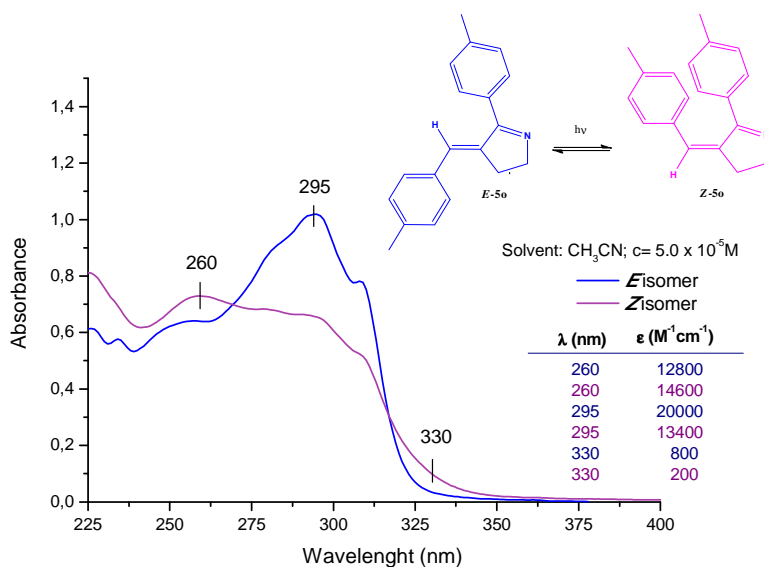
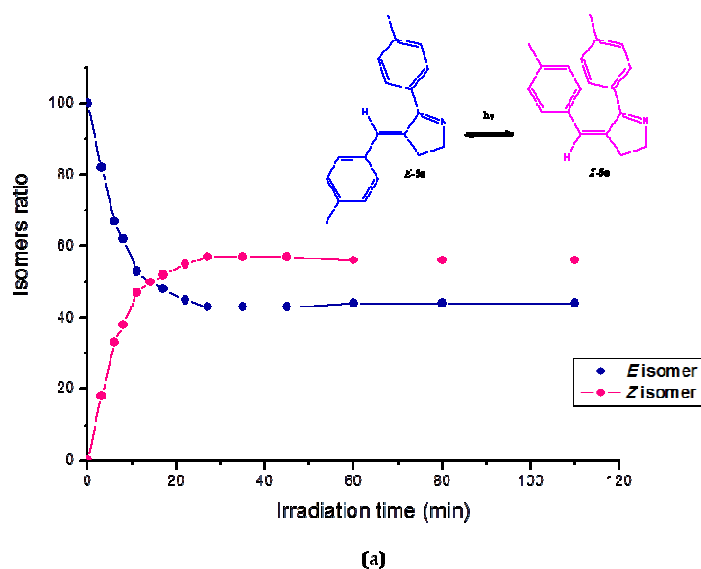


Figure 5.9. UV-Vis spectra of the *E* and *Z* isomers of compound **5o**.

Not only the two isomers of compound **5o** can be isolated, but also the isomers of other compounds can be separated by flash chromatography on silica gel, using hexane/ ethyl acetate (1:2) as eluent. For example, the data of the NMR

spectra of the *Z* isomer of compound **5k** are also shown in the experimental section and appendix A, so it can be compared with the NMR spectra of the thermodynamically more stable isomer (*E*).

As soon as we have both the *E* and *Z* isomers separately, their different behavior against light can be analyzed. For this, we prepared in two distinctive Pyrex NMR tubes two solutions of the same concentration in CDCl₃. In the first NMR tube, we got ready a solution 0.07 M of the *E* isomer of compound **5o**. In turn, in the second NMR tube, we prepared a solution 0.07 M of the *Z* isomer of compound **5o**. Then, both NMR tubes were irradiated in a 125-W medium-pressure Hg lamp and a Pyrex filter, until both solutions reached the PSS. As the samples were directly dissolved in CDCl₃, it was easy to follow the photoisomerization reaction by ¹H NMR at short irradiation intervals. Therefore, ¹H NMR spectra of the two samples were performed every 3 minutes with the aim of tracking the isomerization process of the compounds *E*-**5o** and *Z*-**5o**. Representing the isomers ratio vs. the irradiation time, we obtained the two graphs that are shown in Figure 5.10, (a) corresponding to the sample with 100% of *E*-**5o** isomer at the beginning of the reaction, and (b) corresponding to the sample with 100% of *Z*-**5o** isomer at $t_{\text{irrad}}=0$ min.



5. Photochemical study

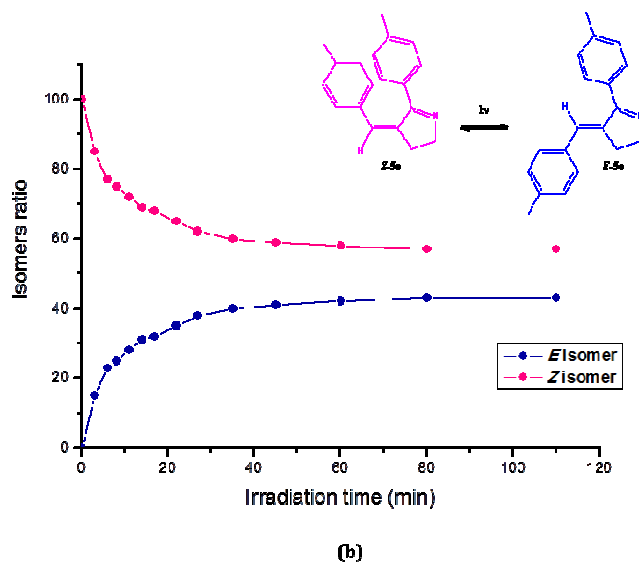


Figure 5.10. Graphs where the isomers ratio is represented vs. the irradiation time (a) starting from a 100% of the *E* isomer, and (b) starting from a 100% of the *Z* isomer of compound 5o.

From Figure 5.10, we can extract the following information:

- Part (a): When we started from 100% of the *E* isomer, the photostationary state was reached after 30 min of irradiation, time after which the isomers ratio remained constant and with a value of 40% (*E*) / 60% (*Z*).
- Part (b): If we started from 100% of the *Z* isomer, it took approx. 35 min to reach the PSS, being the value for the isomers ratio from this point 40% (*E*) / 60% (*Z*).
- This way, we proved that starting from solutions of the same concentration and irradiating under the same conditions the two NMR tubes, the isomers ratio at the photostationary state is independent from the starting isomer (*E* or *Z*), what is a fact consistent with the definition of a molecular switch (see section 2.2.1)

Furthermore, we can compare the results for the isomers ratio at the PSS reached during this experiment, 40% (*E*) / 60% (*Z*), and the value obtained when irradiating in an immersion well reactor, 76% (*E*) / 24% (*Z*) (see table 5.2, entry

15). As it can be seen, there is a big difference between the two results, since in the experiment shown in Figure 5.10 the *Z* isomer is the main isomer at the PSS, whilst when we irradiated in an immersion well reactor, the main isomer was *E*. This might be due to several facts:

- even though the light source was the same in both experiments, the rest of the reaction conditions, such as solvent or concentration, were different;
- in the case of the immersion well reactor, a work-up prior to recording the NMR spectrum is required, time during which the mixture of isomers can revert to the more thermodynamically stable isomer, *E*; and finally,
- as the irradiation process in the immersion well reactor was carried out for longer periods of time, thermal inversion of the *Z* isomer could have taken place in that experiment competing with the photoisomerization process, making it not possible to fully reach the PSS.

On the other hand, from the linear relationship between the first points of each graph of Figure 5.10 (representing $\ln [A_0] / [A]$ vs irradiation time and doing a linear fit), we can calculate the values for the kinetic constants of each process, and therefore, the value of the relative kinetic constant that relates the speed of both processes. In this particular case, if $k_{Z \rightarrow E} = 1$, then $k_{E \rightarrow Z} = 2$, which means that the $E \rightarrow Z$ initial isomerization rate is two times the $Z \rightarrow E$ reaction initial rate.

5.2.1.1. Photochemical and thermal stability of the photoswitches with structure based on the PSB-retinal chromophore.

Finally, we studied the photochemical and thermal stability of this new family of switches based on the PSB-retinal chromophore.

Concerning the photochemical stability of these switches, different compounds have been irradiated for several hours and followed by ^1H NMR, but no signals of other reactions apart from the ones corresponding to the isomerization process were noticed.

On the other hand, with respect to the thermal stability, once the PSS is reached, the mixture of *E/Z* isomers obtained is not stable in most cases for more than several hours at room temperature. There is a thermal back reaction towards the thermodynamically stable isomer (*E*), which allows recovering the initial stage. However, the speed of this thermal reaction depends on the substituents R_1 and R_2 of the molecule. A few examples are shown in Table 5.3, whose results were

obtained after following by ^1H NMR the thermal back reaction to recover the *E* isomer of several compounds.

Table 5.3

R₁	R₂	compound	<i>E</i> isomer recovery*
Me	Ph	5a	12
Me	<i>p</i> -MePh	5b	60
Me	<i>o</i> -MeOPh	5d	156

* time in hours, in the dark at 25°C.

If we compare the data from Table 5.3, we infer that the compound that reverts more easily to the *E* isomer is **5a**, where the phenyl group in R₂ doesn't have any substitution. But when the phenyl group in R₂ has a substituent, such as a *p*-methyl (**5b**) or an *o*-methoxy (**5d**), the recovery of *E* is slower, taking a few days to obtain the pure *E* form. In view of the experimentally obtained data from Table 5.3, the more electron-donor is the substituent, the slower is the return to the thermodynamically stable isomer (*E*). This is due to a higher energy barrier of the thermal transition state.

However, for other compounds such as **5n** (where R₁= Ph and R₂= 2-naphtyl), it is even necessary to heat the mixture of *E/Z* isomers reached at the PSS at 50°C for a few days in order to displace the equilibrium, since leaving the mixture at room temperature for several hours is not enough for the thermal back reaction to take place, and it eventually reverts to the pure *E* form.

This last feature is quite important as the main isomer of the mixture can be easily modified by choosing between light and heat. This could be useful in practical applications in which on/off switching are necessary.

5.2.2. Photochemical aspects of the mechanism of the isomerization reaction of photoswitches with structure based on the PSB-retinal chromophore.

This section will discuss the experimental studies carried out in order to gather information about the mechanism and efficiency of the photochemical reaction.

5.2.2.1. Excited state multiplicity.

When a molecular switch is irradiated, the absorption of a photon takes place, followed by the excitation of an electron to a higher energy state. The molecule goes from the ground state (S_0) to a singlet state (S_n) through an allowed singlet-singlet process. The excited singlet state can either react to give the reaction products (isomerization), or undergo a non radiant intersystem crossing (ISC) process to originate a new triplet state (T_n), being this latter the one that produces the final reaction (see Figure 5.2).

A way of determining which of the two states (S_n or T_n) is the responsible for the photochemical reactivity consists of carrying out the irradiation in the presence of triplet quenchers. Alkenes such as 1,3-pentadiene (*cis*-piperilene, which has a triplet energy of 57 kcal / mol), polyenes, or molecular oxygen (O_2) are a few examples of the most common triplet quenchers.⁵

Molecular oxygen (O_2) is a low energy triplet in its ground state ($^3\Sigma_g$) with two low excitation energy singlets ($^1\Delta_g$, 22.8 kcal/mol, and $^1\Sigma_g$, 37.9 kcal/mol), which means that molecules that have more energetic excited triplet states, $A^*(T_1)$, could be quenched by atmospheric oxygen (Figure 5.11).

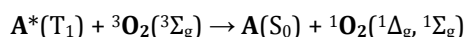


Figure 5.11. Quenching of a triplet state by molecular oxygen.

If the photoisomerization reaction of the switch takes place through triplets, solutions of a certain compound saturated with oxygen or deoxygenated would result in different reaction rates.

Knowing the nature of the excited state involved in the photoisomerization is relevant not only to explore alternative reactive pathways, but also to study the luminescence of these compounds.

⁵ Montalti, M.; Credi, A.; Prodi, L.; Gandolfi, M. T. *Handbook of Photochemistry, 3rd ed.*, CRC Press: Boca Raton, FL, **2006**.

5. Photochemical study

Therefore, the following experiment was performed in order to determine the excited state multiplicity of the reactive state for the new PSB-retinal based photoswitches, which consisted of the simultaneous irradiation of three samples of the same switch that were under different reaction conditions. For this purpose, we prepared 0.05 M solutions of compound **5f** in CDCl_3 in three different Pyrex NMR tubes. The first sample was deoxygenated and used as reference. The second sample was saturated with O_2 (triplet quencher) by bubbling air for 15 minutes. And finally, we deoxygenated the third sample and added *cis*-piperilene (5 equivalents), which is also a common triplet quencher as mentioned before. These three samples were irradiated simultaneously for 15 minutes in a 125-W medium-pressure Hg lamp. Then, the isomers ratio at that given time was measured from the ^1H NMR spectra of the samples, whose results appear in Table 5.4.

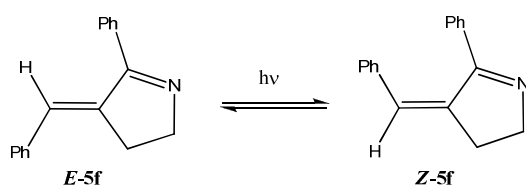


Table 5.4

Sample	% <i>E</i> -5f	% <i>Z</i> -5f
1	80	20
2	77	23
3	78	22

From the obtained data, we deduce that there is no change in the result of the photoisomerization process beyond the experimental error derivative of the NMR technique in any of the aforementioned experiments,⁶ so the progress of the reaction takes place through electronic states of singlet multiplicity, since the triplet quenchers have no effect over the reaction outcome.

⁶ For more detailed info see: Skoog, D. A. *Principios de Análisis Instrumental*, Mc-Graw Hill: Madrid, 2000.

These conclusions are in agreement with the expected results, as previous studies had showed the existence of excited electronic states of singlet multiplicity for analogous compounds.⁷

5.2.2.2. Isomerization quantum yield.

The quantum yield of a photochemical reaction, Φ , determines the efficiency of the process regarding the relationship between the number of photons absorbed by the system and the number of formed or destroyed molecules during the irradiation (Figure 5.12).

$$\Phi = \frac{\text{number of formed or destroyed molecules}}{\text{number of photons absorbed by the system}}$$

Figure 5.12. Equation expressing the quantum yield of a photochemical reaction

Using the previous expression, the isomerization quantum yield was calculated for two representative examples of photoswitches with structure based on the PSB-retinal chromophore, compound **5h** ($R_1 = \text{Ph}$, $R_2 = p\text{-MeOPh}$) and compound **5l** ($R_1 = \text{Ph}$, $R_2 = p\text{-NO}_2\text{Ph}$), following the procedure described in the literature, using *trans*-azobenzene as actinometer.⁸ In chemical actinometry, irradiation times are very short in order to avoid the interference of the reaction products in the light absorption of the starting compound.

The experiment with both switches was performed irradiating at 334 nm with monochromatic light solutions of *trans*-azobenzene in methanol, and **5h** and **5l** in acetonitrile. This method requires that the spectral width of the employed radiation to be short, so a monochromator was used to select the wavelength of the light source (Figure 5.13).

⁷ (a) Shichida, Y. *Photochem. Photobiol.*, **1990**, *52*, 1179. (b) Taiji, M.; Bryl, K.; Nakagawa, M.; Tsuda, M.; Kobayashi, T. *Photochem. Photobiol.*, **1992**, *56*, 1003. (c) Sampedro, D.; Migani, A.; Pepi, A.; Busi, E.; Basosi, R.; Latterini, L.; Elisei, F.; Fusi, S.; Ponticelli, F.; Zanirato, V.; Olivucci, M. *J. Am. Chem. Soc.*, **2004**, *126*, 9349.

⁸ Kuhn, H. J.; Braslavsky, S. E.; Schmidt, R. *Pure Appl. Chem.* **2004**, *76*, 2105.

5. Photochemical study

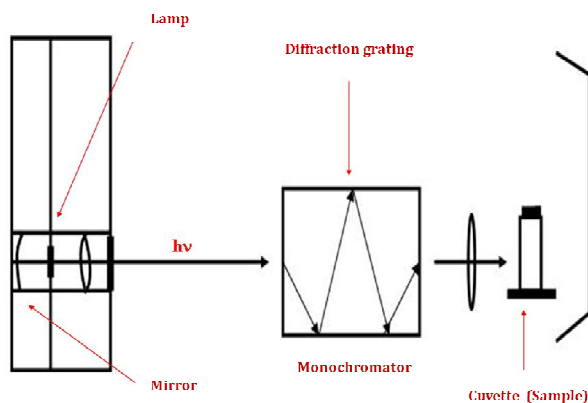


Figure 5.13. Scheme showing the performance of a monochromator.

In the appliance we used for irradiating, the light source is a 500-W Hg(Xe) lamp, being that light collected (through a mirror and lens) and directed towards the inlet slit of a monochromator. According to the manufacturer's specifications, with the inlet and outlet slits adjusted to 2 mm, the spectral width is approx. 20 nm. Finally, the monochromatic light is focused towards a quartz cuvette that contains the sample.

In the first place, a solution of *trans*-azobenzene in methanol was prepared in such way that the value of the absorbance at 358 nm was close to one.⁹ Then, after placing the actinometer solution in a quartz cuvette, the solution was irradiated at 334 nm. Each irradiation period should cause a change in absorbance at 358 nm of about 0.02. We chose $\lambda = 334$ nm for irradiating the samples because it was close to the maximum absorption values of compounds **5h** and **5l**.

Afterwards, a solution in acetonitrile of compounds **5h** and **5l** (100% *E* isomer) was prepared by adjusting the value of the absorbance at 334 nm to the one showed by the actinometer. These solutions were irradiated at 334 nm for a period of time that was fixed after several runs, as it depends on different factors such as the concentration or the irradiation wavelength. It should be pointed out that the conversion obtained after the irradiation time selected is recommended to

⁹ The values of the *trans*-azobenzene quantum yield are measured and tabulated so that the value of the absorbance at 358 nm is close to one. Distant values entail a relevant experimental error.

be around 20% (which means that after irradiating the isomers ratio should be around 80% (*E*)/ 20% (*Z*)). Moreover, the irradiation time of the sample doesn't have to be the same as the irradiation time of the actinometer.

As the concentration of the sample wasn't enough for recording the ¹H NMR spectra, after the selection of the adequate irradiation time, we irradiated three aliquots of each sample for exactly the same amount of time, taking this into account when doing the final calculations.

We calculated the number of photons absorbed by using the following formula:

$$E_p \text{ (mol of photons x cm}^{-2} \text{ x s}^{-1}) = F(\lambda) \times \Delta A(358\text{nm}) / t(\text{s})$$

where $\Delta A(358\text{nm})$ is the change in the absorbance at 358 nm of the *trans*-azobenzene solution when irradiating at 334 nm, and $t(\text{s})$ is the irradiation time responsible for that change. The F factor, which depends on the wavelength, has a value of 3.60×10^{-6} einstein $\times \text{cm}^{-2}$ at 334 nm.

Then, the number of photons absorbed corresponds to E_p multiplied by the irradiation time of the sample (in seconds).

To calculate the number of moles of *Z* isomer formed after irradiating the samples, the solvent of the samples was removed immediately after the irradiation and the residue dried properly. The amount of *Z* isomer formed was quantified by ¹H NMR, using 1,3,5-trimethoxybenzene as internal standard, as the proton signals of this standard didn't overlap with the signals of the isomers of the samples. From the integration of the signals it was possible to know the number of *Z* isomer formed.

Finally, the value for the isomerization quantum yield was the result of the equation shown in Figure 5.12.

Furthermore, at the end of the experiment the actinometer solution was measured again to prove that the light intensity had been constant. All the solutions were kept in the dark when they weren't irradiated.

The values of the isomerization quantum yield for the $E \rightarrow Z$ reaction of compounds **5h** and **5l** obtained were:

- for compound **5h** ($R_1 = \text{Ph}$, $R_2 = p\text{-MeOPh}$): $\Phi_{E \rightarrow Z} = 0.37 \pm 0.04$
- compound **5l** ($R_1 = \text{Ph}$, $R_2 = p\text{-NO}_2\text{Ph}$): $\Phi_{E \rightarrow Z} = 0.72 \pm 0.05$

Therefore, these new prototypes of molecular switches can be considered quite efficient. Moreover, the measured Φ value for compound **5l** is similar to the one obtained for the photoisomerization of the natural retinal chromophore ($\Phi = 0.67$) (see section 2.3.4).¹⁰ In addition to this, the Φ value of the new PSB-retinal based photoswitch **5l** is considerably better than the values described by Feringa and *col.* for overcrowded alkenes ($\Phi = 0.07\text{-}0.55$) (see section 2.5).

The fact that these molecular switches display high Φ values is directly related to the reaction path. As it has been previously described in section 2.6.1 (Figure 2.31), the reaction path for an efficient photoswitch involves that during the photoisomerization process, A^* evolves along a barrierless excited-state path, decays to a conical intersection (CI),¹¹ and finally relaxes also through a barrierless path to the energy minimum of photoproduct B. It requires that the aforementioned reaction path that connects A^* and B to be as simple as possible. This means that efficient molecular switches, such as the ones described in this dissertation, make good use of a great amount of the irradiation energy to generate the photoisomerization product.

5.2.2.3. Luminescence.

Once assessed the nature of the excited state involved in the photoisomerization and the value of the photoisomerization quantum yield, we

¹⁰ (a) Dartnall, H. *Vision Res.*, **1967**, *8*, 339. (b) Birge, R. R.; Einterz, C. M.; Knapp, H. M.; Murray, L. P. *Biophys. J.*, **1988**, *53*, 367 (c) Mathies, R. A.; Lugtenburg, J. In *Handbook of Biological Physics*; Stavenga, D. G., de Grip, W. J., Pugh, E. N. (eds.) Elsevier: Amsterdam, **2000**; Vol. 3, p 56.

¹¹ (a) Bernardi, F.; Olivucci, M.; Robb, M. A. *Chem. Soc. Rev.*, **1996**, 321. (b) Michl, J.; Bonacic-Koutecky, V. *Electronic Aspects of Organic Photochemistry*, Wiley & Sons Inc., New York, **1990**.

aimed for the study of deactivation processes that could diminish the efficiency of the switches with structure based on the PSB-retinal chromophore.

Therefore, we measured the emission and excitation spectra of two illustrative photoswitches: compound **5f** ($R_1 = \text{Ph}$, $R_2 = \text{Ph}$) and compound **5k** ($R_1 = \text{Ph}$, $R_2 = o\text{-BrPh}$).

First of all, a 3.0×10^{-5} M solution of **5f** in deoxygenated acetonitrile at 298 K was measured in a spectrofluorimeter. Only a weak emission band centered at 355 nm was obtained when exciting from 250 to 280 nm (Figure 5.14).

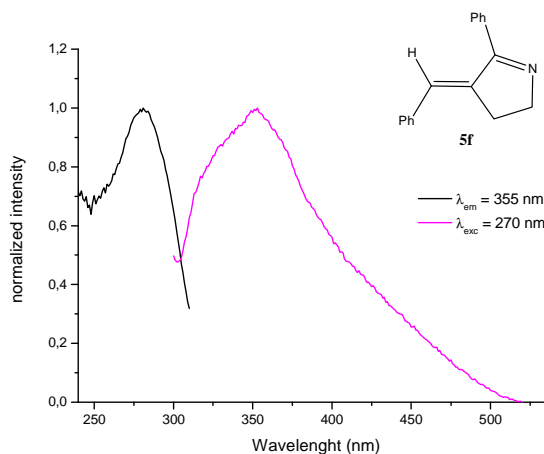


Figure 5.14. Excitation and emission spectra of compound 5f.

Afterwards, the fluorescence lifetime was measured using a 280 nm LED and was found to be 9.80×10^{-10} s. Finally, in order to determine the fluorescence quantum yield, a solution of *trans*-stilbene in deoxygenated hexane was used as standard of fluorescence. A solution of **5f** in deoxygenated acetonitrile was also prepared and the emission spectra for both compounds were measured using an excitation wavelength of 290 nm in a spectrofluorimeter. Under these conditions, a fluorescence quantum yield of $0.016 (\pm 0.005)$ was found.

On the other hand, a 2.6×10^{-5} M solution of **5k** in deoxygenated acetonitrile at 298 K was measured in a spectrofluorimeter. Only a weak emission band centered at 430 nm was obtained when exciting from 270 to 280 nm (Figure 5.15).

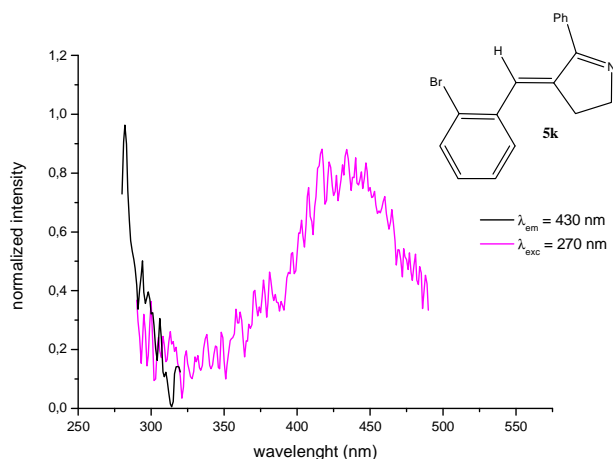


Figure 5.15. Excitation and emission spectra of compound 5k.

Then, the fluorescence lifetime was measured using a 280 nm LED and was found to be 9.64×10^{-10} s. The fluorescence quantum yield was also calculated using a solution of *trans*-stilbene in deoxygenated hexane as standard of fluorescence. A solution of **5k** in deoxygenated acetonitrile was prepared and the emission spectra for both compounds were measured using an excitation wavelength of 290 nm in a spectrofluorimeter. Under these conditions, a fluorescence quantum yield of $0.0005 (\pm 0.0001)$ was found.

The low values of the fluorescence quantum yields for both compounds show that deactivation through fluorescence does not effectively compete with the isomerization process. In fact, these results emphasize the adequate design of these switches as only a small fraction of the light energy is wasted in the radiative decay.

5.2.2.4. Sensitization tests.

As it has been described in section 5.2.2.1, the isomerization process carried out under standard conditions takes place through electronic states of singlet multiplicity (see section 5.1). However, it is known that excited states of different

multiplicity (singlet or triplet) can yield different reaction products.¹² Therefore, we considered attractive the idea of knowing what happened if the isomerization reaction could take place through electronic states of triplet multiplicity. For this purpose, we carried out another experiment in which the isomerization reaction of the photoswitches based on the PSB-retinal chromophore was achieved through sensitized irradiations.

A triplet sensitizer is a chemical compound with triplet energy high enough to be able to transfer its excess energy in the excited state to a molecule that forms a lower energy triplet (Figure 5.16).

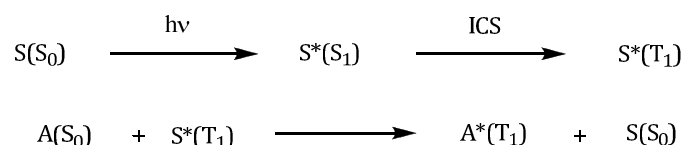


Figure 5.16. Sensitization process of a molecule A.

A good triplet sensitizer should feature intense absorption at the irradiation wavelength, high efficiency of the passage from singlet to triplet state (which means that it must have an intersystem crossing quantum yield close to one) and an excited triplet state lifetime long enough. Another required characteristic in order for the sensitization process to take place is that the triplet energy of the sensitizer must be higher than the triplet energy of the compound that it is going to be sensitized. The most common triplet sensitizers are ketones.¹³

In this particular case, we used thioxanthone as triplet sensitizer, whose UV-Vis spectrum is represented in Figure 5.17(a). The triplet energy of this triplet sensitizer is 63.2 kcal/mol, so any compound with lower triplet energy is sensitive to suffer a triplet energy transfer from thioxanthone.

¹² Turro, N. J.; Ramamurthy, V.; Scaiano, J. C. *Modern Molecular Photochemistry of Organic Molecules*. University Science Books: California, **2010**.

¹³ See ref. 5.

5. Photochemical study

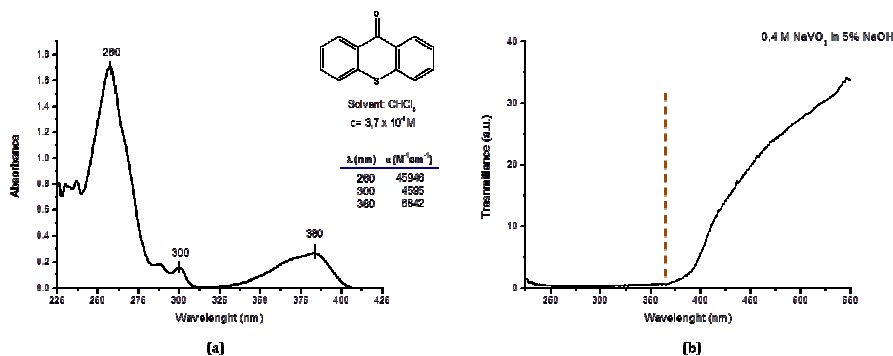


Figure 5.17. (a) UV-Vis spectrum of thioxanthone in CHCl_3 (b) Transmittance spectrum of a 0.4 M solution of NaVO_3 in 5% NaOH .

The next step consisted of the selection of the appropriate light filter with a transmittance spectrum that allowed the selective irradiation with a 125-W medium-pressure Hg lamp of thioxanthone without irradiating the photoswitches. Therefore, we chose a light filter that was composed of a 0.4 M solution of sodium metavanadate (NaVO_3) in 5% NaOH . After measuring the transmittance spectrum of this light filter (see Figure 5.17(b)), we inferred that it was adequate for irradiating the switches, since it avoids the radiation at wavelengths lower than 370 nm, region where thioxanthone absorbs but there is no absorption of the photoswitches.

For irradiation under sensitized conditions, we selected the following switches: compound **5f** ($R_1 = \text{Ph}$, $R_2 = \text{Ph}$), compound **5h** ($R_1 = \text{Ph}$, $R_2 = p\text{-MeOPh}$), and compound **5i** ($R_1 = \text{Ph}$, $R_2 = p\text{-NO}_2\text{Ph}$), as they present no relevant absorptions at wavelengths higher than 370 nm.

Then, in three Pyrex NMR tubes, we prepared 0.1 M solutions of each compound in CDCl_3 and added 1 equivalent of thioxanthone to each sample. Afterwards, we irradiated the three samples until the photostationary state was reached. The values of the isomers ratio at the photostationary state for the sensitized and standard reactions (see Table 5.2) are shown in Table 5.5.

Table 5.5

Entry	Compound	Irradiation conditions	% <i>E</i> isomer*	% <i>Z</i> isomer*
1	5f	Standard	76	24
2		Sensitized	57	43
3	5h	Standard	75	25
4		Sensitized	75	25
5	5l	Standard	30	70
6		Sensitized	50	50

* Isomers ratio at the photostationary state.

From these results, we can infer that the isomers ratio at the PSS under sensitized conditions may be different from the isomers ratio obtained when carrying out the reaction under standard conditions, as observed for compounds **5f** and **5l**. In addition to this, there is a triplet energy transfer from the triplet state of thioxanthone to form the excited triplet state of the switches, which afterwards reacts to give the isomerization product. Therefore, the triplet energy of the photoswitches is lower than 63.2 kcal/mol. In order to find the approximate value of the triplet energy of the photoswitches, it would be necessary to carry out this experiment with diverse triplet sensitizers with different triplet energies, so the values result delimited in an interval of energies. This latter subject and other related studies are still in progress.

5.2.3. Photochemical study of methylated photoswitches with structure based on the PSB-retinal chromophore.

As it has been discussed in section 2.3.4, the natural retinal chromophore is attached to the protein in which is embedded through a protonated Schiff base. Therefore, any attempt to mimic the structure of this chromophore should feature a quaternization of the nitrogen atom that belongs to the imine group. In related compounds, such as fluorenylidene-pyrrolines (FPs) (see section 2.6.3),¹⁴ this

¹⁴ Rivado-Casas, L.; Sampedro, D.; Campos, P. J.; Fusi, S.; Zanirato, V.; Olivucci, M. *J. Org. Chem.* **2009**, *74*, 4666.

quaternization (specifically, methylation) of the nitrogen atom causes a bathochromic shift of the low energy band of approximately 50 nm in the UV spectra compared to the neutral compounds, presenting absorption even in the visible region (see Figure 2.36). As we said before, this permits completing the photoisomerization reaction with solar light, which is a clean and renewable kind of energy. Moreover, methylation also speeds up the photoisomerization process, so that the reaction is 4 times faster with NAFPs than with FPs.

If the methylated photoswitches based on the PSB-retinal studied in this dissertation are irradiated, an induced movement analogous to the one shown in Figure 5.3 is provoked, which consists of the rotation around the C=C double bond to achieve the corresponding *E* or *Z* isomers.

Prior to the irradiation of these methylated compounds, their UV-Vis spectra were recorded, so as to compare the obtained results to the UV-Vis spectra of the neutral compounds. Therefore, we prepared 10^{-5} M solutions of compound **5f** ($R_1 = \text{Ph}$, $R_2 = \text{Ph}$), compound **5h** ($R_1 = \text{Ph}$, $R_2 = p\text{-MeOPh}$), and compound **5i** ($R_1 = \text{Ph}$, $R_2 = p\text{-NO}_2\text{Ph}$) in acetonitrile. Afterwards, the obtained spectra for each compound were plotted in the same axes with the spectrum of their corresponding neutral compound.

In Figure 5.18, the UV-Vis spectra of compounds **5f** and **5f-met** are represented.

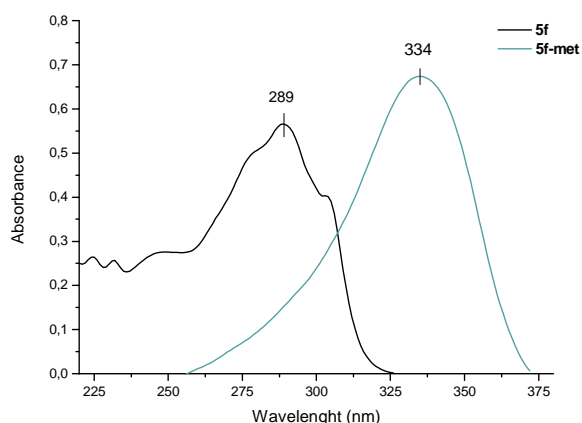


Figure 5.18. UV-Vis spectra of **5f** and **5f-met** in acetonitrile.

We discerned that there was a bathochromic shift of the maximum of the absorption band ($\Delta\lambda_{\text{max}} = 45 \text{ nm}$) when methylating **5f**.

Moreover, the UV-Vis spectra of compounds **5h** and **5h-met** are represented in Figure 5.19.

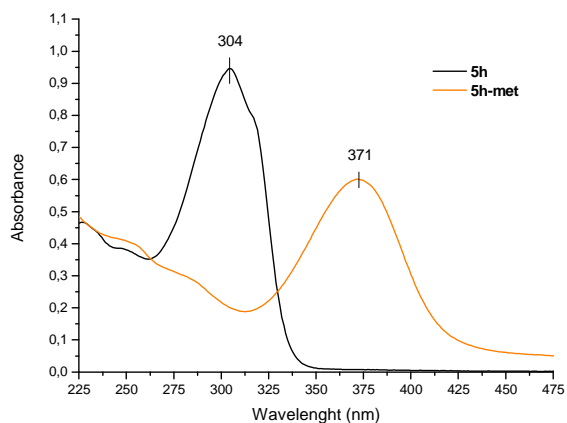


Figure 5.19. UV-Vis spectra of 5h and 5h-met in acetonitrile.

In this case, there was a noticeable bathochromic shift of the maximum of the absorption band ($\Delta\lambda_{\text{max}} = 67 \text{ nm}$) when methylating **5h**.

Finally, in Figure 5.20, the UV-Vis spectra of compounds **5l** and **5l-met** are represented.

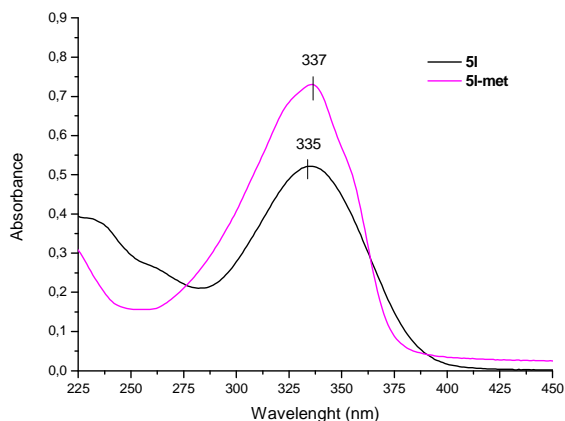


Figure 5.20. UV-Vis spectra of **5I** and **5I-met** in acetonitrile.

Interestingly, there was almost no change in the absorption band after methylating compound **5I** ($\Delta\lambda_{\text{max}} = 2$ nm).

The aforementioned results can be explained according to the relative stabilization of the ground and excited states that occurs when methylating the compounds. This effect was observed in earlier studies on *N*-methylated benzylidene-pyrrolines (see section 2.6.1).¹⁵ In the case of the methylated compounds, this was due to the effect of the (solvated) negative counterion present in solution on the different electronic structure (charge distribution) of the ground and excited states of the switches. In the ground state, the positive charge is found in the nitrogen atom that belongs to the imine group. However, in the excited state, this positive charge is delocalized in the aromatic ring. Therefore, substituents of the aromatic ring that stabilize this positive charge will lead to a stabilization of the excited state.

Regarding **5f** and **5f-met** ($R_1 = \text{Ph}$, $R_2 = \text{Ph}$), the excited state is moderate stabilized after methylating, so the gap between the excited and ground states is reduced, producing a bathochromic shift of the maximum wavelength for absorption ($\Delta\lambda_{\text{max}} = 45$ nm).

¹⁵ See ref. 7(c).

However, in the case of **5h** and **5h-met** ($R_1 = \text{Ph}$, $R_2 = p\text{-MeOPh}$), there is a remarkable stabilization of the excited state due to the presence of an electron-donor group in the phenyl group of substituent R_4 . This causes a significant reduction of the gap between the excited and ground states, and displaces the absorption band towards less energetic regions ($\Delta\lambda_{\text{max}} = 67 \text{ nm}$).

In the last place, what happens with **5l** and **5l-met** ($R_1 = \text{Ph}$, $R_2 = p\text{-NO}_2\text{Ph}$) is that the presence of an electron-withdrawing group in R_4 scarcely destabilizes the excited state, so the gap between the excited and ground states is not altered and there is no change in the absorption band.

With the aim of confirming this trend and obtaining a photoswitch that absorbs in the visible region, we tried to carry out the reaction between the azido phosphonate **3** and 2, 4, 6-trimethoxybenzaldehyde (see section 4.1.1). The presence of three methoxy groups in R_4 should highly stabilize the excited state and produce a considerable displacement of the absorption band. However, after letting the reaction stirring for several weeks and rising the temperature to 40°C , the corresponding azido enone **4** was not obtained.

On the other hand, we also measured the UV-Vis spectrum of **5n** ($R_1 = \text{Ph}$, $R_2 = 2\text{-naphthyl}$). In the following figure, the spectra of compounds **5n** and **5n-met** are represented.

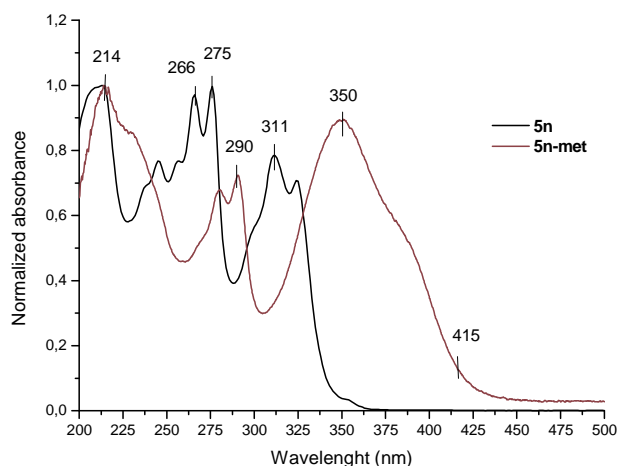
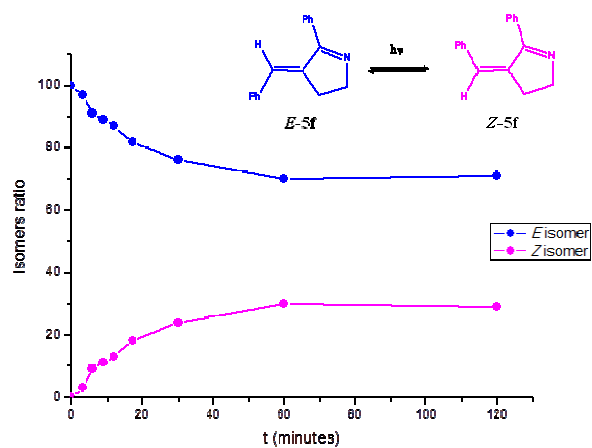


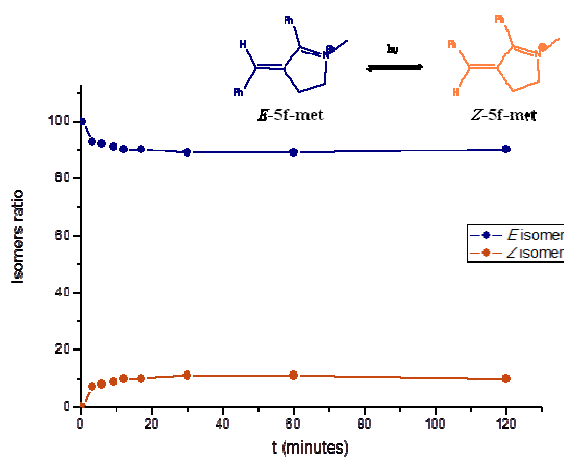
Figure 5.21. UV-Vis spectra of **5n** and **5n-met** in acetonitrile.

In the same way as it happened with compounds **5f** and **5h**, there is a bathochromic shift of the absorption band when methylating compound **5n** ($\Delta\lambda_{\text{max}} \approx 40$ nm), which allows the absorption of light even in the visible region. This fact is quite relevant because low energy light can be used to irradiate this compound, which means that visible and solar light could be used instead of UV light to produce the isomerization reaction, as it occurred when methylating fluorenylidene-pyrrolines (FPs) (see section 2.6.3).

After analyzing the UV-Vis spectra of the methylated photoswitches, we proceeded to irradiate them. In order to compare the isomerization process of the neutral and methylated compounds, we designed the following experiment. In two Pyrex NMR tubes, we prepared 0.1 M solutions of the neutral and methylated compounds of each photoswitch (**5f** / **5f-met**, **5h** / **5h-met**, **5l** / **5l-met** and **5n** / **5n-met**) in CDCl_3 . Then, we irradiated each pair of samples of compounds in a 125-W medium-pressure Hg lamp until the photostationary state was reached, being the reaction followed by ^1H NMR. Representing the isomers ratio vs. the irradiation time starting from 100% of the *E* isomer for each pair of neutral and methylated compounds, we obtained two graphs for each compound such as those shown in Figure 5.22 for compounds **5f** (a) and **5f-met** (b).



(a)



(b)

Figure 5.22. Graphs where the isomers ratio is represented vs. the irradiation time starting from 100% of the *E* isomer (a) of the neutral compound 5f and (b) of the methylated compound 5f-met.

For each of the other pairs of compounds, similar graphs were obtained for the isomerization of the neutral and methylated compounds. The obtained results are summarized in the following table (Table 5.6).

Table 5.6

Entry	Compound	% <i>E</i> <i>isomer</i> *	% <i>Z</i> <i>isomer</i> *	$k_{\text{met/neutral}}$ **
1	5f	70	30	1.5
2	5f-met	90	10	
3	5h	56	44	1.4
4	5h-met	68	32	
5	5l	34	66	1.1
6	5l-met	40	60	
7	5n	48	52	1.2
8	5n-met	75	25	

* Isomers ratio at the photostationary state.

** relative kinetic constants ($k_{\text{met/neutral}}$).

From these results, we can deduce that in all cases the percentage of the *Z* isomer (photochemically obtained isomer) at the photostationary state is higher when the compounds are in their neutral form than if they are methylated.

On the other hand, from the linear relationship between the first points of each graph for each pair of compounds (representing $\ln [A_0] / [A]$ vs. irradiation time and doing a linear fit), we can calculate the values for the kinetic constants of each process, and therefore, the value of the relative kinetic constant that relates the speed of both processes (see Table 5.6). In all cases, being the kinetic constant for the neutral compounds $k_{\text{neutral}} = 1$, we noticed that the $E \rightarrow Z$ isomerization process for the methylated compounds is approx. 1.5 times faster than the $E \rightarrow Z$ reaction for the neutral compounds. Therefore, methylation of the photoswitches caused only a mild acceleration of the speed of the isomerization reaction. However, as it has been already discussed, in related compounds such as FPs,¹⁶ the speed increase was four times higher for the methylated than the neutral compounds.

¹⁶ See ref. 14.

5.2.4. Photochemical study of metallated photoswitches with structure based on the PSB-retinal chromophore.

Finally, we briefly studied the metallated compound (**5f-Ag**) that we had obtained from the reaction of two equivalents of compound **5f** and Ag^+ (Figure 5.23).

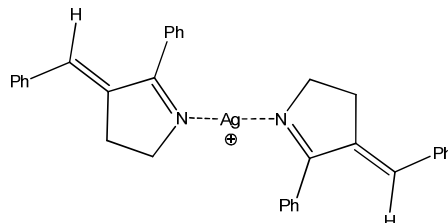


Figure 5.23. Compound **5f-Ag**.

In the first place, the UV-Vis spectrum of a 10^{-5} M solution of compound **5f-Ag** in THF was recorded in order to compare it with the UV-Vis spectrum of **5f** in THF (Figure 5.24).

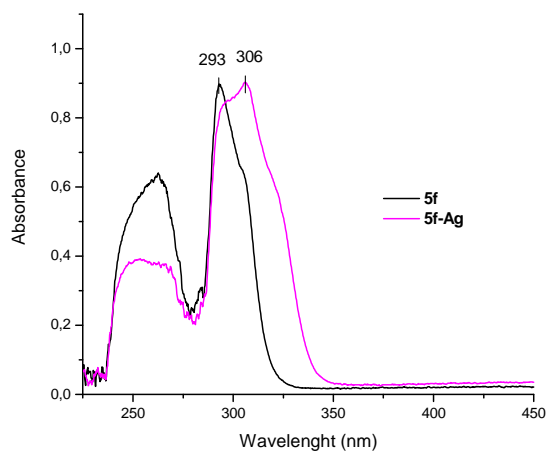


Figure 5.24. Comparison of the UV-Vis spectra of compounds **5f** and **5f-Ag** in THF.

We observed that there was a bathochromic shift of the maximum of the absorption band ($\Delta\lambda_{\text{max}} = 13$ nm) when compound **5f** was coordinated to silver (I). Then, we recorded the emission spectrum of a 10^{-5} M solution of compound **5f-Ag**

in THF to see if there was any difference with the emission spectrum obtained for **5f** in THF (Figure 5.25).

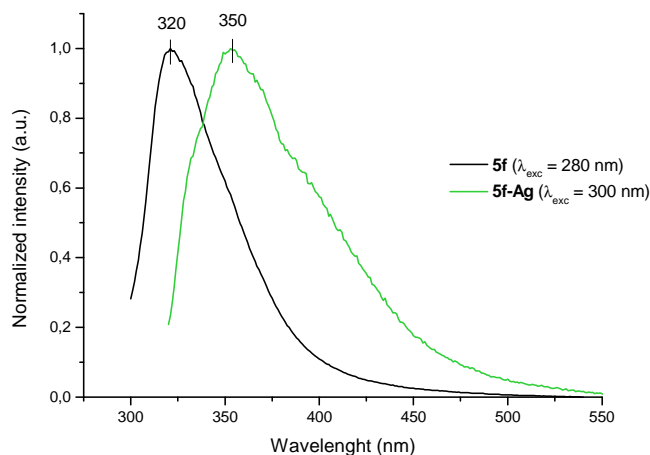


Figure 5.25. Comparison of the emission spectra of compounds **5f and **5f-Ag** in THF.**

We noticed that there was also a bathochromic shift of the maximum of the emission band ($\Delta\lambda_{max} = 30$ nm) when compound **5f** was coordinated to silver (I).

From these results we deduce that there is an effect of the metallic center in the photophysical properties of the compound, so the photochemical properties should be also influenced by the presence of silver (I). However, as silver is easily reduced from Ag (I) to Ag (0) with light, it is not useful to irradiate **5f-Ag**. Therefore, in the near future it is necessary to carry out again this essay with different cations, such as zinc or copper.

5.3. PHOTOCHEMICAL STUDY OF PHOTOSWITCHES WITH STRUCTURE BASED ON THE GFP CHROMOPHORE.

5.3.1. Photochemical study of photoswitches with structure based on the GFP chromophore.

In this section, the photochemical behavior of the photoswitches with structure based on the GFP chromophore will be described. Regarding this kind of prototypes of molecular switches, the irradiation with UV light results in the induced movement shown in Figure 5.26 with green arrows, which corresponds to the rotation around the central C=C double bond so as to obtain the corresponding *Z* or *E* isomers. If we recall what has been mentioned in section 2.3.5, we realize that this photoisomerization process is analogous to the one that occurs in the green fluorescent protein (GFP) chromophore.

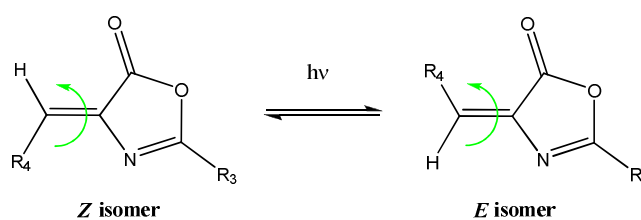


Figure 5.26. *Z/E* photoisomerization process undergone by the molecular switches with structure based on the GFP chromophore.

Prior to the irradiation process, the UV-Vis spectra for all the synthesized compounds were measured. The values for the maximum wavelengths and the extinction coefficients of the bands found for each compound in acetonitrile are displayed in Table 5.7. From these results, we can infer that there is a bathochromic shift of the maximum wavelength of absorption when changing R_3 from a methyl (switch **7i**, entry 8) to a phenyl (switch **7b**, entry 2) or a *p*-tolyl (switch **7s**, entry 17) group due to the extended conjugation. However, there are no significant differences when having as R_3 a phenyl (switch **7b**, entry 2) or a *p*-tolyl (switch **7s**, entry 17) group. On the other hand, there is a red-shift when R_3 = Me and R_4 varies from Ph (switch **7h**, entry 7) to *p*-MeOPh (switch **7j**, entry 9) or *p*-NO₂Ph (switch **7l**, entry 11). This shift is also noticeable when maintaining R_3 = Me and changing R_4 from a phenyl (switch **7h**, entry 7) to a heterocycle such as 3-thiophene (switch **7q**, entry 16). The same effect is observed when another

5. Photochemical study

aromatic ring is added (switch **7p**, entry 15) in R_4 and R_3 remains unchanged. Nevertheless, there is no variation of the maximum wavelength of absorption when having the same R_3 and changing the substituent of the phenyl group of R_4 from *para* (switch **7e**, entry 5) to *ortho* (switch **7f**, entry 6) position. Finally, it must be highlighted that some of the compounds with $R_3 = \text{Ph}$ present absorption in the visible region (see UV-Vis of compound **7c**, Figure 5.27).

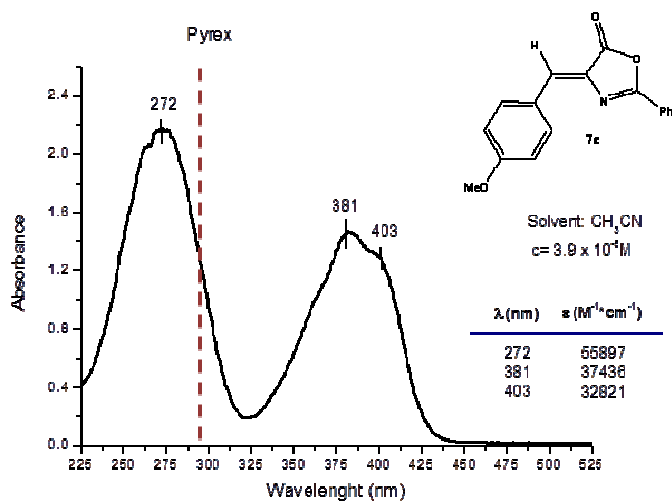


Figure 5.27. UV-Vis absorption spectrum of compound **7c** in acetonitrile.

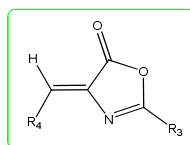
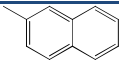
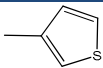


Table 5.7

Entry	R ₃	R ₄	Compound (Z isomer)	$\lambda_{\max}(\text{nm})/\epsilon$ (M ⁻¹ cm ⁻¹) in CH ₃ CN
1	Ph	Ph	7a	360 / 81673
2	Ph	<i>p</i> -MePh	7b	367 / 33333
3	Ph	<i>p</i> -MeOPh	7c	381 / 37436 403 / 32821
4	Ph	<i>o</i> -MeOPh	7d	385 / 12394 403 / 10704
5	Ph	<i>p</i> -BrPh	7e	366 / 37839
6	Ph	<i>o</i> -BrPh	7f	366 / 10492
7	Me	Ph	7h	327 / 26633
8	Me	<i>p</i> -MePh	7i	336 / 39091
9	Me	<i>p</i> -MeOPh	7j	355 / 28261
10	Me	<i>o</i> -MeOPh	7k	363 / 27900
11	Me	<i>p</i> -NO ₂ Ph	7l	350 / 24769
12	Me	<i>p</i> -CNPh	7m	334 / 39000
13	Me	<i>p</i> -MeCO ₂ Ph	7n	331 / 20909
14	Me	<i>p</i> -BrPh	7o	333 / 24407
15	Me		7p	342 / 25490
16	Me		7q	358 / 20679
17	<i>p</i> -MePh	<i>p</i> -MePh	7s	370 / 37273

5. Photochemical study

Besides, the UV-Vis spectra of the compounds shown in Table 5.7 were measured in diverse solvents with different polarity:¹⁷ acetonitrile (polarity 0.460) and chloroform (polarity 0.259), in order to test if there was any solvent effect. To illustrate this, the UV-Vis spectra of compounds **7h** and **7o** in acetonitrile and chloroform are shown respectively in Figures 5.28 and 5.29.

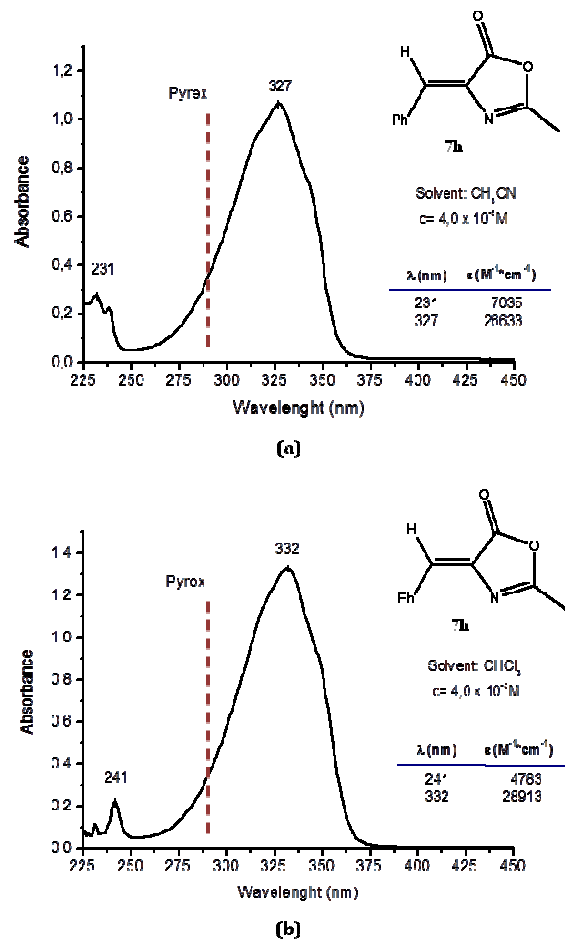
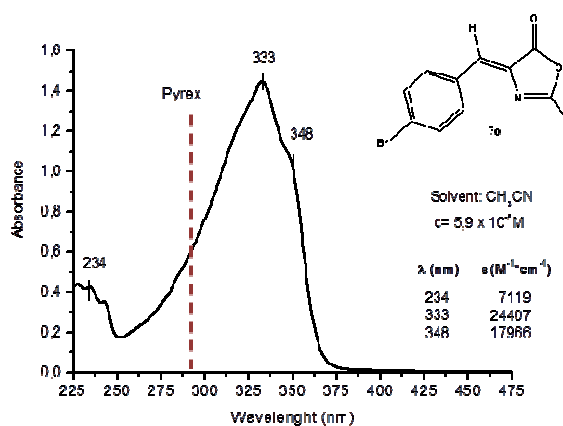
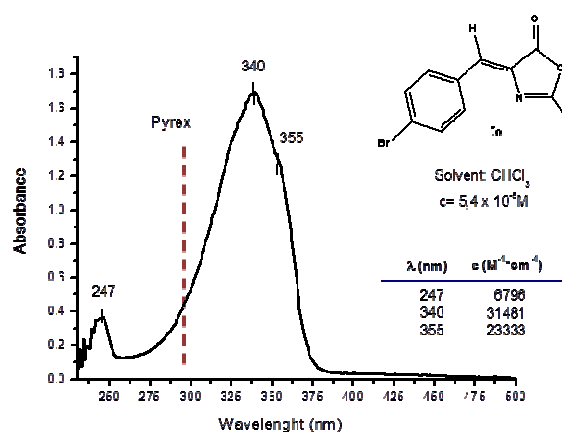


Figure 5.28. UV-Vis absorption spectrum of compound **7h** in (a) acetonitrile and (b) chloroform.

¹⁷ Normalized parameters based on empiric data of solvent polarity (E_T^N). For further info, see: Reichardt, C. *Solvents and solvent effects in organic chemistry 3rd ed.*, Wiley-VCH, Weinheim, 2003, page 418.



(a)



(b)

Figure 5.29. UV-Vis absorption spectrum of compound **7o** in (a) acetonitrile and (b) chloroform.

From Figures 5.28 and 5.29, which are shown above, we deduced that the maximum absorption wavelength of the band suffers a slight red-shift when changing from a polar (acetonitrile) to a non-polar (chloroform) solvent. However, in general terms, we can consider that the UV spectra of both compounds remains almost the same, so we can use them indiscriminately as the photophysical properties, isomerization kinetics and photostationary state composition won't suffer major changes. Nevertheless, in section 5.3.1.3, we will review the effect of using diverse solvents with different polarities in the photoisomerization reaction.

The analysis of the UV-Vis spectra of the photoswitches with structure based on the GFP chromophore deduced that for irradiating the different compounds, a Pyrex filter can be used to avoid radiation below 290 nm (see Figures 5.27, 5.28 and 5.29). As the light source, a 125-W medium-pressure Hg lamp was used. The results for the irradiation in an immersion well reactor of 0.01 M solutions of a selection of photoswitches based on the GFP chromophore in acetonitrile are shown in Table 5.8. The irradiation process of each compound was followed by ^1H NMR, at different time intervals, until the photostationary state (PSS) was reached, since *Z* and *E* isomers have distinctive ^1H NMR signals (see as an example the ^1H NMR spectra for the isomerization process of compound **7k** at different irradiation times in Figure 5.30). Integration of the ^1H NMR signals corresponding to each isomer allowed us to know the isomers ratio at a given irradiation time. Depending on the absorption bands, the irradiated mixture took from 1 to 3 hours to reach the PSS.

From the values obtained for the isomers ratio at the PSS for every compound shown in Table 5.8, we can interpret the following trends. When changing R_3 from a methyl (switch **7h**, entry 5) to a phenyl (switch **7a**, entry 1), there isn't a noticeable change of the isomers ratio at the PSS. However, the values for the isomers ratio at the PSS depend on the substituent of the phenyl group of R_4 , as different results are found in each case, but without being consistent with a regular trend. On the other hand, when having the same R_3 and changing the substituent of the phenyl group of R_4 from *para* (switch **7c**, entry 2) to *orto* (switch **7d**, entry 3) position, it is observed that the percentage of *E* isomer increases. Nevertheless, if another aromatic ring is added (switch **7p**, entry 13) in R_4 and R_3 remains the same, there is no perceptible modification of the isomers ratio at the PSS. Finally, there is also an increase of the percentage of *E* isomer at the PSS when maintaining $\text{R}_3 = \text{Me}$ and changing R_4 from a phenyl (switch **7h**, entry 5) to a heterocycle such as 3-thiophene (switch **7q**, entry 14). Therefore, we conclude that the value of the isomers ratio at the photostationary state can be varied depending on the structure substitution, which also happened with PSB-retinal photoswitches (see section 5.2.1).

Notwithstanding, when we proceeded to irradiate the compounds where the substituent of the phenyl group of R_4 was an electron-withdrawing group, other side reactions took place apart from the photoisomerization process that decreased the reaction yield.

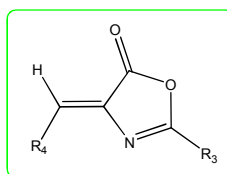


Table 5.8

Entry	R ₃	R ₄	Compound	Ratio at PSS*	
				% Z	% E
1	Ph	Ph	7a	75	25
2	Ph	<i>p</i> -MeOPh	7c	83	17
3	Ph	<i>o</i> -MeOPh	7d	65	35
4**	Ph	<i>p</i> -BrPh	7e	75	25
5	Me	Ph	7h	85	15
6	Me	<i>p</i> -MePh	7i	85	15
7	Me	<i>p</i> -MeOPh	7j	85	15
8	Me	<i>o</i> -MeOPh	7k	64	36
9**	Me	<i>p</i> -NO ₂ Ph	7l	83	17
10**	Me	<i>p</i> -CNPh	7m	75	25
11**	Me	<i>p</i> -MeCO ₂ Ph	7n	80	20
12**	Me	<i>p</i> -BrPh	7o	85	15
13	Me		7p	83	17
14	Me		7q	60	40

* Isomers ratio at the photostationary state.

** Other side reactions take place apart from the photoisomerization. One of these reactions was the [2+2] cycloaddition reaction between two molecules of the photoswitch, which was also observed when irradiating in solid state (see section 5.3.1.5).

5. Photochemical study

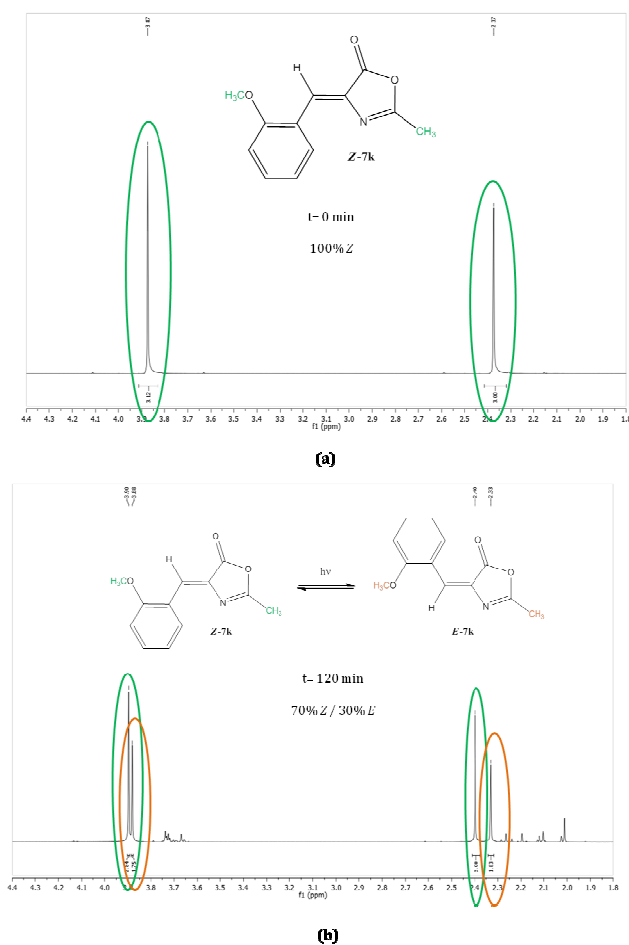


Figure 5.30. ^1H NMR spectra for the isomerization process of compound **7k** at (a) $t = 0$ min, and (b) $t = 120$ min.

As soon as the isomers ratio at the photostationary state has been determined, the following step is trying to separate the two isomers (Z and E) so as to individually characterize and study them. For this purpose, we irradiated a 0.01 M solution of compound **7h** (100% Z isomer at $t = 0$ min) in acetonitrile in an immersion well reactor with a 125-W medium-pressure Hg lamp, and a Pyrex filter, until the PSS was reached. Later, we separated the resulting mixture of isomers by flash chromatography on silica gel, using hexane/ ethyl acetate (10:1) as eluent. By this means we could have the two isomers (Z and E) separately, so we

could record the NMR and UV-Vis spectra of the *E* isomer (see experimental section and appendix A) and contrast it with the thermodynamically more stable isomer (*Z*).

Not only the two isomers of compound **7h** could be isolated following this procedure, but also the isomers of other compounds could be separated by flash chromatography on silica gel, using hexane/ ethyl acetate (10:1) as eluent. For instance, the data of the NMR spectra of the *E* isomer of compound **7k** is shown in the experimental section and appendix A, so it can be compared with the NMR spectra of the thermodynamically stable isomer (*Z*).

Once we have the *Z* and *E* isomers separately, we can perform an experiment to study the kinetics of the isomerization reaction. For this purpose, we prepared in two distinctive Pyrex NMR tubes two solutions of the same concentration in CDCl₃. In the first NMR tube, we got ready a solution 0.07 M of the *Z* isomer of compound **7h**. Next, in the second NMR tube, we prepared a solution 0.07 M of the *E* isomer of compound **7h**. Afterwards, both NMR tubes were irradiated in a 125-W medium-pressure Hg lamp and a Pyrex filter, until both solutions reached the PSS. As the samples were directly dissolved in CDCl₃, it was easy to follow the photoisomerization reaction by ¹H NMR at short irradiation intervals. Therefore, ¹H NMR spectra of the two samples were performed every 3 minutes with the aim of tracking the isomerization process of the compounds **Z-7h** and **E-7h**. Representing the isomers ratio vs. the irradiation time, we obtained the two graphs that are shown in Figure 5.31, (a) corresponding to the sample with 100% of **Z-7h** isomer at the beginning of the reaction, and (b) corresponding to the sample with 100% of **E-7h** isomer at $t_{\text{irrad}}=0$ min.

5. Photochemical study

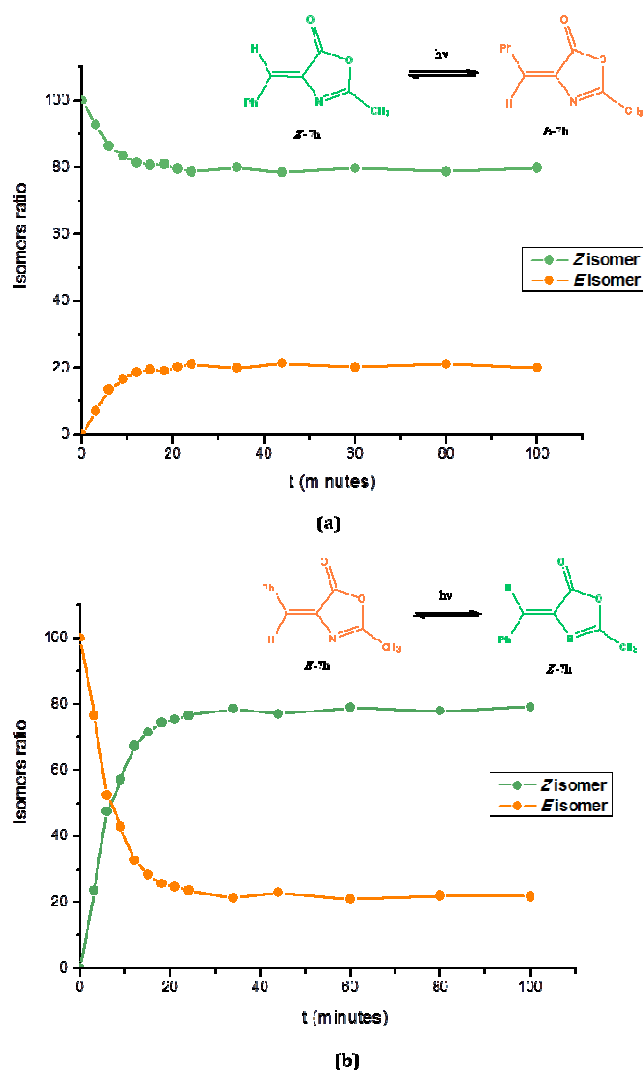


Figure 5.31. Graphs where the isomers ratio is represented vs. the irradiation time (a) starting from a 100% of the Z isomer, and (b) starting from a 100% of the E isomer of compound 7h.

The following conclusions can be inferred out of the graphs represented in Figure 5.31:

- Part (a): When we started from 100% of the *Z* isomer, the photostationary state was reached after 30 min of irradiation, time after which the isomers ratio remained constant and with a value of 79% (*Z*) / 21% (*E*).
- Part (b): If we started from 100% of the *E* isomer, it took approx. 35 min to reach the PSS, being the value for the isomers ratio from this point 79% (*Z*) / 21% (*E*).
- Therefore, we checked that the isomers ratio at the PSS is independent from the starting isomer (*Z* or *E*), as it happened when carrying out this experiment with PSB-retinal photoswitches (see section 5.2.1).

In addition to this, we can compare the results for the isomers ratio at the PSS reached during this experiment, 79% (*Z*) / 21% (*E*), and the value obtained when irradiating in an immersion well reactor, 85% (*Z*) / 15% (*E*) (see Table 5.8, entry 5). As the obtained isomers ratio at the PSS is similar in both cases, we can presume that there isn't a noticeable difference when irradiating under both conditions and that thermal isomerization is not a relevant process for this kind of compounds.

On the other hand, from the linear relationship between the first points of each graph of Figure 5.31 (representing $\ln [A_0] / [A]$ vs irradiation time and doing a linear fit), we can calculate the values for the kinetic constants of each process, and therefore, the value of the relative kinetic constant that relates the speed of both processes. In this particular case, if $k_{Z \rightarrow E} = 1$, then $k_{E \rightarrow Z} = 4.5$, which means that the $E \rightarrow Z$ isomerization process is 4.5 times faster than the $Z \rightarrow E$ reaction.

Besides this experiment, when both samples reached the PSS, we proceeded to heat them at 50°C in the dark for several hours, in order to see if the isomers ratio was altered. By studying the ¹H NMR spectra of the heated samples, we deduced that at that temperature the isomers ratio remained unchanged.

The same whole experiment was carried out with the two isomers (*Z* and *E*) of compound **7k**. Representing values for the isomers ratio vs. the irradiation time extracted from the ¹H NMR spectra, we obtained the two graphs that are shown in Figure 5.32, (a) corresponding to the sample with 100% of **Z-7k** isomer at the beginning of the reaction, and (b) corresponding to the sample with 100% of **E-7k** isomer at $t_{\text{irrad}}=0$ min.

5. Photochemical study

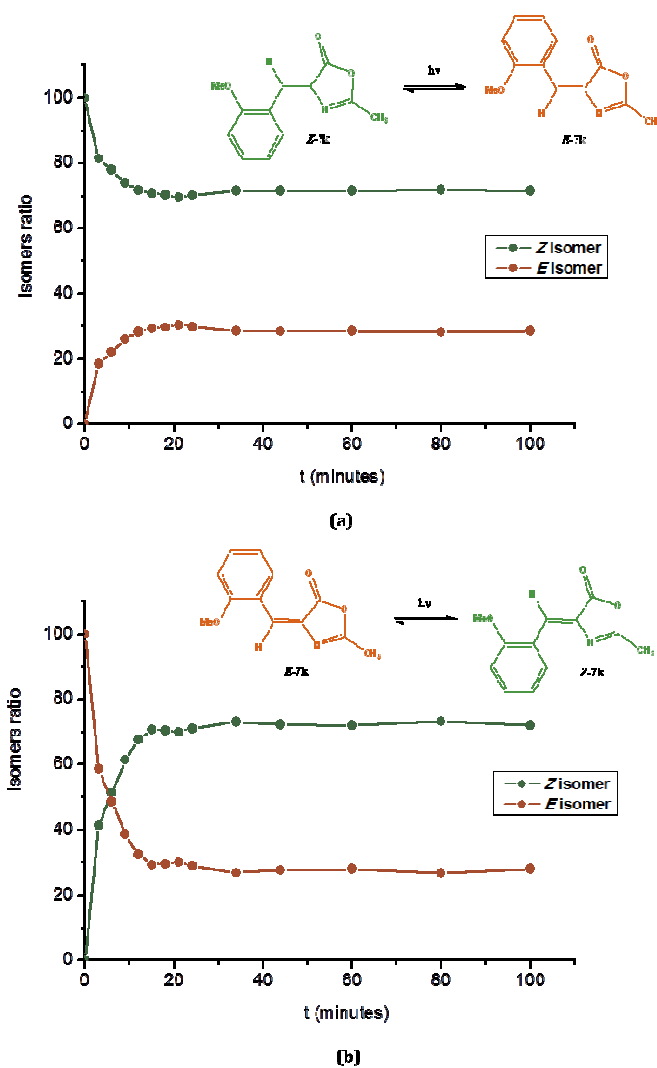


Figure 5.32. Graphs where the isomers ratio is represented vs. the irradiation time (a) starting from a 100% of the Z isomer, and (b) starting from a 100% of the E isomer of compound 7k.

From Figure 5.32 we can infer that the value of the isomers ratio at the PSS for these two processes is 70% (Z) / 30% (E), which is reached after approx. 35 minutes of irradiation.

Moreover, the results for the isomers ratio at the PSS reached during this experiment, 70% (*Z*) / 30% (*E*), and the value obtained when irradiating in an immersion well reactor, 64% (*Z*) / 36% (*E*) (see Table 5.8, entry 8) can be contrasted. As seen with compound **7h**, the obtained isomers ratio at the PSS is similar in both cases, so we can presume that there isn't a discernible difference when irradiating under both conditions and that thermal isomerization is not a significant process for this kind of compounds.

If we calculate the values for the kinetic constants of each process from the first points of each graph of Figure 5.32, we can determine the value of the relative kinetic constant that relates the speed of both processes. In this particular case, if $k_{Z \rightarrow E} = 1$, then $k_{E \rightarrow Z} = 3$, which means that the $E \rightarrow Z$ isomerization process is three times faster than the $Z \rightarrow E$ reaction.

Additionally, when both samples reached the PSS, we heated them at 50°C in the dark for several hours to see if the isomers ratio was altered. From the ¹H NMR spectra of the warmed samples, we inferred that at that temperature the isomers ratio remained unchanged.

5.3.1.1. Selective irradiation of the two isomers (*Z* and *E*) of the photoswitches with structure based on the GFP chromophore.

When we plotted the UV-Vis spectra of solutions of the same concentration in acetonitrile of the two isomers of compound **7h** in the same axes (Figure 5.33), we realized that there were slight differences in the shape of their absorption bands, as it happened with the compounds with structure based on the PSB-retinal (see section 5.2.1, Figure 5.9). Thanks to this effect, we could selectively irradiate in different regions of the absorption spectrum of each isomer with monochromatic light so as to obtain different isomers ratio at the PSS depending on the irradiation wavelength.

5. Photochemical study

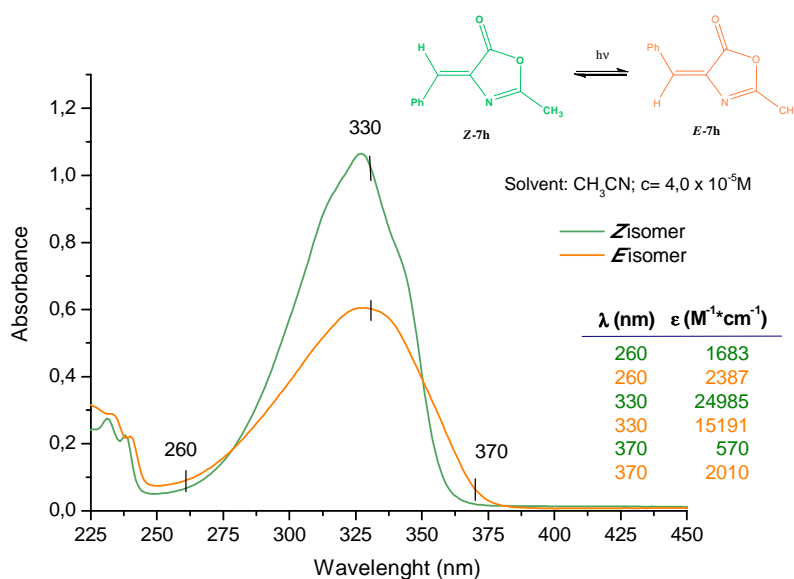


Figure 5.33. UV-Vis spectra of the *Z* and *E* isomers of compound **7h**.

Therefore, we proceeded to design a new experiment. For this purpose, we prepared two solutions of the same concentration (1.08×10^{-4} M in dry acetonitrile) of both isomers (*Z* and *E*), which we planned to separately irradiate in a quartz cuvette using a monochromator as the light source (see section 5.2.2.2, Figure 5.13).

In the first place, we selected for irradiating the maximum wavelength of the band ($\lambda = 330$ nm). Taking a look at Figure 5.33, we saw that the *Z* isomer presented a stronger absorption than the *E* isomer at 330 nm. Then, it was expected that at this wavelength, the $Z \rightarrow E$ isomerization reaction was favoured over the $E \rightarrow Z$ process, as the *Z* isomer rapidly absorbed light to afford the *E* isomer, displacing the equilibrium towards the formation of this product. This way, it was thought that the mixture of isomers at the PSS had to be rich in *E* isomer. To experimentally confirm this fact, we first irradiated the solution of 100% of the *Z* isomer at 330 nm in a monochromator for an hour until the PSS was reached. The reaction was followed by 1H NMR. The isomers ratio at the PSS starting from the *Z* isomer was found to be 43% (*Z*) / 57% (*E*). Afterwards, we irradiated the solution of 100% of the *E* isomer at 330 nm for 3 hours until the PSS was reached. In this case, the isomers ratio at the PSS was the same as when irradiating the *Z* isomer,

since we have mentioned before (see Figures 5.31) that the value of the isomers ratio at the PSS doesn't depend on the starting isomer (for solutions of the same concentration and irradiating under the same conditions), but it depends on the irradiation wavelength. As predicted, the isomers ratio achieved at the PSS at this wavelength (330 nm) was a mixture rich in *E*.

Later we selected an irradiation wavelength from the end of the band (370 nm). At this wavelength, the *E* isomer presented stronger absorption than the *Z* isomer. Specifically at this point, the *E* isomer showed absorption, but the *Z* isomer had almost no absorption. Therefore, the $E \rightarrow Z$ isomerization was greatly favoured over the $Z \rightarrow E$ reaction. This means that the *E* isomer absorbed light to give the *Z* isomer, but the *Z* isomer didn't tend to react to achieve *E* as its absorption was very little. The equilibrium was displaced towards the formation of *Z*, being the main isomer at the PSS. We irradiated a solution of 100% of the *Z* isomer at 370 nm for 10 hours until the PSS was reached, with a value of 83% (*Z*) / 17% (*E*). The irradiation times were longer than at 330 nm as the absorption was really low. However, when irradiating a solution of 100% of the *E* isomer, the same isomers ratio at the PSS was reached in only an hour of irradiation, since the *E* isomer was practically the only isomer that absorbed at this λ . As expected, irradiating at the end of the band we reached a mixture of isomers rich in *Z*.

Finally, we selected a wavelength of the beginning of the band (260 nm). At this wavelength, the *E* isomer absorbed more than *Z*, but the absorption for both isomers was really low. This means that the $E \rightarrow Z$ isomerization was favoured over the $Z \rightarrow E$ reaction, anticipating a mixture rich in *Z* at the PSS. However, unlike the previous cases, we weren't able to reach the PSS as the isomerisation process was really slow due to the low absorption presented by both isomers. We first irradiated a solution of 100% of *Z* isomer at 260 nm for 12 hours and a half and measured the isomers ratio obtained after that irradiation time (which wasn't the value of the PSS), 90% (*Z*) / 10% (*E*). Then, we irradiated at this λ a solution of 100% of the *E* isomer for the same amount of time (12 hours and a half) and obtained a mixture with an isomers ratio of 20% (*Z*) / 80% (*E*) (which wasn't the value of the PSS). Comparing the conversion between isomers that took place in both cases (which weren't the values of the PSS), we concluded that the *E* isomer evolved more rapidly towards the formation of *Z* than the other way round, so if we were capable of irradiating during longer irradiation times, we would achieve a PSS with a mixture of isomers rich in *Z*, which agrees with the expected results.

If we compile the results obtained for each case in a table (Table 5.9), we deduce that we may achieve different isomers ratio at the PSS depending on the selected irradiation wavelength. As mentioned above, this is due to the different absorption that the two isomers present in different regions of the absorption band.

Table 5.9

λ (nm)	(Z/E) ratio at PSS*	t_{irrad} starting from 100% Z**	t_{irrad} starting from 100% E**
260***	mixture rich in Z****	prolonged t_{irrad} , longer than 12 h and a half****	prolonged t_{irrad} , longer than 12 h and a half****
330	43% (Z) / 57% (E)	1 h	3 h
370	83% (Z) / 17% (E)	10 h	1 h

* Isomers ratio at the photostationary state.

** Irradiation time to achieve the PSS, in hours.

*** At $\lambda = 260$ nm, the PSS wasn't reached after the irradiation time.

**** Estimated results according to the expected PSS.

Therefore, we can obtain mixtures of isomers rich in Z at the beginning and end of the absorption band (260 and 370 nm), while mixtures of isomers rich in E are afforded when irradiating at the maximum of the band (330 nm).

5.3.1.2. Irradiation in a photoreactor of the photoswitches with structure based on the GFP chromophore.

The fact that it was possible to use different irradiation wavelengths led us to think that it could be feasible to carry out the irradiation process with less energetic light in order to diminish the contribution of side reactions different from the target photoisomerization, especially in the case of compounds with an electron-withdrawing group in the phenyl group of substituent R₄. Therefore, we irradiated at 360 nm a 2.2×10^{-3} M solution of compound **7o** in CDCl₃ in a quartz cuvette with a monochromator, and followed the photoisomerization process by ¹H NMR, until the photostationary state was reached (Figure 5.34).

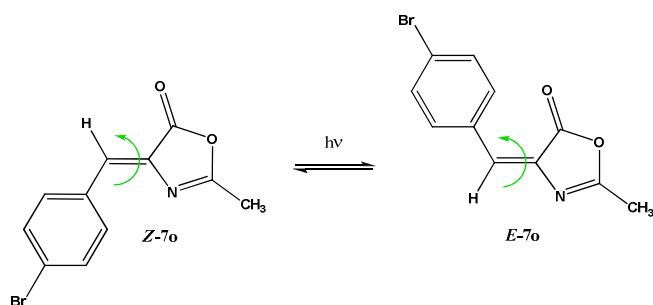


Figure 5.34. Photoisomerization reaction undergone by compound 7o.

Apart from obtaining a value for the isomers ratio at the PSS of 54% (*Z*) / 46% (*E*), which greatly differed from the result obtained when irradiating in a 125-W medium-pressure Hg lamp and a Pyrex filter [85% (*Z*) / 15% (*E*), Table 5.8, entry 12], there were no signals in the ^1H NMR spectra of other side reactions. This meant that the photoisomerization process was taking place exclusively, which was a considerable improvement over the previous irradiation conditions used. Therefore, we decided to repeat the irradiation process of different compounds using a light source with emission wavelength centred at 350 nm in order to compare the two irradiation methods. For this purpose, we prepared 0.01 M solutions of different photoswitches with structure based on the GFP chromophore in acetonitrile, placed them in Pyrex test tubes in a merry-go-round appliance in a photoreactor (Figure 5.35), and irradiated them using lamps with emission wavelength centred at 350 nm (14 lamps \times 8-W/lamp, see experimental section) until the PSS was reached.



Figure 5.35. Image of the photoreactor used for irradiating under these conditions.

5. Photochemical study

The reaction was followed by ^1H NMR. The results for the isomers ratio at the PSS after irradiating under these conditions are shown in Table 5.10. Depending on the photoswitches, the irradiated mixture took from 1 to 2 hours to reach the PSS.

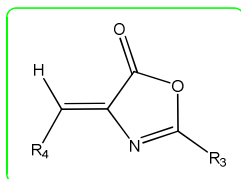


Table 5.10.

Entry	R ₃	R ₄	Compound	Ratio at PSS*	
				% Z	% E
1	Me	Ph	7h	70	30
2	Me	<i>p</i> -MePh	7i	75	25
3	Me	<i>p</i> -MeOPh	7j	42	58
4	Me	<i>o</i> -MeOPh	7k	41	59
5	Me	<i>p</i> -NO ₂ Ph	7l	76	24
6	Me	<i>p</i> -CNPh	7m	62	38
7	Me	<i>p</i> -BrPh	7o	63	37
8	Ph	<i>p</i> -BrPh	7e	36	64

* Isomers ratio at the photostationary state

The following trends can be inferred from the results shown in Table 5.10. When substituting the phenyl group in R₄, different values for the isomers ratio at the PSS are achieved, depending on those substituents. If the substituent of the phenyl group is an electron-donor group, such as methoxy (switch **7j**, entry 3), the percentage of *E* isomer at the PSS increases. The effect is the same whether the substituent is in para or ortho (switch **7k**, entry 4) position. However, when having an electron-withdrawing group, such as nitro (switch **7l**, entry 5), there is no significant change in the isomers ratio. On the other hand, if there is a bromine (switch **7o**, entry 7), the percentage of *E* isomer at the PSS also increases. Moreover, if substituent R₃ is modified from Me (switch **7o**, entry 7) to Ph (switch

7e, entry 8) and R_4 remains the same, the percentage of *E* isomer at the PSS increases a lot. Therefore, the value of the isomers ratio at the PSS can be varied depending on the substituents R_3 and R_4 , which is a great advantage. Even more important is the fact that all of the values for the isomers ratio have been improved with respect to the values obtained for each switch when irradiated with a 125-W medium-pressure Hg lamp (see Table 5.8), since the percentage of *E* isomer has increased in all cases. In addition to this, there was no decomposition of the switches when irradiated under these conditions, so no side reactions were occurring during the irradiation time intervals, which is a further improvement over the previous conditions used.

Irradiating under these improved conditions, mixtures of *Z* and *E* isomers of different compounds bearing electron-withdrawing groups can be subsequently separated in order to individually characterize and study them. With this aim, we irradiated a 0.01 M solution of compound **7o** (100% *Z* isomer at $t=0$ min) in acetonitrile in a photoreactor with lamps (14 lamps x 8-W/lamp) with emission wavelength centred at 350 nm, until the PSS was reached. Then, the resulting mixture of isomers was separated by flash chromatography on silica gel, using hexane/ ethyl acetate (10:1) as eluent. Therefore we could have the two isomers (*Z* and *E*) separately, so we could record the NMR and UV-Vis spectra of the *E* isomer (see experimental section and appendix A) and compare it with the thermodynamically more stable isomer (*Z*).

When the *Z* and *E* isomers are already separated, we can carry out the aforementioned experiment to study the kinetics of the isomerization reaction. Thus, we prepared in two distinctive Pyrex NMR tubes two solutions of the same concentration in $CDCl_3$. In the first NMR tube, we got ready a solution 0.10 M of the *Z* isomer of compound **7o**. Next, in the second NMR tube, we prepared a solution 0.07 M of the *E* isomer of compound **7o**. Afterwards, both NMR tubes were irradiated in a photoreactor (14 lamps x 8-W/lamp) with emission wavelength centred at 350 nm until both solutions reached the PSS. The photoisomerization reaction was followed by 1H NMR at short irradiation intervals. Representing the isomers ratio vs. the irradiation time, we obtained the two graphs that are shown in Figure 5.36, (a) corresponding to the sample with 100% of **Z-7o** isomer at the beginning of the reaction, and (b) corresponding to the sample with 100% of **E-7o** isomer at $t_{irrad}=0$ min.

5. Photochemical study

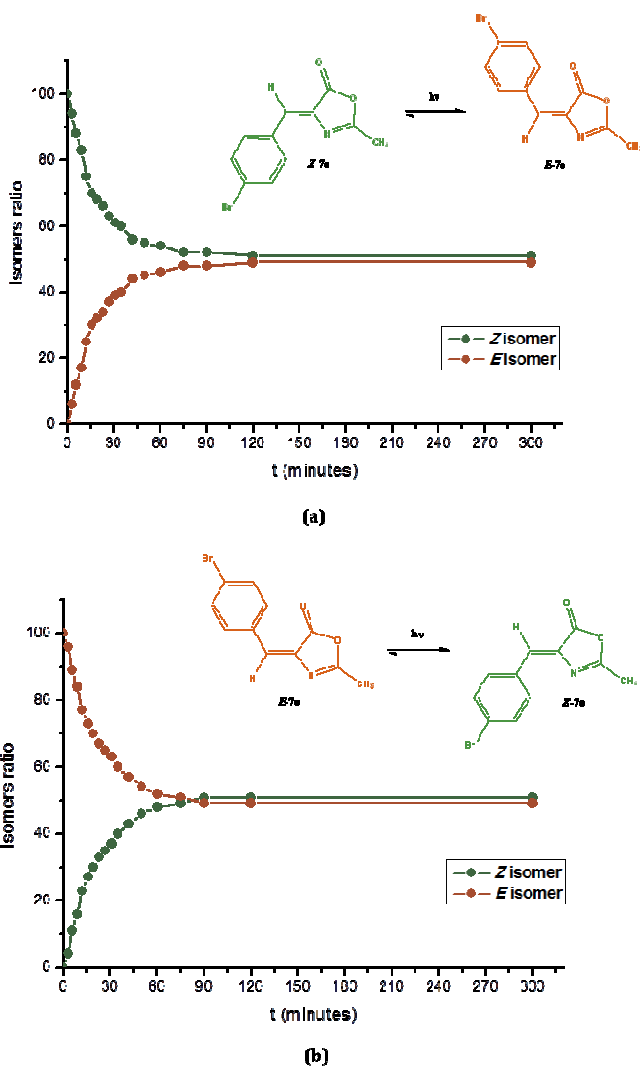


Figure 5.36. Graphs where the isomers ratio is represented vs. the irradiation time in a photoreactor ($\lambda_{\text{irrad}} \approx 350 \text{ nm}$) (a) starting from a 100% of the Z isomer, and (b) starting from a 100% of the E isomer of compound 7o.

From the graphs represented in Figure 5.36 we can deduce that the value of the isomers ratio at the PSS for these two processes is 51% (Z) / 49% (E), which is reached after approx. 85 minutes of irradiation.

We can also compare the results for the isomers ratio at the PSS reached during this experiment, 51% (*Z*) / 49% (*E*), and the value obtained when irradiating a 0.01 M solution of **7o** in CH₃CN in a Pyrex test tube, 63% (*Z*) / 37% (*E*) (see Table 5.10, entry 7). In both experiments, a photoreactor is used for irradiating. However, it is observed that the values for the isomers ratio at the PSS are different in each case, which could be due to the change in the solvent used for irradiating the samples. This fact will be more extensively explained later in section 5.3.1.3.

Moreover, it is possible to calculate the values for the kinetic constants of each process from the first points of each graph of Figure 5.36, and therefore determine the value of the relative kinetic constant that relates the speed of both processes. If we consider $k_{Z \rightarrow E} = 1$, then $k_{E \rightarrow Z} \approx 1$, which means that the *E*→*Z* isomerization process is almost as fast as the *Z*→*E* reaction, so there is no difference in speed.

Afterwards, we decided to repeat the experiment to study the kinetics of the isomerization reaction of compound **7h** when irradiated in a photoreactor instead of with a medium-pressure Hg lamp, as we had already separated both isomers (see Figure 5.31). For that purpose, we designed a similar experiment than the one that we have described for compound **7o**. In Figure 5.37 are shown the two graphs obtained when representing the isomers ratio vs. the irradiation time, (a) corresponding to the sample with 100% of **Z-7h** isomer at the beginning of the reaction, and (b) corresponding to the sample with 100% of **E-7h** isomer at $t_{\text{irrad}}=0$ min.

5. Photochemical study

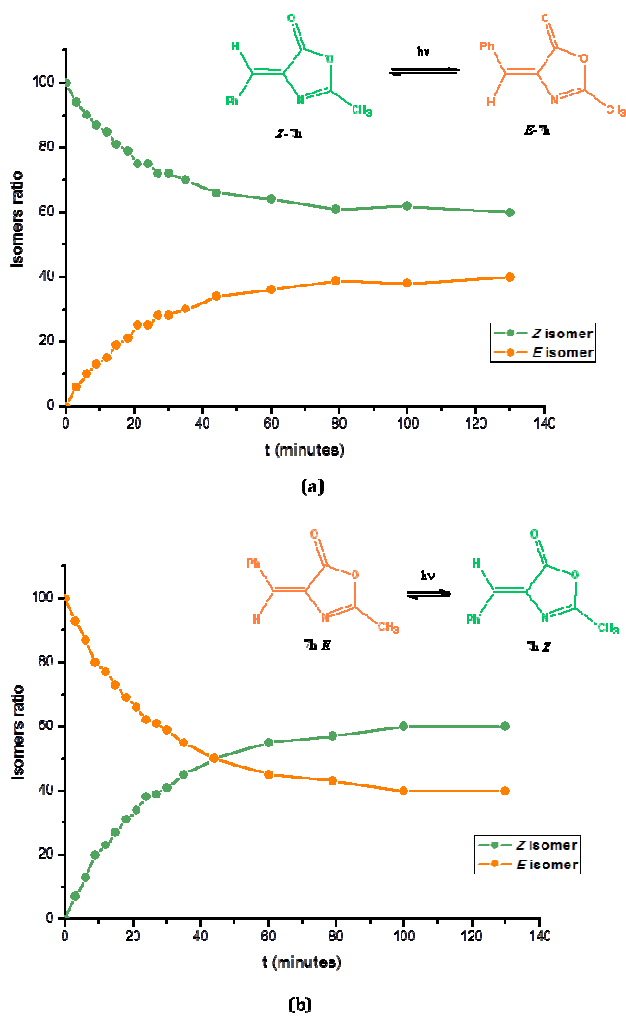


Figure 5.37. Graphs where the isomers ratio is represented vs. the irradiation time in a photoreactor ($\lambda_{\text{irrad}} \approx 350 \text{ nm}$) (a) starting from a 100% of the Z isomer, and (b) starting from a 100% of the E isomer of compound 7h.

From these results we can infer that value of the isomers ratio at the PSS for these two processes is 60% (Z) / 40% (E), which is reached after approx. 80 minutes of irradiation in a photoreactor. If we calculate the values for the kinetic constants of each process from the first points of each graph, we can determine the

value of the relative kinetic constant that relates the speed of both processes. Considering $k_{Z \rightarrow E} = 1$, then $k_{E \rightarrow Z} = 1.7$, which means that the $E \rightarrow Z$ isomerization process is almost two times faster than the $Z \rightarrow E$ reaction.

On the other hand, we can also compare the values for the kinetic constants obtained in this experiment (Figure 5.37) and in the one in which we used a medium-pressure Hg lamp as the light source (Figure 5.31). For the same process, for example the $Z \rightarrow E$ reaction, if $k_{Z \rightarrow E \text{ photoreactor}} = 1$, then $k_{Z \rightarrow E \text{ immersion well}} = 1.4$, which means that the $Z \rightarrow E$ isomerization process is almost 1.4 times faster when irradiating with a medium-pressure Hg lamp than if a photoreactor is used.

5.3.1.3. Solvent dependence of the isomerization reaction of photoswitches with structure based on the GFP chromophore.

As shown in Figures 5.28 and 5.29, there are slight differences in the absorption spectra with solvents of different polarities. In order to study if there was any noticeable effect in the values of the isomers ratio at the PSS obtained when irradiating solutions in different solvents, we designed the following experiment. In different Pyrex test tubes, we prepared 0.01 M solutions of compound **7o** in diverse solvents with different polarities, we placed them in a merry-go-round device, and irradiated in a photoreactor (14 lamps x 8-W/lamp) with emission wavelength centred at 350 nm until all the solutions reached the PSS, being the photoisomerization reaction followed by ^1H NMR. The results for the PSS of all the samples are shown in Table 5.11.

It was observed that when changing one solvent for another, there were slight differences in the values for the isomers ratio at the PSS. For example, when using chloroform as solvent (sample 1), the isomers ratio at the PSS was 55% (*Z*) / 45% (*E*). On the other hand, when using acetonitrile (sample 4), the isomers ratio at the PSS was 63% (*Z*) / 37% (*E*), which means that the percentage of *E* isomer had been reduced. However, the differences between these results weren't related to the polarity of the solvents according to diverser polarity indices found in literature, such as E_{T}^{N} , ϵ , or π^* (Taft).¹⁸ Furthermore, the experimental error derivative of the NMR technique had to be taken into account.¹⁹

¹⁸ See ref. 3.

¹⁹ See ref. 6.

5. Photochemical study

Therefore, we can conclude that in the case of photoswitches with structure based on the GFP chromophore, the value of the isomers ratio at the PSS can be adjusted depending on the light source and the solvent used for the experiment.

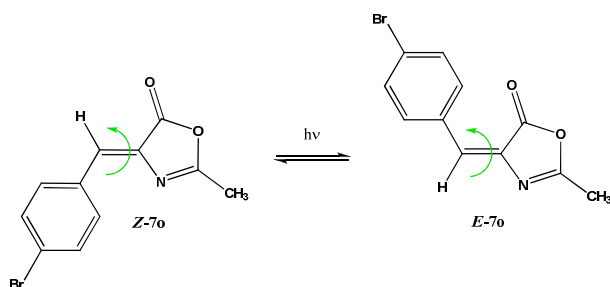


Table 5.11.

Sample	Solvent	Polarity			Ratio at PSS*	
		E_T^N	ϵ	π^*	% Z	% E
1	CHCl ₃	0.259	4.8	0.58	55	45
2	Toluene	0.099	2.4	0.54	60	40
3	THF	0.207	7.6	0.58	63	37
4	CH ₃ CN	0.460	37.5	0.75	63	37
5	MeOH	0.762	32.7	0.60	63	37

* Isomers ratio at the photostationary state

5.3.1.4. Photochemical and thermal stability of the photoswitches with structure based on the GFP chromophore.

Finally, we studied the photochemical and thermal stability of the photoswitches based on the GFP chromophore.

Concerning the photochemical stability of these switches, different compounds have been irradiated for several hours and followed by ¹H NMR, and no signals of other side reactions apart from the ones corresponding to the isomerization process.

On the other hand, with the aim of testing the thermal stability of both isomers, we performed the following experiment. In two different Pyrex NMR tubes, we prepared 0.1 M solutions in CDCl₃ of the two isomers (*Z* and *E*) of compound **7h**, and heated them at 50°C. ¹H NMR spectra were performed for both samples after different time intervals. After heating the samples for several days at this temperature, we realized that there wasn't a noticeable change in any of the samples. Therefore, we changed the solvent to deuterated toluene to be able to heat the samples at higher temperatures. Therefore, we warmed up the samples at 100°C, and followed the reaction by ¹H NMR. This way, we observed that the *Z* isomer remained unchanged when heated for long periods of time. However, the *E* isomer slowly reverted to the *Z* isomer, and after heating for 776 hours, this reversion was fully achieved. This means that the *Z* isomer was thermodynamically more stable than the *E* isomer, as predicted. This result is in agreement with the results obtained when carrying out the computational studies (see section 5.4.2).

In addition to this, we can use this property to tune the switch behaviour, obtaining mixtures of isomers rich in one isomer or another depending on whether we use light or heat.

5.3.1.5. Irradiation of photoswitches with structure based on the GFP chromophore in solid state.

It has been long recognized the important role that the reaction media (solvents with varying characteristics) play in controlling the rates, product distribution and stereochemistry of organic reactions.²⁰ Lately, much effort has been directed towards the use of organized media to modify the photochemical reactivities achieved with isotropic liquids.²¹ The main goal of these studies is using the order of the medium to increase the rate and selectivity of a chemical process. The differences in chemical reactivities occurring in ordered media as compared to isotropic solvent phases are principally due to the physical restraints imposed by the environment. If we think of the structure of the protein in which the GFP chromophore is embedded, we realized that we are dealing with an

²⁰ *Synthetic Organic Photochemistry*. Griesbeck, A. G.; Mattay, J. (eds.) Marcel Dekker: New York, **2005**.

²¹ (a) Kalyanasundaram, K. (ed.) *Photochemistry in Microheterogeneous Systems*. New York: Academic Press, **1987**. (b) Ramamurthy, V. *Photochemistry in Organized & Constrained Media*. New York: VCH, **1991**.

organized medium (see section 2.3.5). The fact that the chromophore is specifically bound to the protein allows it to adopt the precise conformation required to trigger a complex sequence of events after the absorption of a photon. With the aim of resembling more the actual process that takes place in the green fluorescent protein, we decided to carry out the irradiation in solid state.

Similar processes had already been described in literature. For example, when irradiating *trans*-cinnamic acid in solution, an isomerisation process takes place yielding the *cis* isomer with a quantum yield of 0.62 (Figure 5.38(a)). However, irradiation of the crystalline material leads to a [2+2] dimerization rather than isomerization.²² On the other hand, *trans*-1,2-bis(4-pyridyl)ethylene also undergoes a *cis-trans* isomerization upon irradiation in solution (Figure 5.38(b)).²³ But irradiation of its crystals doesn't give any products. These two examples confirm the fact that in crystals the reactant molecules are preorganized.

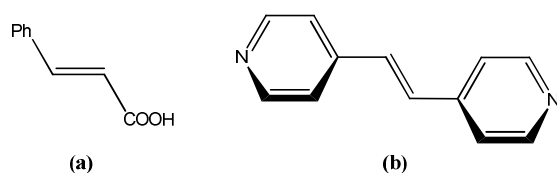


Figure 5.38. (a) *trans*-cinnamic acid (b) *trans*-1,2-bis(4-pyridyl)ethylene.

As an example for the irradiation in solid state we chose compound **7o**. Then, we placed 200 mg of **7o** in a glass plate and irradiated it in a photoreactor (14 lamps x 8-W/lamp) with emission wavelength centred at 350 nm. We followed the reaction by ¹H NMR. A new compound, **11**, was observed as the major product after several days of irradiation. This new product corresponded to the [2 + 2] cycloaddition reaction of the starting compound with itself (Figure 5.39), as it was confirmed by electrospray and ¹H and ¹³C NMR (see experimental section). As in the previous examples, no isomerization process was observed.

²² (a) Cohen, M. D.; Schmidt, G. M. J. *J. Chem. Soc.* **1964**, 1996. (b) Cohen, M. D.; Schmidt, G. M. J.; Sonntag, F. I. *J. Chem. Soc.* **1964**, 2000.

²³ Schmidt, G. M. J. et al. In: *Solid State Photochemistry*. Ginsburg D. (ed.) New York: Verlag Chemie, **1976**.

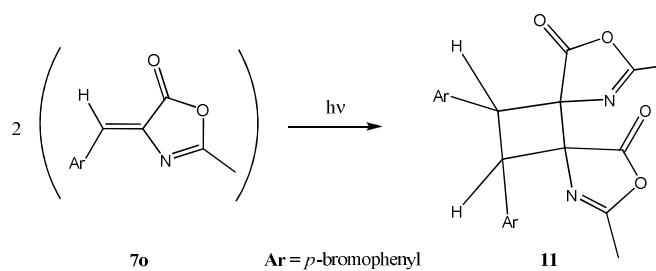


Figure 5.39. Tentative structure of compound 11.²⁴

5.3.2. Photochemical aspects of the mechanism of the isomerization reaction of photoswitches with structure based on the GFP chromophore.

In this section we will talk about the experimental studies carried out in order to gather information about the mechanism and efficiency of the photochemical reaction.

5.3.2.1. Excited state multiplicity.

In the same way as described in section 5.2.2.1 for the photoswitches with structure based on the PSB-retinal, we performed an experiment in order to determine the excited state multiplicity of the GFP-based photoswitches. Therefore, we irradiated simultaneously three samples of the same switch that were under different reaction conditions. In the first place, we prepared 0.05 M solutions of compound **7c** in CDCl₃ in 3 different Pyrex RMN tubes. The first sample was deoxygenated and used as reference. The second sample was saturated with O₂ (triplet quencher) by bubbling air for 15 minutes. At last, we deoxygenated the third sample and added *cis*-piperilene (5 equivalents). The three samples were irradiated simultaneously for 20 minutes in a 125-W medium-pressure Hg lamp. After irradiating, ¹H NMR spectra of the samples were recorded to know the isomers ratio at the given irradiation time. The obtained results are shown in Table 5.12.

As the values of the isomers ratio after irradiating all the samples during the same amount of time were similar in every case,²⁵ we inferred that the progress of

²⁴ X-ray analysis would be required in order to determine the stereochemistry of **11**.

²⁵ See ref. 6.

5. Photochemical study

the reaction took place through electronic states of singlet multiplicity, since the triplet quenchers had no effect over the reaction outcome.

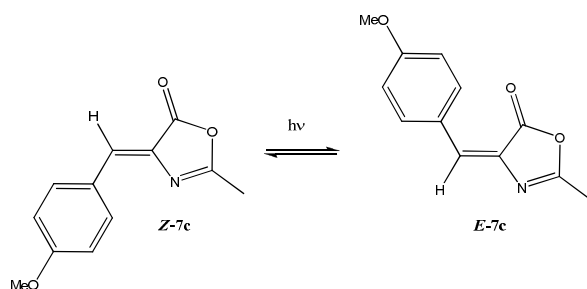


Table 5.12

Sample	% Z-7c	% E-7c
1	80	20
2	79	21
3	81	19

5.3.2.2. Isomerization quantum yield.

The following step consisted in calculating the quantum yield of the photoisomerization reaction of the photoswitches with structures based on the GFP chromophore. For this purpose, we selected the compound **7h** ($R_3 = \text{Me}$, $R_4 = \text{Ph}$) as a representative example of this kind of switches. As we had separately both isomers of **7h**, it was possible to measure the photoisomerization quantum yield of both the $Z \rightarrow E$ reaction and the $E \rightarrow Z$ process. We followed the same procedure used for determining the isomerization quantum yield of PSB-retinal based photoswitches (see section 5.2.2.2), using *trans*-azobenzene as actinometer.²⁶

To begin with, a solution of *trans*-azobenzene in methanol was prepared in such way that the value of the absorbance at 358 nm was close to one.²⁷

²⁶ See ref. 8.

²⁷ See ref. 9.

Afterwards the actinometer solution was irradiated in a quartz cuvette at 334 nm with a monochromator. The change in absorbance of the actinometer solution at 358 nm was approx. 0.02. We chose $\lambda = 334$ nm for irradiating the samples because it was close to the maximum absorption values of both isomers of compound **7h**.

Then, solutions in acetonitrile of both isomers, *Z* and *E*, of compound **7h** were prepared by adjusting the value of the absorbance at 334 nm to the one showed by the actinometer. These solutions were separately irradiated at 334 nm for a period of time that was fixed after several runs, as it depends on different factors such as the concentration or the irradiation wavelength.

As the concentration of the samples wasn't enough for recording the ^1H NMR spectra, after the selection of the adequate irradiation time, we irradiated three aliquots of each sample for exactly the same amount of time, taking this into account when doing the final calculations.

Later, we calculated the number of photons absorbed by using the following formula:

$$E_p \text{ (mol of photons } \times \text{ cm}^{-2} \times \text{ s}^{-1}) = F(\lambda) \times \Delta A(358\text{nm}) / t(\text{s})$$

where $\Delta A(358\text{nm})$ is the change in the absorbance at 358 nm of the *trans*-azobenzene solution when irradiating at 334 nm, and $t(\text{s})$ is the irradiation time responsible for that change. The F factor, which depends on the wavelength, has a value of 3.60×10^{-6} einstein $\times \text{ cm}^{-2}$ at 334 nm.

Then, the number of photons absorbed corresponds to E_p multiplied by the irradiation time of the sample (in seconds).

To calculate the number of moles of *E* (when we started from 100% *Z*) or *Z* (if we started from 100% *E*) isomer formed after irradiating the samples, the solvent was removed immediately after the irradiation and the residue dried properly. The amount of the corresponding *Z* or *E* isomer (depending on the process) formed was quantified by ^1H NMR, using 1,3,5-trimethoxybenzene as internal standard, as the proton signals of this standard didn't overlap with the signals of both isomers of the samples. From the integration of the signals it was possible to know the number of *Z* or *E* isomer formed.

Moreover, at the end of the experiment the actinometer solution was measured again to prove that the light intensity had been constant. All the solutions were kept in the dark when they weren't irradiated.

To end up, the value for the isomerization quantum yield for each process was the result of the equation shown in Figure 5.12.

The values of the isomerization quantum yield for the $Z \rightarrow E$ and the $E \rightarrow Z$ processes of compound **7h** were:

- starting from 100% of the Z isomer: $\Phi_{Z \rightarrow E} = 0.25 \pm 0.01$
- starting from 100% of the E isomer: $\Phi_{E \rightarrow Z} = 0.11 \pm 0.02$

The measured Φ values for the two isomers of this representative switch are similar to the values obtained for the photoisomerization of analogous compounds based on the GFP chromophore.²⁸ These prototypes of molecular switches can be considered pretty efficient.

5.3.2.3. Luminescence.

As soon as the nature of the excited state involved in the photoisomerization and the value of the photoisomerization quantum yield had been determined, we proceeded to study the deactivation processes that could diminish the efficiency of the switches with structure based on the GFP chromophore.

Therefore, we measured the emission and excitation spectra of two illustrative photoswitches: the two isomers (Z and E) of compound **7h** ($R_3 = \text{Me}$, $R_4 = \text{Ph}$), and compound **7o** ($R_3 = \text{Me}$, $R_4 = p\text{-BrPh}$) (only the Z isomer).

In the first place, a 3.6×10^{-5} M solution of **Z-7h** in deoxygenated acetonitrile at 298 K was measured in a spectrofluorimeter. Only a weak emission band centered at 380 nm was obtained when exciting from 250 to 310 nm (Figure 5.40).

²⁸ Abbandonato, G.; Signore, G.; Nifosi, R.; Voliani, V.; Bizzarri, R.; Beltram, F. *Eur. Biophys. J.* **2011**, *40*, 1205.

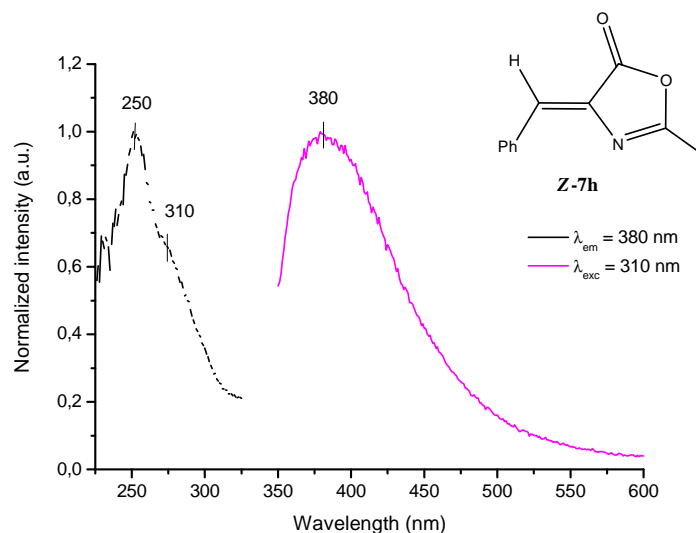


Figure 5.40. Excitation and emission spectra of compound **Z-7h**.

Then, the fluorescence lifetime was measured using a 320 nm LED and was found to be 4.65×10^{-9} s. In the last place, in order to measure the fluorescence quantum yield, a solution of *trans*-stilbene in deoxygenated hexane was used as standard of fluorescence. A solution of **Z-7h** in deoxygenated acetonitrile was also prepared and the emission spectra for both compounds were measured using an excitation wavelength of 290 nm in a spectrofluorimeter. Under these conditions, a fluorescence quantum yield of 2.33×10^{-4} M ($\pm 5.00 \times 10^{-5}$) was found.

After studying the luminescence of the *Z* isomer of compound **7h**, we measured the luminescence of a 3.6×10^{-5} M solution of **E-7h** in deoxygenated acetonitrile at 298 K in a spectrofluorimeter. However, no emission was found for this isomer, which means that the fluorescence quantum yield is really low and it cannot be determined with the available equipment.

On the other hand, a 3.0×10^{-5} M solution of **7o** in deoxygenated acetonitrile at 298 K was measured in a spectrofluorimeter. Only a weak emission band centered at 430 nm was obtained when exciting from 290 to 370 nm (Figure 5.41).

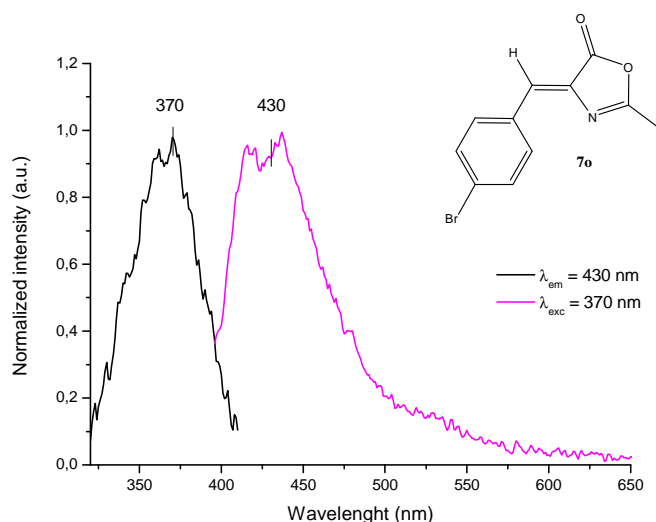


Figure 5.41. Excitation and emission spectra of compound **7o.**

Afterwards, the fluorescence lifetime was measured using a 280 nm LED and was found to be 5.44×10^{-9} s. The fluorescence quantum yield was also calculated using a solution of *trans*-stilbene in deoxygenated hexane as standard of fluorescence. A solution of **7o** in deoxygenated acetonitrile was prepared and the emission spectra for both compounds were measured using an excitation wavelength of 290 nm in a spectrofluorimeter. Under these conditions, a fluorescence quantum yield of $0.005 (\pm 0.001)$ was found.

The low values of the fluorescence quantum yields for both compounds show that deactivation through fluorescence does not effectively compete with the isomerization process. In fact, these results emphasize the adequate design of these switches as only a small fraction of the light energy is wasted in the radiative decay.

5.3.2.4. Sensitization tests.

Finally, a further experiment was carried out that consisted of the isomerization reaction of the photoswitches based on the GFP chromophore through sensitized reaction with thioxanthone, which was the same triplet sensitizer that we had used for irradiating with the PSB-retinal based photoswitches (see section 5.2.2.4). It is recalled that the triplet energy of

thioxanthone is 63.2 kcal/mol, so any compound with lower triplet energy is sensitive to suffer a triplet energy transfer from thioxanthone (see experimental section).

As the appropriate light filter with a transmittance spectrum that allowed the selective irradiation with a 125-W medium-pressure Hg lamp of thioxanthone without irradiating the photoswitches, we chose the same filter as used with PSB-retinal photoswitches. This light filter was composed of a 0.4 M solution of sodium methavanadate (NaVO_3) in 5% NaOH, and avoided the radiation at wavelengths lower than 370 nm, region where thioxanthone absorbed but there was no absorption of the photoswitches (see experimental section).

For irradiation under sensitized conditions, we selected the following switches: compound **7h** ($R_3 = \text{Me}$, $R_4 = \text{Ph}$), compound **7j** ($R_3 = \text{Me}$, $R_4 = p\text{-MeOPh}$), and compound **7l** ($R_3 = \text{Me}$, $R_4 = p\text{-NO}_2\text{Ph}$), as they presented no relevant absorptions at wavelengths higher than 370 nm.

Later, in three Pyrex NMR tubes, we prepared 0.1 M solutions of each compound in CDCl_3 and added 1 equivalent of thioxanthone to each sample. Afterwards, we irradiated the three samples until the photostationary state was reached. The values of the isomers ratio at the PSS for the standard irradiations (see Table 5.8), the irradiations carried out in a photoreactor (see Table 5.10) and the sensitized processes are shown in Table 5.13.

From these results, we could deduce that the isomers ratio at the photostationary state under sensitized conditions was different from the isomers ratio obtained when carrying out the reaction under standard conditions or in a photoreactor. However, there were other side reactions taking place apart from the photoisomerization reaction in all the three cases. This means that there was a triplet energy transfer from the triplet state of thioxanthone to form the excited triplet state of the switches, which afterwards reacted to give the isomerization product and other side reactions. Therefore, the triplet energy of the photoswitches based on the GFP chromophore is lower than 63.2 kcal / mol. With the aim of finding the approximate value of the triplet energy of these photoswitches, it would be necessary to carry out this experiment with diverse triplet sensitizers with different triplet energies, so the values would be delimited in an interval of energies.

Table 5.13

Entry	Compound	Irradiation conditions	% <i>Z</i> isomer*	% <i>E</i> isomer*
1	7h	Standard	85	15
2		Photoreactor	70	30
3		Sensitized**	85	15
4	7j	Standard	85	15
5		Photoreactor	42	58
6		Sensitized**	87	13
7	7l	Standard**	83	13
8		Photoreactor	76	24
9		Sensitized**	70	30

* Isomers ratio at the photostationary state

** Other side reactions take place apart from the photoisomerization.

5.3.3. Study of the azolactone ring opening process with solvents in GFP-based photoswitches.

As discussed in section 4.2.2, GFP-based photoswitches undergo hydrolysis processes with certain reaction solvents. For example, in methanol, they react with the solvent to achieve the corresponding acetoamidoacetate. We used this concept in order to know if any of the two isomers (*Z* or *E*) of these compounds was more stable than the other under these conditions. Therefore, we designed an experiment to figure out if the hydrolysis process was faster in the case of the *Z* isomer or the *E* isomer. For this purpose, we selected the two isomers of compound **7h**, *Z* and *E*. We prepared 0.1 M solutions of the two isomers in CDCl₃ in two different Pyrex NMR tubes, and recorded their ¹H NMR spectra at this point, which were considered as references. Then, we added 0.02 ml of CD₃OD to the two samples, and followed their hydrolysis with deuterated methanol by ¹H NMR. These ¹H NMR spectra were recorded after really short periods of time. The analysis of the final data led us to conclude that both isomers suffered the hydrolysis process almost at the same rate, so no differences were found in the azolactone ring opening of both isomers.

5.4. THEORETICAL STUDY OF PHOTOSWITCHES WITH STRUCTURE BASED ON THE PSB-RETINAL AND THE GFP CHROMOPHORE.

5.4.1. Theoretical calculations of the photoswitches with structure based on the PSB-retinal chromophore.

In this dissertation, theoretical calculations of the photoswitches with structure based on the PSB-retinal chromophore won't be developed as we consider that these compounds have been widely studied in literature.

For instance, different models of the PSB-retinal chromophore have been the subject of several computational studies.²⁹ As an example, the structure of the (*Z*)-penta-3,5-dieniminium cation (*cis*-C₅H₆NH₂⁺) (**12**) is shown in Figure 5.42.

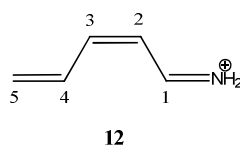


Figure 5.42. Structure of *cis*-C₅H₆NH₂⁺ (**12**).

On the other hand, it has been proved that conformationally locked alkylated or protonated Schiff bases (PSBs), based on a indanylidene pyrrolinium framework, provide the skeleton for the design of a novel class of biomimetic switches that display excited state properties similar to those of the Rh-embedded PSB-retinal chromophore (see section 2.6.1).³⁰ Moreover, a series of computational investigations resulted in the design of a few compounds featuring the rigid framework of 4-(cyclopent-2'-enylidene)-3,4-dihydro-2*H*-pyrrolium cation (CPP, Figure 5.43(a)) which combines the electronic structure and photoisomerization

²⁹ (a) Garavelli, M.; Celani, P.; Bernardi, F.; Robb, M. A.; Olivucci, M. *J. Am. Chem. Soc.* **1997**, *119*, 6891. (b) Garavelli, M.; Vreven, T.; Celani, P.; Bernardi, F.; Robb, M. A.; Olivucci, M. *J. Am. Chem. Soc.* **1998**, *120*, 1285. (c) Garavelli, M.; Bernardi, F.; Olivucci, M.; Vreven, T.; Klein, S.; Celani, P.; Robb, M. A. *Faraday Discuss.* **1998**, *110*, 1. (d) González-Luque, R.; Garavelli, M.; Bernardi, F.; Merchán, M.; Robb, M. A.; Olivucci, M. *Proc. Natl. Ac. Sci. USA* **2000**, *97*, 9379.

³⁰ See ref. 7(c).

mechanism of the protonated Schiff base of retinal and the locked skeleton of diarylidene (DA, Figure 5.43(b)).³¹

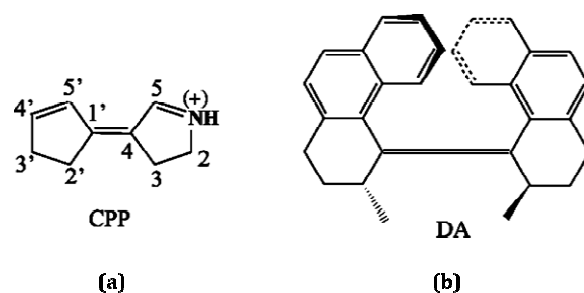


Figure 5.43. Structures of (a) CPP, and (b) DA.

Afterwards, different prototypes of molecular switches based on the PSB-retinal chromophore, such as benzylidene-pyrrolines (BPs, see section 2.6.1), indanylidene-pyrrolines (IPs, see section 2.6.2)³² or fluorenylidene-pyrrolines (FPs, see section 2.6.3)³³ have also been object of study (Figure 5.44).

Finally, the behavior of CPP³⁴ and IPs³⁵ linked to model peptides has been studied as well using computational tools.

³¹ (a) Koumura, N.; Zijlstra, R. W. J.; Van Delden, R. A.; Harada, N.; Feringa, B. L. *Nature* **1999**, *401*, 152. (b) Koumura, N.; Geertsema, E. M.; Meetsma, A.; Feringa, B. L. *J. Am. Chem. Soc.* **2000**, *122*, 12005. (c) Koumura, N.; Geertsema, E. M.; Van Gelder, M. B.; Meetsma, A.; Feringa, B. L. *J. Am. Chem. Soc.* **2002**, *124*, 5037. (d) Feringa, B. L. *Acc. Chem. Res.* **2001**, *34*, 504.

³² (a) Lumento, F.; Zanirato, V.; Fusi, S.; Busi, E.; Latterini, L.; Elisei, F.; Sinicropi, A.; Andruniów, T.; Ferré, N.; Basosi, R.; Olivucci, M. *Angew. Chem. Int. Ed.* **2007**, *46*, 414. (b) Sinicropi, A.; Martin, E.; Ryazantsev, M.; Helbing, J.; Briand, J.; Sharma, D.; Léonard, J.; Haacke, S.; Cannizzo, A.; Chergui, M.; Zanirato, V.; Fusi, S.; Santoro, F.; Basosi, R.; Ferré, N.; Olivucci, M. *Proc. Natl. Ac. Sci. USA* **2008**, *105*, 17642. (c) Melloni, A.; Paccani, R. R.; Donati, D.; Zanirato, V.; Sinicropi, A.; Parisi, M. L.; Martin, E.; Ryazantsev, M.; Ding, W. J.; Frutos, L. M.; Basosi, R.; Fusi, S.; Latterini, L.; Ferre, N.; Olivucci, M. *J. Am. Chem. Soc.* **2010**, *132*, 9310.

³³ Rivado-Casas, L.; Campos, P. J.; Sampedro, D. *Organometallics* **2010**, *29*, 3117.

³⁴ Andruniów, T.; Fantacci, S.; De Angelis, F.; Ferré, N.; Olivucci, M. *Angew. Chem. Int. Ed.* **2005**, *44*, 6077.

³⁵ Sinicropi, A.; Martin, E.; Ryazantsev, M.; Helbing, J.; Briand, J.; Sharma, D.; Léonard, J.; Haacke, S.; Cannizzo, A.; Chergui, M.; Zanirato, V.; Fusi, S.; Santoro, F.; Basosi, R.; Ferré, N.; Olivucci, M. *Proc. Natl. Ac. Sci. USA* **2008**, *105*, 17642.

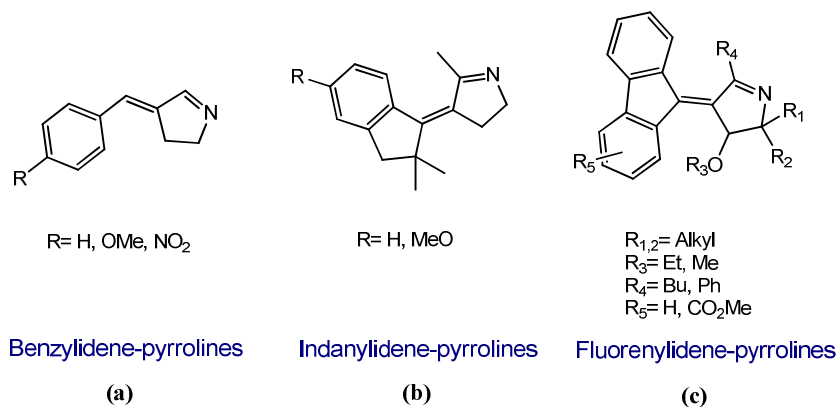


Figure 5.44. Structures of (a) BPs, (b) IPs, and (c) FPs.

In the following paragraphs, it is presented a brief summary of the theoretical calculations done for this type of compounds, in particular for compound **12** (see Figure 5.42), CPP (see Figure 5.43(a)) and BPs (see Figure 5.44(a)).

It should be highlighted that the detailed structure of the excited and ground state potential energy surfaces of the PSB-retinal chromophore model (*Z*)-penta-3,5-dieniminium cation (*cis*-C₅H₆NH₂⁺) (**12**) (see Figure 5.42), and in particular the structure of the excited and ground state reaction path branches has been fully elucidated.³⁶ Moreover, the reduced dimension of the model has permitted the computations of *ab-initio* CASSCF semi-classical trajectories and evaluation of the excited state lifetime and time scale of the photochemical isomerization. It has been proved that **12** provides a reasonable model for more realistic structures. Specially, the two-state two-mode nature of the reaction coordinate computed and observed (both in solution and in the Rh protein) is maintained in the minimal model. Furthermore, the computed ultrafast excited state dynamics is still characterized by two different timescales corresponding to a very initial stretching relaxation (*i.e.* an inversion of the single/double bond positions) and to the following torsional deformation (about the central C₂-C₃ bond) respectively.

In Figure 5.45, the branching vectors (**X**₁ and **X**₂) at the conical intersection (CI S₁/S₀) of **12** are shown. The conical intersection structure features only one highly twisted double bond (about 92^o) and involves two electronic configurations,

³⁶ *Computational Photochemistry*. Olivucci, M. (ed.) Elsevier: Amsterdam, 2005.

an ionic and a covalent state, which differ from the transfer of one electron between the $C_5-C_4-C_3$ - and $-C_2-C_1-N$ fragments. From the structure of the branching plane, it is obvious that in this molecule X_1 and X_2 describe two types of processes. As it can be inferred from Figure 5.45, motion along the X_1 corresponds to a coupled pyramidalization (wagging) modes at the C_1 and C_4 centers of the π -chain. This motion allows for a widening of the $C_4-C_3-C_2-C_1$ dihedral angle leading to a π -bond breaking process. The X_2 mode is characterized by a stretching deformation (a double bond expansion and single bond contraction mode) of the $N=C_1-C_2=C_3-C_4=C_5$ chain segment. Therefore, motion along the X_2 direction would ultimately yield two structures which may be represented by (resonance) formulas with inverted single and double bonds and with the positive charge shifted from the N-terminal to the C_5 -terminal. These two 92° twisted structures will be less stable than the generated motion along the wagging mode since the deformation along X_1 allows for reconstitution of the central double bond providing strong coupling with the Z/E double bond isomerization coordinate. Then, structural analysis of the branching plane suggests that upon decay from the conical intersection, the molecule will generate the Z and E stereoisomers.

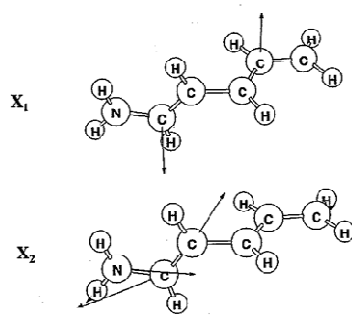


Figure 5.45. Branching plane vectors for the CI structure of **12. The X_1 and X_2 vectors correspond to the derivative coupling (or non-adiabatic coupling) and gradient difference vectors between the S_1 and S_0 states.³⁷**

In addition to this, in Figure 5.46, it is represented the excited state relaxation path of **12**. In this case, the mapping of the low-lying segments of the intersection space (IS), by means of constrained MEP computations, has demonstrated that it ends at a conical intersection with a ca. 70° (CI_{70°) twisted structure. The

³⁷ See ref 35.

intersection space remains then coincident with the reaction path up to the lowest energy intersection (CI_{92°) that has a 92° twisted structure. It should be noticed that in this situation the main locus of excited state (S_1) decay is predicted to be CI_{70° .

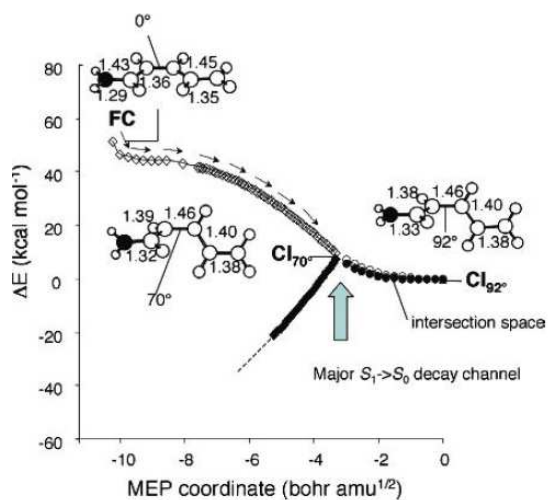


Figure 5.46. The excited state relaxation path of **12**.³⁸

On the other hand, in recent computational work,³⁹ it has been shown that PSBs feature nearly competitive photochemical *Z/E* isomerization paths corresponding to rotary motion about the adjacent double bonds of the chromophore. The existence of these competing paths is clearly undesirable. For this reason, CPP can be considered a good prototype for an efficient molecular switch since its structure is locked by the two five-membered rings (see Figure 543(a)).⁴⁰ These rings also introduce an angular (Bayer) strain that modifies the values of the $\text{N}_1\text{-C}_5\text{-C}_4$ and $\text{C}_1\text{-C}_2\text{-C}_3$ angles of the penta-2,4-dieniminium moiety. Similarly, the inductive effects due to alkyl substitution at the N_1 , C_4 , C_1 , and C_3 must change the S_1 and S_0 positive charge distribution along the chromophore framework.

³⁸ See ref. 35.

³⁹ (a) Ben-Nun, M.; Molnar, F.; Schulten, K.; Martinez, T. J. *Proc. Natl. Acad. Sci. U.S.A.* **2002**, *99*, 1769. (b) Nonella, M. *J. Phys. Chem. B* **2000**, *104*, 11 379. (c) De Vico, L.; Page, C. S.; Garavelli, M.; Bernardi, F.; Basosi, R.; Olivucci, M. *J. Am. Chem. Soc.* **2002**, *124*, 4124.

⁴⁰ See ref. 7(c).

Therefore, the photoisomerization paths for both the *E*-CPP → *Z*-CPP and *Z*-CPP → *E*-CPP processes have been computed (Figure 5.47). Taking a look at Figure 5.47 it is noticeable that the computed *E* → *Z* and *Z* → *E* paths display an energy inflection point in correspondence of a change in direction of the reaction coordinate (first dominated by stretching and then by twisting deformations). Also, it can be pointed out the existence of two planar *S*₁ transition states (**TS_{EXE}** and **TS_{EXZ}**), which implies that the energy surface is symmetric with respect to an out-of-plane deformation and, therefore, *S*₁ clockwise and counterclockwise twisting motions have the same probability to occur. For both the *E* → *Z* and *Z* → *E* paths *S*₁ → *S*₀ decay occurs in the region of a conical intersection (**CI**) displaying a *ca.* 90° central bond. The data of Figure 5.47 also indicate that, similarly to *S*₁ relaxation, *S*₀ relaxation does not involve formation of any intermediate and the system relaxes directly to the energy minimum corresponding to the photoproduct well. Since *Z*-CPP is the photoproduct of *E*-CPP and this is the photoproduct of *Z*-CPP, the two paths in Figure 5.47 describe a complete photocycle leading to a return to the original material after absorption of two photons of similar wavelengths. Finally, it should be noticed that two different *ca.* 90° twisted transition states (**TS_{GSI}** and **TS_{GSII}**) both controlling *E*-CPP → *Z*-CPP and *Z*-CPP → *E*-CPP thermal isomerization have been located *ca.* 40 kcal mol⁻¹ above the *S*₀ equilibrium structures. Such barriers guarantee that the thermal isomerization will not compete with the photochemical process in these species.

Therefore, the ability of CPP to function as an efficient molecular switch has been demonstrated through theoretical calculations (see section 2.6.1).

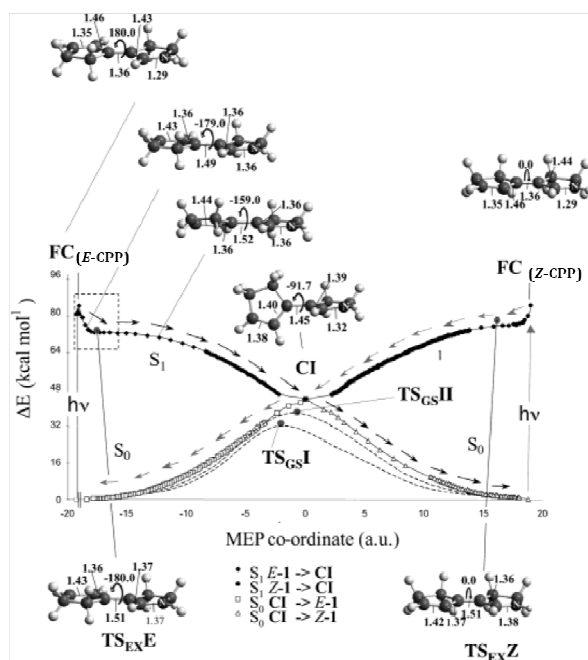


Figure 5.47. Energy profiles along the four MEPs describing the relaxation from the FC points of the *E*-CPP and *Z*-CPP stereoisomers and their (common) CI point.⁴¹

Finally, another prototype of photoswitch (**13**, see Figure 5.48) that belongs to the benzylidene-pyrroline family has also been computed in order to study its photochemical behavior. The structure of **13** is analogous to the structure of the photoswitches presented in this dissertation. Therefore, the computational data obtained for **13** might resemble those resulting from the study of our new prototypes of molecular switches.

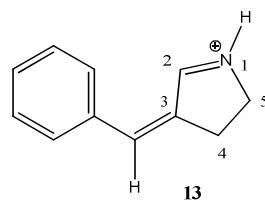


Figure 5.48. Structure of **13**.

⁴¹ See ref. 7(c).

In Figure 5.49 are represented the energy profiles along the minimum energy path (MEP) describing the excited-state relaxation of **E-13**. It is observed that **E-13** is planar, whereas **Z-13** features a 6° twist about the central double bond and a 45° twist about the adjacent unlocked single bond. Presumably, the phenyl ring is twisted out-of-plane by the steric interaction with the heterocycle hydrogen. The corresponding destabilization also accounts for the higher stability ($-1.2 \text{ kcal mol}^{-1}$) of **E-13** with respect to **Z-13**. The **TS_{GSI}** connecting the two forms features a *ca.* 80° twisted central double bond, and is located $43.9 \text{ kcal mol}^{-1}$ above **E-13**. Thus, as for **CPP**, such a high barrier indicates that the *E* and *Z* forms will not thermally interconvert at room temperature.

On the other hand, the excited-state surfaces of **13** (Figure 5.49) and **CPP** (Figure 5.47) present remarkable differences. In the first place, **13** has two low-lying $\pi\pi^*$ excited states separated by less than 2 kcal mol^{-1} . At **FC**, the CASSCF level of theory yields a spectroscopic state corresponding to S_2 , while the lower S_1 state corresponds to a dark state located $2.4 \text{ kcal mol}^{-1}$ lower in energy. When dynamic correlation is included, the spectroscopic state is pushed down by $5.3 \text{ kcal mol}^{-1}$, while the dark state is pushed up by only $0.3 \text{ kcal mol}^{-1}$. Thus, at the CASPT2 level, the energy order of the spectroscopic and dark state is inverted. Notice that due to this inversion the S_2/S_1 crossing found at the CASSCF level does no longer occur. Then, at the CASPT2 level the spectroscopic state is the lowest excited state along the entire reaction coordinate.

Secondly, the S_1 path features a minimum **MIN_{EX}** and a transition state **TS_{MINEX→CI}** (located $1.6 \text{ kcal mol}^{-1}$ higher in energy) connecting **MIN_{EX}** to a conical intersection **CI_{S1/S0}**. The comparison of the structures of **E-13** and **MIN_{EX}** reveals that, as it happened with **CPP**, the initial relaxation of the molecule is dominated by a stretching (as the central double bond expands from 1.36 \AA to 1.39 \AA) coupled with a limited 4° torsional deformation about the central double bond, and a 3° deformation about the adjacent unlocked single bond. The evolution of **MIN_{EX}** is dominated by twisting about both the central double bond and the adjacent unlocked single bond. Such deformation causes the hydrogen atom in *ortho*-position to approach one of the hydrogen atoms placed at C_4 of the pyrroline ring. The distance between these two atoms changes from 2.22 \AA at **MIN_{EX}** to 2.02 \AA in **TS_{MINEX→CI}**. This steric interaction is partially avoided by the twisting of the phenyl ring (3° in **MIN_{EX}**, 13° in **TS_{MINEX→CI}**) that slowly returns to planarity once surpassed the transition state. The lowest energy point of the S_1 energy surface corresponds to the conical intersection structure **CI_{S1/S0}** featuring a *ca.* 90° twisted

central double bond. Despite the small computed barrier, $\text{TS}_{\text{MIN}_{\text{EX}} \rightarrow \text{CI}}$ may allow partial or complete energy redistribution at MIN_{EX} . In practical terms the approx. 10 kcal mol⁻¹ photon energy separating FC and MIN_{EX} may be, at least partially, redistributed. To sum up, due to the presence of a transient I^* which corresponds to MIN_{EX} along the photoisomerization path of $E\text{-13}$, this prototype of photoswitch cannot be considered efficient (see section 2.6.1).

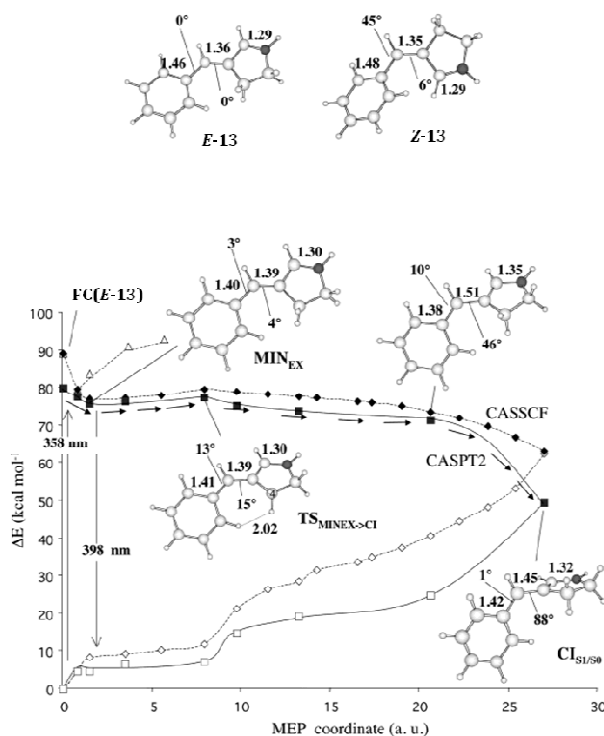


Figure 5.49. Energy profiles along the MEP describing the excited-state relaxation ($\text{FC}(E\text{-13}) \rightarrow \text{MIN}_{\text{EX}} \rightarrow \text{TS}_{\text{MIN}_{\text{EX}} \rightarrow \text{CI}} \rightarrow \text{CI}_{\text{S1/S0}}$) of $E\text{-13}$. Full and open diamonds indicate the CASSCF S_1 and S_0 energies, respectively; full and open squares indicate the CASPT2 S_1 and S_0 energies; open triangles indicate the CASSCF S_2 energies. The structures (geometrical parameters in Å and degrees) document the progression along this path and the equilibrium structures of the $E\text{-13}$ and $Z\text{-13}$ stereoisomers.⁴²

⁴² See ref. 7(c).

The similarities between previously reported BPs and the new prototypes of molecular switches have led us to not consider necessary the computational study of these latter compounds.

5.4.2. Theoretical calculations on the thermal and photochemical isomerization of the photoswitches based on the GFP chromophore.

5.4.2.1. Computational details.

For the thermal reactivity (ground state theoretical calculations), the common hybrid functional B3LYP was used.⁴³ It is based on Becke's three parameter scheme, consisting of the Slater exchange,⁴⁴ the exchange functional of Becke88,⁴⁵ and the HF exchange, as well as a mixture of the correlation functionals of Vosco–Wilk–Nusair⁴⁶ and Lee–Yang–Par.⁴⁷ The standard split-valence 6-31G* basis set⁴⁸ was employed. Geometry was fully optimized without any symmetry constraint for all model compounds. Optimized structures were characterized as minima or saddle points by frequency calculations, which also allowed obtaining the ZPE and thermal corrections. For the transition structures, also intrinsic reaction coordinates were calculated at the same level of theory.^{49,50}

For the photochemical reaction, the geometries were computed using fully unconstrained *ab initio* quantum chemical computations in the framework of a CASPT2//CASSCF strategy.⁵¹ This required the geometry to be computed at the complete active space self-consistent field (CASSCF) level of theory and the

⁴³ Becke, A. D. *J. Chem. Phys.* **1993**, *98*, 5648. (d) Olivucci, M.; Robb, M. A.; Bernardi, F. In *Conformational Analysis of Molecules in Excited States*; Waluk, J. (ed.) Wiley-VCH: New York, **2000**. (e) Robb, M. A.; Garavelli, M.; Olivucci, M.; Bernardi, F. In *Reviews in Computational Chemistry*; Lipkowitz, K. B.; Boyd, D. B. (ed.) Wiley-VCH: New York, **2000**.

⁴⁴ Slater, J. C. *Quantum Theory of Molecules and Solids, Vol. 4: The Self-Consistent Field for Molecules and Solids*; McGraw Hill: New York, **1974**.

⁴⁵ Becke, A. D. *Phys. Rev. B*, **1988**, *38*, 3098.

⁴⁶ Vosco, S. H.; Wilk, L.; Nusair, M. *Can. J. Phys.* **1980**, *58*, 1200.

⁴⁷ Lee, C.; Yang, W.; Parr, R. G. *Phys. Rev. B* **1988**, *37*, 785.

⁴⁸ Hariharan, P. C.; Pople, J. A. *Theor. Chim. Acta* **1973**, *28*, 213.

⁴⁹ Gonzalez, C.; Schlegel, H. B. *J. Chem. Phys.* **1989**, *90*, 2154.

⁵⁰ Gonzalez, C.; Schlegel, H. B. *J. Phys. Chem.* **1990**, *94*, 5523.

⁵¹ a) Sampedro, D. in *Photochemistry: UV/VIS Spectroscopy, Photochemical Reactions and Photosynthesis*; Maes, K. J., Willems, J. M. (eds.) Nova Science Publishers, **2011** b) *Computational Photochemistry*, Olivucci, M. (ed.) Elsevier: Amsterdam, **2005**.

corresponding energy profile to be re-evaluated at the multiconfigurational second-order Møller-Plesset perturbation theory level. This methodology has proven valuable for the study of related compounds.⁵² The Gaussian 03 program package⁵³ was used for CASSCF computations. The energy of the CASSCF geometries was recalculated using the CASPT2 method implemented in MOLCAS-6.4,⁵⁴ taking into account the effect of dynamic electron correlation. All CASPT2 results were obtained using a state average with equal weights for each state. Both CASSCF and CASPT2 calculations were performed using the standard 6-31G* basis set. We included in our calculations the complete π system. Thus, the active space was formed by 12 electrons in 12 orbitals: π and π^* orbitals from the aromatic ring, C=C and C=N and C=O double bonds. We also checked the influence of the active space by computing vertical transitions with expanded active spaces of (14,13) and (16,14).

Bulk solvent effects on the UV-spectra have been included using the polarizable continuum model (PCM)⁵⁵ as implemented in MOLCAS-6.4. The molecule is considered as included in a cavity surrounded by an infinite medium with the dielectric constant corresponding to the specific solvent. The standard value of 36.64 for acetonitrile was used in these calculations. The UV-spectrum was computed under non-equilibrium conditions, that is, only solvent electronic polarization is in equilibrium with excited-state electron density. Thus, only fast solvent degrees of freedom are considered. This kind of calculations is more

⁵² See ref 7(c).

⁵³ Frisch, M. J.; Trucks, G. W.; Schlegel, H. B.; Scuseria, G. E.; Robb, M. A.; Cheeseman, J. R.; Montgomery Jr., J. A.; Vreven, T.; Kudin, K. N.; Burant, J. C.; Millam, J. M.; Iyengar, S. S.; Tomasi, J.; Barone, V.; Mennucci, B.; Cossi, M.; Scalmani, G.; Rega, N.; Petersson, G. A.; Nakatsuji, H.; Hada, M.; Ehara, M.; Toyota, K.; Fukuda, R.; Hasegawa, J.; Ishida, M.; Nakajima, T.; Honda, Y.; Kitao, O.; Nakai, H.; Klene, M.; Li, X.; Knox, J. E.; Hratchian, H. P.; Cross, J. B.; Adamo, C.; Jaramillo, J.; Gomperts, R.; Stratmann, R. E.; Yazyev, O.; Austin, A. J.; Cammi, R.; Pomelli, C.; Ochterski, J. W.; Ayala, P. Y.; Morokuma, K.; Voth, G. A.; Salvador, P.; Dannenberg, J. J.; Zakrzewski, V. G.; Dapprich, S.; Daniels, A. D.; Strain, M. C.; Farkas, O.; Malick, D. K.; Rabuck, A. D.; Raghavachari, K.; Foresman, J. B.; Ortiz, J. V.; Cui, Q.; Baboul, A. G.; Clifford, S.; Cioslowski, J.; Stefanov, B. B.; Liu, G.; Liashenko, A.; Piskorz, P.; Komaromi, I.; Martin, R. L.; Fox, D. J.; Keith, T.; Al-Laham, M. A.; Peng, C. Y.; Nanayakkara, A.; Challacombe, M.; Gill, P. M. W.; Johnson, B.; Chen, W.; Wong, M. W.; Gonzalez, C. and Pople, J. A.; Gaussian, Inc., Wallingford CT, **2004**.

⁵⁴ Karlström, G.; Lindh, R.; Malmqvist, P.-Å.; Roos, B. O.; Ryde, U.; Veryazov, V.; Widmark, P.-O.; Cossi, M.; Schimmelpfennig, B.; Neogrady, P.; Seijo, L. *Comput. Mater. Sci.* **2003**, *28*, 222.

⁵⁵ Tomasi, J.; Mennucci, B.; Cammi, R. *Chem. Rev.* **2005**, *105*, 2999.

adequate to compute vertical excitation energies, as those needed for the UV-spectra.

5.4.2.2. Thermal isomerization.

We started our computational study by exploring the relative stability of the different isomers, including the steric and electronic factors introduced by the substituents R_3 and R_4 , which could affect the thermal isomerization. In section 4.2.1, we described the different compounds with structure based on the GFP chromophore that can be easily generated from a common synthetic route. This kind of compounds shows some differences that allow the classification of the products depending on:

- The α -aminoacid (compound **6**) used in the synthesis: methyl vs. phenyl group (substituent R_3) in the oxazolone ring.
- The substituent in the benzaldehyde derivative: electron donating vs. electron withdrawing groups in substituent R_4 .
- The position of the substituent in the phenyl group of substituent R_4 : *ortho*- vs. *para*- substitution.

We computed both isomers (*Z* and *E*) of several compounds in order to explore the effect of substitution according to the three main categories described above. First, we explored the effect of the methyl vs. the phenyl groups (substituent R_3) in the oxazolone ring by computing the isomers of **7h** and **7a** (see Figure 5.50). The detailed geometry specifications can be found in Appendix C as cartesian coordinates.

As can be seen, the change in substituent R_3 of the methyl group for a phenyl doesn't produce any significant variation in neither the geometries nor the relative energies. All four compounds are planar and the bond distances are very similar, as only variations in the third decimal were found, including C=N bond close to the modified substituent. Moreover, the energetics is the same as variations are below the theoretical threshold for the method used. Thus, from a thermal reactivity point of view, the inclusion of Ph or Me should provide similar results. However, the inclusion of a phenyl group should be relevant for the photochemical reactivity as the extended conjugation leads to a red-shift in the UV spectrum.

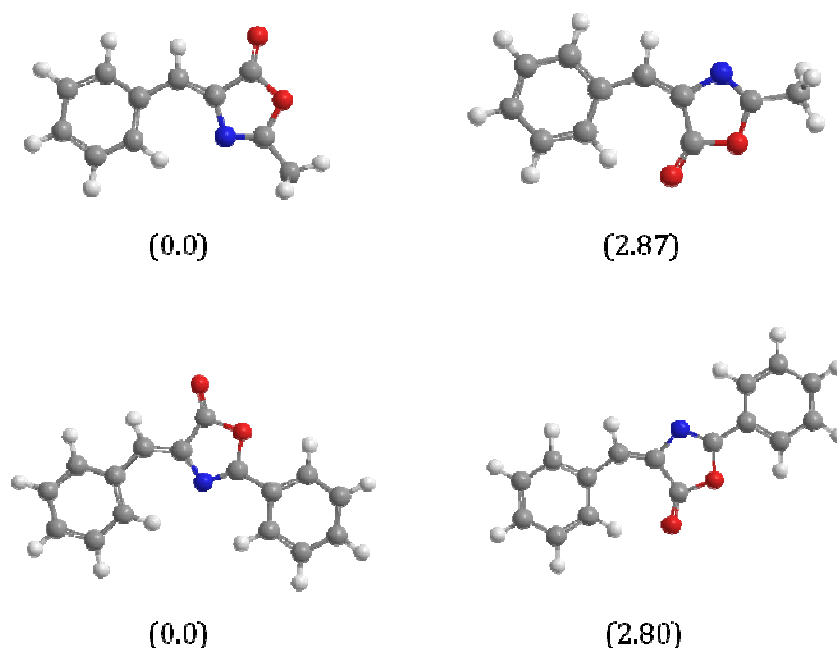


Figure 5.50. *Z* and *E* isomers and relative energies (kcal/mol) for compounds **7h** (top of the image) and **7a** (bottom of the image).

Next, we explored the effect of the electronic character of the substituent in the phenyl group of substituent R_4 by computing compounds **7v** and **7c**,⁵⁶ in which an electron withdrawing (cyano) or electron donating (methoxy) group is attached to the phenyl ring. The obtained results are shown in Figure 5.51.

Again, the influence of the electronic character of the substituent in the phenyl group of substituent R_4 is scarce. A slight variation in the central C=C was found (1.358 Å in the cyano-substituted compound (**7v**) vs. 1.361 Å in the methoxy product (**7c**)). The same distance has a value of 1.359 Å in the parent, unsubstituted product **7a**. This fact could be related to an increased energy barrier for thermal isomerization in the former compound, although the difference is very small.

⁵⁶ The compound **7v** hasn't been synthesized. It has only been studied computationally in order to check the influence of having an electron withdrawing (ciano) group attached to the phenyl ring of R_4 .

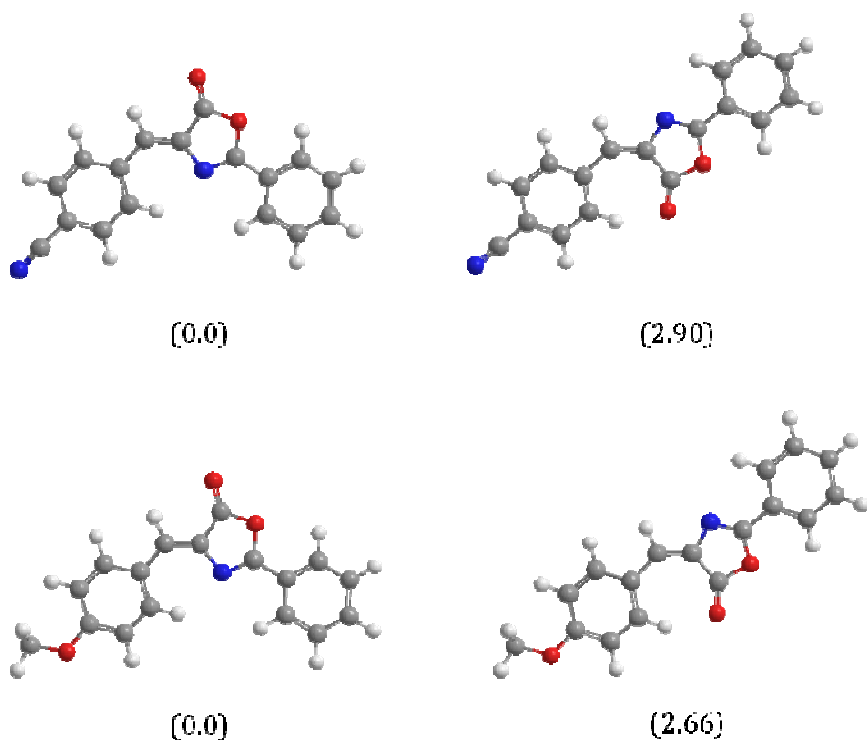


Figure 5.51. *Z* and *E* isomers and relative energies (kcal/mol) for compounds 7v (top of the image) and 7c (bottom of the image).

Finally, the effect of substitution in the *ortho* position in the phenyl group of substituent R_4 was explored by computing compound 7f (Figure 5.52).

In the case of *ortho*-substituted compounds, four different isomers can exist. Two of them are *Z* while the other two are *E*. For every central C=C configuration, two different isomers are possible due to the orientation of the substituent in the aromatic ring. In this case, due to the size of the bromine atom, the two isomers in which the Br atom is located near to the oxazolone ring are clearly more unstable due to steric reasons. This causes the molecule to move away from the planar disposition common to other compounds, especially in the case where the Br atom is very close to the carbonyl moiety. Moreover, in the other two isomers with the Br atom far away from the oxazolone ring, a similar behavior is found in the

relative stability of *Z* and *E* isomers, the planar disposition of both molecules and the central C=C distance (1.359 Å for the most stable isomer).

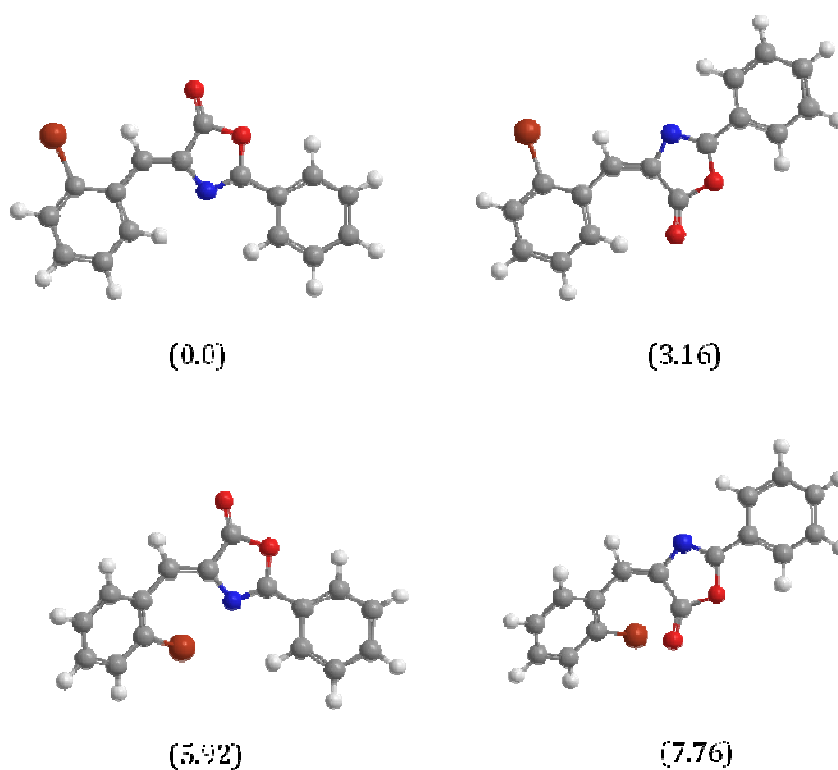


Figure 5.52. *Z* and *E* isomers and relative energies (kcal/mol) for compound 7f.

At last, we checked the feasibility for the thermal isomerization, which has been experimentally studied in section 5.3.1.4. As shown before, only minor variations can be expected for the thermal reaction as the three types of modifications experimentally included in the structure seem to have very limited effects in the energy and structure of the different isomers. Thus, we explored the thermal isomerization path in the compound 7a, which has one of the simplest structures among this type of compounds.

The transition structure connecting both isomers is shown in Figure 5.53. This geometry is placed 61.9 kcal/mol higher in energy than the most stable

5. Photochemical study

isomer. As can be seen, the geometry features a twist of 87.5° between both rings consistent with the *E* / *Z* isomerization process together with a slight central C=C bond elongation (1.368 \AA vs. 1.359 \AA) in the most stable isomer while the torsion angle between the vinylic hydrogen atom and the oxazolone ring is only 39° . Although the double bond character is maintained in this transition structure, the deformation of the geometry clearly points to a C=C isomerization, as showed by the pyramidalization in the C atom next to the aromatic ring and the dihedral angle between rings.

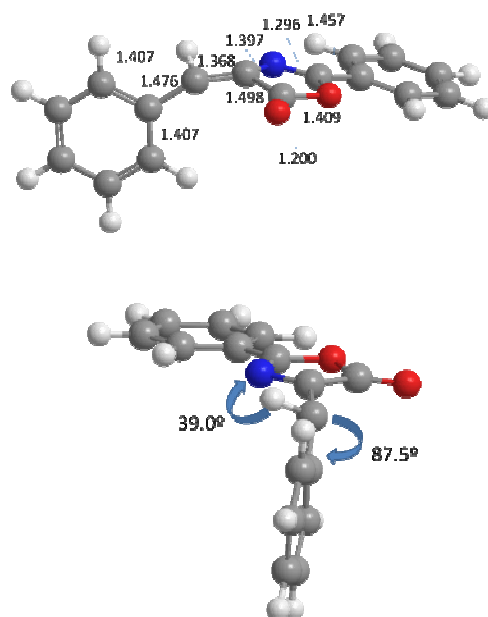


Figure 5.53. Transition structure for the ground state isomerization of 7a.

A frequency calculation on the transition structure allowed us to obtain the transition vector as shown in Figure 5.54, with an imaginary frequency of 182.7449 cm^{-1} . The main deformation associated with this vector is the hydrogen atom movement connecting the transition structure to the two valleys in the potential energy surface relative to the *E* and *Z* isomers.

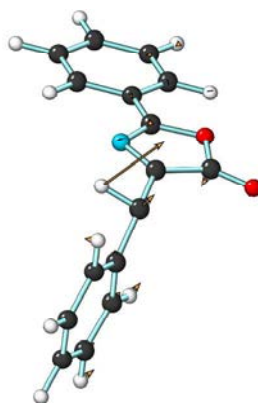


Figure 5.54. Transition vector for the isomerization of 7a.

As a final step for the transition structure characterization, we performed an Intrinsic Reaction Coordinate (IRC) calculation, whose results are shown in Figure 5.55.

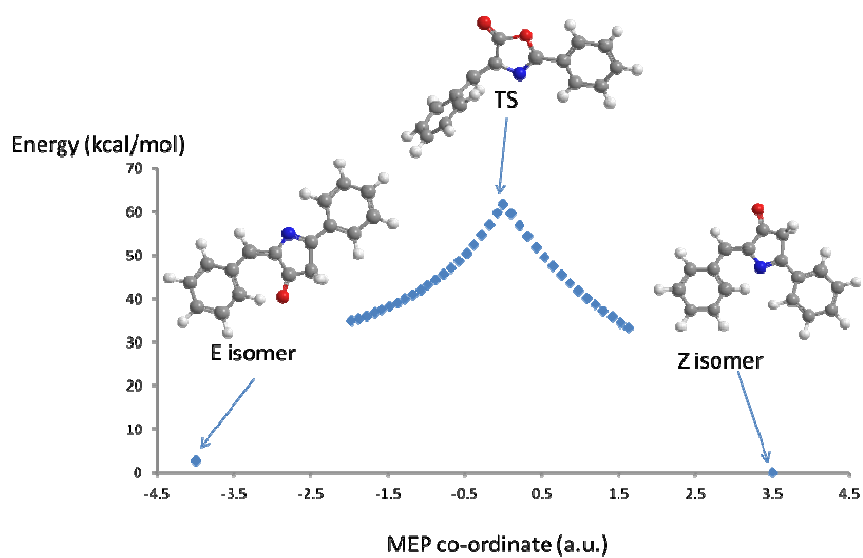


Figure 5.55. IRC starting from the computed transition structure of 7a.

As a final verification of the transition structure, the two isomers are obtained after computing the reaction path starting from the transition structure in both directions.

As explained above, only slight modifications are expected for the synthetic variations of the structure. The high energy value computed for the transition structure is in agreement with the thermal stability found for this type of compound. As shown in section 5.3.1.4, these compounds were found to be stable to isomerization for days at room temperature, and isomerization was detected only after heating in toluene at 100°C.

5.4.2.3. Absorption Spectrum.

As explained above, the optimized geometry is completely planar, as expected by the extended conjugation and the absence of steric hindrance. Figure 5.56 shows the geometry computed at the CASSCF level. The absorption spectrum corresponding to the three lowest-lying singlet excited-states (S_1 , S_2 , S_3) was calculated for compound **7h**,⁵⁷ and the results are shown in Table 5.14.

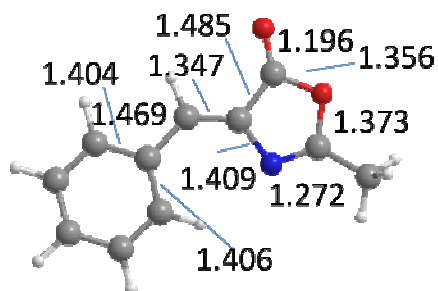


Figure 5.56. Ground state geometry for 7h.

⁵⁷ In the following sections, we chose to study compound **7h** instead of **7a** because it required a lower computational cost. Moreover, it has been proved experimentally that changing R_3 from a methyl to a phenyl group didn't affect the photochemical properties of the photoswitch.

Table 5.14. Experimental (CH₃CN) and vertical CASPT2 transition energies (gas phase), orbital transitions and oscillator strengths (f) for 7h.

Band, eV (nm)	State	E _{CASPT2} , eV (nm)	Transition	f	Relative f
3.80 (327)	S ₃	6.78 (183)	¹ (π,π*)	0.05	1
	S ₂	5.09 (244)	¹ (π,π*)	0.0007	0.014
	S ₁	4.87 (255)	¹ (π,π*)	0.002	0.04

The Franck-Condon (FC) vertical excitation energies and oscillator strengths can be compared with the corresponding experimental data (see Figure 5.28). The experimental UV spectrum of **7h** shows a strong absorption band at 327 nm in acetonitrile, even though the absorption band is slightly solvent dependent ($\lambda_{\text{max}}=332$ nm in CHCl₃). The computational spectrum features a strong absorption at 183 nm. However, this band is located at higher energies and, therefore, is irrelevant for the photoprocesses under study. Two more bands appear at lower energies with similar oscillator strengths. Both bands share a π,π* character but the transition is located in different places. While for S₂ the excitation is located in the central C=C bond, in S₁ the excitation is located in the central C=C and the aromatic ring. Thus, in terms of efficient photoisomerization, both bands could provide a competent reaction path. However in S₂, as the excitation is exclusively located in the central C=C double bond, the photoisomerization could be more effective. In any case, transition to both S₂ and S₁ would ultimately lead to the same reaction path (see more information below).

After comparing the experimental and theoretical spectra, the qualitative picture is reasonably well reproduced although the quantitative values are blue-shifted. The reason for these differences could be the environment effect (gas phase vs. solvent) or a reduced active space. In order to explore the effect of the solvent, the transition spectrum for **7h** in acetonitrile was also computed and results are shown in Table 5.15.

Table 5.15. Experimental (CH_3CN) and vertical CASPT2 transition energies (PCM, CH_3CN), orbital transitions and oscillator strengths (f) for 7h.

Band, eV (nm)	State	E_{CASPT2} , eV (nm)	Transition	f	Relative f
3.80 (327)	S_3	5.62 (221)	$^1(\pi, \pi^*)$	0.85	1
	S_2	5.35 (232)	$^1(\pi, \pi^*)$	0.001	0.001
	S_1	4.88 (255)	$^1(\pi, \pi^*)$	0.003	0.003

As can be seen, the qualitative picture is quite similar to the computed spectrum in gas phase. The main difference is the stabilization of S_3 or, most probably, an alteration in the states energy order. In CH_3CN , an ionic excited state would be stabilized and thus, would show a lower energy value. Thus, the excited state located as S_3 in gas phase and acetonitrile represent different states. While in gas phase S_3 is covalent and the excitation is mainly located in the aromatic ring, the S_3 excited state computed using PCM is clearly ionic and charge transfer takes place from the oxazolone ring to the aromatic ring. This fact is reflected in the dipolar moment of this state (2.70 D vs. the value of 5.70 of the ground state) and the modification in charges in both rings, as shown in Figure 5.57. However, from a practical point of view this transition is still not relevant for the photoisomerization as it is located at high energies. The lowest-lying S_2 and S_1 states show similar features than those found in gas phase. In both cases the transitions are located in the central $\text{C}=\text{C}$ double bond and both the maxima of absorption and oscillator strengths are quite similar to the gas phase. Thus, the qualitative picture is maintained when the solvent is considered through the PCM method.

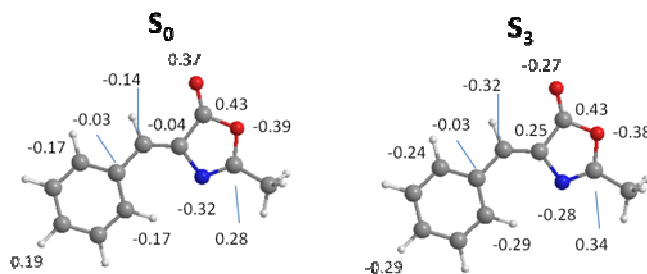


Figure 5.57. Ground and excited (S_3) states charges.

The effect of the active space was also checked by increasing the number of orbitals and electrons included. Specifically, the non-bonding n orbital in the nitrogen atom was included in the active space. Results are summarized in Table 5.16.

Table 5.16. Experimental (CH₃CN) and vertical CASPT2 transition energies (gas phase), orbital transitions and oscillator strengths (f) for 7h with a (14,13) active space.

Band, eV (nm)	State	E _{CASPT2} , eV (nm)	Transition	f	Relative f
3.80 (327)	S ₃	5.50 (226)	¹ (π,π*)	0.001	0.14
	S ₂	4.87 (255)	¹ (π,π*)	0.007	1
	S ₁	4.84 (257)	¹ (n,π*)	0.002	0.3

As can be seen, a new transition appears after the inclusion of the nitrogen lone pair. This transition has an n,π* character and corresponds with the transition at lower energies. However, the oscillator strength values show that the main absorption is still the (π,π*) transition. In the experimental spectrum, this band would probably hide the less intense n,π* transition.

The active space was further increased by including one of the non-bonding oxazolone oxygen atoms n orbital. This orbital could be relevant as far as it could be conjugated with the C=N bond and, therefore, it could affect the chromophore. The obtained results are summarized in Table 5.17.

Table 5.17 Experimental (CH₃CN) and vertical CASPT2 transition energies (gas phase), orbital transitions and oscillator strengths (f) for 7h with a (16,14) active space.

Band, eV (nm)	State	E _{CASPT2} , eV (nm)	Transition	f	Relative f
3.80 (327)	S ₃	5.50 (226)	¹ (π,π*)	0.0007	0.35
	S ₂	4.87 (255)	¹ (π,π*)	0.002	1
	S ₁	3.68 (338)	¹ (n,π*)	0.0005	0.25

The resulting computed spectrum features a low-energy transition at 338 nm. However, the oscillator strength value, together with the electronic n,π^* character of the transition suggests that this absorption is not relevant for the photochemistry.

Although the quantitative spectrum could not be reproduced, the most relevant features are present in our simple model in gas-phase with an active space of (12,12). A further increase in the active space and basis-set could lead to a quantitative match with the experimental spectrum. However, as we will see, this is not critical for the qualitative mechanistic picture obtained.

5.4.2.4. Photoisomerization

As explained above, both S_2 and S_1 can be populated. In both cases, wave function analysis shows electronic transitions between the π and π^* orbitals of the central C=C double bond. However, as both the energy and electronic character are very similar, initial relaxation would lead to S_1 population either directly after light absorption or through a S_2/S_1 surface crossing. The computed geometry for the CI S_2/S_1 is shown in Figure 5.58.

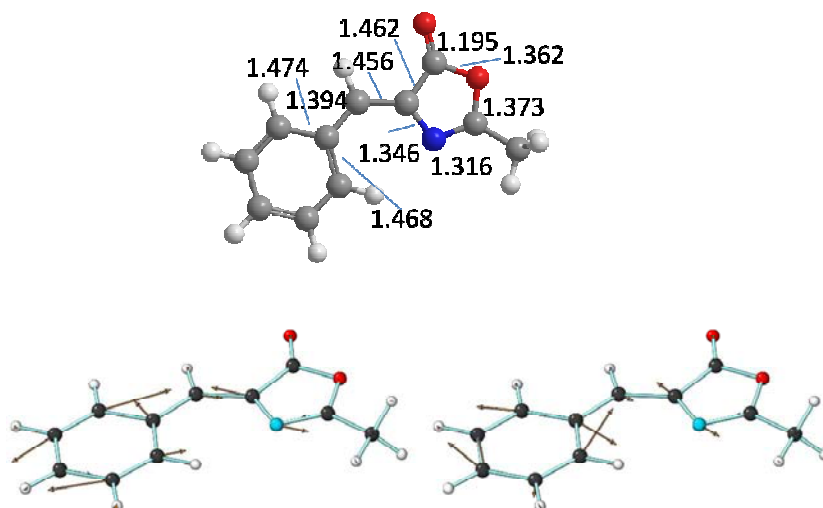


Figure 5.58. Geometry and derivative coupling and gradient difference vectors for the CI S_2/S_1 .

From the analysis of the **FC** (Figure 5.56) and the **CI S₂/S₁** (Figure 5.58) geometries it is evident that the relaxation in S₂ takes place by preserving the planarity of the system. The conical intersection point is easily reached by deformation along the stretching coordinate. The branching plane associated with this CI also corresponds with an in-plane deformation as can be seen by the vector shown in Figure 5.58. Once the S₁ state is reached, either by direct population or through the previous CI point, relaxation continues to be dominated by the stretching coordinate. In both cases, the same minimum in the S₁ potential energy surface (**Min S₁**) was reached. The geometry is shown in Figure 5.59.

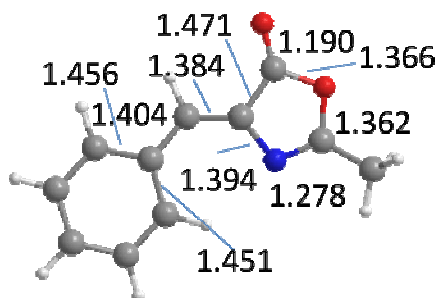


Figure 5.59. Geometry for the Min S₁.

While the system planarity is maintained in **Min S₁**, the central C=C bond recovers its double bond character. The same happens with the N=C bond and the C-N connecting them lengthens. This is probably due to bond switching caused by S₂ in the region between **FC** and **CI S₂/S₁**. This minimum is the responsible of fluorescence in this type of compound. The ground state is located 99.5 kcal/mol below S₁ in this geometry. This provides a wavelength of 288 nm for the computed emission from this minimum. This value can be compared with the experimental emission found at 380 nm (see section 5.3.2.3). The computed emission is considerably blue-shifted with respect to the experimental value. This discrepancy could be attributed to the same factors already considered in the absorption spectrum paragraph. After inclusion of the solvent through a PCM calculation or by increasing the active space to (16,14) the computed value for the emission was consistently the same. However, it should be noted that the experimental Stokes shift (45 nm) is very close to the computational Stokes shift (44 nm for the S₁ absorption). This agreement provides a validation for the level of theory used as

the qualitative picture of the potential energy surfaces is well described and all of the electronic states involved are equally weighted.

Relaxation to the ground state can be done through light emission as explained before or through a conical intersection point. In previous sections the photochemistry and photophysics of this type of compounds have been described (see sections 5.3.1 and 5.3.2). Fluorescence emission is responsible of only a minor percentage of ground state population, while *E* / *Z* isomerization is the main reaction pathway. To explain this behavior a conical intersection point connecting the planar **Min S₁** previously described and the ground state was searched. The geometry of **CI S₁/S₀** is shown in Figure 5.60 together with the branching space vectors.

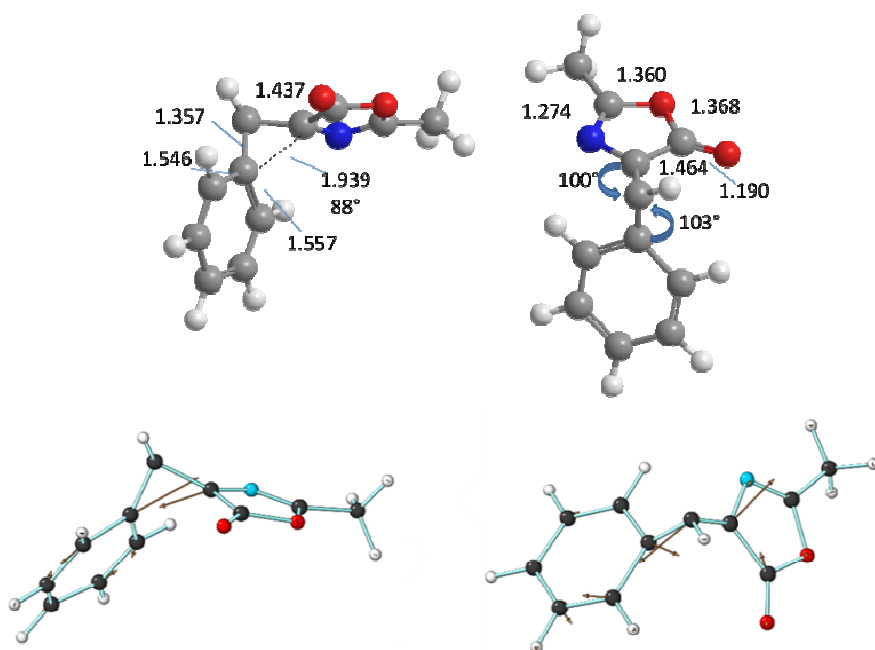


Figure 5.60. Geometry and derivative coupling and gradient difference vectors for the **CI S₁/S₀**.

This CI point is located *ca.* 12 kcal/mol higher in energy with respect to the **Min S₁**. The geometry is clearly distorted in **CI S₁/S₀** as shown in Figure 5.60. The main geometrical changes corresponds with the simultaneous rotation of both

rings (100° and 103°) together with the generation of a kink structure in the central C=C double bond (C-C-C angle 88° , C-C distance 1.939\AA). This CI point features the typical geometry related with a space-saving hula-twist type. Specifically, the two rings are highly twisted and the central C=C double bond is elongated. In contrast with this, the branching space vectors do not show clear components along these two twisting angles as the degeneracy, as shown by the derivative coupling and gradient difference vectors, is mainly lifted by stretching deformations. For the derivative coupling vector (Figure 5.60, left) the deformation is dominated by the C-C-C angle while for the gradient difference vector (Figure 5.60, right) the deformation corresponds with central C-C bond stretching. Thus, the simultaneous change of the twist angles for both rings (hula-twist motion) does not belong to the branching space. After the CI point is reached, the degeneracy can be lifted by moving in any direction within the branching space as defined by the vectors shown in Figure 5.60. To clarify the photoproduct generation from this CI, we computed the different products obtained when relaxing in the ground state in the four different directions pointed out by the branching space vectors. In all four cases, optimization in the ground state leads to the formation of the more stable Z isomer. Similarly, optimization in the S_1 excited state lead to the planar **Min S₁**. This suggests a sloped conical intersection point, in agreement with the relative energy of **Min S₁** and **CI S₁/S₀**. Due to the topology of the conical intersection point, the static point of view provided by the calculations does not allow to provide quantitative information on the photoisomerization process, including the photoreaction quantum yield. This type of data can be only obtained through dynamics calculations. However, the qualitative picture is in agreement with the experimental results obtained.

Figure 5.61 shows the critical points along the potential energy surface computed for compound **7h**.

5. Photochemical study

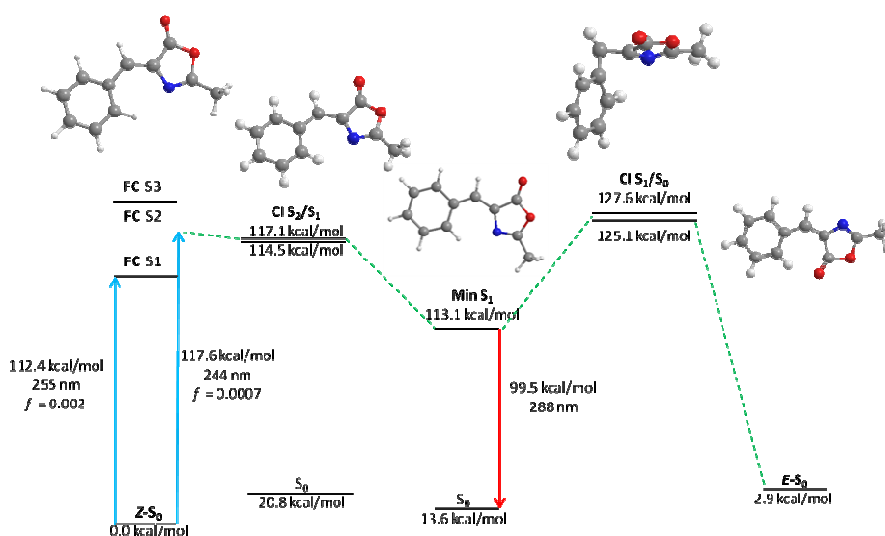


Figure 5.61. Critical points along the 7h potential energy surfaces.

5.4.5.5. Comparison with the GFP chromophore

As explained in previous sections (see sections 5.3.1 and 5.3.2), the main photochemical and photophysical deactivation pathway for the excited state states in the switches under investigation is the Z/E photoisomerization. While the starting material recovery seems to be a competitive pathway as determined by the photoreaction quantum yield, this is not the case for the fluorescence deactivation. This is clearly in contrast with the GFP chromophore which was first used as template for the design of the family of compounds under study. In fact, the wild-type GFP is strongly fluorescent. This fluorescence disappears in solution although it can be recovered in a cold matrix. These facts imply, on one hand, the strong effect caused by the protein environment and, on the other hand, the inherent fluorescence deactivation in the GFP chromophore. This fluorescence can be tuned by temperature suggesting a barrier that hampers this deactivation. When fluorescence is not the main deactivation channel, photoisomerization is usually invoked to explain the non-radiative deactivation. Thus, fluorescence and photoisomerization compete in the GFP chromophore and related compounds, including those under study here. Although the chemical structure for both types of compounds is quite similar, their photophysical and photochemical behavior are

different. This should be reflected in the computed potential energy surface for both types of compounds.

Figure 5.62 represents schematically the computed potential energy surface for compound **7h** as detailed above. The reaction path features a planar minimum responsible for the fluorescence and a conical intersection point which mediates in the photoisomerization reaction. The energy profile qualitatively explains the experimental results found. In the case of the GFP anionic chromophore a similar diagram is shown in Figure 5.63.⁵⁸

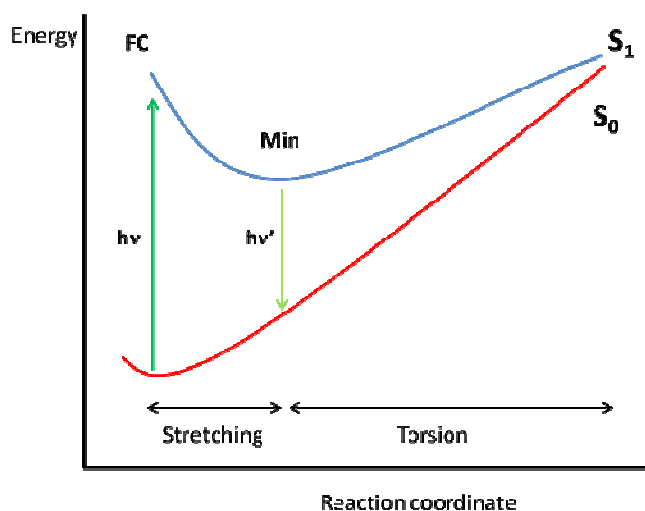


Figure 5.62. Mechanistic picture for **7h** and related compounds.

⁵⁸ Martín, M. E.; Negri, F., Olivucci, M. *J. Am. Chem. Soc.* **2004**, *126*, 5452.

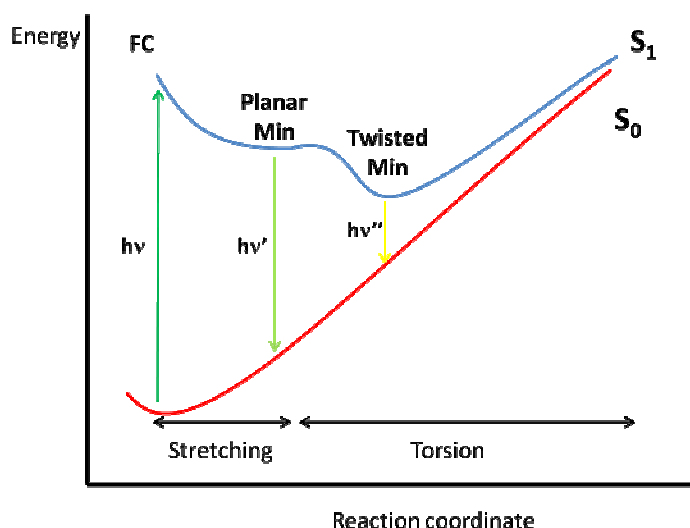


Figure 5.63. Mechanistic picture for the anionic GFP chromophore.

As shown in Figures 5.62 and 5.63, the main difference between the computed potential energy surfaces for both types of compounds is the presence of a stable, twisted minimum in S_1 in the case of the GFP chromophore. This slight variation in the potential energy surface has deep implications in the photophysics. First, the presence of two different minima in the excited state allow for the emission from two different geometries which, in turn, provide two different deactivation channels for the excited state that do not correspond with photoisomerization. In this case, the emissions were located in the visible (507 nm) and infrared (958 nm). Second, a transition state is located between the two minima. Although the computed energy barrier is small, the region of the potential energy surface relates with the photoisomerization is more difficult to reach.

Finally, the presence of a very stable minimum in the excited state causes a higher energy difference between the minimum and the conical intersection. We searched for a twisted minimum similar to that found in the case of the GFP chromophore to check the general mechanistic picture for the compounds under study as shown in Figure 5.62. This minimum was found and the geometry is shown in Figure 5.63.

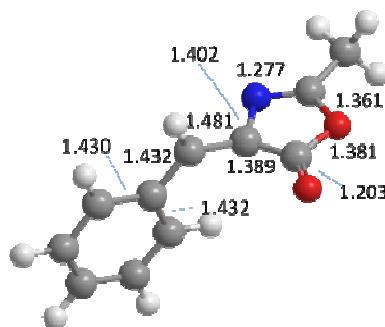


Figure 5.63. Geometry for the Twisted Min S_1 of 7h.

This geometry features an 80.3° twist in the central C=C bond and is similar to the geometry described in the case of the GFP chromophore. However, in this case the energy for the minimum is 129.1 kcal/mol, that is, higher in energy than the **CI** S_1/S_0 . Even more, the computed emission from this minimum provides a value of 467 nm. As explained before, emission from related wavelengths was not experimentally found. Thus, in the case of these compounds the twisted minimum as shown in Figure 5.63 seems that it is not relevant for neither the photoisomerization nor the fluorescence.

CHAPTER 6

Practical applications

As soon as the photochemical study of the new prototypes of molecular switches based on the PSB-retinal and GFP chromophores has been performed, the next goal is to introduce these units in more complex structures with the aim of being able to photocontrol their function. As stated in section 4.1.1, one of the features that should be fulfilled by an efficient molecular switch is the fact of having suitable anchoring points for linkage to other systems. Therefore, the structure of the photoswitches that have been so far synthesized has to be adequately modified to be able to be cross-linked to the target biomolecules.

In this chapter, we present our efforts to design, synthesize and computationally explore new molecular switches that can be inserted in more complex biomolecules, in particular peptides. After achieving the first step, the photochemical study of the cross-linked peptides with the appropriate techniques will be described.

As done previously, this chapter will be sorted into two different sections. We will first talk over the tests performed with the compounds with structure based on the green fluorescent protein (GFP) chromophore. Afterwards, we will review the studies carried out with the photoswitches with structure based on the protonated Schiff base (PSB) of the retinal chromophore.

6.1. INTRODUCTION

As discussed at the beginning of this dissertation (see Chapter 1), the use of light to induce a mechanical movement at the molecular level has been object of study in the last years.¹

Several approaches have been performed to chemically modifying a biomolecule in order to provide it with light-controlled function. However, these chemical modifications should meet the following requirements:²

- they must absorb light effectively (present a high molar extinction coefficient or two-photon cross-section) at a wavelength compatible with biological systems (longer than 340 nm, ideally much longer, up to 800 nm);
- they have to undergo a photochemical reaction with high efficiency to reduce the light dosage required;
- they must provoke a change in the biomolecule activity by altering it.
- they should be stable to biological conditions, and inert (non-toxic) both before and after irradiation.

One of these strategies involves the use of molecular switches based on *E/Z* isomerizations, which have been already used in different contexts to control diverse properties.³ Among the numerous photoswitches achieved, systems based on azobenzene have been widely employed, since it meets most of the criteria outlined above. For instance, azobenzenes have been lately employed as

¹ (a) Balzani, V.; Credi, A.; Venturi, M. *Molecular Devices and Machines: Concepts and Perspectives for the Nanoworld*. Wiley-VCH Verlag, Germany, **2008**. (b) Drexler, K.-E. *Nanosystems: Molecular Machinery, Manufacturing and Computation*. John Wiley: New York, 1992. (c) Sauvage, J.-P. *Molecular Machines and Motors*; Springer Verlag, Heidelberg, 2001; Vol. 99 (d) Bossi, M. L.; Aramendía, P. F. J. *Photochem. Photobio. C* **2011**, *12*, 154.

² Beharry, A. A.; Woolley, G. A. *Chem. Soc. Rev.* **2011**, *40*, 4422.

³ (a) Cacciapaglia, R.; Stefano, S. D.; Mandolini, L. *J. Am. Chem. Soc.* **2003**, *125*, 2224. (b) Joussetme, B.; Blanchard, P.; Gallego-Planas, N.; Delaunay, J.; Allain, M.; Richomme, P.; Levillain, E.; Roncali, J. *J. Am. Chem. Soc.* **2003**, *125*, 2888. (c) Shinkai, S.; Minami, T.; Kusano, Y.; Manabe, O. *J. Am. Chem. Soc.* **1983**, *105*, 1851.

photoswitches in biological applications,⁴ photomodification of polymers⁵ and to induce photomechanical movements in liquid crystals.⁶

Azobenzene derivatives present many favourable properties. Firstly, they feature strong light absorption and photoisomerize with efficiency. Also, the isomerization process induces a pronounced change in geometry as well as dipole moment, which is mainly responsible for all the photoinduced transformations triggered by this photochemical reaction. While the *trans* conformation is near planar and has a dipole moment near zero, the *cis* isomer adopts a bent conformation with its phenyl rings twisted ca. 55° out of the plane from the azo group and has a dipole moment of 3 D.⁷ Last, but not least, an enormous diversity of azobenzene derivatives are synthetically accessible and a detailed knowledge of the relation between substitution and properties is available.

Therefore, the preparation and characterization of novel photoswitches different from azobenzenes in properties such as size, wavelength of absorption, reactivity, polarity and isomerization mechanism represent an attractive research target. The discovery of new or alternative prototypes could expand the applicability of the switch concept to diverse and increasingly complex molecular systems.

⁴ (a) See ref. 2 (b) Renner, C.; Moroder, L. *ChemBioChem* **2006**, *7*, 868.

⁵ Natansohn, A.; Rochon, P. *Chemical Reviews* **2002**, *102*, 4139.

⁶ Yu, Y.; Nakano, M.; Ikeda, T. *Nature* **2003**, *425*, 145.

⁷ (a) Fliegl, H.; Kohn, A.; Hattig, C.; Ahlrichs, R. *J. Am. Chem. Soc.* **2003**, *125*, 9821. (b) Tsuji, T.; Takeuchi, H.; Egawa, T.; Konaka, S. *J. Am. Chem. Soc.* **2001**, *123*, 6381.

6.2. APPLICATIONS OF PHOTOSWITCHES WITH STRUCTURE BASED ON THE GFP CHROMOPHORE.

6.2.1. Synthesis of the appropriate GFP-based photoswitches for the linkage to more complex biomolecules.

As seen in section 4.2.1, the synthetic route to achieve GFP-based photoswitches involved less synthetic steps, and with better yields, than the one to obtain PSB-retinal based photoswitches. Then, we decided to study first this type of compounds.

For this purpose, it was required that the compounds had two points of linkage, and if possible, one at each end of the switch. For instance, any functional group capable of undergoing nucleophilic substitution, such as $-\text{CH}_2\text{Br}$ or $-\text{NHCOCH}_2\text{Cl}$, would be useful. Therefore, we decided to synthesize the compounds represented in Figure 6.1. The compounds bearing NHBoc groups could be subsequently deprotected and reacted with chloroacetyl chloride to give the chloroacetamide groups.

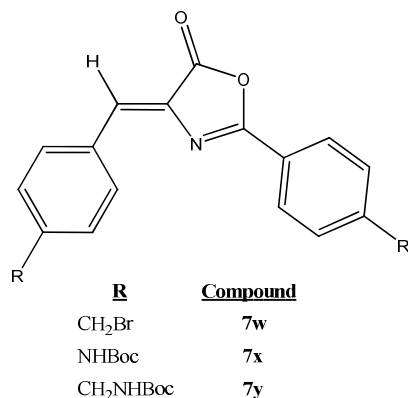


Figure 6.1. Structure of compounds 7w, 7x and 7y.

First of all, we carried out the synthesis of compound **7w**.

We started off by protecting the carboxylic acid of glycine as a methyl ester with chloroacetyl chloride in MeOH (Figure 6.2).

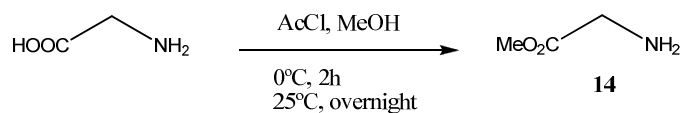


Figure 6.2

Then, the formation of an amide bond between the amino group of **14** and the carboxylic acid of *p*-toluic acid was performed with TBTU and *N,N*-diisopropylethylamine (DIEA) in acetonitrile (Figure 6.3).

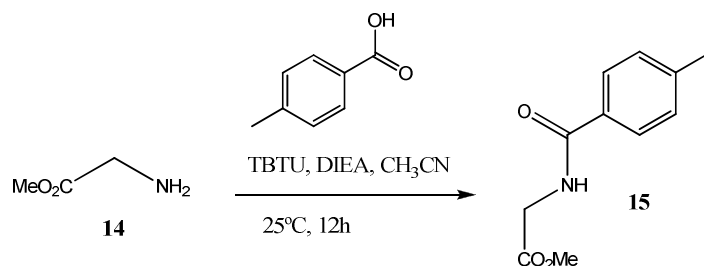


Figure 6.3

Afterwards, the methyl ester of **15** was deprotected with lithium hydroxide monohydrate in MeOH/H₂O (Figure 6.4).

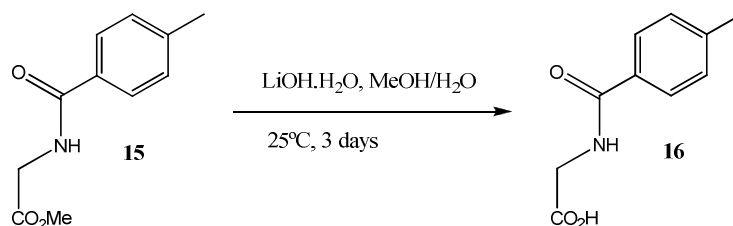


Figure 6.4

Later, the photoswitch **7s** was obtained using the classical conditions for the formation of azalactones described in section 4.2.1 (Figure 4.16)⁸ starting from **16**

⁸Audia, J. E.; Droste, J. J.; Nissen, J. S.; Murdoch, G. L.; Evrard, D. A. *J. Org. Chem.* **1996**, *61*, 7937.

and *p*-tolualdehyde in acetic anhydride, using anhydrous sodium acetate as base (Figure 6.5).

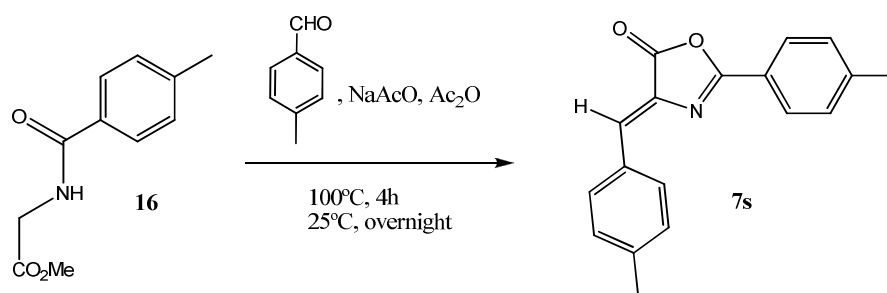


Figure 6.5

Finally, the two benzylic positions of **7s** were dibrominated with *N*-bromosuccinimide and benzoyl peroxide in CCl_4 to achieve the photoswitch **7w** (Figure 6.6).⁹

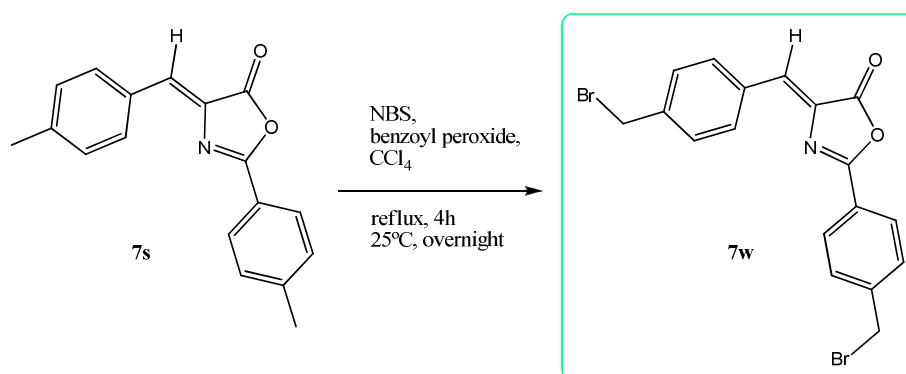


Figure 6.6

After that, we proceeded to synthesize compounds **7x** and **7y**.

Firstly, we protected respectively 4-aminobenzoic acid and 4-(aminomethyl)benzoic acid with Boc anhydride in THF/ H_2O using sodium carbonate decahydrate as base (Figure 6.7).¹⁰

⁹ Djerassi, C. *Chem. Rev.* **1948**, *43*, 271.

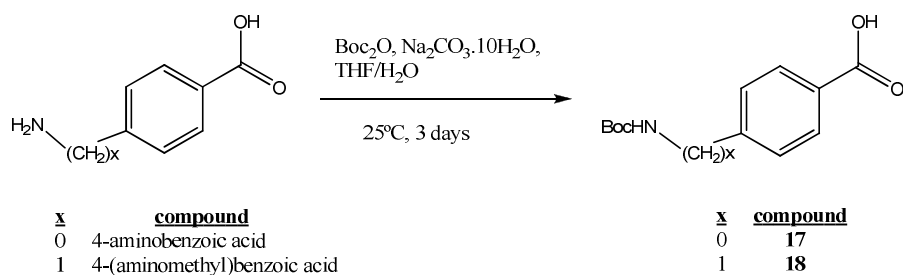


Figure 6.7

Then, the formation of an amide bond between the amino group of **14** and the carboxylic acid of **17** or **18** was performed with TBTU and *N,N*-diisopropylethylamine (DIEA) in acetonitrile (Figure 6.8).

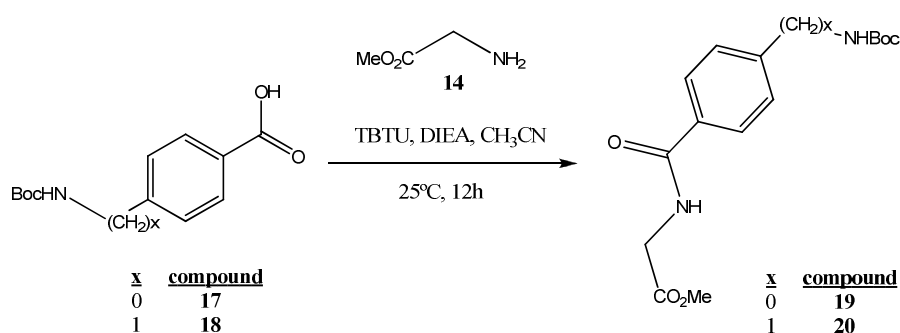


Figure 6.8

Afterwards, the methyl ester of **19** or **20** was deprotected with lithium hydroxide monohydrate in MeOH/H₂O (4:1) (Figure 6.9)

¹⁰ Tarbell, D. S.; Yamamoto, Y.; Pope, B. M. *Proc. Natl. Acad. Sci. USA*, **1972**, *69*, 730.

6. Practical applications

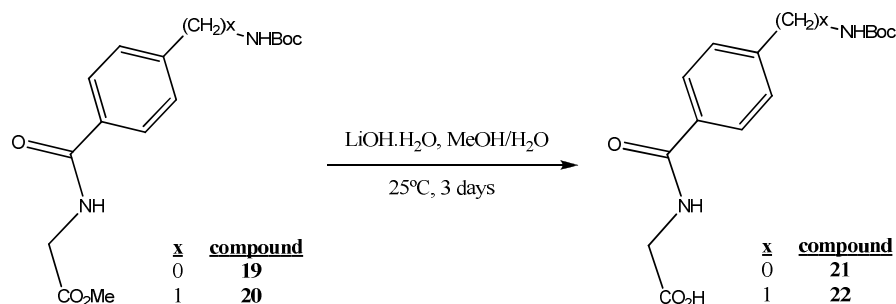


Figure 6.9

On the other hand, the corresponding aldehydes bearing NHBoc groups were also synthesized as indicated in the following paragraphs.

In the first place, we protected the carboxylic acid of 4-aminobenzoic acid or 4-(aminomethyl)benzoic acid as a methyl ester with chloroacetyl chloride in MeOH. Then, we protected the amino group of **23** or **24** with Boc anhydride in THF/H₂O using sodium carbonate decahydrate as base (Figure 6.10).

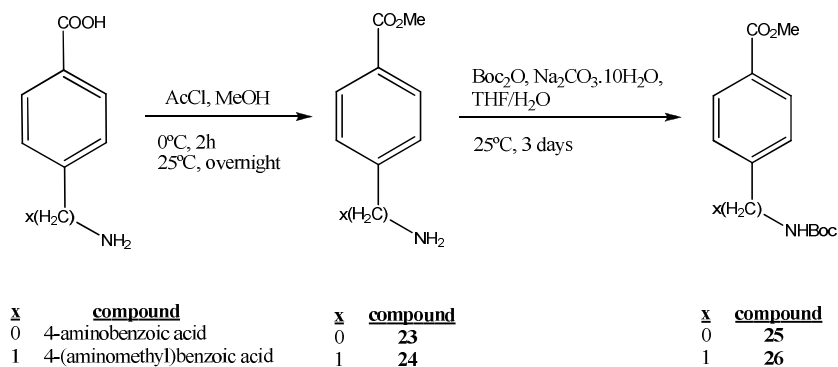


Figure 6.10

The following step was reducing the ester group of **25** or **26** to an alcohol with LiBH₄ in dry THF. Finally, the oxidation of the alcohol group to an aldehyde with Dess-Martin periodinane in dichloromethane was performed (Figure 6.11).

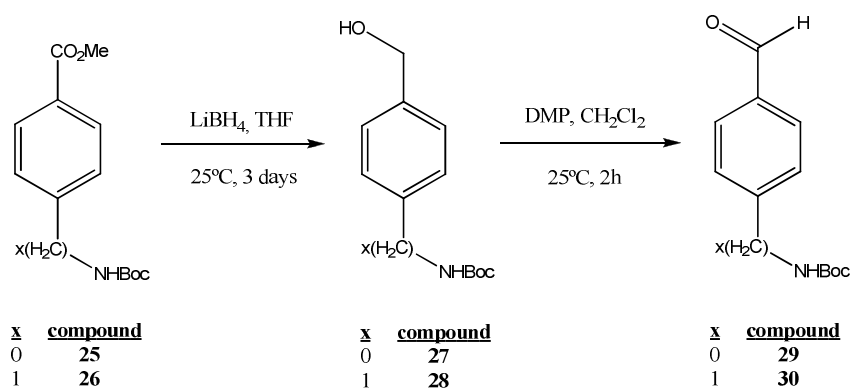


Figure 6.11

Once synthesized the α -aminoacid (**21** or **22**) and the corresponding aldehyde (**29** or **30**), the target oxazolone (**7x** or **7y**) was obtained using the classical conditions for the formation of azalactones (Figure 6.12).¹¹

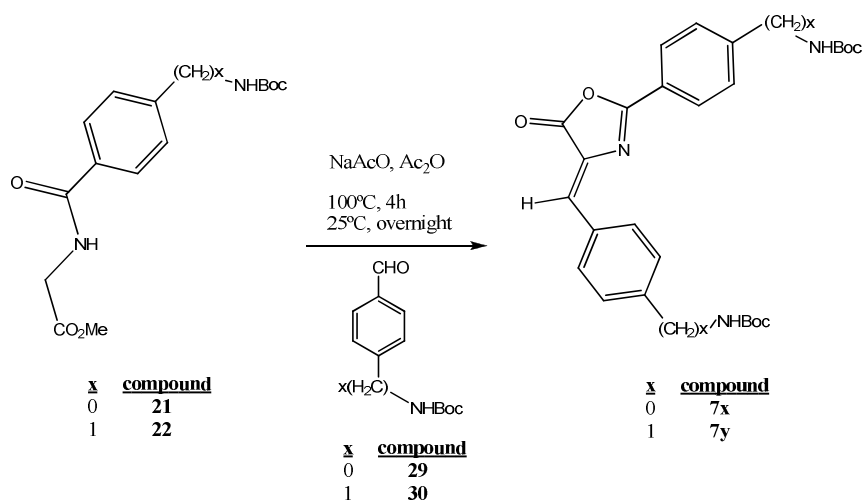


Figure 6.12

¹¹ See ref. 8.

6. Practical applications

In the next step, we deprotected the two amino groups protected with Boc from each switch (**7x** or **7y**) with H_3PO_4 (85%) in dichloromethane to achieve the photoswitch **7z** or **7 α** (Figure 6.13).

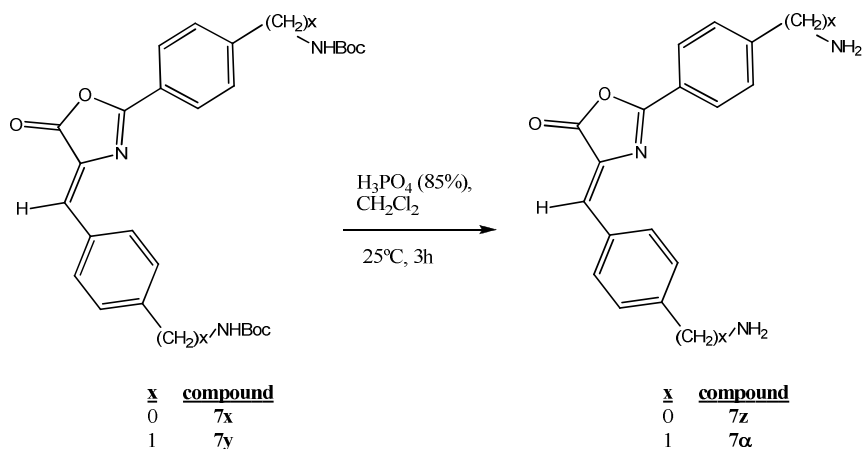


Figure 6.13

The last step was the formation of the chloroacetamide groups at each end of the molecule with chloroacetyl chloride in aqueous sodium carbonate to obtain the corresponding photoswitch **7 β** or **7 γ** (Figure 6.14).

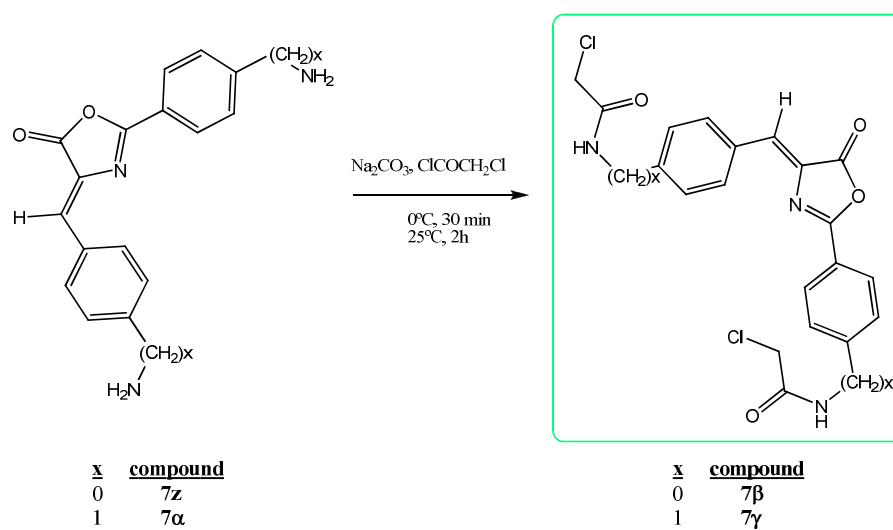


Figure 6.14

6.2.2. Linkage of the synthesized GFP-based photoswitches to model peptides.¹²

As soon as we synthesized the suitable molecular switches **7w**, **7β** and **7γ**, we tried to link them to the appropriate peptide for each case. For this purpose, we followed the methodology used in the laboratory of Prof. Woolley in the University of Toronto.¹³ As the peptide cross-linking reaction will be further described in section 6.3, here we will only state the reaction conditions used for the linkage of the switches to the peptides. Thus, to a 2 mM solution of the switch (**7w**, **7β** or **7γ**) in DMSO was added a solution of 0.5 mM of the adequate peptide in sodium phosphate buffer (pH= 8, 50 mM), so that the solvent system for the reaction was adjusted to DMSO/water (1:4). The reaction was heated at 40°C, kept in the dark and followed by MALDI. It should be noted that the indicated concentrations correspond to the final concentrations in the reaction mixture. However, the expected crosslinked peptide wasn't obtained in any of the cases. A new product different from the target one was observed instead. We purified by HPLC this product in order to characterize it by ESI-MS. The analysis of the mass spectra allowed us to observe that the molecular weight was 18 units higher than the expected crosslinked peptide. If we recall the hydrolysis reaction that occurred when having dissolved the GFP-based compounds in certain solvents (see section 4.2.2), we realize that we were dealing with the same problem here. Thus, the switch was hydrolyzed in the reaction medium prior to binding to the peptide. Afterwards, we tried to carry out the reaction under different reaction conditions. For this purpose, instead of using sodium phosphate buffer in DMSO/water, we used an organic solvent such as DMF and a base such as piperidine. The reaction was followed by MALDI. However, after several days of reaction most of the initial peptide remained unreacted. Only the product that corresponded to the hydrolysis of the switch was found in a small proportion, which was obtained due to the presence of minimum traces of water in both reagents. Another problem that must be taken into account is that even if we were able to achieve the crosslinked peptide using anhydrous conditions, the purification of the product wouldn't be

¹² This part of the study was performed during my stay in the laboratory of Prof. Woolley at the University of Toronto, Toronto, Canadá.

¹³ (a) Woolley, G. A. *Acc. Chem. Res.* **2005**, *38*, 486. (b) Burns, D. C.; Zhang, F.; Woolley, G. A. *Nat. Protoc.* **2007**, *2*, 251. (c) Samanta, S.; Woolley, G. A. *ChemBioChem* **2011**, *12*, 1712.

possible since purification by HPLC requires acetonitrile/water (containing 0.1% of trifluoroacetic acid) as mobile phase.

In order to check the speed rate of the hydrolysis of these compounds under similar conditions, we carried out the following experiment. To a solution of compound **7 β** in 1.5 ml of DMSO was added 1.5 ml of water. The UV-Vis spectrum of the resulting solution was measured at $t=0$ min and at different time intervals. The resulting spectra are plotted altogether in Figure 6.15.

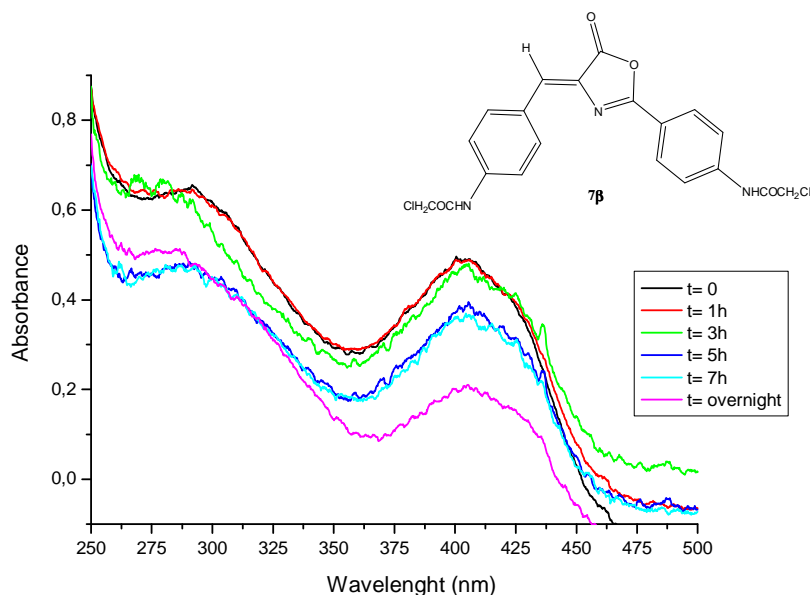


Figure 6.15. UV spectra of a solution of **7 β** in DMSO/H₂O at different time intervals.

From Figure 6.15 it can be inferred that **7 β** was not stable for several hours under these conditions, since it is noticeable that the compound began to be hydrolyzed after 3 hours of reaction. This is reflected in the decrease of the intensity of the absorption band corresponding to the switch as time goes by.

Therefore, we conclude that any application in which this type of compounds could be included would require the adequate reaction conditions and handling so as to avoid hydrolysis. In that case, this kind of compounds would be useful, given the good features that they present as molecular switches (see section 5.3).

6.3. APPLICATIONS OF PHOTOSWITCHES WITH STRUCTURE BASED ON THE PSB-RETINAL CHROMOPHORE.

6.3.1. Synthesis of the appropriate PSB-retinal based photoswitches for the linkage to more complex biomolecules.

As discussed in section 4.1.1, previously reported PSB-retinal-based molecular switches (see section 2.6) had a lack of practical ability to act as efficient switches in real applications due to the absence of convenient structures to be incorporated in a complex system. However, the retrosynthetic analysis (see Figure 4.3) of the new prototypes of photoswitches based on the PSB-retinal chromophore presented in this dissertation suggested that the modification of the substructure, so as to present two binding sites, is possible.

In the first place, we thought of functionalizing one of the available switches that we had already synthesized, in particular **5o** (Figure 6.16).

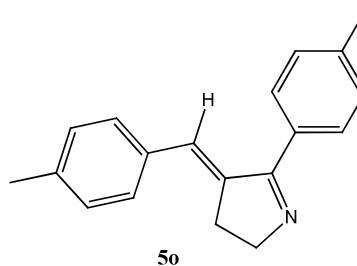


Figure 6.16. Structure of compound 5o.

For this purpose, we tried different methods for the bromination of benzylic positions:

- NBS, benzoyl peroxide, CCl_4 ;¹⁴
- Br_2 , glacial HAcO ;¹⁵
- IBX, DMSO;¹⁶ and

¹⁴ See ref. 9.

¹⁵ Breslow, R.; Posner, J. *Org. Synth.* **1967**, *47*, 62; *Org. Synth.* **1973**, *Coll. Vol. 5*, 514.

- NBS, SiCl₄, CH₃CN.¹⁷

Notwithstanding, none of these methods achieved the target dibrominated product, since no reaction was observed in any of the cases.

Therefore, we decided to design a new switch that belonged to this family but had two amino groups at both extremes of the substructure. This could allow for an easy introduction into a peptide due to the versatile reactivity that this functional group features. For instance, the placing of amino groups at the end of the switch unit permitted the synthesis of a thiol-reactive chloroacetamide derivative (**5r**) suitable for site-specific insertion into a Cys-containing peptide as an intramolecular cross-link (Figure 6.17).

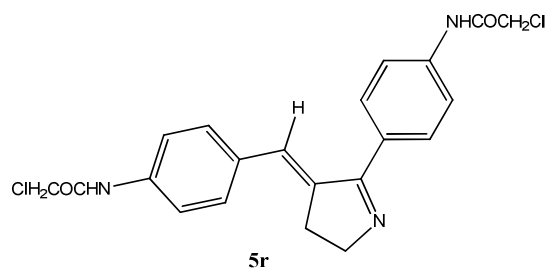


Figure 6.17. Structure of compound **5r**.

The synthetic route followed so as to achieve **5r** was similar to the one already described for compounds that belonged to the same family of photoswitches based on the PSB-retinal chromophore (see section 4.1.1, Figure 4.9). The reaction scheme pursued for the synthesis of this compound is outlined in Figure 6.18.

¹⁶ Satam, V.; Harad, A.; Rajule, R.; Pati, H. *Tetrahedron* **2010**, *66*, 7659.

¹⁷ Salama, T. A.; Novák, Z. *Tetrahedron Lett.* **2011**, *52*, 4026.

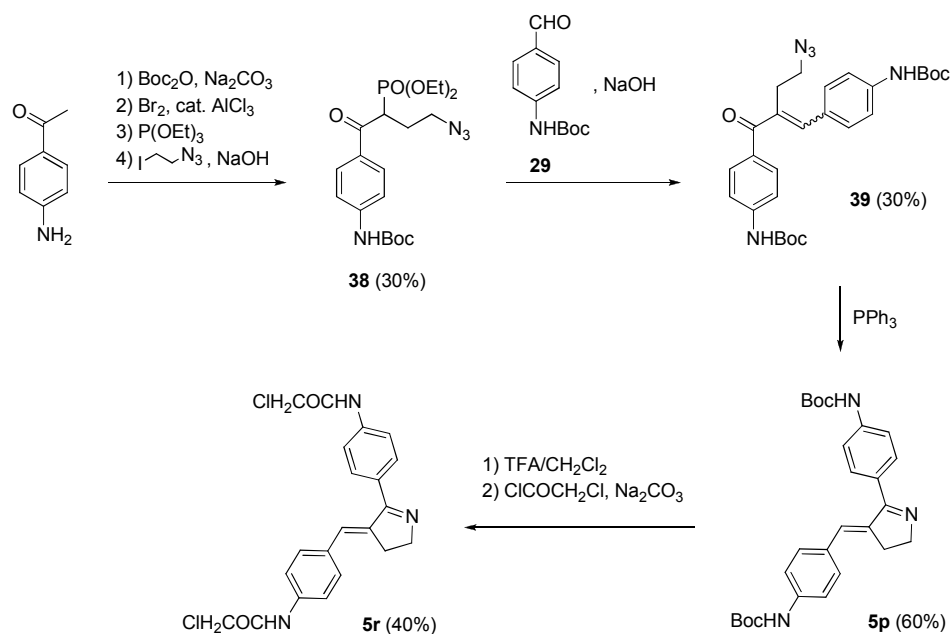


Figure 6.18. Synthesis of the new PSB-retinal based photoswitch 5r.

In the following paragraphs, the synthetic route to obtain **5r** is divided into each of its steps.

First, 4-aminoacetophenone was Boc-protected using di-*tert*-butyl dicarbonate in the presence of sodium carbonate in THF/ H_2O (5:1) (Figure 6.19).¹⁸The resulting mixture was stirred at 25°C for 3 days. The corresponding work-up afforded **31** in a 90 % yield as a white solid.

¹⁸ Tarbell, D. S.; Yamamoto, Y.; Pope, B. M. *Proc. Natl. Acad. Sci. USA*, **1972**, *69*, 730.

6. Practical applications

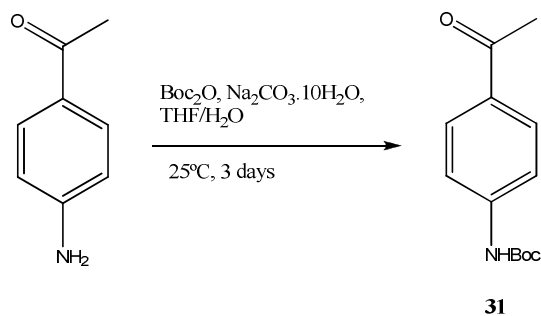


Figure 6.19.

Then, the acetophenone **31** was brominated with Br_2 in THF containing a catalytic amount of AlCl_3 to obtain *t*-butyl 4-(2-bromoacetyl)phenylcarbamate (**32**) in a 50% yield as a yellow solid (Figure 6.20).¹⁹

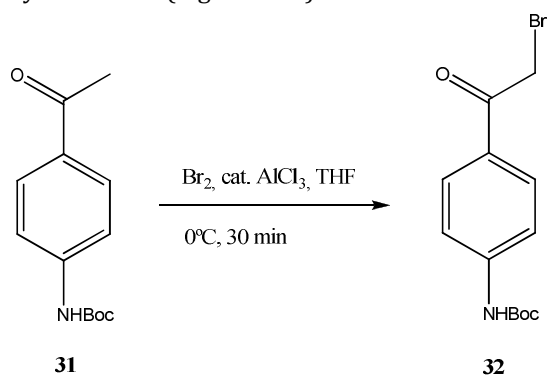


Figure 6.20.

Later, the bromoacetophenone **32** was treated with triethyl phosphite at 160°C for 3 hours²⁰ to give *t*-butyl 4-(2-(diethoxyphosphino)acetyl)phenylcarbamate **33** in a 85% yield as a colourless oil (Figure 6.21).

¹⁹ Goslinski, T.; Golankiewicz, B.; De Clercq, E.; Balzarini, J. *J. Med. Chem.* **2002**, *45*, 5052.

²⁰ Nagata, W.; Wakabayashi, T.; Hayase, Y. *Organic Synthesis* **1973**, *53*, 44; **1988**, *Coll. Vol. 6*, 448.

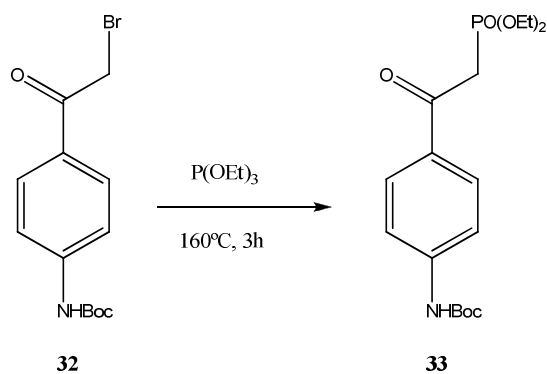


Figure 6.21.

Then, the introduction in **33** of an ethyl azide side chain with 2-iodoethylazide by means of a phase-transfer procedure²¹ using tetrabutylammonium bisulfate and aqueous sodium hydroxide in CH_2Cl_2 at reflux for 36 hours affords the azido phosphonates **34** in a 30% yield (Figure 6.22).

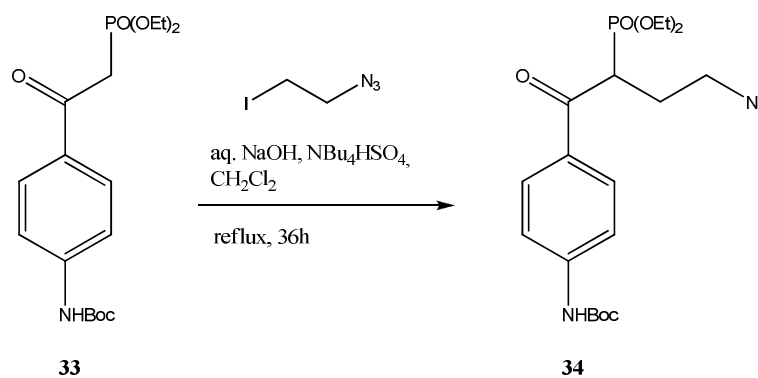


Figure 6.22.

In the case of the synthesis of the photoswitch **5p** the step corresponding to the Wittig-Horner reaction was modified since the conditions used for other PSB-retinal based compounds (see Figure 4.7) didn't work. Therefore, the reaction between the azido-phosphonate **34** and the aldehyde **29** was carried out with

²¹ Snider, B. B.; Zhou, J. *J. Org. Chem.* **2005**, *70*, 1087.

6. Practical applications

aqueous NaOH and tetrabutylammonium bisulfate in THF. The mixture was stirred at 25°C for 3 weeks. This led to the formation of the azido enone **35** in a 30% yield as yellowish oil (Figure 6.23). Although a 9:1 mixture of *E* and *Z* isomers of the azido enone **35** is obtained, we didn't try to separate them. As it has been discussed in section 4.1.1, both isomers afforded the same product in the following step of the synthesis.

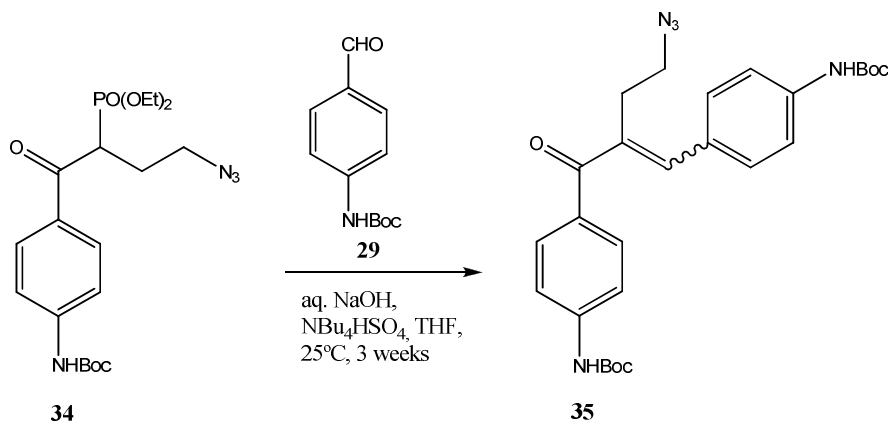


Figure 6.23.

After performing an intramolecular aza-Wittig reaction of **35** with triphenylphosphine in diethyl ether for 1 day at 25°C, only the *E* isomer of the switch **5p** was found as the final product. **5p** was obtained as a yellow solid in a 80% yield (Figure 6.24).

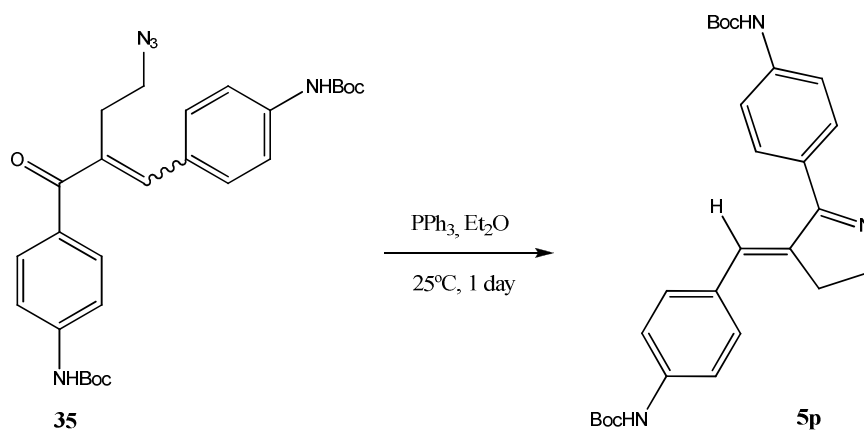


Figure 6.24.

The next step was the Boc-deprotection of the two amino groups located at each end of the molecule. The treatment of compound **5p** with 1 ml of TFA/ CH_2Cl_2 (1:1) for half an hour at 25°C afforded the switch **5q** as an orange oil in a 95% yield (Figure 6.25).²²

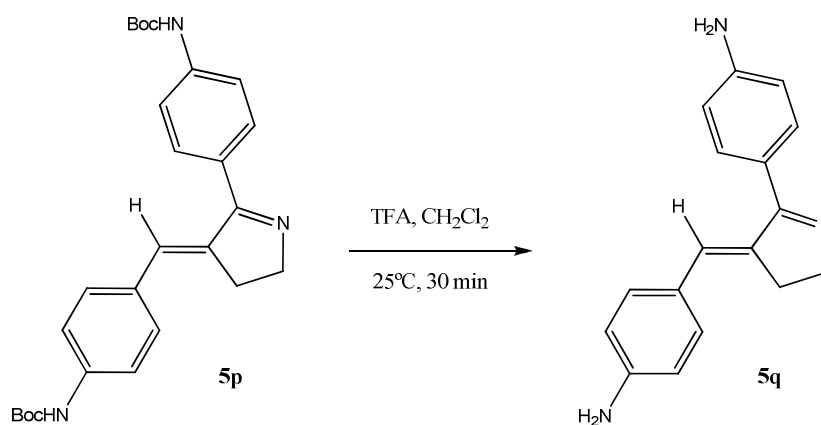


Figure 6.25.

²² Ripka, A. S.; Bohacek, R.S.; Rich, D.H. *Bioorg. Med. Chem. Lett.* **1998**, *8*, 357.

Finally, the two chloroacetamide groups were formed by dissolving **5q** in aqueous sodium carbonate (pH= 8) and adding chloroacetyl chloride at 0°C. The resulting mixture was stirred for half an hour at 0°C and 2 hours at 25°C to achieve the photoswitch **5r** as a brown solid in a 40% yield (Figure 6.26).

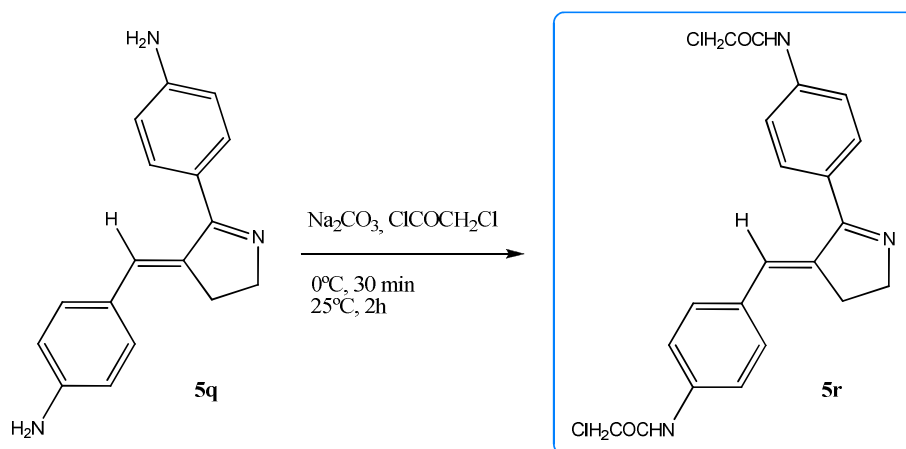


Figure 6.26.

Once synthesized, the photochemical behavior of compounds **5p** and **5r** was studied to see if they met the requirements to be considered efficient. The presence of the two amino groups within the structure, together with the added phenyl ring could modify both the UV-Vis absorption spectrum and the photochemical properties in relation with the parent benzylidene-pyrroline (see section 2.6.1) through extended conjugation. Thus, a longer wavelength of absorption and a higher isomerization quantum yield were envisaged for these new compounds. Moreover, the expected bathochromic shift of the maximum wavelength for absorption was important as the use of low-energy light is essential for biological applications. On the other hand, the extended conjugation provided by the two phenyl groups could limit alternative reaction pathways that lower photoisomerization efficiency, such as single bond rotation.²³ In the following subsections the conducted computational and experimental studies for these switches are described.

²³ Sampedro, D.; Migani, A.; Pepi, A.; Busi, E.; Basosi, R.; Latterini, L.; Elisei, F.; Fusi, S.; Ponticelli, F.; Zanirato, V.; Olivucci, M. *J. Am. Chem. Soc.* **2004**, *126*, 9349.

6.3.1.1. Computational study of the synthesized photoswitch **5r** for the linkage to more complex systems.

The geometry of the critical points of the designed switch **5r**, and its corresponding protonated compound **5r-H⁺**, were computed using fully unconstrained ab initio quantum chemical computations in the framework of a CASPT2//CASSCF strategy.²⁴ This required the geometries to be computed at the complete active space self-consistent field (CASSCF) level of theory and the corresponding energy profile to be re-evaluated at the multiconfigurational second-order Møller-Plesset perturbation theory level. This methodology has proven valuable for the study of related compounds (see section 5.4.1).¹⁷ The Gaussian 03 program package²⁵ was used for CASSCF computations. The energy of the CASSCF geometries was recalculated using the CASPT2 method implemented in MOLCAS-6.4,²⁶ taking into account the effect of dynamic electron correlation. The CASPT2 calculations involved the standard IPEA shift of 0.25.²⁷ All CASPT2 results were obtained from a CASSCF reference function with three roots and a state average with equal weights for each state. Both CASSCF and CASPT2 calculations were performed using the standard 6-31G* basis set. The size of the molecule prevented us from using the complete π system in the active space. Accordingly, we included in our calculations only the seven occupied π orbitals

²⁴ a) Sampedro, D. in *Photochemistry: UV/VIS Spectroscopy, Photochemical Reactions and Photosynthesis*; Maes, K. J.; Willems, J. M. (eds.) Nova Science Publishers, **2011**. b) *Computational Photochemistry*, Olivucci, M. (ed.) Elsevier: Amsterdam, **2005**.

²⁵ Frisch, M. J.; Trucks, G. W.; Schlegel, H. B.; Scuseria, G. E.; Robb, M. A.; Cheeseman, J. R.; Montgomery Jr., J. A.; Vreven, T.; Kudin, K. N.; Burant, J. C.; Millam, J. M.; Iyengar, S. S.; Tomasi, J.; Barone, V.; Mennucci, B.; Cossi, M.; Scalmani, G.; Rega, N.; Petersson, G. A.; Nakatsuji, H.; Hada, M.; Ehara, M.; Toyota, K.; Fukuda, R.; Hasegawa, J.; Ishida, M.; Nakajima, T.; Honda, Y.; Kitao, O.; Nakai, H.; Klene, M.; Li, X.; Knox, J. E.; Hratchian, H. P.; Cross, J. B.; Adamo, C.; Jaramillo, J.; Gomperts, R.; Stratmann, R. E.; Yazyev, O.; Austin, A. J.; Cammi, R.; Pomelli, C.; Ochterski, J. W.; Ayala, P. Y.; Morokuma, K.; Voth, G. A.; Salvador, P.; Dannenberg, J. J.; Zakrzewski, V. G.; Dapprich, S.; Daniels, A. D.; Strain, M. C.; Farkas, O.; Malick, D. K.; Rabuck, A. D.; Raghavachari, K.; Foresman, J. B.; Ortiz, J. V.; Cui, Q.; Baboul, A. G.; Clifford, S.; Cioslowski, J.; Stefanov, B. B.; Liu, G.; Liashenko, A.; Piskorz, P.; Komaromi, I.; Martin, R. L.; Fox, D. J.; Keith, T.; Al-Laham, M. A.; Peng, C. Y.; Nanayakkara, A.; Challacombe, M.; Gill, P. M. W.; Johnson, B.; Chen, W.; Wong, M. W.; Gonzalez, C. and Pople, J. A.; Gaussian, Inc., Wallingford CT, **2004**.

²⁶ Karlström, G.; Lindh, R.; Malmqvist, P.-Å.; Roos, B. O.; Ryde, U.; Veryazov, V.; Widmark, P.-O.; Cossi, M.; Schimmelpfennig, B.; Neogrady, P.; Seijo, L. *Comput. Mater. Sci.* **2003**, *28*, 222

²⁷ Ghigo, G.; Roos, B. O.; Malmqvist, P. Å. *Chem. Phys. Lett.* **2004**, *396*, 142.

higher in energy and the seven virtual π^* orbitals lower in energy in order to get 2760615 different excitations. The most stable occupied and the less stable virtual orbitals were left outside the active space. Selection of the orbital was made in basis of ROHF calculations. Thus, the active space was formed by 14 electrons in 14 orbitals: π and π^* orbitals from both aromatic rings, C=C and C=N double bonds.

The computed vertical transitions for **E-5r** in its neutral and protonated forms were carried out in the gas phase. The obtained results are shown in Table 6.1.

Table 6.1. Experimental and Franck-Condon vertical CASPT2 excitation energies (gas phase), orbital transitions and oscillator strengths (f) for E-5r in neutral (DMSO) and protonated (water) forms.

Switch	Band, eV (nm)	State	E_{CASPT2} , eV (nm)	Transition	f	Relative f
5r	-----	S ₂	5.22 (238)	¹ (π, π^*)	0.011	1
	3.96 (313)	S ₁	5.20 (239)	¹ (π, π^*)	0.006	0.54
5r-H⁺	4.77 (260)	S ₂	4.35 (285)	¹ (π, π^*)	0.27	0.28
	3.32 (375)	S ₁	3.34 (362)	¹ (π, π^*)	0.95	1

As it will be seen in the next subsection, experimental and theoretical data compare reasonably well. Moreover, strong π - π^* absorptions were found in both systems, neutral and protonated. It should be noted that the neutral species wasn't water soluble. As expected, the protonated form shows a band maximum at longer wavelength. Therefore, we can conclude that the photoswitch is predicted to feature better photophysical properties in an acidic medium.

6.3.1.2. Experimental study of the synthesized photoswitches **5p** and **5r** for the linkage to more complex systems.

First of all, the UV-Vis spectrum of a 4×10^{-5} M solution of the photoswitch **5p** in acetonitrile was measured, which is represented in Figure 6.27.

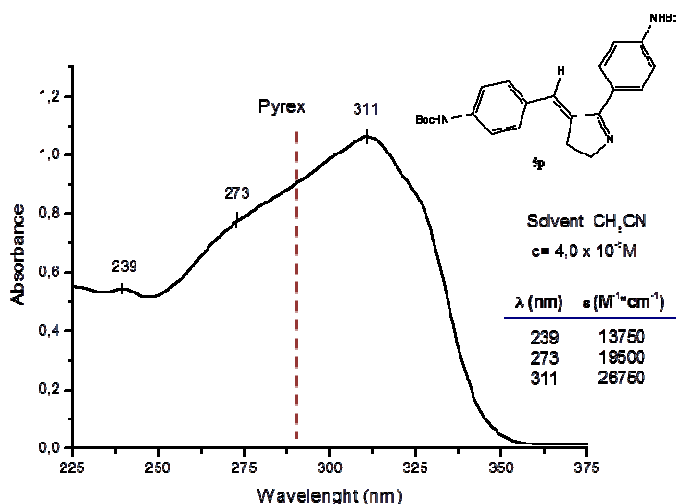


Figure 6.27. UV-Vis spectrum of a $4 \times 10^{-5}M$ solution of **5p** in acetonitrile.

After analyzing the UV-Vis spectrum, we inferred that a Pyrex filter could be used in order to avoid radiation below 290 nm. Thus, we irradiated a 0.1 M solution of **5p** in $CDCl_3$ in a Pyrex NMR tube using a 125-W medium-pressure Hg lamp through a Pyrex filter until the photostationary state (PSS) was reached. The isomerization reaction was followed by 1H NMR.

It should be noted that the composition of the PSS is relevant when it comes to practical applications as it will determine the macroscopic modification induced for the switch once incorporated in a complex system. In the case of **5p**, PSS was composed by a mixture of *ca.* 40% (*E*) / 60% (*Z*), being this rate stable overnight at $25^\circ C$ if the sample is kept in the dark. Furthermore, the equilibrium between isomers *E* and *Z* could be displaced from the PSS after heating at $50^\circ C$ for several hours, eventually reverting to the pure *E* form. Therefore, the main isomer could be easily modified by choosing between light and heat. This can be important in practical applications in which on/off switching cycles are necessary.

We then aimed for a direct measurement of the switching efficiency. Thus, we evaluated the isomerization quantum yield of **5p** using *trans*-azobenzene as actinometer (see experimental section). We obtained an average value of $0.6 (\pm 0.1)$ after several runs. It should be noted that this value for the quantum yield is

comparable to the one found for the Rh chromophore (0.67)²⁸ and bigger than those reported for biarylidene (0.07-0.55).²⁹ In addition to this, this result is similar to the one obtained for **5l**, which belongs to the same family of photoswitches (see section 5.2.2.2). This means that **5p** can efficiently use the light energy into the switching process and show very promising features for its use in practical applications.

On the other hand, we studied the deactivation processes that could diminish the efficiency of **5p**. For this purpose, we measured the emission and excitation spectra of a 5×10^{-5} M solution of **5p** in deoxygenated acetonitrile at 25°C (Figure 6.28). Only a weak emission band centered at 395 nm was obtained when exciting from 240 nm to 330 nm (see experimental section). Afterwards, we measured the fluorescence lifetime using a 280 nm LED and it was found to be 4.20×10^{-10} seconds. Moreover, using an excitation wavelength of 310 nm, an upper limit for the fluorescence quantum yield of 0.01 was found. This value shows that deactivation through fluorescence does not effectively compete with the isomerization process. In fact, this result emphasizes the adequate design of these switches as only a small fraction of the light energy is wasted in the radiative decay.

Therefore, we can conclude that photoswitch **5p** presents the right features to be considered efficient and a good prototype to be included in more complex systems.

²⁸ Mathies, R. A.; Lugtenburg, J. In *Handbook of Biological Physics*; Stavenga, D. G., de Grip, W. J., Pugh, E. N. (eds.) Elsevier: Amsterdam, **2000**; Vol. 3, p 56.

²⁹ Feringa, B. L. *J. Org. Chem.* **2007**, *72*, 6635.

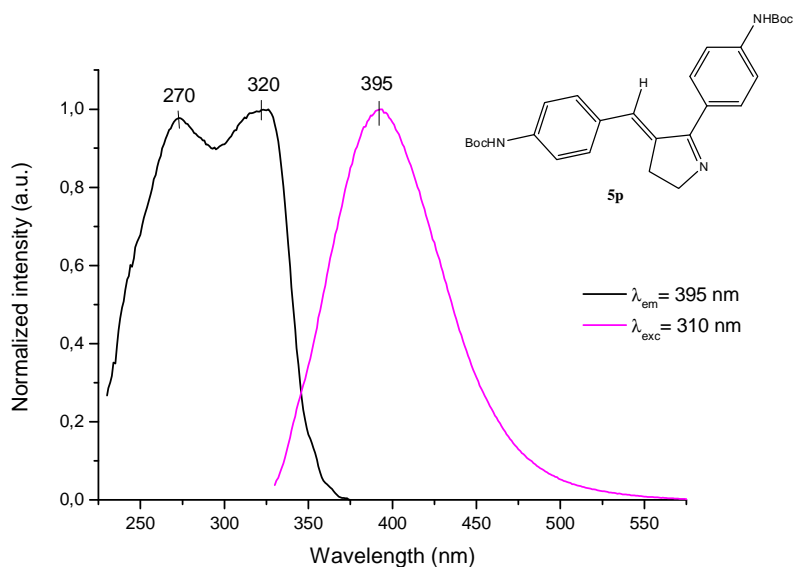


Figure 6.28. Excitation and emission spectra of a $5 \times 10^{-5}\text{M}$ solution of **5p** in deoxygenated acetonitrile.

However, the compound that is actually going to be attached to other biomolecules is **5r**. Therefore, we also recorded the UV-Vis spectrum of this compound in order to check if there was any change in the absorption band. In this case, the solvent used for preparing the sample of the *E* (thermodynamically stable) isomer of **5r** was deuterated dimethyl sulfoxide (DMSO- d_6). In Figure 6.29 it can be observed that the maximum wavelength of absorption for this isomer (*E*) is located at 313 nm, which is similar to the value found for **5p** (311 nm). Then, there was no noticeable shift of the absorption band when changing the NHBoc groups to N HCOCH_2Cl .

For determining the exact concentration of the solution of *E*-**5r** used for recording the UV-Vis spectrum and the value of the molar extinction coefficient at 313 nm, we used the following strategy. A solution of unknown concentration of *E*-**5r** in DMSO- d_6 was prepared in a Pyrex NMR tube and its ^1H NMR spectrum was recorded with a known concentration of 1,2-dichloroethane as internal standard. The intensity ratio of the ^1H signals of 1,2-dichloroethane and the α -chloroacetamido group of *E*-**5r** permitted the determination of the concentration of *E*-**5r** in the NMR sample. An aliquot of the NMR sample was then taken and

diluted, and its UV-Vis spectrum was recorded (see Figure 6.29). Thus, the molar extinction coefficient was calculated to be $46850 \text{ M}^{-1}\text{cm}^{-1}$ in DMSO at 313 nm. This value was later used for calculating the concentration of the stock solution of cross-linked peptide (see section 6.3.3.1).

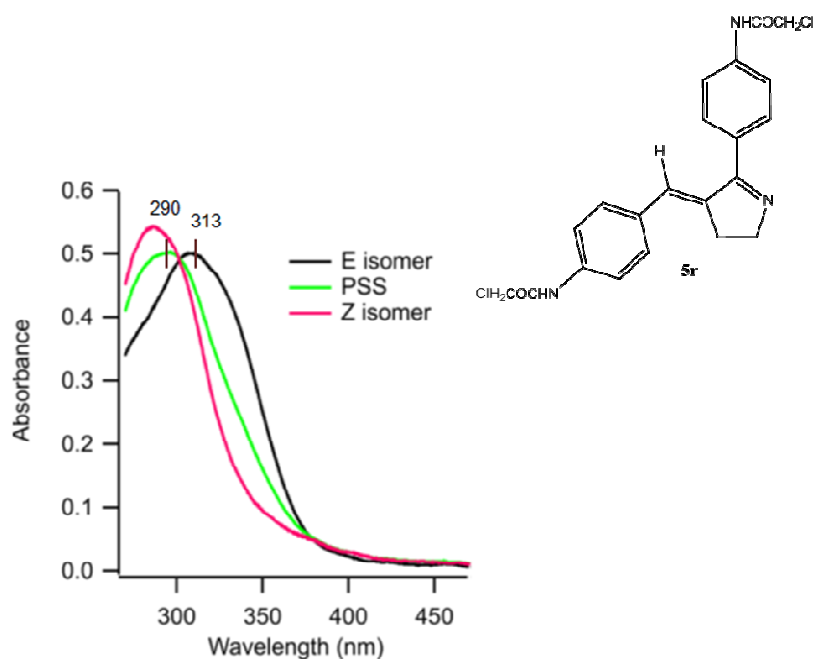


Figure 6.29. UV-Vis spectra of the pure *E* isomer of **5r** in deuterated DMSO, the PSS obtained with 365 nm irradiation (40% (*E*) / 60% (*Z*), determined by ^1H NMR), and the calculated spectrum of the pure *Z* isomer.

Then, the same NMR sample used for calculating the concentration of the solution of *E*-**5r** and the molar extinction coefficient was irradiated using a 365 nm LED until the PSS was reached. The isomers ratio at this stage was found to be 40% (*E*) / 60% (*Z*). Afterwards, an aliquot of the irradiated NMR sample was taken and diluted so as to record its UV-Vis spectrum. In Figure 6.29 is shown the UV-Vis spectrum of the PSS for **5r**. Once we had the spectra of the pure *E* isomer of **5r** and the mixture of isomers at the PSS, it was possible to calculate the UV-Vis spectrum of the pure *Z* isomer, which is also shown in Figure 6.29.

6.3.2. Linkage of the synthesized PSB-retinal based photoswitch **5r** to a model peptide.³⁰

6.3.2.1. Selection and synthesis of the adequate model peptide for the linkage to **5r**.

First of all, the adequate model peptide for the linkage to **5r** was selected.

For this purpose, the change in end-to-end distance of **5r** upon isomerization was estimated using molecular dynamics simulations (see experimental section). In Figure 6.30 it is shown the calculated change in end-to-end distance between the sulfur atom attachment points for the *E* and *Z* forms of **5r**.

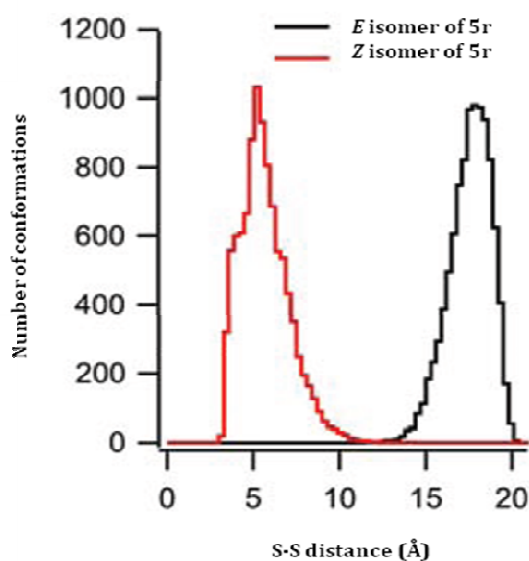


Figure 6.30. Calculated change in the end-to-end distance between S atom attachment points for the *E* and *Z* forms of the photoswitch **5r**.

From Figure 6.30 it can be inferred that *E/Z* isomerization produces a large (~ 10 Å) change in the mean end-to end distance with very little overlap between

³⁰ (a) This part of the study was also performed during my stay in the laboratory of Prof. Woolley at the University of Toronto, Toronto, Canada. (b) Blanco-Lomas, M.; Samanta, S.; Campos, P. J.; Woolley, G. A.; Sampedro, D. *J. Am. Chem. Soc.* **2012**, *134*, 6960.

isomers. The size of this conformational change is significantly greater than those in many azobenzene-based photoswitches.³¹ Azobenzene derivatives specifically designed to undergo large changes in end-to-end distance upon photoisomerization have exhibited lower photoisomerization efficiencies or more complex conformational distributions than those exhibited by **5r**.³² Photocontrol of peptide α -helical structure can be achieved by matching the end-to-end distance of a photoswitchable cross-linker in one isomeric state with the distance between cross-linker attachment points in the peptide.³³ The average S-S distance for the *E* isomer of **5r** was found to be 17 Å (see Figure 6.30). On the other hand, the average S-S distance for the *Z* isomer was 6 Å. From this results we can conclude that the end-to end distance of the *E* isomer matches well with the distance between Cys side chains with an $i, i + 11$ sequence spacing in a peptide α -helix, whereas the *Z* isomer is too short to permit normal helix formation with this Cys side-chain spacing. The peptide SS-11, studied previously as an ideal helix-forming sequence in water,³⁴ was chosen as target for photocontrol by **5r**. This peptide is long enough to confer aqueous solubility on the relatively hydrophobic cross-linker.

The peptide SS-11 (Ac-WGACEAAAAREAAARCAAAREAAAREAQ-NH₂, Figure 6.31) was prepared by standard protocols for Fmoc-based solid-phase peptide synthesis, and purified by HPLC afterwards (see experimental section).

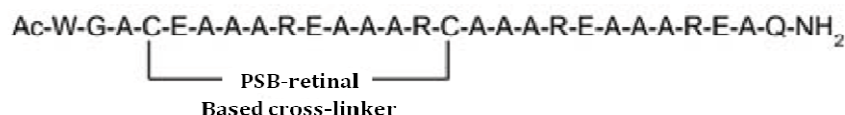


Figure 6.31. Scheme of peptide SS-11 cross-linked to the PSB-retinal based photoswitch.

³¹ See ref. 2.

³² (a) Standaert, R. F.; Park, S. B. *J. Org. Chem.* **2006**, *71*, 7952. (b) Zhang, F.; Sadovskii, O.; Woolley, G. A. *ChemBioChem* **2008**, *9*, 2147.

³³ (a) Burns, D. C.; Flint, D. G.; Kumita, J. R.; Feldman, H. J.; Serrano, L.; Zhang, Z.; Smart, O. S.; Woolley, G. A. *Biochemistry* **2004**, *43*, 15329. (b) Flint, D. G.; Kumita, J. R.; Smart, O. S.; Woolley, G. A. *Chem. Biol.* **2002**, *9*, 391.

³⁴ See ref. 13(a).

The resulting peptide was then dissolved in 200 μ l of water. This solution was later used for the cross-linking reaction to the photoswitch.

6.3.2.2. Cross-linking reaction of peptide SS-11 to photoswitch **5r**.

Cross-linking of the peptide SS-11 to **5r** was performed following the methodology used in the laboratory of prof. Woolley in the University of Toronto.³⁵ A 0.5 mM solution of the peptide SS-11 in 60 mM tris Buffer at pH 8 containing 2 mM TCEP was stirred at 25°C under N₂ atmosphere for 30 minutes. Then, to the reaction mixture was added a 2 mM solution of crosslinker **5r** in DMSO and the solvent system for the reaction was adjusted to 20% DMSO and 80% water. The mixture was stirred at 40°C overnight, kept in the dark and followed by MALDI. It should be noted that the indicated concentrations correspond to the final concentrations in the reaction mixture. Afterwards, the solvent was removed using a high vacuum pump, and the crosslinked peptide was purified by HPLC. It was then dissolved in 100 μ l of 5 mM sodium phosphate buffer (pH= 7). This concentrated stock solution was later used for the photochemical study of the cross-linked peptide.

On the other hand, since **5r** is not a symmetrical molecule, two distinct species result when it reacts with a peptide to form an intramolecular cross-link. This is due to the fact that the Cys4 residue (see Figure 6.31) can react with either of the two chloroacetamide groups of **5r**. In Figure 6.32 is shown the HPLC chromatogram of *E* and *Z* isomers of the cross-linked peptide under ambient light. It must be noted that the two regioisomers of the *Z*-linked peptide are resolved under the selected separation conditions, while those of the *E*-linked peptide are not.

³⁵ See ref. 13.

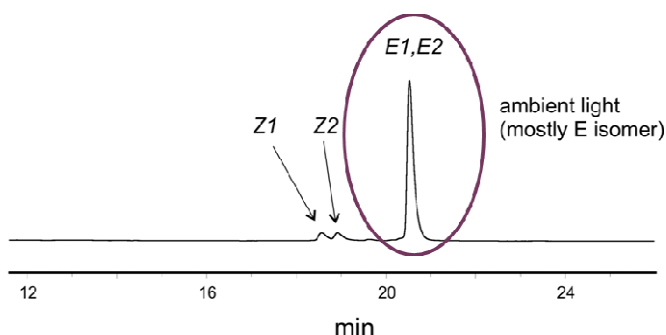


Figure 6.32. HPLC traces of 5r-cross-linked SS-11 under ambient light.

Since the end-to-end distance change caused by isomerization is the same for both species, we did not attempt to characterize these isomers separately for conformational analysis.

6.3.3. Photochemical study of the cross-linked peptide.

6.3.3.1. Photochemical study of the cross-linked peptide dissolved in sodium phosphate buffer at pH 7.

First of all, we had to determine the concentration of the available stock solution of the cross-linked peptide. For this purpose, we took 2 μL of the concentrated stock solution and diluted it to 140 μL with DMSO. Then, the UV-Vis spectrum of this diluted cross-linked peptide solution was recorded. From this UV-Vis spectrum and the molar extension coefficient of **5r** ($46850 \text{ M}^{-1}\text{cm}^{-1}$) in DMSO, the concentration of the stock solution was calculated.

Afterwards, we prepared a 13 mM solution in 5 mM sodium phosphate buffer (pH= 7) of the cross-linked peptide from the concentrated stock solution. This later solution was used for recording the different UV-Vis spectra before and after irradiating at 20°C (Figure 6.33). The blue line corresponds to the UV-vis spectrum of the SS-11 peptide cross-linked with **5r** in the dark-adapted *E* form. Then, the sample was irradiated with 365 nm light until the PSS was reached. As it has been said before in section 6.3.1.2, the isomers ratio for **5r** at this stage was found to be 40% (*E*) / 60% (*Z*). The UV-Vis spectrum of the PSS after irradiating with 365 nm light is represented in Figure 6.33 with a yellow line. We also found that when

using 400 nm light instead of 365 nm light for irradiating, a similar isomers ratio at the PSS was obtained, as the shape of the UV-Vis spectrum of this later PSS was nearly the same (Figure 6.33, green line).

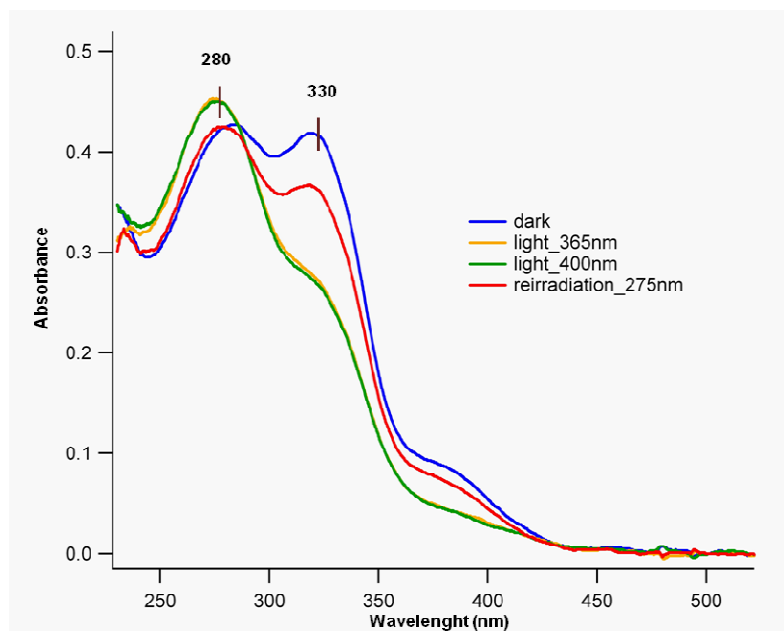


Figure 6.33. UV-Vis spectra of the cross-linked peptide of the dark-adapted *E* form and the photostationary state at pH 7 after irradiating with 365, 400 and 275 nm lights at 20°C.

After irradiating with 365 or 400 nm light, the sample was reirradiated with 275 nm light in order to recover the thermodynamically stable *E* isomer. The UV-Vis spectrum of the PSS reached irradiating at 275 nm is represented in Figure 6.33 with a red line. In addition to the fact that irradiating with 275 nm light doesn't fully recover the initial isomer, this wavelength is too energetic for being used in biological applications. Therefore, we decided to irradiate with blue light (446 nm) instead of with 275 nm light so as to recover the dark-adapted form. The UV-Vis spectra at the photostationary state after irradiating the cross-linked peptide in 20 mM phosphate buffer (at pH= 7) with 365 nm light (black dotted line) and reirradiating with blue light (blue line) at 20°C are shown in Figure 6.34(a). Multiple rounds of photoswitching of the cross-linked peptide at pH 7 using alternating 365 nm and blue light at 20°C were performed (Figure 6.34(b)),

but there was no evidence of photo-bleaching or photo-oxidation. Therefore, the cross-linked peptide is photostable.

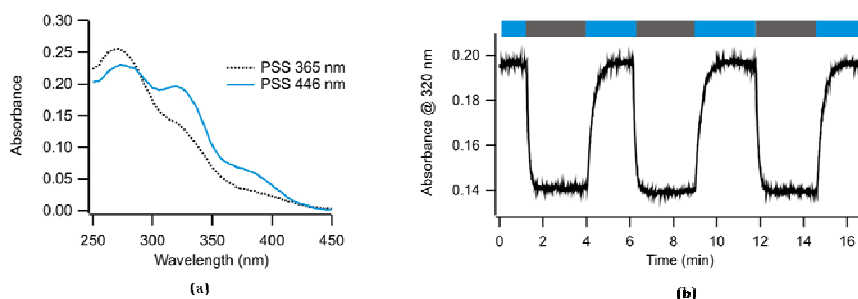


Figure 6.34. (a) UV-Vis spectra of the cross-linked peptide at pH 7 at the photostationary state after irradiating with 365 and 446 nm lights at 20°C. (b) Multiple rounds of photoswitching of the cross-linked peptide at pH 7 using alternating 365 nm and blue light at 20°C.

Then, the CD spectra of the cross-linked peptide before and after irradiating with 365 nm light were recorded. The obtained results are represented in Figure 6.35 along with the spectrum of the uncross-linked SS-11 peptide (blue line). From Figure 6.35 it can be inferred that cross-linking the SS-11 peptide with the *E* form of **5r** leads to a stabilization of the α -helical content (navy blue line), and the peptide is essentially fully helical at 20°C. Irradiation with 365 nm light to achieve an isomers ratio at the PSS of 40% (*E*) / 60% (*Z*) leads to a marked decrease in helicity, as predicted (navy blue dotted line). It should be pointed out that at different temperatures (5°C, green lines, and 40°C, red lines) takes place a similar process; however, at low temperatures the stabilization is more remarkable than at higher temperatures.

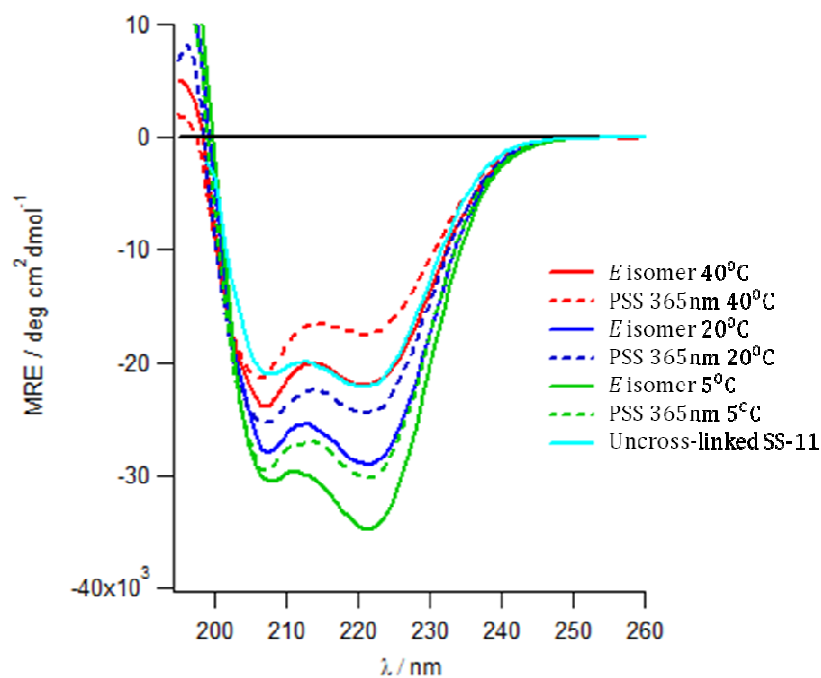


Figure 6.35. CD spectra of cross-linked SS-11 peptide at the indicated temperatures (20 mM sodium phosphate buffer, pH 7).

6.3.3.2. Photochemical study of the cross-linked peptide dissolved in sodium phosphate buffer at different pHs.

Although the experiments were initially carried out at pH 7, we realized that the chromophore was predicted to have a pK_a of 7.4 ± 0.2 (ACD/iLabs, see experimental section), a value significantly lower than that of the Schiff base of rhodopsin.³⁶ Therefore, at pH 7, the N atom of the imine bond of the cross-linker (Figure 6.36) was partially protonated. This means that at lower pH values, such as pH 5, the Schiff base moiety is protonated, while at higher pHs (*i.e.* pH 9) is in its neutral form.

³⁶ Kolodner, P.; Lukashev, E. P.; Ching, Y. C.; Rousseau, D. L. *Proc. Natl. Ac. Sci. USA* **1996**, *93*, 11618.

6. Practical applications

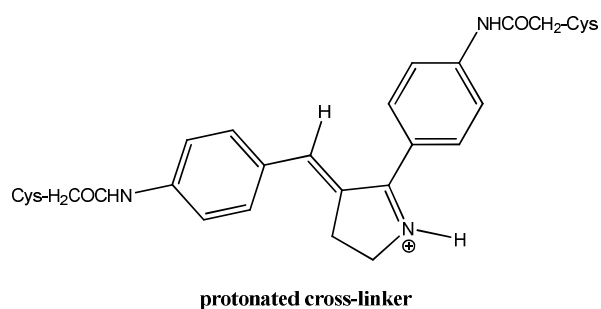


Figure 6.36

Thus, we decided to record the UV-Vis spectrum of the cross-linked peptide at different pH values at 20°C (Figure 6.37).

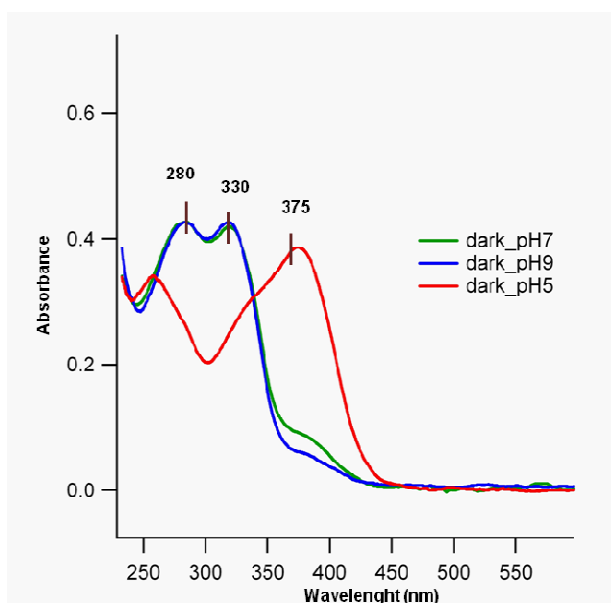


Figure 6.37. UV-Vis spectra of the SS-11 peptide cross-linked with 5r in the dark-adapted *E* form in sodium phosphate buffer at different pHs (pH 5, 7 and 9) at 20°C.

From Figure 6.37 it can be inferred that lowering the pH to 5.0 (red line) caused a bathochromic shift in the spectrum (from 330 to 375 nm, $\Delta\lambda = 45$ nm)

consistent with the protonation of the Schiff base moiety,³⁷ while this longer-wavelength band appeared only partially at pH 7.0 (green line). On the other hand, the UV-Vis spectrum of the cross-linked peptide at pH 9 (blue line) resembled that of pH 7. In this case, there was almost no absorption at 375 nm. The shift of the absorption band when having pH 5 is relevant as lower energetic light can be used for irradiating. However, it would be more convenient to have this absorption band at physiological pH.

Presumably, the pKa of the photoswitch could be raised so that the Schiff base would be protonated at physiological pH by the appropriate introduction of electron-donating substituents. Alternatively, the amino group could be quaternized to maintain a permanent positive charge, as has been done previously with other PSB-retinal based photoswitches (see sections 2.6 and 4.1.2).³⁸

At pH 5, the molar extinction coefficient was calculated to be 24 700 M⁻¹ cm⁻¹ at 375 nm, a value that compares well to those of azobenzene photoswitches, which typically are ~20000 M⁻¹ cm⁻¹.³⁹

Then, we irradiated at 20°C a solution in 20 mM sodium phosphate buffer (pH= 9) of the cross-linked peptide to check if there was any difference with respect to the irradiation at pH 7 (Figure 6.38). The observed behavior was pretty similar to the case at pH 7. The blue line corresponds to the UV-Vis spectrum of the SS-11 peptide cross-linked with **5r** in the dark-adapted *E* form. When the sample was irradiated with 365 nm light until the PSS was reached (dotted black line), it was observed an increase of the band corresponding to the *Z* isomer ($\lambda_{\text{max}}= 280$ nm). If 400 nm light was used for irradiating instead of 365 nm light (dotted blue line), it was also noticeable an increase of the band of the *Z* form.

³⁷ (a) See ref. 35. (b) Nielsen, I. B.; Petersen, M. Å.; Lammich, L.; Nielsen, M. B.; Andersen, L. *H. J. Phys. Chem. A* **2006**, *110*, 12592. (c) Petersen, M. A.; Nielsen, I. B.; Kristensen, M. B.; Kadziola, A.; Lammich, L.; Andersen, L. H.; Nielsen, M. B. *Org. Biomol. Chem.* **2006**, *4*, 1546.

³⁸ (a) See ref. 23. (b) Rivado-Casas, L.; Sampedro, D.; Campos, P. J.; Fusi, S.; Zanirato, V.; Olivucci, M. *J. Org. Chem.* **2009**, *74*, 4666.

³⁹Rau, H. In *Photochromism: Molecules and Systems*; Durr, H., Bouas-Laurent, H. (eds.); Elsevier: Amsterdam, **1990**.

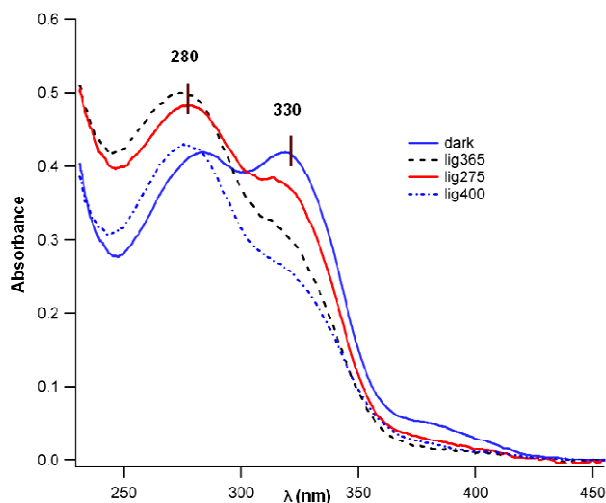


Figure 6.38. UV-Vis spectra of the cross-linked peptide of the dark-adapted *E* form and the photostationary state at pH 9 after irradiating with 365, 400 and 275 nm lights at 20°C.

Moreover, after irradiating with 365 light, the sample was reirradiated with 275 nm light to recover the thermodynamically stable *E* isomer. However, the 275 nm light didn't fully recover the initial isomer.

Since the photochemical behaviour when having the sample of the cross-linked peptide at pH 9 was similar to pH 7, we moved on to performing the experiments at pH 5.

First of all, we irradiated at 20°C a solution in 20 mM sodium phosphate buffer (pH= 5) of the cross-linked peptide. The results are shown in Figure 6.39. The blue line corresponds to the UV-Vis spectrum of the SS-11 peptide cross-linked with **5r** in the dark-adapted *E* form. Irradiation with 365 nm light (dotted red line) and 400 nm light (green line) until the PSS led to an increase of the band corresponding to the *Z* isomer ($\lambda_{\text{max}}= 280$ nm). It should be highlighted that either one light or the other resulted in the same change in the UV-Vis spectrum. Therefore, as violet light (400 nm) is less energetic and more adequate for being used in biological applications, it was used as the light source in the rest of the experiments.

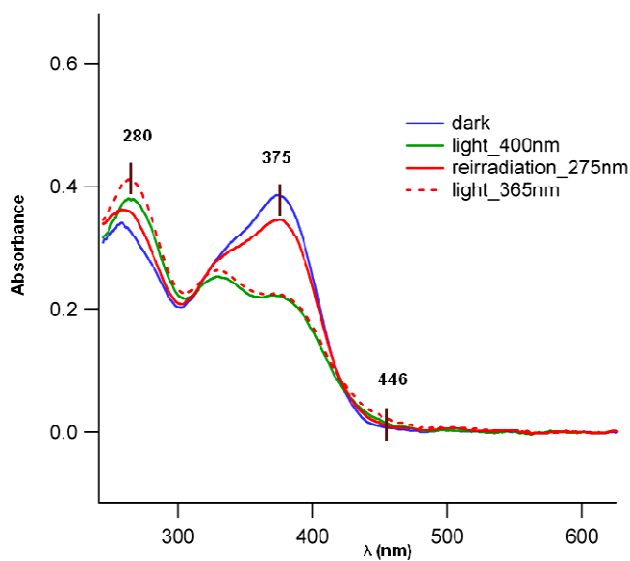


Figure 6.39. UV-Vis spectra of the cross-linked peptide of the dark-adapted *E* form and the photostationary state at pH 5 after irradiating with 365, 400 and 275 nm lights at 20°C.

Reirradiation with 275 nm light almost completely recovered the dark-adapted *E* form. Although this is a good feature, it has been discussed before that this light source is too energetic for being used in future biological applications.

When analyzing the shape of the UV-Vis spectrum for the PSS after irradiation with 400 nm light, we realized that the *Z* isomer had decreased absorbance at 375 nm and exhibited a long wavelength tail. This long wavelength tail enabled photoswitching of the chromophore back to the *E* isomer with blue light (446 nm).

The UV-Vis spectra of the dark-adapted *E* form of the cross-linked peptide (black line) and of the PSS after irradiating the cross-linked peptide in 20 mM phosphate buffer (at pH= 5) with violet light (400 nm) (violet line) and reirradiating with blue light (446 nm) (blue line) at 20°C are shown in Figure 6.40(a). Multiple rounds of photoswitching of the cross-linked peptide at pH 5 using alternating violet and blue light at 20°C were performed (Figure 6.40(b)). As it happened when irradiating at pH 7, there was no evidence of photo-bleaching or

photo-oxidation at this pH. Thus, we can consider that the cross-linked peptide is photostable.

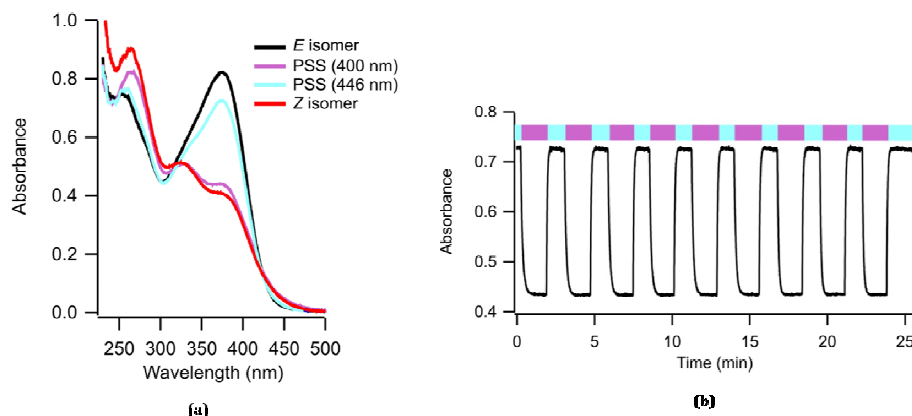


Figure 6.40. (a) UV-Vis spectra of the cross-linked peptide at pH 5 at the photostationary state after irradiating with violet (400 nm) and blue (446 nm) lights at 20°C. (b) Multiple rounds of photoswitching of the cross-linked peptide at pH 5 using alternating violet and blue light at 20°C.

After reaching the PSS by irradiation with 400 nm light, the relaxation of the *Z* isomer to the thermodynamically stable *E* form was monitored at 50°C by measuring absorbance at 375 nm as a function of time (Figure 6.41). The thermal relaxation curve was fitted to a single exponential equation to calculate the relaxation lifetime. The half life was found to be approx. 10 hours at 50°C. This slow thermal relaxation allowed the separation of the *E* and *Z* isomers by HPLC (Figure 6.42).

Once separated the *Z* isomer, the UV-Vis spectrum of a solution of the pure *Z* isomer in 20 mM sodium phosphate at pH 5 at 20°C was recorded. The resulting spectrum is shown in Figure 6.40(a). Having the UV-Vis spectra of the *E* and *Z* pure forms, it was possible to determine the isomers ratio at the PSS after irradiating with violet and blue light. At the PSS after irradiating with violet light (400 nm), the isomer ratio was 7% (*E*) / 93% (*Z*), which means that the photochemical isomer *Z* was almost obtained completely. Reirradiation with blue light (446 nm) gave an isomers ratio at the PSS of 78% (*E*) / 22% (*Z*). Therefore, the *E* isomer was practically recovered.

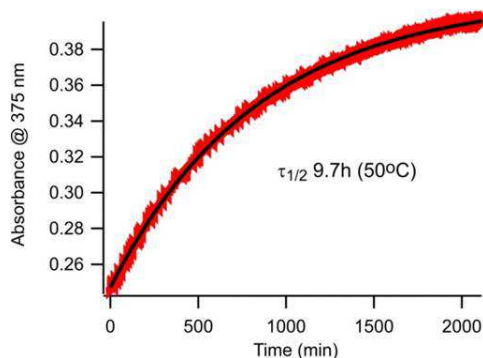


Figure 6.41. Thermal relaxation of the Z form of 5r cross-linked SS-11 after exposure to 400 nm light in 20 mM sodium phosphate buffer at pH 5.

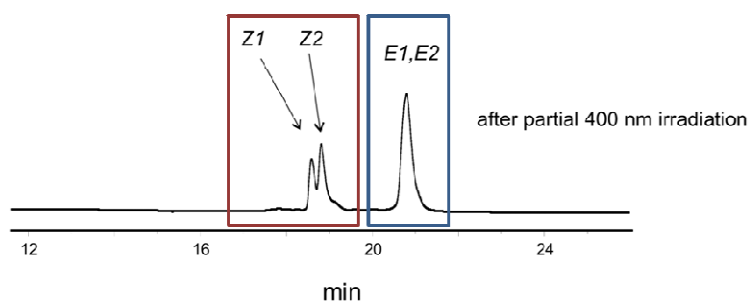


Figure 6.42. HPLC traces of 5r cross-linked SS-11 after exposure to 400 nm light to produce the Z isomer.

On the other hand, the quantum yield for the $E \rightarrow Z$ isomerization of the cross-linked peptide in 20 mM sodium phosphate buffer at pH 5 was determined using a *trans*-azobenzene-modified peptide as actinometer (see experimental section).⁴⁰ After doing this experiment, the value found for the $E \rightarrow Z$ isomerization quantum yield was $\Phi_{E \rightarrow Z} \approx 0.24$. This value was slightly lower than the one found for the photoswitch **5p** ($\Phi_{E \rightarrow Z} \approx 0.6$); however, it was considered quite efficient.

Finally, we recorded the CD spectra of the cross-linked peptide in 20 mM phosphate buffer at pH 5 at 20°C, before and after irradiating with violet and blue

⁴⁰ Borisenko, V.; Woolley, G. A. *J. Photoch. Photobio. A* **2005**, *173*, 21.

6. Practical applications

lights. The obtained results are represented in Figure 6.43, along with the CD spectrum of the pure *Z* form (previously purified by HPLC). From Figure 6.43 we can conclude that cross-linking the SS-11 peptide with the *E* form of **5r** led to a stabilization of the α -helical content, and that the peptide was essentially fully helical at 20°C. Irradiation with 400 nm light to produce the 7% (*E*) / 93% (*Z*) PSS led to a marked decrease in helicity, as predicted.

Since the cross-linker is near the N-terminus of the peptide, conformational distortion is likely to be focused there, with the rest of the peptide remaining helical (Figure 6.44). The observed conformational change was fully reversible to the 78% (*E*) / 22% (*Z*) PSS upon irradiation with blue light.

It is unlikely that the photoswitch itself contributes significantly to the observed CD change, since no induced CD signal was seen at wavelengths where only the photoswitch absorbs (Figure 6.45).

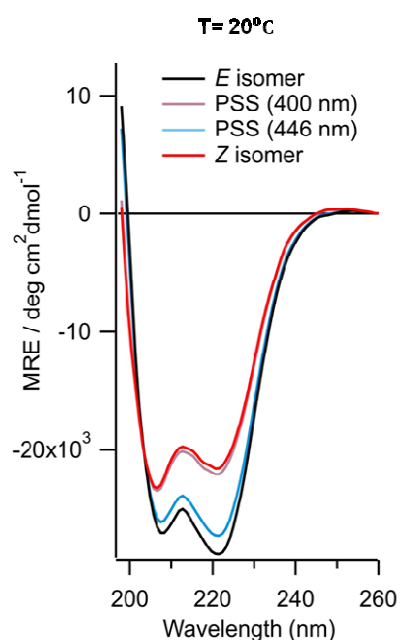


Figure 6.43. CD spectra of cross-linked SS-11 peptide at 20°C (20 mM sodium phosphate buffer, pH 5).

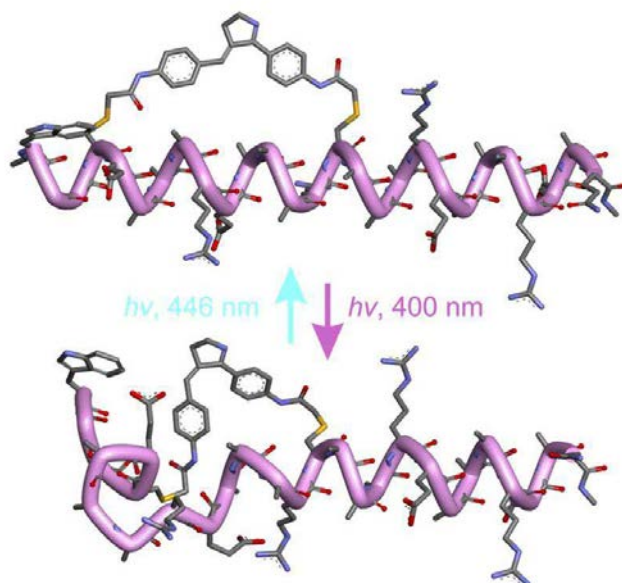


Figure 6.44. Sketch of the cross-linked peptide with the photoswitch in the helix-stabilizing *E* form (top of the image) and showing disruption of the helical structure by the *Z* form of the photoswitch (bottom of the image).

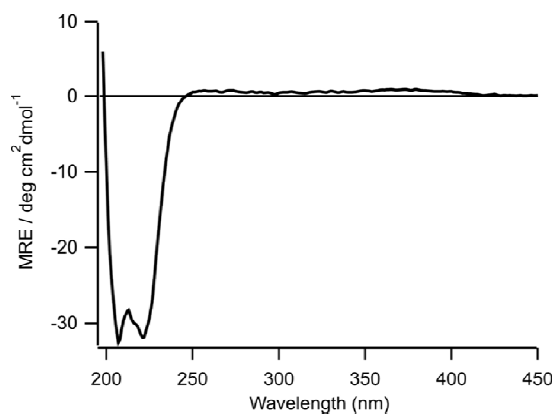


Figure 6.45. CD spectrum obtained for dark-adapted 5r-cross-linked SS-11 in 20 mM sodium phosphate buffer at pH 5 at 20°C. Note the absence of any significant CD signal at wavelengths where the chromophore alone absorbs.

6. Practical applications

It should be pointed out that at different temperatures (5°C, green lines, and 40°C, red lines) took place a similar process. In Figure 6.46, the CD spectra after irradiating with violet and blue lights at different temperatures are represented, along with the CD spectrum of the uncross-linked SS11. It is noticeable that at low temperatures the stabilization was more remarkable than at higher temperatures.

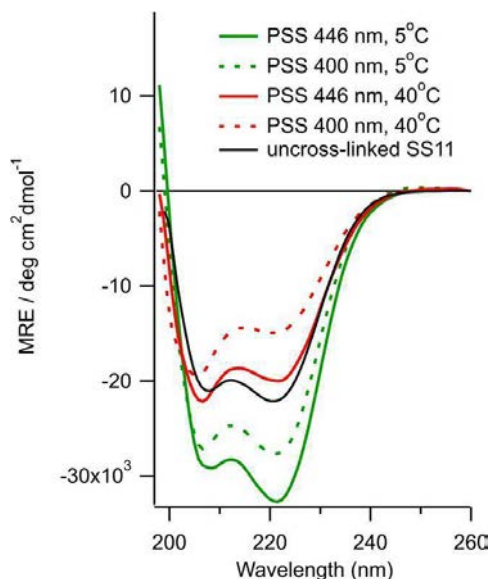


Figure 6.46. CD spectra of cross-linked SS-11 peptide at the indicated temperatures (20 mM sodium phosphate buffer, pH 5).

To sum up, the designed switch functions effectively for the photocontrol of peptide conformation in an aqueous environment using visible wavelengths. Furthermore, the slow thermal relaxation process enables each conformational isomer to be produced with a brief light pulse and maintained on time scales of biological interest. Therefore, the large conformational change that occurs upon isomerization and the efficiency of the photoswitching make this PSB-retinal based photoswitch an attractive candidate for peptide and protein photocontrol that can be applied to a wide variety of targets. Further modification of the substructure of the photoswitch may make even longer wavelength switching possible, as is observed in the natural PSB-retinal chromophore. This methodology may also be

used for other applications in which a change in structure results in a change in the function of the target biomolecule.

The good features presented by this compound could be used in the future to provoke structural changes in biomolecules with biological activity. As the function of a biomolecule is directly related to its structure, merely by the photoinduced isomerization of the switch linked to the biomolecule, we would be able to photocontrol the action of the target biomolecule.

CHAPTER 7

Conclusions

From the study carried out along this thesis, the following conclusions can be drawn:

- Firstly, the synthesis of different prototypes of molecular switches with structures based on the structure of natural chromophores can be achieved through versatile synthetic routes:
 - on the one hand, diverse compounds with structure based on the protonated Schiff base of the retinal chromophore have been synthesized and characterized. The substituents in the substructure have been modified to tune the photochemical and photophysical properties of the switches. The analysis of 2-D NMR experiments and X-ray diffraction has allowed confirming that the compounds are initially in their *E* form.
 - on the other hand, various compounds with structure based on the green fluorescent protein chromophore have been synthesized and characterized as well. Also, the substituents in the substructure have been modified to tune the photochemical and photophysical features of the switches. From the X-ray diffraction results it can be inferred that the compounds are initially in their *Z* form.
- It has been analyzed the effect of varying the solvent when recording the UV-Vis spectra for both types of compounds. The conclusion reached is that it makes no difference whether to use acetonitrile or chloroform for the irradiation process.
- The photochemical study of the two families of molecular switches synthesized has been carried out, from which the following trends can be highlighted:
 - the modification of the substituents present in the structure of the photoswitches entails obtaining different isomers ratio at the PSS;
 - it is possible to achieve the separation of the less thermodynamically stable isomer for both kinds of compounds. In both cases, the shape of the UV-Vis spectra of the two isomers is slightly different. Therefore, there are regions of the spectra where one isomer absorbs more than the other;

7. Conclusions

- the selective irradiation of the photoswitches with structure based on the GFP chromophore leads to different isomers ratio at the PSS as a function of the irradiation wavelength;
 - both types of compounds are photostable;
 - thermal isomerization for both families of photoswitches takes place from the less thermodynamically stable isomer to the thermodynamically stable isomer. In the case of the compounds with structure based on the GFP chromophore this process only occurs when heating the samples in toluene at 100^oC
 - the photoswitches with structure based on the PSB-retinal chromophore can be considered efficient as they present high values for the $E \rightarrow Z$ isomerization quantum yield.
 - the photoswitches with structure based on the GFP chromophore are also quite efficient as they show moderate values for the $E \rightarrow Z$ and $Z \rightarrow E$ isomerization quantum yields.
 - the photoisomerization reaction is plausible under sensitized conditions.
- The conclusions drawn from the theoretical study of the photoswitches with structure based on the GFP chromophore are consistent with the experimental results.
 - It is not viable the linkage of the photoswitches with structure based on the GFP chromophore using the standard methodology described by Woolley and *col.*
 - Once performed the photochemical study of the photoswitches with structure based on the PSB-retinal chromophore, these units have been included in more complex systems, in particular peptides. The efficient behavior of these photoswitches has been kept when bound to the peptide. The reversible isomerization of the obtained cross-linked peptide has been possible by alternating violet (400 nm) and blue (446 nm) light.

CHAPTER 8

Experimental section

8.1. GENERAL COMMENTS.

Solvents and reagents:

All solvents were distilled prior to use. Moreover, certain solvents, such as acetonitrile, tetrahydrofuran, diethyl ether and dichloromethane were purified with the solvent purification system Pure Solvtm 4-MD. On the other hand, the employed reagents were of commercial grades.

Chromathography:

Thin layer chromatography (TLC) was performed using Polygram Sil G/UV254 F₂₅₄ plates (0.2 mm silica gel layer with fluorescence indicator on pre-coated plastic sheets).

Column chromatography was carried out with silica gel (230-240 mesh) as stationary phase. Usual eluents were mixtures of hexane / ethyl acetate.

Characterization techniques:

- Nuclear Magnetic Resonance:

¹H and ¹³C spectra were recorded on a Bruker ARX-300 and/or a Bruker Avance 400 spectrometers. The usual solvent was CDCl₃ with TMS as internal standard. However, other deuterated solvents such as acetonitrile, toluene, methanol or water were also used. Chemical shifts (δ) are given in ppm and coupling constants in hertz. Multiplicity of the signals are abbreviated as follows: (s) = singlet, (d) = doublet, (t) = triplet, (q) = quatriplet, (dd) = doublet of doublets, (dt) = doublet of triplets, (m) = multiplet.

- Chromatography-Mass Spectrometry:

Gas chromatography/mass spectrometry (GC/MS) measurements were performed with a Hewlett-Packard HP G1800B GCD System, provided with HP-5 column and mass spectroscopy detector of electronic impact with quadruple filter (I.E. 71 eV).

- **Electrospray-Mass Spectrometry:**

Electrospray mass spectra were obtained on an HP 5989B apparatus with an HP 59987A interface in either positive-ion mode (ES+) or negative-ion mode (ES-). High resolution mass spectrometry was performed in a HP Bruker Microtof-Q with an Apollo II electrospray source, and was registered in positive ion mode.

- **X-ray diffraction:**

The crystals were mounted in inert oil on glass fibers and transferred to a Nonius Kappa CCD diffractometer equipped with an Oxford Instruments low-temperature attachment. Data were collected by monochromatic Mo K α radiation ($\lambda = 0.71073 \text{ \AA}$) Scan type $\omega\psi$ and Φ . Absorption corrections: numerical (based on multiple scans). The structures were solved by Sir98 and refined on F2 using the program SHELXL-97.¹ All non-hydrogen atoms were anisotropically refined and hydrogen atoms were included using a mixed model.

- **Melting point:**

Values were obtained on a Büchi B-545 apparatus, with capillary tubes, and were not corrected.

- **UV-Vis:**

Absorption molecular spectra were recorded on a Hewlett-Packard HP 8451A Diode Array UV-Vis spectrophotometer. Quartz cuvettes (1.0 cm path length) were used for the measurements.

- **Luminescence:**

Luminescence spectra were recorded at room temperature with a Jobin-Yvon Horiba Fluorolog 3-22 Tau-3 spectrofluorimeter. Data was analyzed with the Origin 6.1 program. Fluorescence lifetime recording was performed with a 280 or 320 nm Horiba Jobin Yvon IBH NanoLED excitation Source with a nanoLED controller module HJY-IBH FluoroHub-B.

¹ Seldrick, G. M. *SHELXL-97*. University of Göttingen: Göttingen, Germany, 1997.

Lamps and photochemical instruments:

Standard irradiation of the samples in photochemical reactors was carried out with a 125-W medium-pressure Hg lamp (Photochemical Reactors LTD (UK)) and a Pyrex filter (except in the case of compound **5e**, where Quartz was used instead of Pyrex) (Figure 8.1). The sample solutions were placed in an immersion well reactor or a Pyrex/quartz NMR tube.

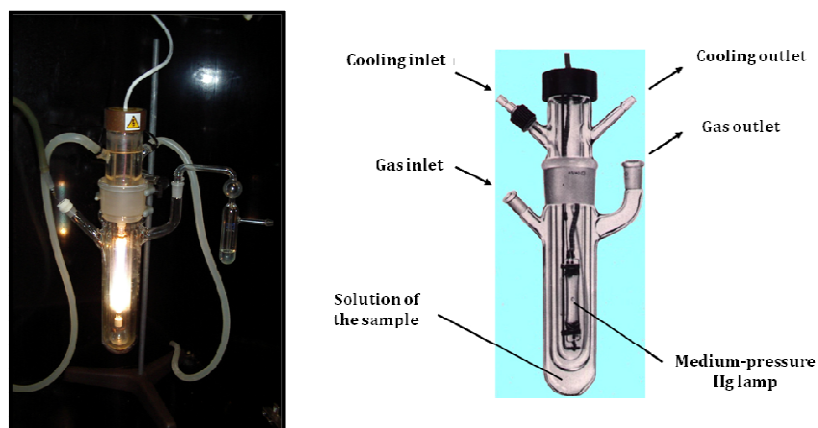


Figure 8.1. Lamps and photochemical reactors.

The emission spectrum of a Hg lamp is shown in Figure 8.2.

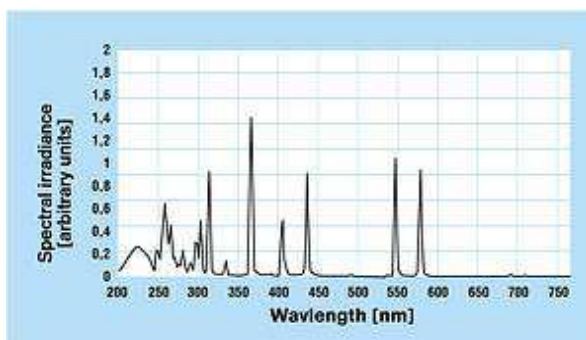


Figure 8.2. Emission spectrum of a Hg lamp.

- Monochromator:

For irradiating with monochromatic light, an Oriel Cornestone 130 1/8m monochromator was used, being the light source a 500 W Hg arc lamp placed in a proper lamp housing. The samples were placed in quartz cuvettes (1.0 cm path length) (Figure 8.3).



Figure 8.3. Oriel Cornestone 130 1/8m monochromator.

- Photoreactor:

For irradiating with less energetic light, a Luzchem UV/Vis photoreactor (LZC-4, Figure 8.4(a)) was used, provided with LZC-UVA lamps with emission wavelength centred at 350 nm (14 lamps x 8-W lamp, Figure 8.4(b)).

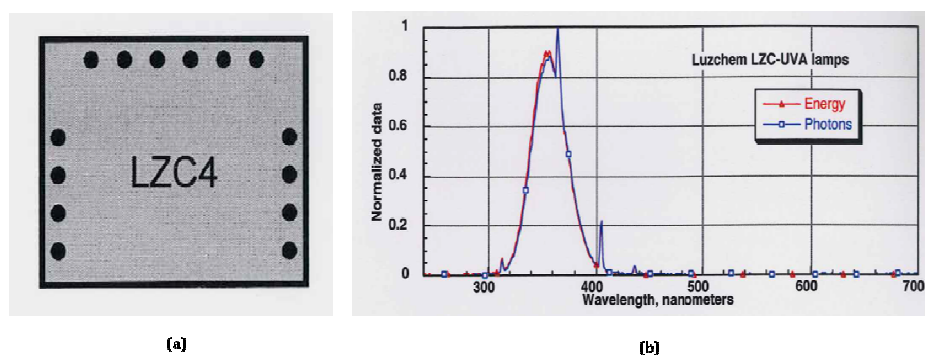


Figure 8.4. (a) LZC4 UV/Vis photoreactor. (b) Emission spectrum of LZC-UVA lamps.

8.2. SYNTHESIS OF BIOMIMETIC MOLECULAR SWITCHES.

8.2.1. Synthesis of neutral photoswitches switches with structure based on the protonated Schiff base of retinal (PSB-retinal) chromophore.

The general procedure for the synthesis of compounds **5(a-o)** is represented in the following figure:

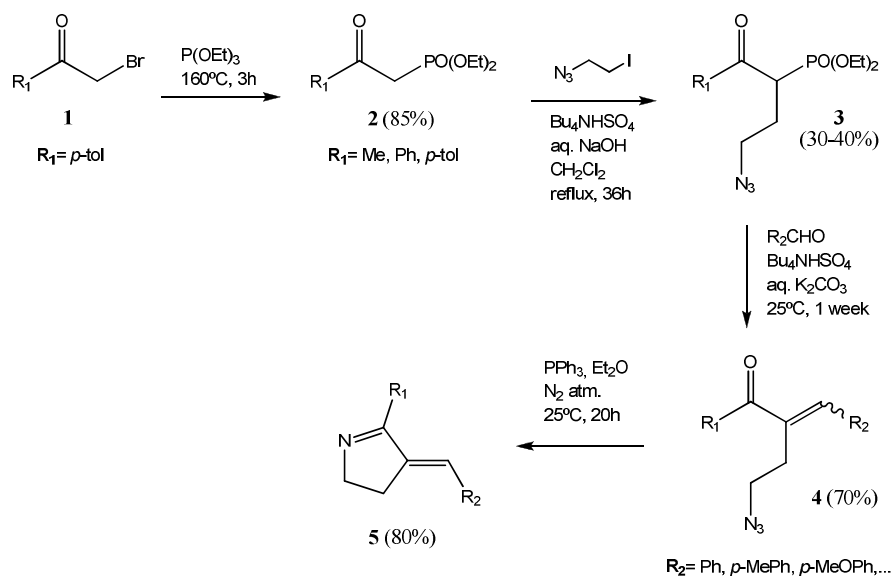


Figure 8.5. Synthetic route to afford new PSB-retinal based photoswitches.

In the following paragraphs are described the steps taken so as to obtain the target photoswitches **5(a-o)**.

- Synthesis of phosphonates (**2**):

When the phosphonate (**2**) with the adequate R₁ group was not commercially available, it was synthesized by treatment of the corresponding 2-bromoketone (**1**) with triethyl phosphite at 160^oC for 3 hours.²

² Nagata, W.; Wakabayashi, T.; Hayase, Y. *Org. Syn.* **1973**, *53*, 44; **1988**, *Coll. Vol. 6*, 448.

- Synthesis of azido phosphonates (**3**):

To a mixture of the phosphonate (**2**) (1 equiv.) and 2-iodoethylazide (2.5 equiv.) in CH₂Cl₂ (5 ml) was added a solution of tetrabutylammonium hydrogen sulfate (1 equiv.) in sodium hydroxide 2M (2 equiv.), and the resulting mixture was refluxed for 36 hours.³ Later, it was cooled and treated with water (50 ml) and CH₂Cl₂ (50 ml). The organic layer was separated and concentrated under reduced pressure. The resulting residue was dissolved in Et₂O (100 ml) in order to precipitate tetrabutylammonium iodide. The salt was filtered off, and the filtrate was dried (Na₂SO₄) and concentrated under reduced pressure to give a colorless oil. The resulting product was purified by flash chromatography on silica gel (1:1 hexanes/EtOAc) to afford (**3**) with the adequate R₁ group in 30-40% yield.

- Synthesis of azido enones (**4**):

To azido phosphonate (**3**) (1 equiv.) were added K₂CO₃ (28 equiv.), H₂O (10ml), tetrabutylammonium hydrogen sulfate (0.2 equiv.) and the aldehyde with the adequate R₂ group (1.5 equiv.), and the resulting mixture was stirred for 1 week at room temperature.² The reaction was followed by TLC (5:1 hexanes/EtOAc) until the total consumption of azido phosphonate (**3**). Then, the solvent was removed and water (50ml) was added before extracting with CH₂Cl₂ (3 x 50ml). The organic layers were combined, dried (Na₂SO₄), and concentrated under reduced pressure. The residual oil was purified by chromatography on silica gel (5:1 hexanes/EtOAc) to give the azido enone (**4**) as a 9:1 mixture of *E* and *Z* isomers in 70% yield. The two isomers could be separated by chromatography on silica gel (10:1 hexanes/EtOAc); however, it was possible to carry out the next step by using the 9:1 mixture of *E* and *Z* isomers.

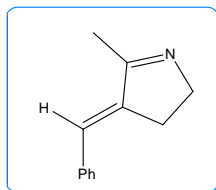
- Synthesis of switches (**5a-o**):

To a dry diethyl ether solution (20ml) of (**4**) (1 equiv.) was added Ph₃P (3 equiv.).⁴ The resulting mixture was stirred for 24 h under nitrogen at room temperature and concentrated under reduced pressure. The resulting solid was purified by chromatography on silica gel (1:4 hexanes/EtOAc) to obtain the *E* isomer of (**5a-o**) in 60-85% yield.

The corresponding data for each compound (**5a-o**) are described below:

³ Snider, B. B.; Zhou, J. *J. Org. Chem.* **2005**, *70*, 1087.

• (*E*)-4-benzylidene-5-methyl-3,4-dihydro-2*H*-pyrrole (**5a**)



Empiric formula: C₁₂H₁₃N

Molecular weight: 171.12

Yield: 85 %

¹H NMR (300 MHz, CDCl₃): δ (ppm) 7.48 (d, *J* = 7.4 Hz, 2H), 7.70 (t, *J* = 7.6 Hz, 2H), 7.29 (t, *J* = 13.0 Hz, 1H), 6.73 (s, 1H), 4.02 (m, 2H), 2.89 (m, 2H), 2.24 (s, 3H).

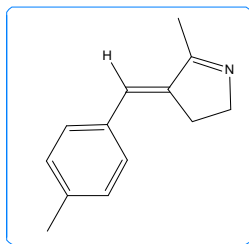
¹³C NMR (300MHz, CDCl₃): δ (ppm) 173.06, 142.99, 137.05, 128.88, 128.74, 127.90, 124.90, 58.97, 29.81, 16.31.

UV-VIS (CH₃CN): λ (nm) 277 (ε = 7640 M⁻¹cm⁻¹), 288 (ε = 8681 M⁻¹ cm⁻¹), 303 (ε = 5851 M⁻¹cm⁻¹).

ES-MS (+) (C₁₂H₁₃N + H): calc. 172.1121, found 172.1122.

Observations: Brown oil

• (*E*)-5-methyl-4-(4-methylbenzylidene)-3,4-dihydro-2*H*-pyrrole (**5b**)



Empiric formula: C₁₃H₁₅N

Molecular weight: 185.13

Yield: 82 %

¹H NMR (300 MHz, CDCl₃): δ (ppm) 7.38 (d, *J* = 8.1 Hz, 2H), 7.21 (d, *J* = 8.0 Hz, 2H), 6.71 (s, 1H), 4.02 (m, 2H), 2.88 (m, 2H), 2.38 (s, 3H), 2.23 (s, 3H).

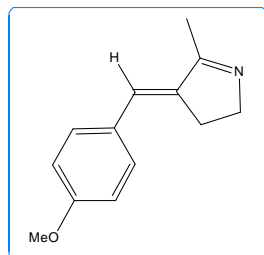
¹³C NMR (300MHz, CDCl₃): δ (ppm) 173.30, 142.24, 138.15, 134.44, 129.66, 129.01, 124.99, 59.16, 29.29, 21.59, 16.49.

UV-VIS (CH₃CN): λ (nm) 287 (ε = 7345 M⁻¹cm⁻¹), 300 (ε = 5715 M⁻¹ cm⁻¹), 305 (ε = 4790 M⁻¹cm⁻¹).

ES-MS (+) (C₁₃H₁₅N + H): calc. 186.1277, found 186.1279.

Observations: Brown oil

• (*E*)-4-(4-methoxybenzylidene)-5-methyl-3,4-dihydro-2*H*-pyrrole (**5c**)



Empiric formula: C₁₃H₁₅NO

Molecular weight: 201.12

Yield: 80 %

¹H NMR (300 MHz, CDCl₃): δ (ppm) 7.40 (d, *J* = 8.8 Hz, 2H), 6.91 (d, *J* = 8.8 Hz, 2H), 6.65 (s, 1H), 3.98 (m, 2H), 3.80 (s, 3H), 2.80 (m, 2H), 2.20 (s, 3H).

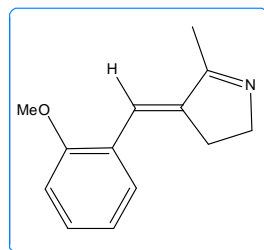
¹³C NMR (300MHz, CDCl₃): δ (ppm) 174.39, 159.51, 139.24, 130.45, 129.17, 126.35, 114.14, 57.39, 55.30, 29.65, 15.61.

UV-VIS (CH₃CN): λ (nm) 296 (ε = 26636 M⁻¹cm⁻¹).

ES-MS (+) (C₁₃H₁₅NO + H): calc. 202.1226, found 202.1235.

Observations: Brown oil

• (*E*)-4-(2-methoxybenzylidene)-5-methyl-3,4-dihydro-2*H*-pyrrole (**5d**)



Empiric formula: C₁₃H₁₅NO

Molecular weight: 201.12

Yield: 80 %

¹H NMR (300 MHz, CDCl₃): δ (ppm) 7.50 (m, 1H), 7.28 (m, 1H), 7.11 (s, 1H), 6.96 (m, 2H), 3.98 (m, 2H), 3.88 (s, 3H), 2.85 (m, 2H), 2.25 (s, 3H).

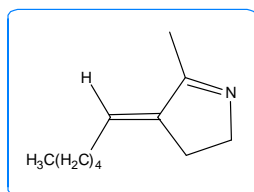
¹³C NMR (300MHz, CDCl₃): δ (ppm) 173.52, 157.50, 143.02, 131.40, 129.26, 128.19, 120.59, 118.91, 110.74, 58.84, 55.64, 29.76, 16.50.

UV-VIS (CH₃CN): λ (nm) 275 (ε = 8938 M⁻¹cm⁻¹), 291 (ε = 6818 M⁻¹cm⁻¹), 312 (ε = 4713 M⁻¹cm⁻¹).

ES-MS (+) (C₁₃H₁₅NO + H): calc. 202.1226, found 202.1228.

Observations: Brown oil

• (*E*)-4-hexylidene-5-methyl-3,4-dihydro-2*H*-pyrrole (**5e**)



Empiric formula: C₁₁H₁₉N
Molecular weight: 165.15
Yield: 75%

¹H NMR (300 MHz, CDCl₃): δ (ppm) 5.80 (s, 1H), 3.90 (m, 2H), 2.51 (m, 2H), 2.14 (m, 2H), 2.09 (s, 3H), 1.47 (m, 2H), 1.35 (m, 4H), 0.93 (m, 3H).

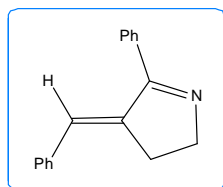
¹³C NMR (300MHz, CDCl₃): δ (ppm) 171.93, 143.31, 126.62, 57.58, 31.71, 30.62, 28.78, 26.89, 22.68, 15.94, 14.18.

UV-VIS (CH₃CN): λ (nm) 232 (ε = 15000 M⁻¹cm⁻¹).

ES-MS (+) (C₁₁H₁₉N + H): calc. 166.1590, found 166.1591.

Observations: Brown oil

• (*E*)-4-benzylidene-5-phenyl-3,4-dihydro-2*H*-pyrrole (**5f**)



Empiric formula: C₁₇H₁₅N
Molecular weight: 233.12
Yield: 82%

¹H NMR (300 MHz, CDCl₃): δ (ppm) 7.65 (m, 2H), 7.40 (m, 7H), 7.26 (m, 1H), 6.83 (s, 1H), 4.21 (m, 2H), 3.06 (m, 2H).

¹³C NMR (300MHz, CDCl₃): δ (ppm) 174.94, 142.12, 137.02, 134.55, 129.63, 128.92, 128.79, 128.60, 128.49, 127.92, 127.76 (d, *J* = 2.3 Hz), 59.68, 31.00.

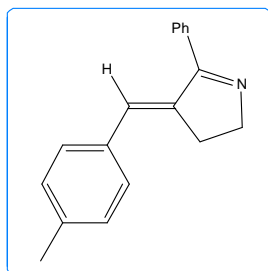
UV-VIS (CH₃CN): λ (nm) 231 (ε = 10059 M⁻¹cm⁻¹), 248 (ε = 10806 M⁻¹cm⁻¹), 289 (ε = 22232 M⁻¹cm⁻¹), 303 (ε = 15717 M⁻¹cm⁻¹).

ES-MS (+) (C₁₇H₁₅N + H): calc. 234.1277, found 234.1284.

Melting point: 103-105°C

Observations: White solid

• (*E*)-4-(4-methylbenzylidene)-5-phenyl-3,4-dihydro-2*H*-pyrrole (**5g**)



Empiric formula: C₁₈H₁₇N

Molecular weight: 247.14

Yield: 70%

¹H NMR (300 MHz, CDCl₃): δ (ppm) 7.64 (m, 2H), 7.45 (m, 3H), 7.31 (d, *J* = 8.2 Hz, 2H), 7.17 (d, *J* = 8.1 Hz, 2H), 6.80 (s, 1H), 4.19 (m, 2H), 3.03 (m, 2H), 2.35 (s, 3H).

¹³C NMR (300MHz, CDCl₃): δ (ppm) 175.06, 141.17, 137.96, 134.63, 134.19, 129.56, 129.34, 128.90, 128.78, 128.45, 127.74 (d, *J* = 1.9 Hz), 59.62, 30.97, 21.36.

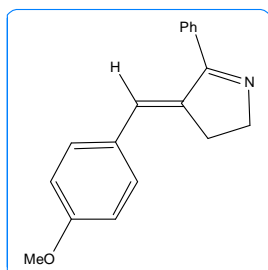
UV-VIS (CH₃CN): λ (nm) 283 (ε = 21154 M⁻¹cm⁻¹), 296 (ε = 24808 M⁻¹cm⁻¹), 309 (ε = 19231 M⁻¹cm⁻¹).

ES-MS (+) (C₁₈H₁₇N + H): calc. 248.1434, found 248.1430.

Melting point: 64-66°C

Observations: Orange solid

• (*E*)-4-(4-methoxybenzylidene)-5-phenyl-3,4-dihydro-2*H*-pyrrole (**5h**)



Empiric formula: C₁₈H₁₇NO

Molecular weight: 263.

Yield: 83%

¹H-NMR (300 MHz, CDCl₃): δ (ppm) 7.62 (m, 2H), 7.42 (m, 2H), 7.32 (d, *J* = 8.7 Hz, 2H), 6.87 (d, *J* = 8.8 Hz, 2H), 6.76 (s, 1H), 4.16 (m, 2H), 3.75 (s, 3H), 2.97 (m, 2H).

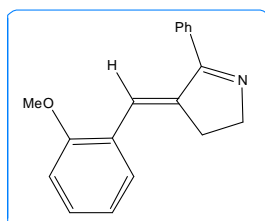
¹³C-NMR (300MHz, CDCl₃): δ (ppm) 174.87, 159.12, 139.66, 134.43, 130.19, 129.42, 129.35, 128.58, 128.25, 127.33, 127.24, 59.28, 55.07, 30.63.

UV-VIS (CH₃CN): λ (nm) 226 (ε = 12467 M⁻¹cm⁻¹), 249 (ε = 10345 M⁻¹cm⁻¹), 304 (ε = 24934 M⁻¹cm⁻¹), 317 (ε = 20689 M⁻¹cm⁻¹).

ES-MS (+) (C₁₈H₁₇NO + H): calc. 264.1383, found 264.1389.

Observations: Brown oil

- (*E*)-4-(2-methoxybenzylidene)-5-phenyl-3,4-dihydro-2*H*-pyrrole (**5i**)



Empiric formula: C₁₈H₁₇NO

Molecular weight: 263.

Yield: 85%

¹H-NMR (300 MHz, CDCl₃): δ (ppm) 7.69 (m, 2H), 7.46 (d, *J* = 7.7 Hz, 1H), 7.38 (m, 3H), 7.21 (m, 2H), 6.94 (t, *J* = 7.5 Hz, 1H), 6.77 (d, *J* = 8.3 Hz, 1H), 4.08 (m, 2H), 3.61 (s, 3H), 2.90 (m, 2H).

¹³C-NMR (300MHz, CDCl₃): δ (ppm) 174.45, 156.98, 141.42, 134.23, 129.24, 128.91, 128.52, 128.01, 127.93, 125.59, 121.74, 119.92, 110.50, 58.95, 54.72, 30.77.

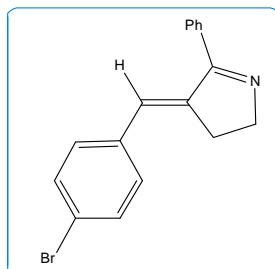
UV-VIS (CH₃CN): λ (nm) 237 (ε = 13840 M⁻¹cm⁻¹), 281 (ε = 15225 M⁻¹cm⁻¹), 294 (ε = 13840 M⁻¹cm⁻¹), 317 (ε = 14189 M⁻¹cm⁻¹).

ES-MS (+) (C₁₈H₁₇NO + H): calc. 264.1383, found 264.1394.

Melting point: 111-113°C

Observations: White solid

- (*E*)-4-(4-bromobenzylidene)-5-phenyl-3,4-dihydro-2*H*-pyrrole (**5j**)



Empiric formula: C₁₇H₁₄BrN

Molecular weight: 311.03

Yield: 74%

¹H-NMR (300 MHz, CDCl₃): δ (ppm) 7.63 (m, 2H), 7.46 (m, 5H), 7.26 (d, *J* = 8.6 Hz, 2H), 6.74 (s, 1H), 4.20 (m, 2H), 2.99 (m, 2H).

¹³C-NMR (300MHz, CDCl₃): δ (ppm) 174.74, 142.80, 135.94, 134.33, 131.74, 130.34, 129.71, 128.73, 128.53, 126.47, 121.80, 59.75, 30.82.

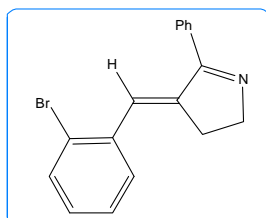
UV-VIS (CH₃CN): λ (nm) 282 ($\epsilon = 47716 \text{ M}^{-1}\text{cm}^{-1}$), 295 ($\epsilon = 43147 \text{ M}^{-1}\text{cm}^{-1}$), 311 ($\epsilon = 23350 \text{ M}^{-1}\text{cm}^{-1}$).

ES-MS (+) (C₁₇H₁₄BrN + H): calc. 312.0382, found 312.0385.

Melting point: 120-122^oC

Observations: White solid

• (*E*)-4-(2-bromobenzylidene)-5-phenyl-3,4-dihydro-2*H*-pyrrole (**5k**)



Empiric formula: C₁₇H₁₄BrN

Molecular weight: 311.03

Yield: 77%

¹H-NMR (300 MHz, CDCl₃): δ (ppm) 7.71 (m, 2H), 7.57(t, $J = 9.2 \text{ Hz}$, 2H), 7.47 (m, 3H), 7.33 (t, $J = 7.3 \text{ Hz}$, 1H), 7.14 (m, 2H), 4.77 (m, 2H), 2.95 (m, 2H).

¹³C-NMR (300MHz, CDCl₃): δ (ppm) 174.28, 143.75, 136.76, 134.10, 132.95, 129.75, 129.07, 128.78, 128.58, 128.44, 127.26, 126.40, 124.99, 59.28, 30.37.

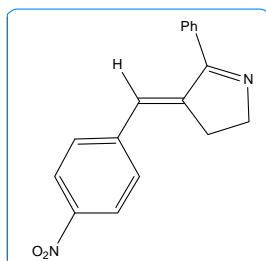
UV-VIS (CH₃CN): λ (nm) 235 ($\epsilon = 15015 \text{ M}^{-1}\text{cm}^{-1}$), 240 ($\epsilon = 14114 \text{ M}^{-1}\text{cm}^{-1}$), 282 ($\epsilon = 18182 \text{ M}^{-1}\text{cm}^{-1}$), 292 ($\epsilon = 17117 \text{ M}^{-1}\text{cm}^{-1}$).

ES-MS (+) (C₁₇H₁₄BrN + H): calc. 312.0382, found 312.0388.

Melting point: 106-108^oC

Observations: White solid

• (*E*)-4-(4-nitrobenzylidene)-5-phenyl-3,4-dihydro-2*H*-pyrrole (**5l**)



Empiric formula: C₁₇H₁₄N₂O₂

Molecular weight: 278.11

Yield: 76%

¹H-NMR (300 MHz, CDCl₃): δ (ppm) 8.23 (d, *J* = 8.8 Hz, 2H), 7.66 (m, 2H), 7.57 (d, *J* = 8.9 Hz, 2H), 7.50 (m, 3H), 6.90 (s, 1H), 4.30 (m, 2H), 3.10 (m, 2H).

¹³C-NMR (300MHz, CDCl₃): δ (ppm) 174.47, 146.61, 146.19, 143.64, 133.90, 129.96, 129.34, 128.67, 125.51, 125.43, 123.93, 123.87, 60.03, 31.30.

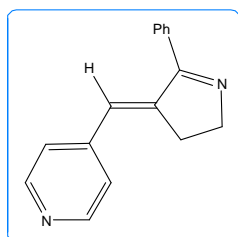
UV-VIS (CH₃CN): λ (nm) 233 (ε = 10150 M⁻¹cm⁻¹), 262 (ε = 7026 M⁻¹cm⁻¹), 335 (ε = 13684 M⁻¹cm⁻¹).

ES-MS (+) (C₁₇H₁₄N₂O₂ + H): calc. 279.1128, found 279.1133.

Melting point: 119-121^oC

Observations: Pale orange solid

• (*E*)-4-((5-phenyl-2*H*-pyrrol-4(3*H*-ylidene)methyl)pyridine (**5m**)



Empiric formula: C₁₆H₁₄N₂

Molecular weight: 234.12

Yield: 65%

¹H-NMR (300 MHz, CDCl₃): δ (ppm) 8.64 (m, 2H), 7.65 (m, 2H), 7.51 (m, 3H), 7.30 (m, 2H), 6.77 (s, 1H), 4.29 (m, 2H), 3.11 (m, 2H).

¹³C-NMR (300MHz, CDCl₃): δ (ppm) 174.48, 150.19, 146.69, 144.43, 133.93, 130.02, 128.76, 128.72, 125.10, 123.03, 59.98, 31.25.

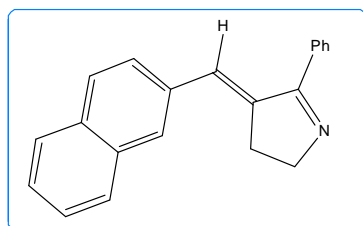
UV-VIS (CH₃CN): λ (nm) 245 (ε = 10028 M⁻¹cm⁻¹), 275 (ε = 18384 M⁻¹cm⁻¹), 284 (ε = 19304 M⁻¹cm⁻¹), 300 (ε = 12368 M⁻¹cm⁻¹).

ES-MS (+) (C₁₆H₁₄N₂ + H): calc. 235.1230, found 235.1232.

Melting point: 99-101^oC

Observations: Brown solid

• (*E*)-4-(naphthalen-1-ylmethylene)-5-phenyl-3,4-dihydro-2*H*-pyrrole (**5n**)



Empiric formula: C₂₁H₁₇N

Molecular weight: 283.14

Yield: 60%

¹H-NMR (300 MHz, CDCl₃): δ (ppm) 7.89 (s, 1H), 7.83 (m, 3H), 7.70 (m, 2H), 7.57 (m, 1H), 7.51 (m, 5H), 7.01 (s, 1H), 4.28 (m, 2H), 3.20 (m, 2H).

¹³C-NMR (300MHz, CDCl₃): δ (ppm) 175.20, 142.46, 134.63, 134.50, 133.46, 132.89, 129.81, 128.92, 128.62, 128.56, 128.33, 128.25, 127.76, 126.59, 126.56, 59.70, 31.18.

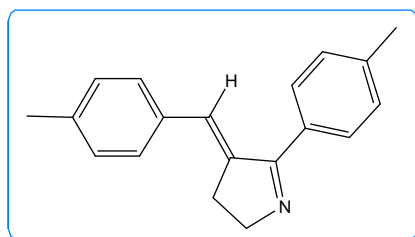
UV-VIS (CH₃CN): λ (nm) 245 (ε = 26342 M⁻¹cm⁻¹), 266 (ε = 34448 M⁻¹cm⁻¹), 275 (ε = 34853 M⁻¹cm⁻¹), 311 (ε = 28368 M⁻¹cm⁻¹), 324 (ε = 24316 M⁻¹cm⁻¹).

ES-MS (+) (C₂₁H₁₇N + H): calc. 284.1434, found 284.1439.

Melting point: 153-155°C

Observations: Yellow solid

(E)-4-(4-methylbenzylidene)-5-p-tolyl-3,4-dihydro-2H-pyrrole (5o)



Empiric formula: C₁₉H₁₉N

Molecular weight: 261.15

Yield: 80%

¹H-NMR (400 MHz, CDCl₃): δ (ppm) 7.55 (d, *J* = 8.0 Hz, 2H), 7.32 (d, *J* = 8.1 Hz, 2H), 7.27 (d, *J* = 7.9 Hz, 2H), 7.19 (d, *J* = 8.0 Hz, 2H), 6.82 (s, 1H), 4.19 (m, 2H), 3.05 (m, 2H), 2.42 (s, 3H), 2.36 (s, 3H).

¹³C-NMR (400 MHz, CDCl₃): δ (ppm) 174.91, 141.27, 139.56, 137.88, 134.29, 131.69, 131.69, 129.32, 129.14, 128.89, 128.74, 127.68, 59.44, 31.01, 21.47, 21.35.

UV-VIS (CH₃CN): λ (nm) 254 (ε = 12623 M⁻¹cm⁻¹), 294 (ε = 20118 M⁻¹cm⁻¹), 309 (ε = 15385 M⁻¹cm⁻¹).

ES-MS (+) (C₁₉H₁₉N + H): calc. 262.1590, found 262.1598.

Melting point: 83-85°C

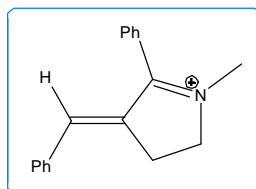
Observations: Orange solid

8.2.2. Synthesis of methylated photoswitches switches with structure based on the PSB-retinal chromophore.

The methylated photoswitches were synthesized as follows: to a solution of the neutral photoswitch (1 equivalent) in dry toluene (2 ml), under nitrogen atmosphere, was added methyl triflate CF₃SO₃CH₃ (1 equivalent). The resulting

mixture was stirred vigorously for 10 minutes at room temperature. After this time, the *N*-methylated compound precipitates and can be separated by filtration. Finally, the methylated photoswitch is dried well in a high vacuum pump, being not necessary further purification. The corresponding data for each methylated compound are described below:

- **(*E*)-4-benzylidene-1-methyl-5-phenyl-3,4-dihydro-2*H*-pyrrolium (5f-met)**



Empiric formula: C₁₈H₁₈N

Molecular weight: 248.14

Yield: 95%

¹H NMR (300 MHz, CD₃CN): δ (ppm) 7.74 (m, 3H), 7.57 (m, 7H), 7.05 (s, 1H), 4.41 (m, 2H), 3.43 (m, 2H), 3.40 (s, 3H).

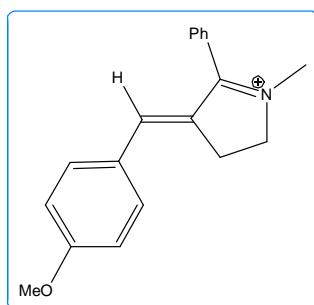
¹³C NMR (300MHz, CD₃CN): δ (ppm) 180.48, 144.62, 139.45, 135.09, 133.72, 132.23, 131.84, 130.45, 130.13, 129.89, 125.98, 60.52, 39.24, 27.76.

UV-VIS (CH₃CN): λ (nm) 334 (ε = 19418 M⁻¹cm⁻¹).

ES-MS (+) (C₁₈H₁₈N): calc. 248.1434, found 248.1441.

Observations: Brown oil

- **(*E*)-4-(4-methoxybenzylidene)-1-methyl-5-phenyl-3,4-dihydro-2*H*-pyrrolium (5h-met)**



Empiric formula: C₁₉H₂₀NO

Molecular weight: 278.15

Yield: 90%

¹H NMR (300 MHz, CD₃CN): δ (ppm) 7.76 (m, 3H), 7.55 (m, 4H), 7.04 (m, 3H), 4.36 (m, 2H), 3.86 (s, 3H), 3.40 (m, 2H), 3.35 (s, 3H).

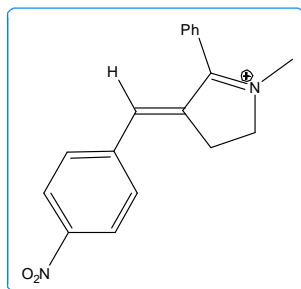
¹³C NMR (300MHz, CD₃CN): δ (ppm) 180.83, 163.32, 144.80, 136.39, 134.26, 133.57, 130.45, 129.83, 127.88, 126.22, 115.71, 60.00, 56.37, 38.74, 27.75.

UV-VIS (CH₃CN): λ (nm) 254 ($\epsilon = 7921 \text{ M}^{-1}\text{cm}^{-1}$), 287 ($\epsilon = 5624 \text{ M}^{-1}\text{cm}^{-1}$), 371 ($\epsilon = 11901 \text{ M}^{-1}\text{cm}^{-1}$).

ES-MS (+) (C₁₉H₂₀NO): calc. 278.1539, found 278.1542.

Observations: Brown oil

- (*E*)-1-methyl-4-(4-nitrobenzylidene)-5-phenyl-3,4-dihydro-2*H*-pyrrolium (**51-met**)



Empiric formula: C₁₈H₁₇N₂O₂

Molecular weight: 293.13

Yield: 97%

¹H NMR (300 MHz, CD₃CN): δ (ppm) 8.23 (d, $J = 8.7 \text{ Hz}$, 2H), 7.73 (m, 5H), 7.59 (m, 2H), 7.11 (s, 1H), 4.44 (m, 2H), 3.44 (m, 5H).

¹³C NMR (300MHz, CD₃CN): δ (ppm) 180.33, 149.32, 143.24, 141.45, 140.98, 133.97, 132.41, 130.51, 129.99, 129.85, 125.57, 124.93, 60.93, 39.66, 27.76.

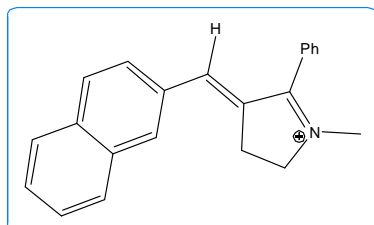
UV-VIS (CH₃CN): λ (nm) 337 ($\epsilon = 23408 \text{ M}^{-1}\text{cm}^{-1}$).

ES-MS (+) (C₁₈H₁₇N₂O₂): calc. 293.1285, found 293.1285.

Melting point: 112-114^oC

Observations: Brown solid

- (*E*)-1-methyl-4-(4-nitrobenzylidene)-5-phenyl-3,4-dihydro-2*H*-pyrrolium (**51-met**)



Empiric formula: C₂₂H₂₀N

Molecular weight: 298.16

Yield: 85%

¹H NMR (300 MHz, CD₃CN): δ (ppm) 8.13 (m, 1H), 7.93 (m, 3H), 7.76 (m, 3H), 7.60 (m, 5H), 7.23 (s, 1H), 4.42 (m, 2H), 3.57 (m, 2H), 3.42 (s, 3H).

^{13}C NMR (300MHz, CD_3CN): δ (ppm) 180.52, 144.94, 144.89, 139.51, 135.12, 133.99, 133.80, 133.31, 132.71, 130.53, 129.92, 129.77, 129.45, 128.67, 128.13, 127.58, 126.02, 60.52, 39.27, 27.87.

UV-VIS (CH_3CN): λ (nm) 214 ($\epsilon = 18250 \text{ M}^{-1}\text{cm}^{-1}$), 280 ($\epsilon = 12500 \text{ M}^{-1}\text{cm}^{-1}$), 290 ($\epsilon = 13250 \text{ M}^{-1}\text{cm}^{-1}$), 350 ($\epsilon = 16500 \text{ M}^{-1}\text{cm}^{-1}$).

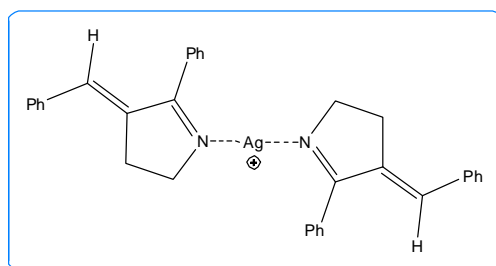
ES-MS (+) ($\text{C}_{22}\text{H}_{20}\text{N}$): calc. 298.1583, found 298.1583.

Melting point: 179-181 $^\circ\text{C}$

Observations: Orange solid

8.2.3. Synthesis of metallated photoswitches switches with structure based on the PSB-retinal chromophore.

The synthesis of the compound **5f-Ag** was performed by adding silver triflate AgSO_3CF_3 (1 equivalent, 0.15 mmol, 40 mg) to a solution of **5f** (2 equivalents, 0.30 mmol, 72 mg) in 20 ml of dry THF under nitrogen atmosphere. The resulting mixture is stirred overnight in the dark. After this time, the reaction mixture is concentrated under reduced pressure to achieve a silver (I) complex, called **5f-Ag**, in a 95% yield. The spectroscopic data of **5f-Ag** are the following:



Empiric formula: $\text{C}_{34}\text{H}_{30}\text{AgN}_2^+$

Molecular weight: 573.15

Yield: 95%

^1H NMR (400 MHz, CDCl_3): δ (ppm) 7.55 (m, 3H), 7.40 (m, 7H), 6.83 (s, 1H), 4.34 (m, 2H), 3.19 (m, 2H).

^{13}C NMR (400 MHz, CDCl_3): δ (ppm) 179.84, 139.51, 135.60, 134.44, 133.64, 130.95, 129.37, 129.34, 129.14, 128.91, 128.14, 60.96, 30.29.

UV-VIS (THF): λ (nm) 306.

ES-MS (+) ($\text{C}_{34}\text{H}_{30}\text{AgN}_2^+$): calc. 573.1453, found 575.1465.

Observations: Brown oil

8.2.4. Synthesis of molecular switches with structure based on the green fluorescent protein (GFP) chromophore.

The synthetic reaction followed to achieve the photoswitches **7(a-s)** is shown in Figure 8.6.⁴

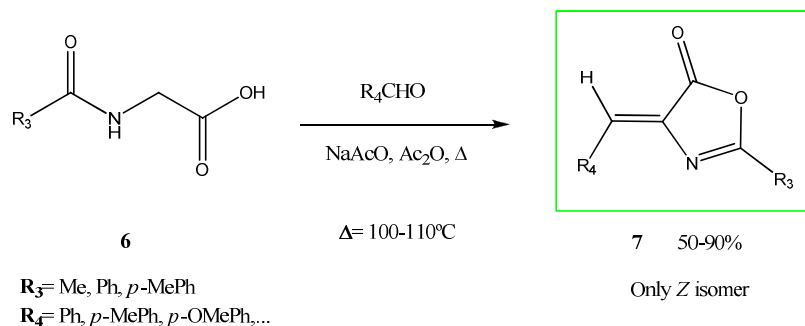


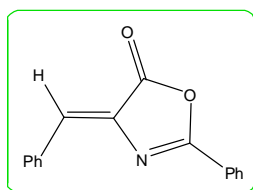
Figure 8.6. Synthetic route to achieve the GFP-based photoswitches 7.

Furthermore, the general procedure for the synthesis of azalactones **7(a-s)** is the following: to the compound **6** with the adequate substituent R_3 (1 equivalent, 20 mmol) and sodium acetate (1 equivalent, 20 mmol) in 18.4 ml of acetic anhydride, was added the corresponding aldehyde with the required R_4 group (1 equivalent, 20 mmol). The resulting mixture was stirred for 4 hours at $100-110^\circ\text{C}$. Then, the mixture was left stirring overnight at 25°C . After this time, the target azalactone precipitated, and was separated by filtration and washed with 100 ml of cold Et_2O . The resulting solid was purified by flash chromatography on silica gel (2:1 hexanes/ EtOAc) to obtain the Z isomer of (**7a-s**) in 50-90% yield.

The corresponding data for each compound (**7(a-s)**) are reported below:

⁴ Audia, J. E.; Droste, J. J.; Nissen, J. S.; Murdoch, G. L.; Evrard, D. A. *J. Org. Chem.* **1996**, *61*, 7937.

• (Z)-4-benzylidene-2-phenyloxazol-5(4H)-one (7a)



Empiric formula: C₁₆H₁₁NO₂

Molecular weight: 249.08

Yield: 85%

¹H-NMR (300 MHz, CDCl₃): δ (ppm) 8.17 (m, 4H), 7.54 (m, 6H), 7.23 (s, 1H).

¹³C-NMR (300MHz, CDCl₃): δ (ppm) 167.77, 163.63, 133.60, 133.47, 133.35, 132.58, 131.90, 131.33, 129.05, 129.02, 128.48, 125.66.

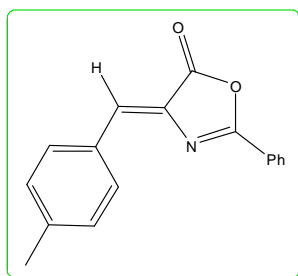
UV-VIS (CH₃CN): λ (nm) 258 (ε = 30876 M⁻¹cm⁻¹), 345 (ε = 66235 M⁻¹cm⁻¹), 360 (ε = 81673 M⁻¹cm⁻¹), 379 (ε = 57769 M⁻¹cm⁻¹).

ES-MS (+) (C₁₆H₁₁NO₂ + H): calc. 250.0863, found 250.0859.

Melting point: 157-159°C

Observations: Yellow solid

• (Z)-4-(4-methylbenzylidene)-2-phenyloxazol-5(4H)-one (7b)



Empiric formula: C₁₇H₁₃NO₂

Molecular weight: 263.09

Yield: 85%

¹H-NMR (300 MHz, CDCl₃): δ (ppm) 8.14 (d, J = 8.5 Hz, 2H), 8.07 (d, J = 8.1 Hz, 2H), 7.57 (d, J = 7.2 Hz, 1H), 7.51 (d, J = 7.7 Hz, 2H), 7.25 (d, J = 8.1 Hz, 2H), 7.18 (s, 1H), 2.39 (s, 3H).

¹³C-NMR (300MHz, CDCl₃): δ (ppm) 167.87, 163.01, 142.17, 133.83, 133.23, 132.62, 132.10, 130.95, 129.80, 128.97, 128.33, 125.75, 21.90.

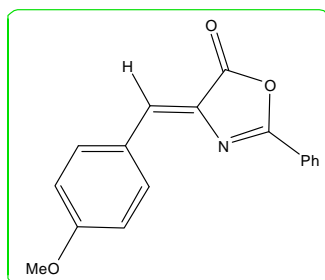
UV-VIS (CH₃CN): λ (nm) 245 (ε = 11111 M⁻¹cm⁻¹), 350 (ε = 26389 M⁻¹cm⁻¹), 367 (ε = 33333 M⁻¹cm⁻¹), 390 (ε = 25278 M⁻¹cm⁻¹).

ES-MS (+) (C₁₇H₁₃NO₂ + H): calc. 264.1019, found 264.1024.

Melting point: 128-130°C

Observations: Yellow solid

• (Z)-4-(4-methoxybenzylidene)-2-phenyloxazol-5(4H)-one (**7c**)



Empiric formula: $C_{17}H_{13}NO_3$

Molecular weight: 279.09

Yield: 60%

1H -NMR (300 MHz, $CDCl_3$): δ (ppm) 8.16 (t, $J = 7.9$ Hz, 4H), 7.53 (m, 3H), 7.19 (s, 1H), 6.98 (d, $J = 8.8$ Hz, 2H), 3.87 (s, 3H).

^{13}C -NMR (300MHz, $CDCl_3$): δ (ppm) 168.08, 162.53, 162.28, 134.70, 133.08, 131.99, 131.19, 128.99, 128.24, 126.66, 125.93, 114.61, 55.56.

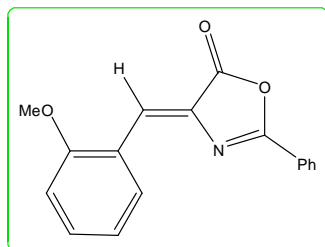
UV-VIS (CH_3CN): λ (nm) 272 ($\epsilon = 55897 M^{-1}cm^{-1}$), 381 ($\epsilon = 37436 M^{-1}cm^{-1}$), 403 ($\epsilon = 32821 M^{-1}cm^{-1}$).

ES-MS (+) ($C_{17}H_{13}NO_3 + H$): calc. 280.0968, found 280.0968.

Melting point: 138-140 $^{\circ}C$

Observations: Yellow solid

• (Z)-4-(2-methoxybenzylidene)-2-phenyloxazol-5(4H)-one (**7d**)



Empiric formula: $C_{17}H_{13}NO_3$

Molecular weight: 279.09

Yield: 87%

1H -NMR (300 MHz, $CDCl_3$): δ (ppm) 8.87 (dd, $J = 7.9, 1.7$ Hz, 1H), 8.18 (m, 2H), 7.88 (s, 1H), 7.54 (m, 3H), 7.43 (m, 1H), 7.10 (m, 1H), 6.93 (d, $J = 8.4$ Hz, 1H), 3.92 (s, 3H).

^{13}C -NMR (300MHz, $CDCl_3$): δ (ppm) 168.04, 163.17, 159.44, 133.25, 133.13, 133.07, 132.60, 129.04, 128.40, 126.12, 125.96, 122.78, 121.14, 110.91, 55.82.

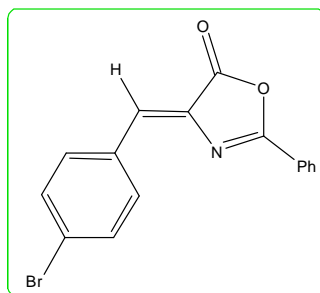
UV-VIS (CH_3CN): λ (nm) 255 ($\epsilon = 5775 M^{-1}cm^{-1}$), 385 ($\epsilon = 12394 M^{-1}cm^{-1}$), 403 ($\epsilon = 10845 M^{-1}cm^{-1}$).

ES-MS (+) ($C_{17}H_{13}NO_3 + H$): calc. 280.0968, found 280.0966.

Melting point: 246-248 $^{\circ}C$

Observations: Yellow solid

• (Z)-4-(4-bromobenzylidene)-2-phenyloxazol-5(4H)-one (**7e**)



Empiric formula: $C_{16}H_{10}NO_2Br$

Molecular weight: 326.99

Yield: 63%

1H -NMR (300 MHz, $CDCl_3$): δ (ppm) 8.19 (m, 2H), 8.08 (m, 2H), 7.58 (m, 5H), 7.17 (s, 1H)

^{13}C -NMR (300MHz, $CDCl_3$): δ (ppm) 167.52, 164.06, 133.89, 133.79, 133.73, 132.52, 132.36, 130.23, 129.15, 128.60, 126.06, 125.54.

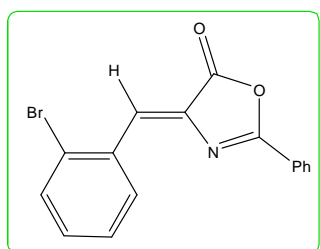
UV-VIS (CH_3CN): λ (nm) 251 ($\epsilon = 12162 M^{-1}cm^{-1}$), 347 ($\epsilon = 29730 M^{-1}cm^{-1}$), 366 ($\epsilon = 37839 M^{-1}cm^{-1}$), 386 ($\epsilon = 27027 M^{-1}cm^{-1}$).

ES-MS (+) ($C_{16}H_{10}NO_2Br + H$): calc. 327.9968, found 327.9968.

Melting point: 221-223 $^{\circ}C$

Observations: Yellow solid

• (Z)-4-(2-bromobenzylidene)-2-phenyloxazol-5(4H)-one (**7f**)



Empiric formula: $C_{16}H_{10}NO_2Br$

Molecular weight: 326.99

Yield: 85%

1H -NMR (300 MHz, $CDCl_3$): δ (ppm) 8.94 (dd, $J = 7.9, 1.4$ Hz, 1H), 8.23 (d, $J = 7.4$ Hz, 2H), 7.77 (s, 1H), 7.70 (m, 2H), 7.59 (m, 2H), 7.51 (t, $J = 7.6$ Hz, 1H), 7.34 (m, 1H).

^{13}C -NMR (300MHz, $CDCl_3$): δ (ppm) 167.30, 164.69, 134.74, 133.82, 133.65, 133.52, 133.18, 132.10, 129.35, 129.15, 128.69, 127.89, 127.55, 125.52.

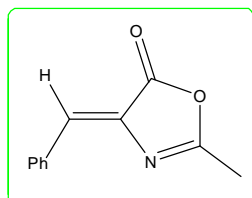
UV-VIS (CH₃CN): λ (nm) 254 ($\epsilon = 5902 \text{ M}^{-1}\text{cm}^{-1}$), 351 ($\epsilon = 9344 \text{ M}^{-1}\text{cm}^{-1}$), 366 ($\epsilon = 10492 \text{ M}^{-1}\text{cm}^{-1}$), 386 ($\epsilon = 7049 \text{ M}^{-1}\text{cm}^{-1}$).

ES-MS (+) (C₁₆H₁₀NO₂Br + H): calc. 327.9968, found 327.9965.

Melting point: 130-132^oC

Observations: Yellow solid

• **(Z)-4-benzylidene-2-methyloxazol-5(4H)-one (7h)**



Empiric formula: C₁₁H₉NO₂

Molecular weight: 187.06

Yield: 80%

¹H-NMR (300 MHz, CDCl₃): δ (ppm) 8.10 (m, 2H), 7.46 (m, 3H), 7.17 (s, 1H), 2.43 (s, 3H).

¹³C-NMR (300MHz, CDCl₃): δ (ppm) 168.02, 166.36, 133.36, 132.79, 132.41, 131.76, 131.38, 129.13, 15.93.

UV-VIS (CH₃CN): λ (nm) 231 ($\epsilon = 7035 \text{ M}^{-1}\text{cm}^{-1}$), 327 ($\epsilon = 26633 \text{ M}^{-1}\text{cm}^{-1}$).

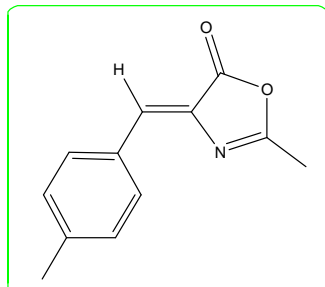
UV-VIS (CHCl₃): λ (nm) 241 ($\epsilon = 4783 \text{ M}^{-1}\text{cm}^{-1}$), 332 ($\epsilon = 28913 \text{ M}^{-1}\text{cm}^{-1}$).

ES-MS (+) (C₁₁H₉NO₂ + H): calc. 188.0708, found 188.0708.

Melting point: 144-146^oC

Observations: Yellow solid

• **(Z)-2-methyl-4-(4-methylbenzylidene)oxazol-5(4H)-one (7i)**



Empiric formula: C₁₂H₁₁NO₂

Molecular weight: 201.08

Yield: 75%

¹H-NMR (300 MHz, CDCl₃): δ (ppm) 7.97 (d, $J = 8.3 \text{ Hz}$, 2H), 7.24 (d, $J = 8.3 \text{ Hz}$, 2H), 7.12 (s, 1H), 2.40 (s, 3H), 2.39 (s, 3H).

$^{13}\text{C-NMR}$ (300MHz, CDCl_3): δ (ppm) 168.11, 165.62, 142.08, 132.34, 131.80, 131.79, 130.59, 129.79, 21.87, 15.76.

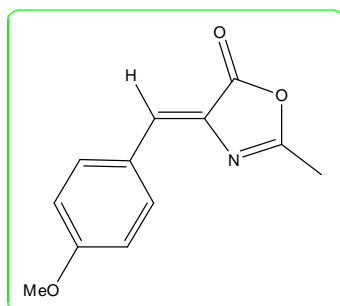
UV-VIS (CH_3CN): λ (nm) 236 ($\epsilon = 9091 \text{ M}^{-1}\text{cm}^{-1}$), 243 ($\epsilon = 9091 \text{ M}^{-1}\text{cm}^{-1}$), 336 ($\epsilon = 39091 \text{ M}^{-1}\text{cm}^{-1}$).

ES-MS (+) ($\text{C}_{12}\text{H}_{11}\text{NO}_2 + \text{H}$): calc. 202.0863, found 202.0855.

Melting point: 126-128 $^\circ\text{C}$

Observations: Yellow solid

• (Z)-4-(4-methoxybenzylidene)-2-methyloxazol-5(4H)-one (**7j**)



Empiric formula: $\text{C}_{12}\text{H}_{11}\text{NO}_3$

Molecular weight: 217.07

Yield: 50%

$^1\text{H-NMR}$ (300 MHz, CDCl_3): δ (ppm) 8.10 (d, $J = 8.9 \text{ Hz}$, 2H), 7.15 (s, 1H), 7.00 (d, $J = 8.9 \text{ Hz}$, 2H), 3.91 (s, 3H), 2.43 (s, 3H).

$^{13}\text{C-NMR}$ (300MHz, CDCl_3): δ (ppm) 168.31, 165.11, 162.24, 134.45, 131.72, 130.57, 126.32, 114.64, 55.64, 15.50.

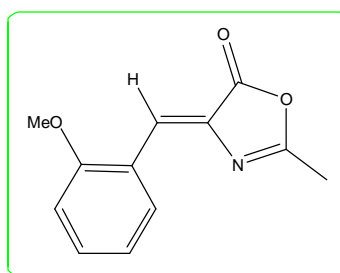
UV-VIS (CH_3CN): λ (nm) 244 ($\epsilon = 7174 \text{ M}^{-1}\text{cm}^{-1}$), 355 ($\epsilon = 28261 \text{ M}^{-1}\text{cm}^{-1}$).

ES-MS (+) ($\text{C}_{12}\text{H}_{11}\text{NO}_3 + \text{H}$): calc. 218.0812, found 218.0812.

Melting point: 106-108 $^\circ\text{C}$

Observations: Yellow solid

• (Z)-4-(2-methoxybenzylidene)-2-methyloxazol-5(4H)-one (**7k**)



Empiric formula: $\text{C}_{12}\text{H}_{11}\text{NO}_3$

Molecular weight: 217.07

Yield: 82%

¹H-NMR (300 MHz, CDCl₃): δ (ppm) 8.62 (dd, *J* = 7.9, 1.7 Hz, 1H), 7.40 (m, 1H), 7.04 (t, *J* = 7.9 Hz, 1H), 6.91 (d, *J* = 8.4 Hz, 1H), 3.89 (s, 3H), 2.40 (s, 3H).

¹³C-NMR (300MHz, CDCl₃): δ (ppm) 167.97, 165.46, 159.03, 132.80, 132.48, 131.69, 125.60, 122.11, 120.84, 110.68, 55.56, 15.62.

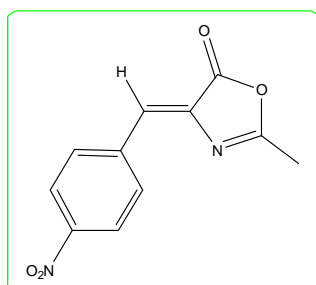
UV-VIS (CH₃CN): λ (nm) 245 (ε = 11111 M⁻¹cm⁻¹), 350 (ε = 26389 M⁻¹cm⁻¹), 367 (ε = 33333 M⁻¹cm⁻¹), 390 (ε = 25278 M⁻¹cm⁻¹).

ES-MS (+) (C₁₂H₁₁NO₃ + H): calc. 218.0812, found 218.0818.

Melting point: 147-149°C

Observations: Yellow solid

• **(*Z*)-2-methyl-4-(4-nitrobenzylidene)oxazol-5(4*H*)-one (7l)**



Empiric formula: C₁₁H₈N₂O₄

Molecular weight: 232.05

Yield: 90%

¹H-NMR (300 MHz, CDCl₃): δ (ppm) 8.27 (m, 4H), 7.14 (s, 1H), 2.46 (s, 3H).

¹³C-NMR (300MHz, CDCl₃): δ (ppm) 168.66, 167.02, 148.47, 139.10, 135.72, 132.73, 127.67, 127.65, 124.03, 16.41.

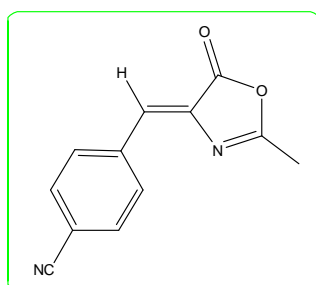
UV-VIS (CH₃CN): λ (nm) 350 (ε = 24769 M⁻¹cm⁻¹).

ES-MS (+) (C₁₁H₈N₂O₄ + H): calc. 233.0557, found 233.0556.

Melting point: 178-180°C

Observations: Yellow solid

• **(*Z*)-4-((2-methyl-5-oxooxazol-4(5*H*)-ylidene)methyl)benzonitrile (7m)**



Empiric formula: C₁₂H₈N₂O₂

Molecular weight: 212.06

Yield: 80%

¹H-NMR (300 MHz, CDCl₃): δ (ppm) 8.18 (d, *J* = 8.3 Hz, 2H), 7.71 (d, *J* = 8.3 Hz, 2H), 7.08 (s, 1H), 2.44 (s, 3H).

¹³C-NMR (300MHz, CDCl₃): δ (ppm) 168.23, 167.05, 137.30, 135.31, 132.51, 132.32, 128.24, 118.50, 113.90, 15.95.

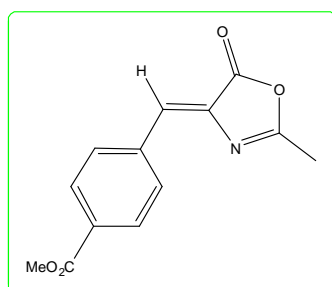
UV-VIS (CH₃CN): λ (nm) 235 (ε = 12121 M⁻¹cm⁻¹), 332 (ε = 20909 M⁻¹cm⁻¹), 351 (ε = 13636 M⁻¹cm⁻¹).

ES-MS (+) (C₁₂H₈N₂O₂ + H): calc. 213.0659, found 213.0654.

Melting point: 182-184^oC

Observations: Yellow solid

• (Z)-methyl-4-((2-methyl-5-oxooxazol-4(5H)-ylidene)methyl)benzoate (**7n**)



Empiric formula: C₁₃H₁₁NO₄

Molecular weight: 245.07

Yield: 60%

¹H-NMR (300 MHz, CDCl₃): δ (ppm) 8.07 (q, 4H), 7.07 (s, 1H), 3.93 (s, 3H), 2.41 (s, 3H).

¹³C-NMR (300MHz, CDCl₃): δ (ppm) 171.03, 167.34, 167.20, 166.25, 137.08, 134.23, 131.81, 131.50, 129.75, 129.24, 52.27, 15.64.

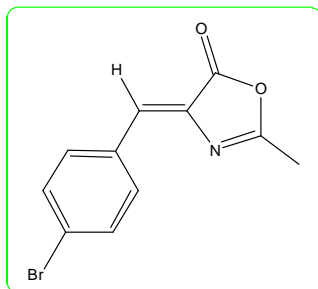
UV-VIS (CH₃CN): λ (nm) 231 (ε = 8500 M⁻¹cm⁻¹), 321 (ε = 33500 M⁻¹cm⁻¹), 334 (ε = 39000 M⁻¹cm⁻¹), 351 (ε = 26000 M⁻¹cm⁻¹).

ES-MS (+) (C₁₃H₁₁NO₄ + H): calc. 246.0761, found 246.0755.

Melting point: 221-223^oC

Observations: Yellow solid

• (Z)-4-(4-bromobenzylidene)-2-methyloxazol-5(4H)-one (**7o**)



Empiric formula: $C_{11}H_8BrNO_2$

Molecular weight: 264.97

Yield: 72%

1H -NMR (300 MHz, $CDCl_3$): δ (ppm) 7.91 (d, $J = 8.6$ Hz, 2H), 7.54 (d, $J = 8.6$ Hz, 2H), 7.01 (s, 1H), 2.39 (s, 3H).

^{13}C -NMR (300MHz, $CDCl_3$): δ (ppm) 167.50, 166.61, 133.45, 133.07, 132.14, 132.01, 129.72, 125.82, 15.76.

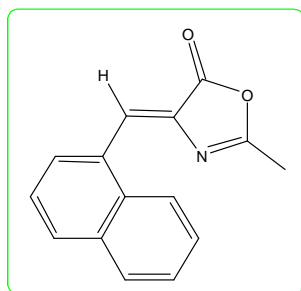
UV-VIS (CH_3CN): λ (nm) 227 ($\epsilon = 7457 M^{-1}cm^{-1}$), 234 ($\epsilon = 7119 M^{-1}cm^{-1}$), 243 ($\epsilon = 6101 M^{-1}cm^{-1}$), 333 ($\epsilon = 24407 M^{-1}cm^{-1}$), 348 ($\epsilon = 17966 M^{-1}cm^{-1}$).

ES-MS (+) ($C_{11}H_8BrNO_2 + H$): calc. 265.9813, found 265.9813.

Melting point: 151-153 $^{\circ}C$

Observations: Yellow solid

• (Z)-2-methyl-4-(naphthalen-1-ylmethylene)oxazol-5(4H)-one (**7p**)



Empiric formula: $C_{15}H_{11}NO_2$

Molecular weight: 237.08

Yield: 61%

1H -NMR (300 MHz, $CDCl_3$): δ (ppm) 8.33 (m, 2H), 7.85 (m, 3H), 7.52 (m, 2H), 7.26 (s, 1H), 2.41 (s, 3H).

^{13}C -NMR (300MHz, $CDCl_3$): δ (ppm) 167.99, 165.99, 134.44, 133.86, 133.18, 132.69, 131.62, 130.97, 129.17, 128.68, 128.15, 127.86, 127.69, 126.76, 15.63.

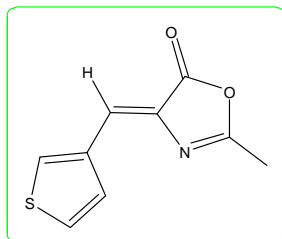
UV-VIS (CH_3CN): λ (nm) 278 ($\epsilon = 13333 M^{-1}cm^{-1}$), 289 ($\epsilon = 15490 M^{-1}cm^{-1}$), 342 ($\epsilon = 25490 M^{-1}cm^{-1}$).

ES-MS (+) ($C_{15}H_{11}NO_2 + H$): calc. 238.0863, found 238.0861.

Melting point: 128-130°C

Observations: Yellow solid

• (Z)-2-methyl-4-(thiophen-1-ylmethylene)oxazol-5(4H)-one (**7q**)



Empiric formula: C₉H₇NO₂S

Molecular weight: 193.02

Yield: 74%

¹H-NMR (300 MHz, CDCl₃): δ (ppm) 7.67 (m, 1H), 7.55 (m, 1H), 7.37 (m, 1H), 7.13 (m, 1H), 2.41 (s, 3H).

¹³C-NMR (300MHz, CDCl₃): δ (ppm) 167.39, 165.19, 137.10, 135.36, 134.63, 130.18, 127.99, 124.62, 15.81.

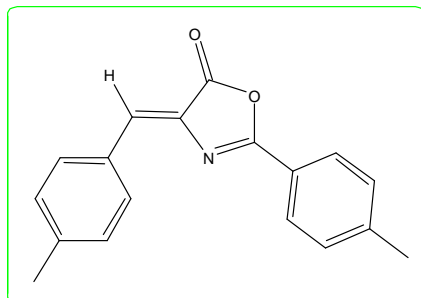
UV-VIS (CH₃CN): λ (nm) 232 (ε = 2780 M⁻¹cm⁻¹), 291 (ε = 4615 M⁻¹cm⁻¹), 358 (ε = 20679 M⁻¹cm⁻¹).

ES-MS (+) (C₉H₇NO₂S + H): calc. 194.0270, found 194.0277.

Melting point: 124-126°C

Observations: Pale yellow solid

• (Z)-4-(4-methylbenzylidene)-2-p-tolyloxazol-5(4H)-one (**7s**)



Empiric formula: C₁₈H₁₅NO₂

Molecular weight: 277.11

Yield: 52%

¹H-NMR (300 MHz, CDCl₃): δ (ppm) 8.09 (m, 4H), 7.31 (m, 4H), 7.21 (s, 1H), 2.46 (s, 3H), 2.43 (s, 3H).

¹³C-NMR (300MHz, CDCl₃): δ (ppm) 168.09, 163.27, 144.33, 142.06, 132.72, 132.58, 131.54, 131.11, 129.85, 128.45, 123.03, 22.06, 21.85.

UV-VIS (CH₃CN): λ (nm) 270 ($\epsilon = 14091 \text{ M}^{-1}\text{cm}^{-1}$), 355 ($\epsilon = 28636 \text{ M}^{-1}\text{cm}^{-1}$), 370 ($\epsilon = 37273 \text{ M}^{-1}\text{cm}^{-1}$), 390 ($\epsilon = 29091 \text{ M}^{-1}\text{cm}^{-1}$).

ES-MS (+) (C₁₈H₁₅NO₂ + H): calc. 278.1176, found 278.1168.

Melting point: 173-175^oC

Observations: Yellow solid

8.2.4. Stability of the GFP-based photoswitches in different solvents.

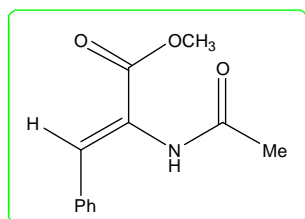
40 mg of compound **7h** were dissolved in several flasks in different solvents:

- o 10 ml dichloromethane
- o 10 ml acetonitrile
- o 10 ml methanol
- o 10 ml aqueous sodium hydroxide (1M)

All the solutions were stirred at room temperature for 2 weeks and the reaction was followed by TLC, using hexane /ethyl acetate (1:1) as eluent.

After that time, the solvent of each reaction mixture was concentrated under reduced pressure. The resulting solid for each case was analyzed by ¹H NMR. In the flasks with CH₂Cl₂ and CH₃CN, **7h** was recovered unchanged. In the case of the aqueous NaOH solution, hydrolysis of **7h** to give the acetaminoacid **8** took place. On the other hand, when having MeOH as solvent, it reacted with compound **7h** to give the acetamidoacetate **9**, whose spectroscopic data are the following:

• (Z)-methyl 2-acetamido-3-phenylacrylate (**9**)



Empiric formula: C₁₂H₁₃NO₃

Molecular weight: 219.09

Yield: 70%

¹H-NMR (400 MHz, CD₃OD): δ (ppm) 7.57 (d, $J = 6.7 \text{ Hz}$, 2H), 7.41 (d, $J = 4.7\text{Hz}$, 2H), 7.37 (m, 3H), 3.80 (s, 3H), 2.10 (s, 3H).

¹³C-NMR (300MHz, CD₃OD): δ (ppm) 173.25, 167.15, 135.14, 134.77, 130.90, 130.72, 129.72, 126.29, 52.95, 22.46.

ES-MS (+) (C₁₂H₁₃NO₃ + Na): calc. 242.0788, found 242.0796.

Observations: White solid

8.3. PHOTOCHEMICAL STUDY.

8.3.1. Irradiation of neutral and methylated photoswitches with structure based on the PSB-retinal chromophore.

- Irradiation of the neutral and methylated photoswitches with structure based on the PSB-retinal chromophore until the PSS.

In all cases, a 125-W medium-pressure Hg lamp was used for irradiating the photoswitches with structure based on the PSB-retinal chromophore.

Moreover, several types of irradiation conditions were used:

- Type A: A 0.1M solution of the compound in CDCl₃, directly in a Pyrex NMR tube, with a Pyrex filter. These conditions were used whenever the amount of compound available wasn't enough for irradiating in an immersion reactor.
- Type B: A 0.01 M solution in CH₃CN, in an immersion well reactor, with a Pyrex filter. These are the standard conditions for performing the irradiation.
- Type C: a 0.1 M solution in CDCl₃, directly in a Quartz NMR tube, with a Quartz filter. It was only used for the irradiation of **5e**.

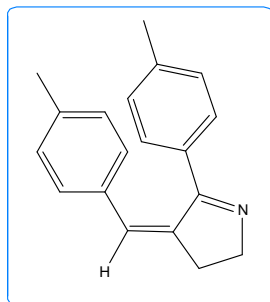
The irradiation process of each compound was followed by ¹H NMR, at different time intervals, until the photostationary state (PSS) was reached, since *E* and *Z* isomers have distinctive ¹H NMR signals. Integration of the ¹H NMR signals corresponding to each isomer allowed us to know the isomers ratio at a given irradiation time.

- Separation of the less thermodynamically stable isomer (*Z*) of the PSB-retinal based photoswitches.

A 0.01 M solution of the compound **5o** or **5k** (100% *E* isomer at t=0 min) in acetonitrile was irradiated in an immersion well reactor with a 125-W medium-pressure Hg lamp, and a Pyrex filter, until the PSS was reached. The reaction was followed by ¹H NMR. Later, the resulting mixture of isomers was separated by flash

chromatography on silica gel, using hexane/ ethyl acetate (1:2) as eluent. The corresponding data for the *Z* isomers of compounds **5o** and **5k** are the following:

(*Z*)-4-(4-methylbenzylidene)-5-*p*-tolyl-3,4-dihydro-2*H*-pyrrole (Z-5o**)**



Empiric formula: C₁₉H₁₉N

Molecular weight: 261.15

Yield: 15%

¹H-NMR (400 MHz, CDCl₃): δ (ppm) 7.13 (d, *J* = 8.0 Hz, 2H), 6.92 (s, 1H), 6.84 (d, *J* = 7.8 Hz, 2H), 6.72 (q, *J* = 8.2 Hz, 4H), 4.07 (m, 2H), 2.96 (m, 2H), 2.24 (s, 3H), 2.19 (s, 3H).

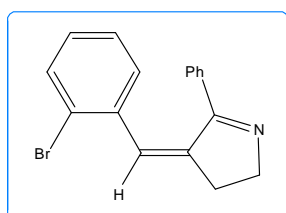
¹³C-NMR (400 MHz, CDCl₃): δ (ppm) 172.94, 140.04, 138.80, 136.58, 133.29, 132.68, 129.31, 128.29, 128.25, 127.95, 126.17, 57.71, 35.88, 21.44, 21.23.

UV-VIS (CH₃CN): λ (nm) 260 (ε = 14600 M⁻¹cm⁻¹), 295 (ε = 13400 M⁻¹cm⁻¹).

ES-MS (+) (C₁₉H₁₉N + H): calc. 262.1590, found 262.1598.

Observations: Orange solid

• **(*Z*)-4-(2-bromobenzylidene)-5-phenyl-3,4-dihydro-2*H*-pyrrole (**Z-5k**)**



Empiric formula: C₁₇H₁₄BrN

Molecular weight: 311.03

Yield: 10%

¹H-NMR (300 MHz, CDCl₃): δ (ppm) 7.40 (dd, *J* = 8.0, 0.9 Hz, 1H), 7.14 (m, 2H), 7.08 (m, 1H), 6.98 (m, 2H), 6.90 (s, 1H), 6.83 (td, *J* = 8.0, 1.8 Hz, 1H), 6.57 (m, 2H), 4.14 (m, 2H), 3.03 (m, 2H).

¹³C-NMR (300MHz, CDCl₃): δ (ppm) 172.86, 142.13, 136.80, 135.39, 132.41, 131.79, 128.99, 128.67, 128.15, 127.67, 126.14, 125.72, 123.15, 58.25, 34.83.

ES-MS (+) (C₁₇H₁₄BrN + H): calc. 312.0382, found 312.0388.

Observations: White solid

- Determination of relative kinetic constants.

Once separated the two isomers (*E* and *Z*) of compound **5o**, the simultaneous irradiation of both isomers was carried out.

In two distinctive Pyrex NMR tubes, two solutions of the same concentration in CDCl₃ were prepared: the first one corresponding to a solution 0.07 M of the *E* isomer of compound **5o**, and the second one being a solution 0.07 M of the *Z* isomer of compound **5o**. Both NMR tubes were irradiated in a 125-W medium-pressure Hg lamp and a Pyrex filter, until both solutions reached the PSS. The photoisomerization reaction was followed by ¹H NMR at short irradiation intervals. For each given time, the isomers ratio was calculated from the relationship between the ¹H NMR signals corresponding to each isomer. From the first four values of isomers ratio obtained for each sample, the kinetic constant of each process was calculated by representing $\ln [A_0] / [A]$ vs irradiation time and doing a linear fit. Then, the value of the relative kinetic constant that relates the speed of both processes could be determined as well. Data processing was performed using the OriginPro 8 program.

8.3.2. Irradiation of photoswitches switches with structure based on the GFP chromophore.

- Irradiation of photoswitches with structure based on the GFP chromophore until the PSS.

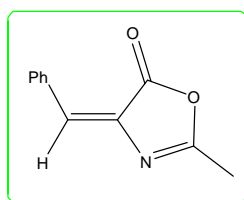
In the first place, 0.01 M solutions of different photoswitches in acetonitrile were prepared and irradiated in an immersion well reactor using a 125-W medium-pressure Hg lamp until the PSS was reached. The reaction was followed by ¹H NMR.

Afterwards, the irradiation process of several compounds was carried out again using a light source with emission wavelength centred at 350 nm in order to compare the two irradiation methods. For this aim, 0.01 M solutions of the selected photoswitches with structure based on the GFP chromophore in acetonitrile were prepared. Then, they were placed in Pyrex test tubes in a merry-go-round appliance in a photoreactor, and were irradiated using lamps with emission wavelength centred at 350 nm (14 lamps x 8-W/lamp) until the PSS was reached.

- Separation of the less thermodynamically stable isomer (*E*) of the GFP based photoswitches.

• Firstly, a 0.01 M solution of compound **7h** or **7k** (100% *Z* isomer at $t=0$ min) in acetonitrile was irradiated in an immersion well reactor with a 125-W medium-pressure Hg lamp, and a Pyrex filter, until the PSS was reached. The reaction was followed by ^1H NMR. Afterwards, the resulting mixture of isomers was separated by flash chromatography on silica gel, using hexane/ ethyl acetate (10:1) as eluent. The corresponding data for the *E* isomers of compounds **7h** and **7k** are the following:

- (*E*)-4-benzylidene-2-methyloxazol-5(4*H*)-one (**E-7h**)



Empiric formula: $\text{C}_{11}\text{H}_9\text{NO}_2$

Molecular weight: 187.06

Yield: 25%

$^1\text{H-NMR}$ (300 MHz, CDCl_3): δ (ppm) 8.092 (m, 2H), 7.456 (m, 3H), 7.409 (s, 1H), 2.342 (s, 3H).

$^{13}\text{C-NMR}$ (300MHz, CDCl_3): δ (ppm) 165.002, 163.871, 139.799, 133.634, 132.506, 131.925, 131.721, 128.918, 15.518.

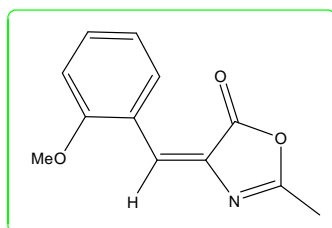
UV-VIS (CH_3CN): λ (nm) 330 ($\epsilon = 15191 \text{ M}^{-1}\text{cm}^{-1}$).

ES-MS (+) ($\text{C}_{11}\text{H}_9\text{NO}_2 + \text{H}$): calc. 188.0708, found 188.0708.

Melting point: 142-144 $^\circ\text{C}$

Observations: Yellow solid

- (*E*)-4-(2-methoxybenzylidene)-2-methyloxazol-5(4*H*)-one (**E-7k**)



Empiric formula: $\text{C}_{12}\text{H}_{11}\text{NO}_3$

Molecular weight: 217.07

Yield: 82%

$^1\text{H-NMR}$ (300 MHz, CDCl_3): δ (ppm) 8.42 (dd, $J = 7.9, 1.7$ Hz, 1H), 7.89 (s, 1H), 7.43 (m, 1H), 7.02 (m, 1H), 6.91 (dd, $J = 8.4, 0.8$ Hz, 1H), 3.88 (s, 3H), 2.32 (s, 3H).

$^{13}\text{C-NMR}$ (300MHz, CDCl_3): δ (ppm) 165.23, 163.28, 158.79, 134.21, 133.42, 132.87, 131.40, 121.29, 120.43, 110.67, 55.84, 15.42.

UV-VIS (CH_3CN): λ (nm) 241 ($\epsilon = 6300 \text{ M}^{-1}\text{cm}^{-1}$), 311 ($\epsilon = 11000 \text{ M}^{-1}\text{cm}^{-1}$), 326 ($\epsilon = 12400 \text{ M}^{-1}\text{cm}^{-1}$), 361 ($\epsilon = 17000 \text{ M}^{-1}\text{cm}^{-1}$).

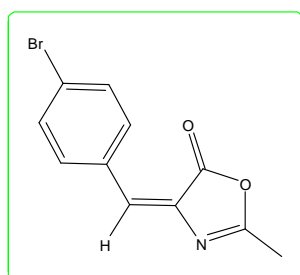
ES-MS (+) ($\text{C}_{12}\text{H}_{11}\text{NO}_3 + \text{H}$): calc. 218.0812, found 218.0818.

Melting point: 145-147 $^\circ\text{C}$

Observations: Yellow solid

On the other hand, a 0.01 M solution of compound **7o** (100% *Z* isomer at $t=0$ min) in acetonitrile was irradiated in a photoreactor using lamps with emission wavelength centred at 350 nm (14 lamps x 8-W/lamp) until the PSS was reached. The reaction was followed by ^1H NMR. Afterwards, the resulting mixture of isomers was separated by flash chromatography on silica gel, using hexane/ ethyl acetate (10:1) as eluent. The corresponding data for the *E* isomer of compound **7o** are the following:

• (*E*)-4-(4-bromobenzylidene)-2-methyloxazol-5(4*H*)-one (**E-7o**)



Empiric formula: $\text{C}_{11}\text{H}_8\text{BrNO}_2$

Molecular weight: 264.97

Yield: 15%

$^1\text{H-NMR}$ (300 MHz, CDCl_3): δ (ppm) 7.96 (d, $J = 8.4$ Hz, 2H), 7.57 (d, $J = 8.5$ Hz, 2H), 7.31 (s, 1H), 2.34 (s, 3H).

$^{13}\text{C-NMR}$ (300MHz, CDCl_3): δ (ppm) 164.88, 164.20, 138.08, 134.08, 133.18, 132.13, 131.26, 126.30, 15.47.

UV-VIS (CH_3CN): λ (nm) 237 ($\epsilon = 10851 \text{ M}^{-1}\text{cm}^{-1}$), 336 ($\epsilon = 23404 \text{ M}^{-1}\text{cm}^{-1}$).

ES-MS (+) ($\text{C}_{11}\text{H}_8\text{BrNO}_2 + \text{H}$): calc. 265.9813, found 265.9813.

Observations: Pale yellow solid

- Determination of relative kinetic constants.

Once separated the two isomers (*Z* and *E*) of the compounds **7h**, **7k** and **7o**, the simultaneous irradiation of both isomers was performed.

For this purpose, two solutions of the same concentration in CDCl₃ were prepared in two different Pyrex NMR tubes: the first one corresponding to a solution 0.07 M of the *Z* isomer of the compound **7h**, **7k** or **7o**, and the second one being a solution 0.07 M of the *E* isomer of compound **7h**, **7k** or **7o**.

In the case of the compound **7h** or **7k**, both NMR tubes were irradiated in a 125-W medium-pressure Hg lamp and a Pyrex filter, until both solutions reached the PSS. On the other hand, in the case of compound **7o**, both NMR tubes were irradiated in a photoreactor using lamps with emission wavelength centred at 350 nm (14 lamps x 8-W/lamp) until both solutions reached the PSS. In all cases, the photoisomerization reaction was followed by ¹H NMR at short irradiation intervals. For each given time, the isomers ratio was calculated from the relationship between the ¹H NMR signals corresponding to each isomer. From the first four values of isomers ratio obtained for each sample, the kinetic constant of each process could be determined by representing ln [A₀] / [A] vs irradiation time and doing a linear fit. Then, the value of the relative kinetic constant that relates the speed of both processes could be also calculated. Data processing was done using the OriginPro 8 program.

- Selective irradiation of the two isomers (*Z* and *E*) of **7h**.

The two isomers (*Z* and *E*) of compound **7h** were irradiated separately with monochromatic light at different irradiation wavelengths: at the beginning (260 nm), maximum (330 nm) and the end of the absorption band (370 nm). The intensity of the monochromatic light in all cases was the same, being all the experiments carried out under the same conditions.

For this aim, 1.08 x 10⁻⁴M solutions of each isomer in dry acetonitrile were prepared. 3 ml of the abovementioned solutions were irradiated at the selected wavelengths in a quartz cuvette (1.0 cm path length) using a monochromator until the PSS was reached (except in the case of irradiation at 260 nm). The reaction was followed by ¹H NMR. The work up prior to recording the NMR spectra required the

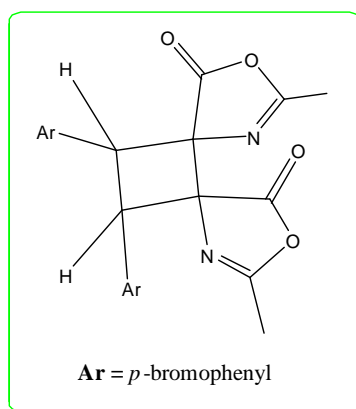
concentration of the solvent (acetonitrile) under reduced pressure, being the sample later redissolved in CDCl_3 .

Data processing was carried out using the OriginPro 8 program.

- Irradiation in solid state of **7o**.

For irradiating in solid state, 200 mg of **7o** were placed in a glass plate. Then, the sample was irradiated in a photoreactor (14 lamps x 8-W/lamp) with emission wavelength centred at 350 nm. The reaction was followed by ^1H NMR until it was over. Afterwards, the resulting solid was purified by chromatography on silica gel, using hexane/ ethyl acetate (1:1) as eluent. The spectroscopic data of compound **11** are the following:

- [2+2] cycloadduct of **7o** (**11**):



Empiric formula: $\text{C}_{22}\text{H}_{16}\text{Br}_2\text{N}_2\text{O}_4$

Molecular weight: 529.95

Yield: 15%

^1H -NMR (300 MHz, CDCl_3): δ (ppm) 7.46 (dd, $J = 18.5, 8.6$ Hz, 4H), 4.58 (s, 1H), 2.21 (s, 3).

^{13}C -NMR (300MHz, CDCl_3): δ (ppm) 175.96, 163.83, 132.25, 131.68, 130.50, 123.29, 71.89, 55.45, 15.56.

ES-MS (+) ($\text{C}_{22}\text{H}_{16}\text{Br}_2\text{N}_2\text{O}_4 + \text{H}$): calc. 530.9550, found 532.9535.

Observations: White solid

8.3.3. Photochemical aspects of the mechanism of the isomerization reaction.

- Excited state multiplicity

In order to determine the excited state multiplicity of the reactive state of both families of photoswitches, the simultaneous irradiation of three samples of the same switch that were under different reaction conditions was performed.

For this purpose, 0.05 M solutions of compound **5f** or **7j** in CDCl₃ were prepared and placed in three different Pyrex NMR tubes. The first sample was deoxygenated and used as reference. The second sample was saturated with O₂ (triplet quencher) by bubbling air for 15 minutes. Finally, to the third sample, once deoxygenated, 5 equivalents of *cis*-piperilene (triplet quencher) were added. The three samples were irradiated simultaneously for 15-20 minutes in a 125-W medium-pressure Hg lamp. After irradiating, the ¹H NMR spectra of the samples were recorded and from these data, the value of the isomers for each sample was calculated.

- Isomerization quantum yield

The isomerization quantum yield of different PSB-retinal based photoswitches (**5h**, **5l** and **5p**), and the two isomers (*Z* and *E*) of the GFP-based photoswitch **7h**, was calculated following the procedure described in the literature, using *trans*-azobenzene as actinometer.⁵

In the first place, a solution of *trans*-azobenzene in methanol was prepared in such way that the value of the absorbance at 358 nm was close to one.⁶ Then, after placing the actinometer solution in a quartz cuvette, the solution was irradiated at 334 (in the case of **5h**, **5l** and **7h**) or 313 nm (in the case of **5p**) using a monochromator. Each irradiation period should cause a change in absorbance at 358 nm of about 0.02.

⁵ Kuhn, H. J.; Braslavsky, S. E.; Schmidt, R. *Pure Appl. Chem.* **2004**, *76*, 2105.

⁶ The values of the *trans*-azobenzene quantum yield are measured and tabulated so that the value of the absorbance at 358 nm is close to one. Distant values entail a relevant experimental error.

Afterwards, a solution in acetonitrile of the corresponding switch was prepared by adjusting the value of the absorbance at 334/313 nm to the one showed by the actinometer. These solutions were irradiated at 334/313 nm for a period of time that was fixed after several runs. The conversion obtained after the irradiation time selected is recommended to be around 20%.

Three aliquots of each sample were irradiated for exactly the same amount of time because the concentration of the sample wasn't enough for recording the ^1H NMR spectra. This was taken into account when doing the final calculations.

The number of photons absorbed by the sample was calculated by using the following formula:

$$E_p \text{ (mol of photons x cm}^{-2} \text{ x s}^{-1}\text{)} = F(\lambda) \text{ x } \Delta A(358\text{nm}) / t(\text{s})$$

where $\Delta A(358\text{nm})$ is the change in the absorbance at 358 nm of the *trans*-azobenzene solution when irradiating at 334/313 nm, and $t(\text{s})$ is the irradiation time responsible for that change. The F factor, which depends on the wavelength, has a value of 3.60×10^{-6} einstein $\times \text{cm}^{-2}$ at 334 nm, and of 5.30×10^{-6} einstein $\times \text{cm}^{-2}$ at 313 nm.

Then, the number of photons absorbed corresponds to E_p multiplied by the irradiation time of the sample (in seconds).

To calculate the number of moles of the less thermodynamically stable isomer formed after irradiating the samples, the solvent of the samples was removed and the residue dried properly. This value was quantified by ^1H NMR, using 1,3,5-trimethoxybenzene as internal standard, as the proton signals of this standard didn't overlap with the signals of the isomers of the samples. From the integration of the signals it was possible to know the number of moles of the less thermodynamically stable isomer formed.

Finally, the value for the isomerization quantum yield was the result of the following equation:

$$\Phi = \frac{\text{number of formed or destroyed molecules}}{\text{number of photons absorbed by the system}}$$

At the end of the experiment the actinometer solution was measured again to prove that the light intensity had been constant. All the solutions were kept in the dark when they weren't irradiated.

- Luminescence

The luminescence properties of a few compounds with structures based on the PSB-retinal and the GFP chromophore were studied: **5f**, **5k**, **5f-Ag**, **5p**, the two isomers (*Z* and *E*) of **7h** and **7o**.

In the first place, a *ca.* 10⁻⁵M solution of each switch in deoxygenated acetonitrile (except in the case of **5f-Ag**, where deoxygenated THF was used instead) was prepared. The excitation and emission spectra were recorded using a spectrofluorimeter. For measuring the fluorescence lifetime, a LED light source with the appropriate emission wavelength was used.

Finally, the fluorescence quantum yield was calculated using a solution of *trans*-stilbene in deoxygenated hexane as standard of fluorescence. Afterwards, a solution of the corresponding photoswitch in deoxygenated acetonitrile was prepared and the emission spectra for both compounds were measured using an excitation wavelength of 290 nm in a spectrofluorimeter. Data processing was performed using the OriginPro 8 program.

- Sensitization tests

For irradiation under sensitized conditions, several photoswitches with structures based on the PSB-retinal and the GFP chromophore were selected: **5f**, **5h**, **5l**, **7h**, **7j** and **7l**, as they present no relevant absorptions at wavelengths higher than 370 nm.

In all cases, thioxanthone was used as triplet sensitizer. On the other hand, the light filter chosen for cutting the emission of light at wavelengths below 370

nm was composed of a 0.4 M solution of sodium metavanadate (NaVO_3) in 5% NaOH. This solution was placed in an immersion well reactor.

Then, in three Pyrex NMR tubes, 0.1 M solutions of each compound in CDCl_3 were prepared, and 1 equivalent of thioxanthone was added to each sample. The three samples were placed outside of the immersion well reactor and were later irradiated with a 125-W medium pressure Hg lamp until the PSS was reached. The reactions were followed by ^1H NMR.

8.4. APPLICATIONS OF PHOTOSWITCHES WITH STRUCTURE BASED ON THE PSB-RETINAL CHROMOPHORE.

8.4.1. Synthesis of the appropriate PSB-retinal based photoswitches for the linkage to more complex biomolecules.

The synthetic scheme followed to obtain the photoswitches **5p** and **5r** is represented in the following figure:

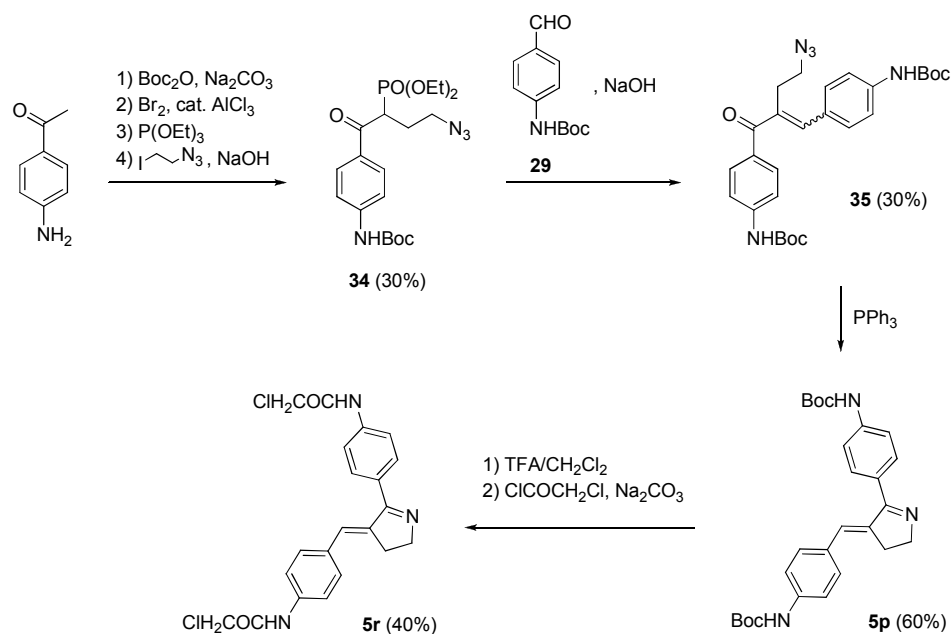


Figure 8.7

- Synthesis of *t*-butyl 4-(4-azido-2-(diethoxyphosphino)butanoyl) phenylcarbamate (**34**):

In the first place, 4'-aminoacetophenone was Boc-protected using di-*tert*-butyl dicarbonate in the presence of sodium carbonate as described.⁷

The resulting product (**31**) was brominated with Br₂ in THF containing a catalytic amount of AlCl₃⁸ to afford *t*-butyl 4-(2-bromoacetyl) phenylcarbamate (**32**).

This (**32**) was treated with triethyl phosphite at 160°C for 3 hours⁹ to give *t*-butyl 4-(2-(diethoxyphosphino)acetyl) phenylcarbamate (**33**).

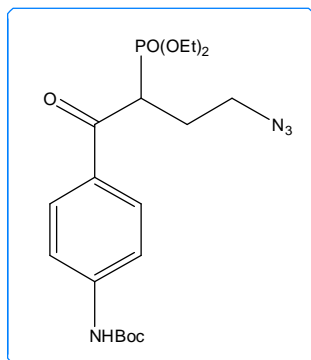
To a mixture of the phosphonate **33** (1.12 g, 3 mmol) and 2-iodoethylazide (1.50 g, 7.6 mmol) in CH₂Cl₂ (5 mL) was added a solution of tetrabutylammonium hydrogen sulfate (1 g, 3 mmol) in sodium hydroxide 2M (3.3 mL, 6 mmol), and the resulting mixture was refluxed for 36 hours.¹⁰ The mixture was cooled and combined with water (50 mL) and CH₂Cl₂ (50 mL). The organic layer was separated and concentrated under reduced pressure. The resulting residue was dissolved in Et₂O (100 mL) to precipitate tetrabutylammonium iodide. The salt was filtered off, and the filtrate was dried (Na₂SO₄) and concentrated under reduced pressure to give a colorless oil. The resulting product was purified by flash chromatography on silica gel (1:1 hexanes/EtOAc) to afford (**34**) in 30% yield as a colorless oil.

⁷ Tarbell, D. S.; Yamamoto, Y.; Pope, B. M. *Proc. Natl. Acad. Sci. USA*, **1972**, *69*, 730.

⁸ Goslinski, T.; Golankiewicz, B.; De Clercq, E.; Balzarini, J. *J. Med. Chem.* **2002**, *45*, 5052.

⁹ Nagata, W.; wakabayashi, T.; Hayase, Y. *Organic Synthesis* **1973**, *53*, 44; **1988**, *Coll. Vol. 6*, 448.

¹⁰ Snider, B. B.; Zhou, J. *J. Org. Chem.* **2005**, *70*, 1087.



Empiric formula: C₁₉H₃₀N₄O₆P

Molecular weight: 440.19

Yield: 30%

¹H NMR (300MHz, CDCl₃): δ (ppm) 7.98 (d, *J* = 8.8 Hz, 2H), 7.48 (d, *J* = 8.8 Hz, 2H), 6.71 (s, 1H), 4.09 (m, 4H), 3.45 (m, 1H), 3.23 (m, 1H), 2.50 (m, 1H), 2.20 (m, 1H), 1.53 (s, 9H), 1.24 (m, 6H).

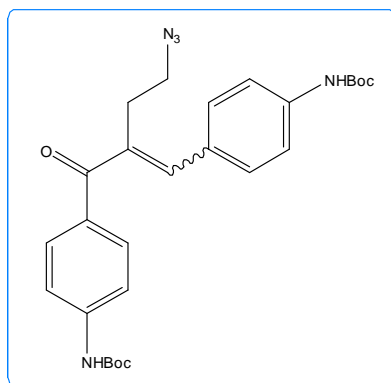
¹³C NMR (300MHz, CDCl₃): δ (ppm) 193.68 (d, *J* = 10 Hz), 152.54, 144.18, 134.61, 130.53, 117.49, 81.37, 63.78 (d, *J* = 5.7 Hz), 63.04 (d, *J* = 5.8 Hz), 49.6 (d, *J* = 26.5 Hz), 43.76 (d, *J* = 129.2 Hz), 28.36 (d, *J* = 5.2 Hz), 27.15 (d, *J* = 3.7 Hz), 16.28 (d, *J* = 5.6 Hz).

ES-MS (+) (C₁₉H₃₀N₄O₆P + H): calc. 441.1897, found 441.1893.

Observations: Colourless oil

- Preparation of (*E*)-2-(4-aminobenzylidene)-1-(4-aminophenyl)-4-azidobutan-1-one protected with Boc (**35**):

To the phosphonate **34** (0.3 g, 0.7 mmol) and *t*-butyl 4-formylphenylcarbamate (0.24 g, 1 mmol) in THF was added a solution of tetrabutylammonium hydrogen sulfate (40 mg, 0.1 mmol) in 2M sodium hydroxide (0.5 mL, 1 mmol), and the resulting mixture was stirred for 3 weeks at room temperature. The reaction was followed by TLC (3:1 hexanes/EtOAc) until the phosphonate **34** was totally consumed. Then, the solvent was removed and water (50 mL) was added before extracting with CH₂Cl₂ (3 x 50 mL). The organic layers were combined, dried (Na₂SO₄), and concentrated under reduced pressure. The residual oil was purified by chromatography on silica gel (3:1 hexanes/EtOAc) to give 100 mg (30%) of **35** as a yellowish oil.



Empiric formula: $C_{27}H_{33}N_5O_5$

Molecular weight: 507.24

Yield: 30%

$^1\text{H NMR}$ (300MHz, CDCl_3): δ (ppm) 7.76 (d, J = 8.6 Hz, 2H), 7.43 (m, 6H), 7.18 (s, 1H), 6.70 (s, 1H), 6.60 (s, 1H), 3.54 (t, J = 6.9 Hz, 2H), 3.04 (m, 2H), 1.53 (s, 18H).

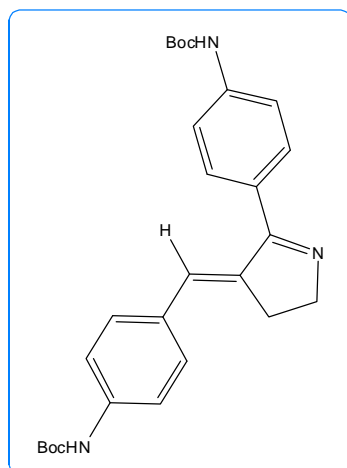
$^{13}\text{C NMR}$ (300MHz, CDCl_3): δ (ppm) 197.63, 152.55, 152.38, 143.31, 142.24, 139.25, 136.54, 132.70, 131.37, 130.42, 129.66, 118.34, 117.56, 81.41, 81.15, 50.06, 29.84, 28.41, 22.84.

ES-MS (+) ($C_{27}H_{33}N_5O_5 + \text{Na}$): calc. 530.2374, found 530.2376.

Observations: Yellowish oil

- Synthesis of (*E*)-4-(4-(4-aminobenzylidene)-3,4-dihydro-2*H*-pyrrol-5-yl)aniline protected with Boc (**5p**):

To a dry diethyl ether solution (20 mL) of (**35**) (0.45 g, 0.9 mmol) was added Ph_3P (0.7 g, 2.7 mmol).⁴ The resulting mixture was stirred for 24 h under nitrogen at room temperature and concentrated under reduced pressure. The resulting solid was purified by chromatography on silica gel (1:4 hexanes/EtOAc) to obtain 244 mg (60%) of (**5p**) as a yellow solid.



Empiric formula: $C_{27}H_{33}N_3O_4$

Molecular weight: 463.26

Yield: 60%

1H NMR (300MHz, $CDCl_3$): δ (ppm) 7.59 (d, $J = 8.6$ Hz, 2H), 7.45 (d, $J = 8.5$ Hz, 2H), 7.37 (q, $J = 8.9$ Hz, 4H), 6.78 (s, 1H), 6.69 (s, 1H), 6.61 (s, 1H), 4.18 (m, 2H), 3.03 (m, 2H), 1.54 (s, 9H), 1.52 (s, 9H).

^{13}C NMR (300MHz, $CDCl_3$): δ (ppm) 174.36, 152.58, 152.50, 140.71, 139.59, 137.99, 131.78, 129.69, 129.61, 129.05, 127.18, 118.22, 118.11, 80.79, 59.34, 30.94, 28.31.

UV-VIS (CH_3CN): λ (nm) 239 ($\epsilon = 13002 M^{-1}cm^{-1}$), 273 ($\epsilon = 18440 M^{-1}cm^{-1}$), 311 ($\epsilon = 26005 M^{-1}cm^{-1}$).

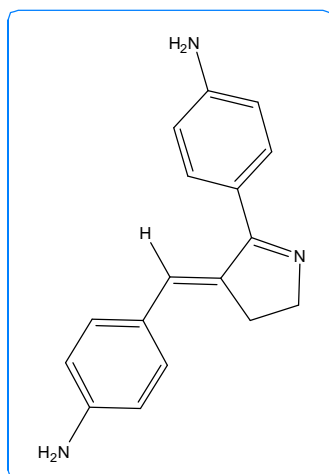
ES-MS (+) ($C_{27}H_{33}N_3O_4 + H$): calc. 464.2544, found 464.2553.

Observations: Yellow solid

- Preparation of (*E*)-2-chloro-*N*-(4-(4-(4-(2-chloroacetamido)benzylidene)-3,4-dihydro-2*H*-pyrrol-5-yl)phenyl)acetamide (**5r**):

To a solution of compound (**5p**) (10 mg, 0.02 mmol) in CH_2Cl_2 (0.5 mL), was added trifluoroacetic acid (0.5 mL) and the resulting mixture was stirred at room temperature for 30 minutes.¹¹ Then, the solvent was concentrated under reduced pressure to afford the deprotected (*E*)-4-(4-(4-(4-aminobenzylidene)-3,4-dihydro-2*H*-pyrrol-5-yl)aniline (**5q**) in a 100% yield as an orange oil.

¹¹ Ripka, A. S.; Bohacek, R.S.; Rich, D.H. *Bioorg. Med. Chem. Lett.* **1998**, *8*, 357.



Empiric formula: $C_{17}H_{17}N_3$

Molecular weight: 263.15

Yield: 100%

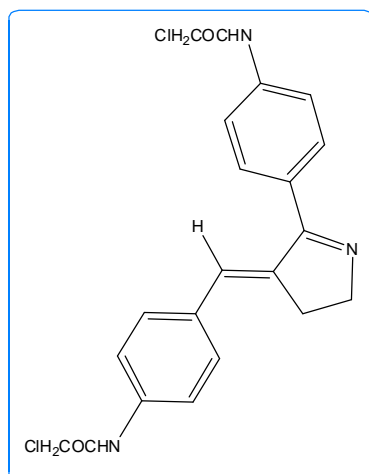
1H NMR (300MHz, CD_3OD): δ (ppm) 7.52 (d, $J = 8.7$ Hz, 2H), 7.55 (s, 1H), 7.41 (d, $J = 8.6$ Hz, 2H), 6.79 (d, $J = 8.7$ Hz, 2H), 6.75 (d, $J = 8.7$ Hz, 2H), 4.07 (m, 2H), 3.38 (m, 2H).

^{13}C NMR (300MHz, CD_3OD): δ (ppm) 179.05, 156.56, 145.57, 134.50, 133.39, 130.67, 129.91, 126.24, 116.66, 115.18, 114.20, 50.09, 30.45.

ES-MS (+) ($C_{17}H_{17}N_3 + H$): calc. 264.1495, found 264.1494.

Observations: Orange oil

Without further purification, the resulting product (**5q**) was dissolved in aqueous Na_2CO_3 (pH = 8) and cooled to $0^\circ C$. Then, chloroacetyl chloride (16 μL , 0.2 mmol) was added, and the mixture was stirred vigorously for 30 min at $0^\circ C$ and later 2 hours at room temperature. The resulting precipitate was filtered from the aqueous solution, washed with water and dried in a high vacuum pump to give **5r** in 40% yield as a brown solid.



Empiric formula: $C_{21}H_{19}N_3O_2Cl_2$

Molecular weight: 415.09

Yield: 60%

1H NMR (400MHz, DMSO- d_6): δ 10.61 (s, 1H), 10.47 (s, 1H), 7.63 (m, 8H), 7.06 (s, 1H), 4.30 (s, 2H), 4.28 (s, 2H), 4.01 (s, 2H), 2.84 (m, 2H).

UV-VIS (DMSO): λ (nm) 313 ($\epsilon = 46850 M^{-1}cm^{-1}$).

ES-MS (+) ($C_{21}H_{19}N_3O_2Cl_2 + H$): calc. 416.0927, found 416.0923.

Observations: Brown solid

8.4.2. Linkage of the synthesized PSB-retinal based photoswitch 5r to a model peptide.

- Selection and synthesis of the adequate model peptide for the linkage to 5r:
 - *Molecular dynamics simulation of the free photoswitchable cross-linkers:*

Cross-linker end-to-end distance distributions were calculated using molecular dynamics methods running under Hyperchem 8.0 (Hypercube Inc.) essentially as described previously.¹² Models of linkers were built and minimized using the Amber molecular mechanics force field (Amber99) with the linkage to a Cys side-chain terminated with the $C\alpha$ atom as a methyl group. All amide bonds had the *trans* geometry. Multiple 10 ns runs were performed at 300K using a variety of starting geometries. Cross-linker distributions were built from sulfur-to-sulfur distances measured at 1 ps time steps.

¹² Chi, L., Sadowski, O., Woolley, G. A. *Bioconjug. Chem.* **2006**, *17*, 670.

- *Peptide synthesis:*

Peptide SS-11 (Ac-WGACEAAAAREAAARCAAAREAAAAREAQ-NH₂) was prepared by standard protocols for Fmoc-based solid-phase peptide synthesis. It was HPLC-purified on a Zorbax SB-C18 column with a linear gradient of 5-70% acetonitrile/water (containing +0.1% trifluoroacetic acid) over the course of 35 min.

The molecular composition of the peptide was confirmed by MALDI-MS [M]⁺: calc. for C₁₁₂H₁₈₂N₄₂O₃₇S₂ 2773.1 Da, found 2773.5 Da.

- **Cross-linking reaction of peptide SS-11 to photoswitch **5r**:**

Cross linking of the peptide SS-11 was performed in 60 mM Tris Buffer at pH 8 containing 2 mM TCEP. To the reaction mixture, a final concentration of 0.5 mM peptide, 2 mM of cross-linker (**5r**) was added, and the solvent was composed of 20% DMSO and 80% water. The mixture was stirred at 40°C overnight. DMSO was removed using a high vacuum pump, and the cross-linked peptide was purified with HPLC using a Zorbax SB-C18 column with a linear gradient of 5-70% acetonitrile/water (containing +0.1% trifluoroacetic acid) over the course of 35 min.

The cross-linked peptide was characterized by ESI-MS (+): m/z (C₁₃₃H₁₉₉N₄₅O₃₉S₂+H) calc.: 3117.5, found: 3116.45.

For the HPLC-resolution of *E* and *Z* isomers of cross-linked peptide, the same C18 column with a different linear gradient of 5-50% acetonitrile/water (containing +0.1% trifluoroacetic acid) over a period of 25 min was employed.

8.4.3. Photochemical study of the cross-linked peptide.

- **Molar extinction coefficient determination:**

To determine the molar extinction coefficient, a ¹H NMR spectrum of (**5r**) in DMSO-*d*₆ was recorded with a known concentration of 1,2-dichloroethane as internal standard. The intensity ratio of the ¹H signals of 1,2-dichloroethane and the α-chloroacetamido group of (**5r**) permitted determination of the concentration of

(5r) in the NMR sample. The sample was then diluted, and the UV-Vis spectrum was recorded. The molar extinction coefficient was calculated to be $46850 \text{ M}^{-1}\text{cm}^{-1}$ in DMSO at 313 nm.

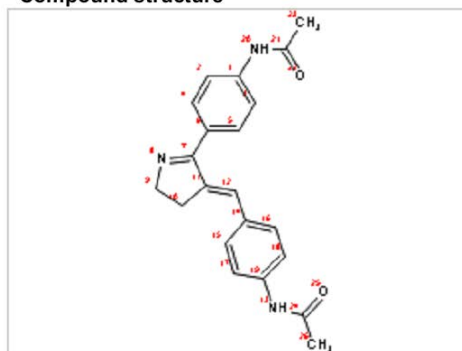
A 2 μL concentrated stock solution of cross-linked peptide in 10 mM sodium phosphate buffer (pH 7) was diluted to 140 μL with DMSO, and the UV-Vis spectrum of this peptide solution was recorded. From this UV-Vis spectrum and the molar extension coefficient of the cross-linker ($46850 \text{ M}^{-1}\text{cm}^{-1}$) in DMSO, the concentration of the stock solution was calculated. Afterward the stock solution was diluted with sodium phosphate buffer (pH 5), and the UV-Vis spectra was recorded to determine the molar extinction coefficient in aqueous solution.

- Estimated pKa:

The following figure shows the output of the pKa predictions from ACD/Ilabs:

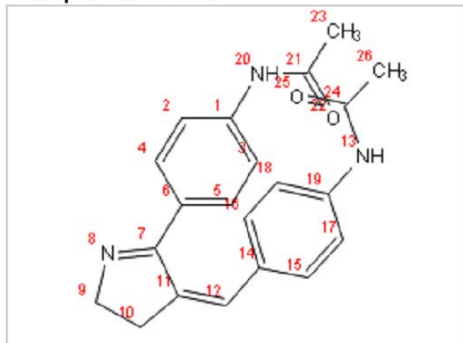
 **ACD/Labs**
I-Lab 2.0 - ilab.acdlabs.com
ACD/Labs Monday 2nd of April 2012 07:36:18 PM. Algorithm Version: v12.1.0.50374

Compound structure



Ionic form : H2L
 $\text{pKa}_1(\text{HL}/\text{H}+\text{L}; 20) = 14.81 \pm 0.70$
 $\text{pKa}_2(\text{H2L}/\text{H}+\text{HL}; 13) = 14.80 \pm 0.70$
 $\text{pKa}_3(\text{H3L}/\text{H}+\text{H2L}; 8) = 7.39 \pm 0.20$
 $\text{pKa}_4(\text{H4L}/\text{H}+\text{H3L}; 13) = -1.14 \pm 0.50$
 $\text{pKa}_5(\text{H5L}/\text{H}+\text{H4L}; 20) = -4.64 \pm 0.50$

Compound structure



Ionic form : H2L

pKa₁(HL/H+L; 20) = 14.81 ± 0.70pKa₂(H2L/H+HL; 13) = 14.80 ± 0.70pKa₃(H3L/H+H2L; 8) = 7.39 ± 0.20pKa₄(H4L/H+H3L; 13) = -1.14 ± 0.50pKa₅(H5L/H+H4L; 20) = -4.64 ± 0.50

Figure 8.8. Output of the pKa predictions from ACD/Ilabs.

- Determination of the $E \rightarrow Z$ isomerization quantum yield of the cross-linked peptide:

The $E \rightarrow Z$ isomerization quantum yield of the cross-linked peptide in sodium phosphate buffer at pH 5.0 was determined with using an azobenzene cross-linked peptide as an actinometer.¹³

The experiment was carried out with a diode array UV-Vis spectrophotometer (Ocean Optics Inc., USB4000) coupled to a temperature controlled cuvette holder (Quantum Northwest, Inc.). A solution of diacetamido azobenzene cross-linked peptide FK11 in 20 mM sodium phosphate buffer at pH 7, with absorbance of 0.5 at 365 nm, was irradiated with 367 nm light at 25°C for times between 5-15 seconds such that the $E \rightarrow Z$ isomerization was kept below 20%. A 1 cm path length quartz cuvette was used for the experiment and the beam of 367 nm light was applied at an angle perpendicular to the measuring beam. The $E \rightarrow Z$ conversion was calculated by comparing this UV-Vis spectra with the 100% dark and 100%Z spectra of diacetamido azobenzene cross-linked peptide FK11.

¹³ Borisenko, V., Woolley, G.A. *J. Photochem. Photobiol. A. Chem.* **2005**, *173*, 21.

Then, a solution of our cross-linked peptide in 20 mM sodium phosphate buffer at pH 5.0 of the same absorbance (0.5) was treated in precisely the same manner, and the $E \rightarrow Z$ conversion was also calculated using spectra obtained for the pure (HPLC isolated) isomers. The ratio of times required for the same %conversion (<20%) was used to calculate a quantum yield of 0.24 for the cross-linked peptide.

- Spectroscopic characterization of the cross-linked peptide (UV-Vis and CD spectra):

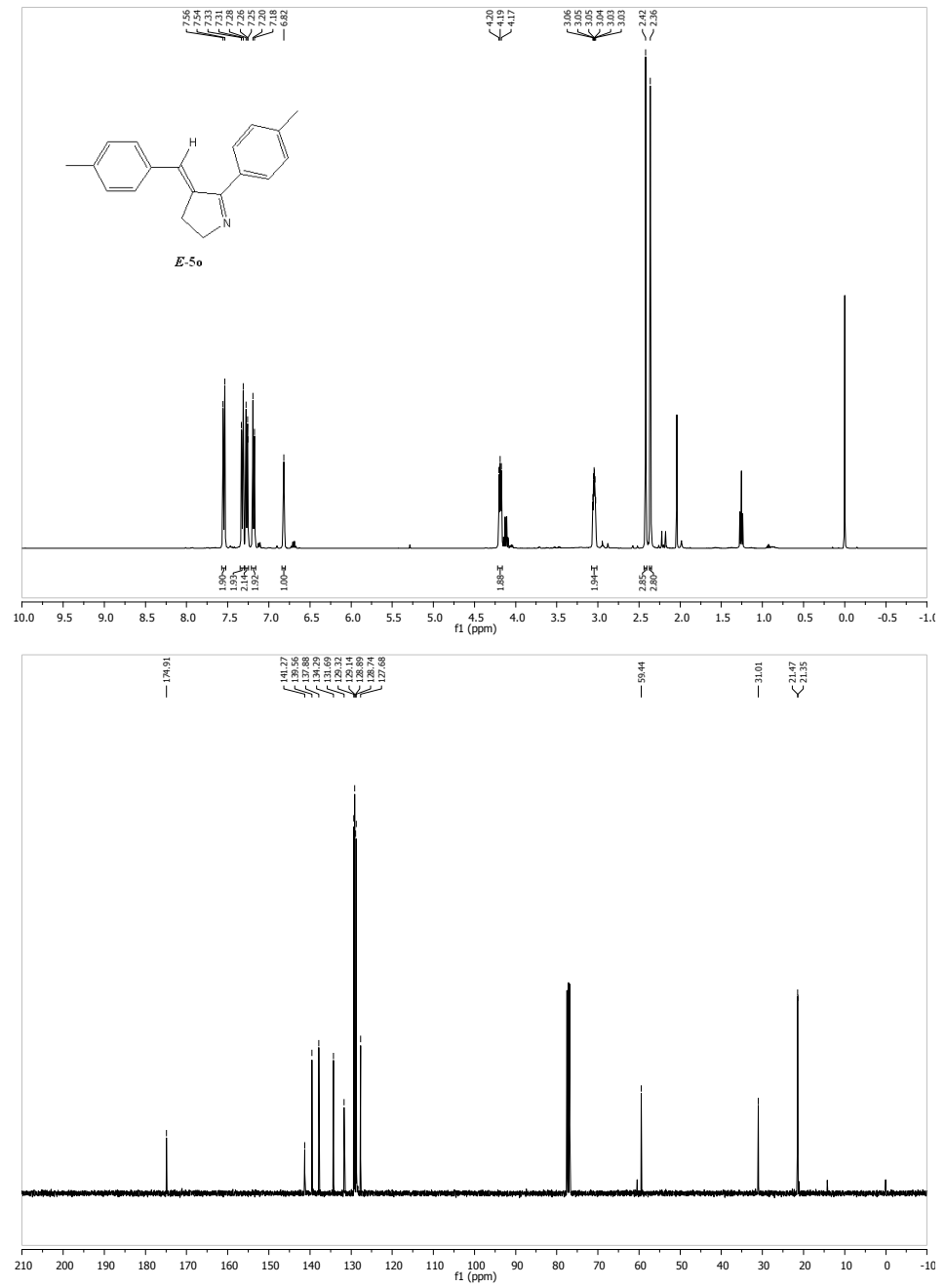
UV spectra were measured with a diode array UV-Vis spectrophotometer (Ocean Optics Inc., USB4000) coupled to a temperature controlled cuvette holder (Quantum Northwest, Inc.). Thermal relaxation of the Z to the E isomer was measured with Perkin Elmer Lambda 35 UV-Vis spectrophotometer coupled with a temperature controlled cuvette holder. A 1 cm path length cuvette was used for all UV-vis. After reaching the PSS by irradiation with 400 nm light, the relaxation of the Z to the E isomer was monitored at 50 °C by measuring absorbance at 375 nm as a function of time. Thermal relaxation curves were fitted to a single exponential equation to calculate the relaxation lifetime. The LEDs used for irradiation were 365 nm (~600 mW, LEDengin LZ4-40U610), 395-405 nm (~460 mW, LEDengin LZ1-10UA05) and 446 nm (Luxeon III Star LED - Royal Blue Lambertian, 340 mW @ 700mA).

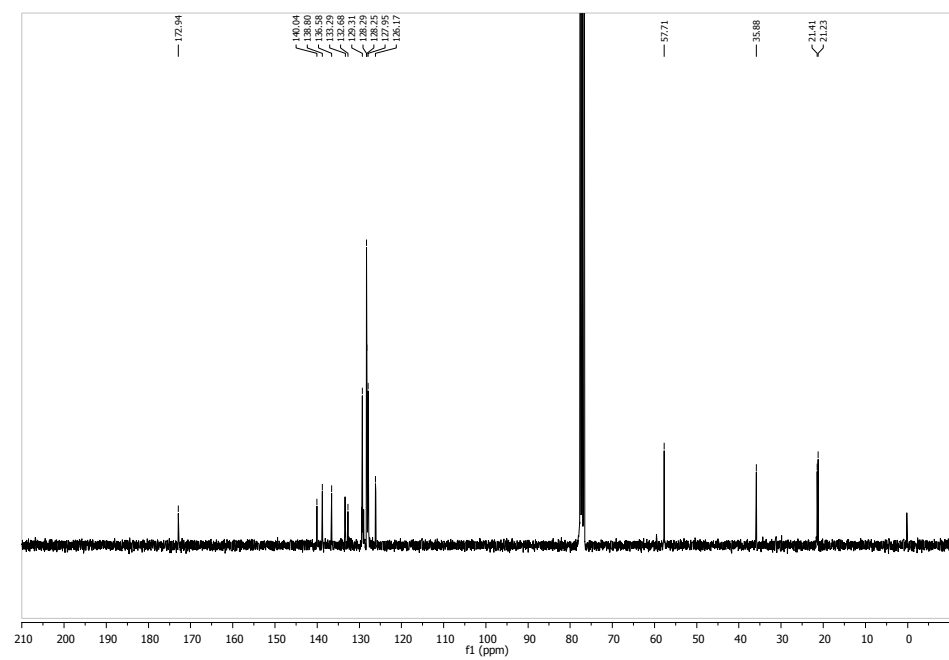
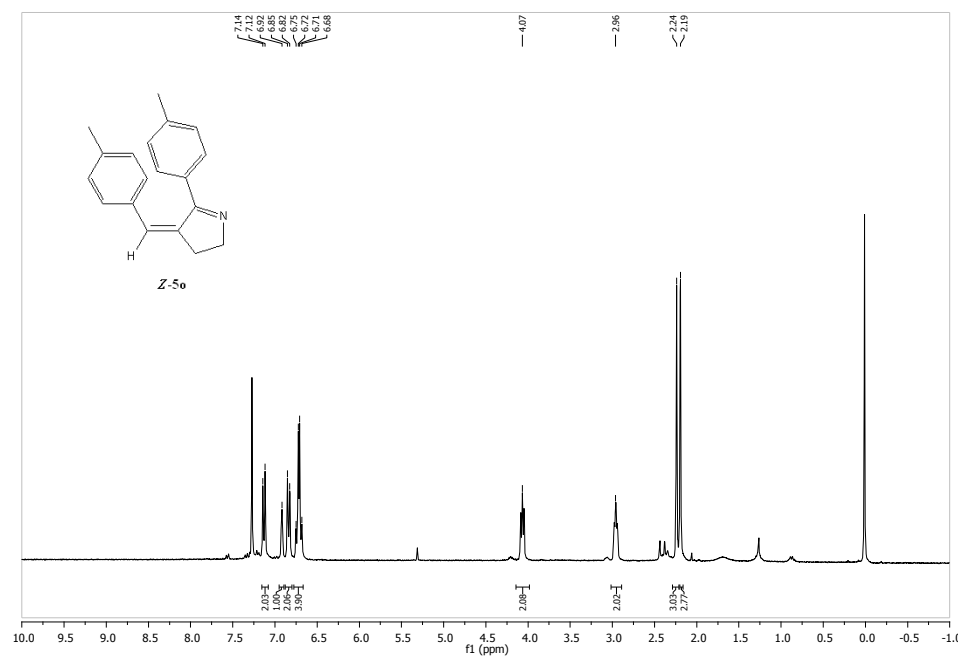
After irradiation with 400 nm light for 10 min, a solution of cross-linked peptide in sodium phosphate buffer (pH 5.0) was injected into the HPLC. The both E and Z isomers were isolated (HPLC conditions mentioned above), immediately frozen using liquid nitrogen and lyophilized in dark. The solid, pure E and Z isomers were dissolved in sodium phosphate buffer (pH 5.0), and the UV-Vis spectra were recorded.

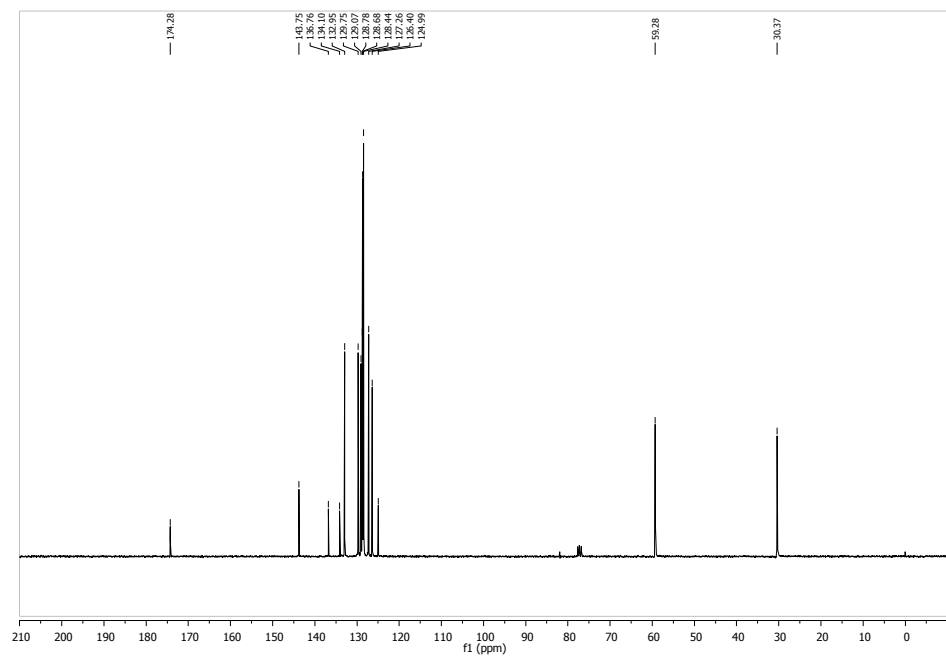
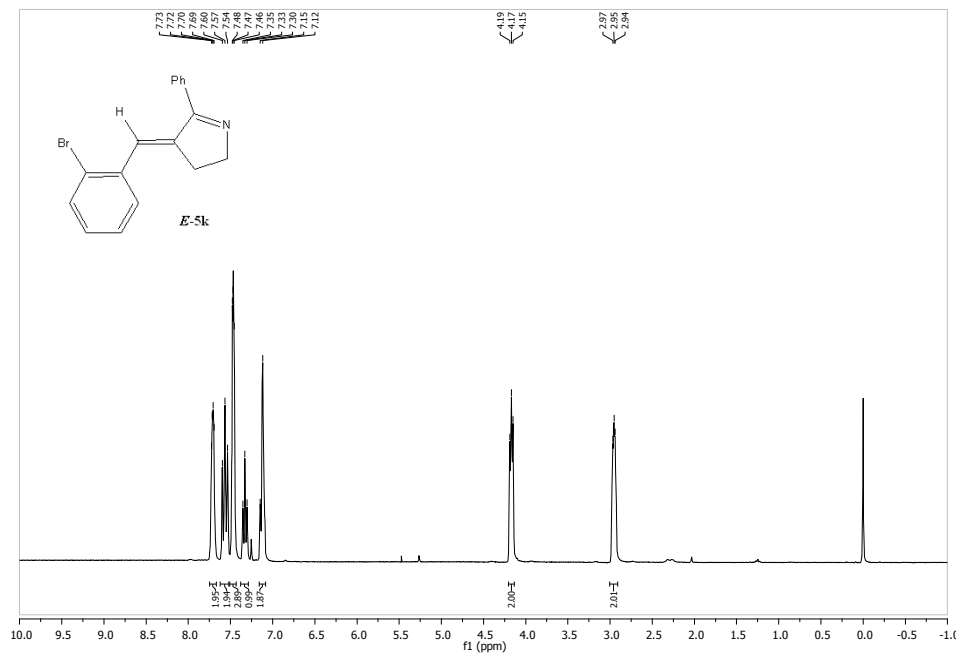
CD spectra were obtained at 5°C, 20°C, and 40°C for both dark-adapted and irradiated peptides. Each spectrum was acquired from 260 nm to 205 nm (1 nm step) with an integration time of 2 s at each wavelength and 3 scans were averaged, smoothed, and baseline subtracted. All CD measurements were carried out in a 1 mm cuvette with peptide concentrations of 50 μ M in 20 mM sodium phosphate buffer at pH 5.0 and of 100 μ M in 10 mM sodium phosphate buffer at pH 7.0. For CD spectra of the irradiated peptide, samples were irradiated using LEDs directly in the CD instrument.

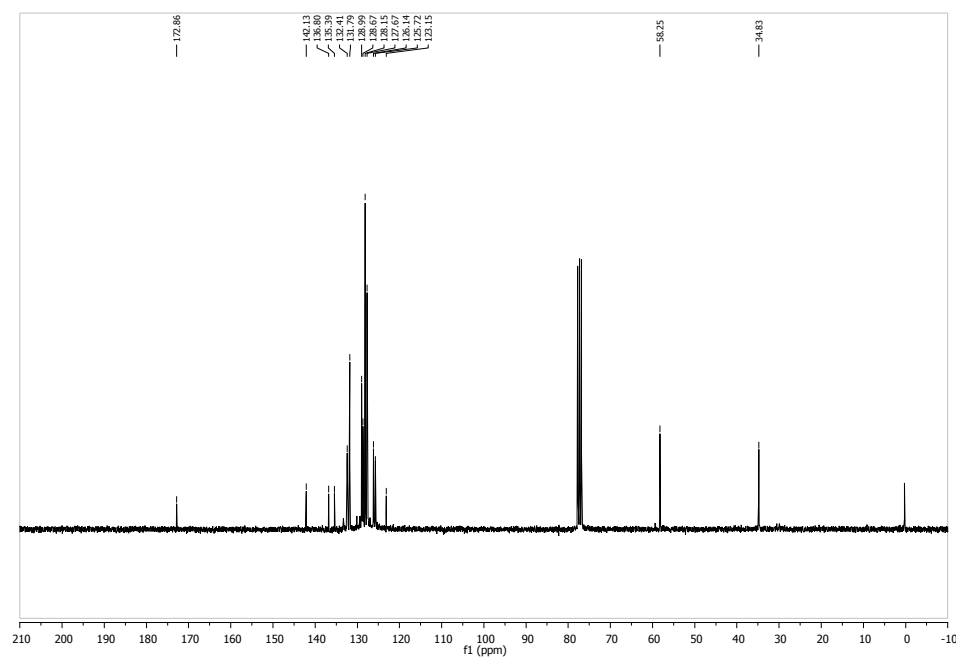
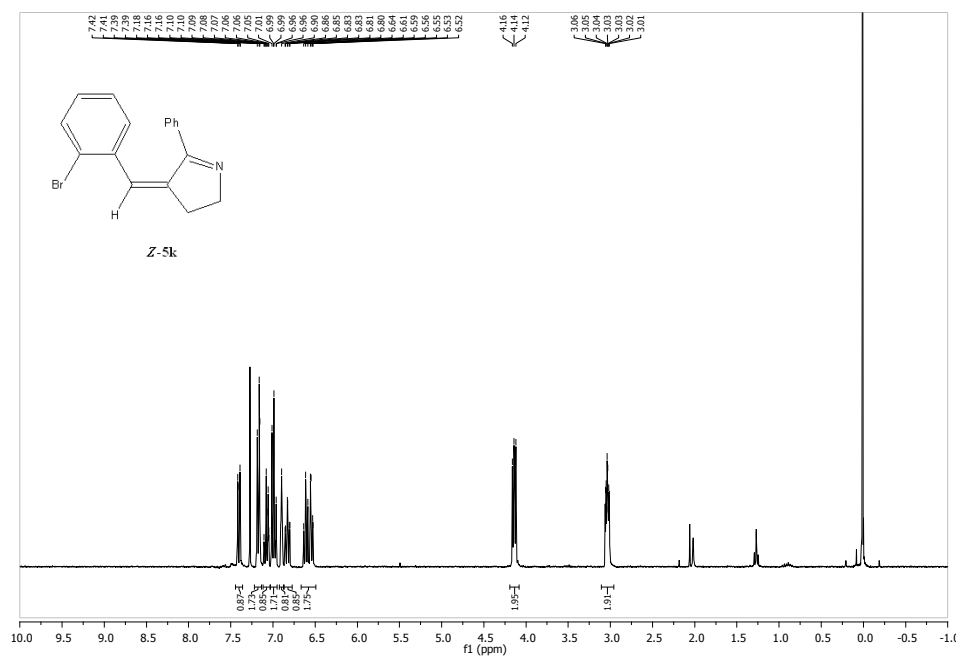
APPENDIX A

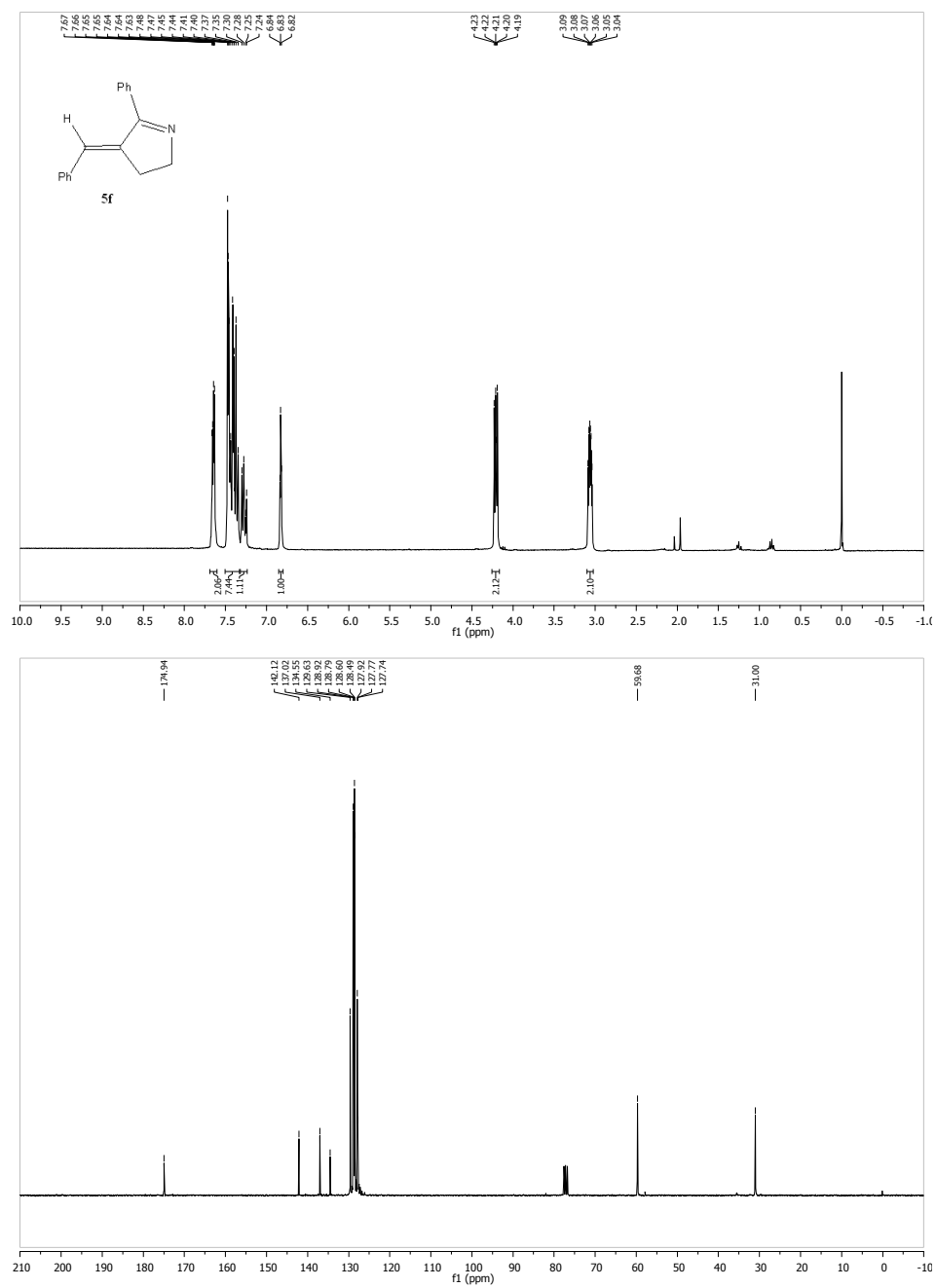
Selected NMR spectra

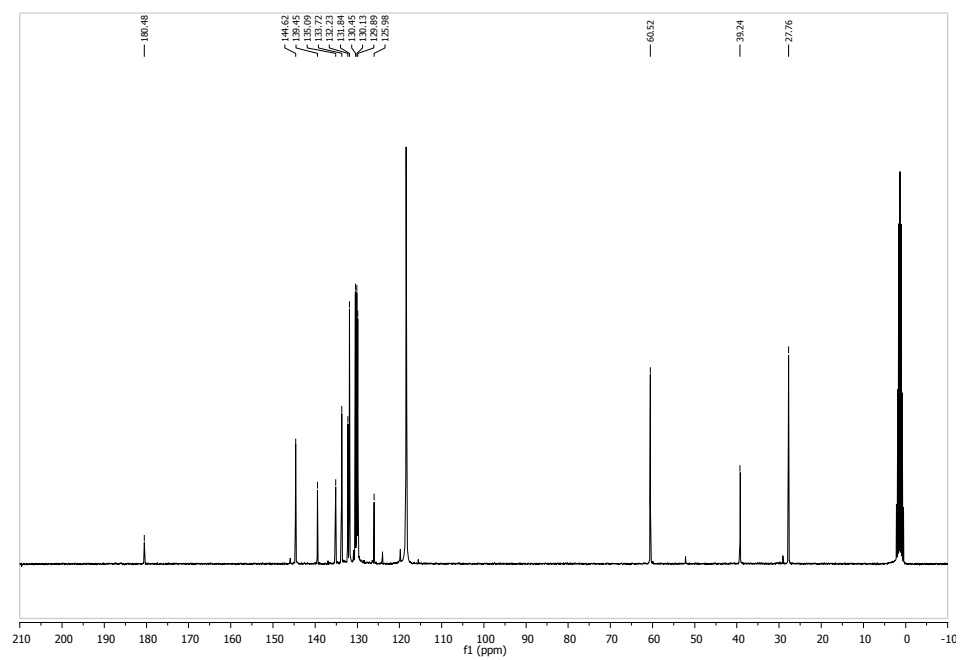
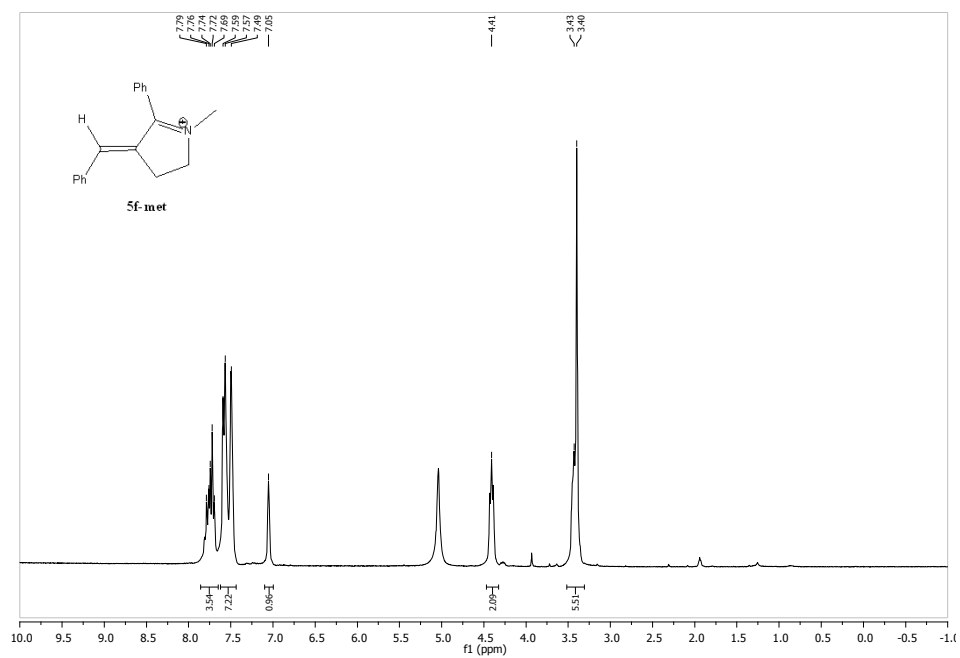


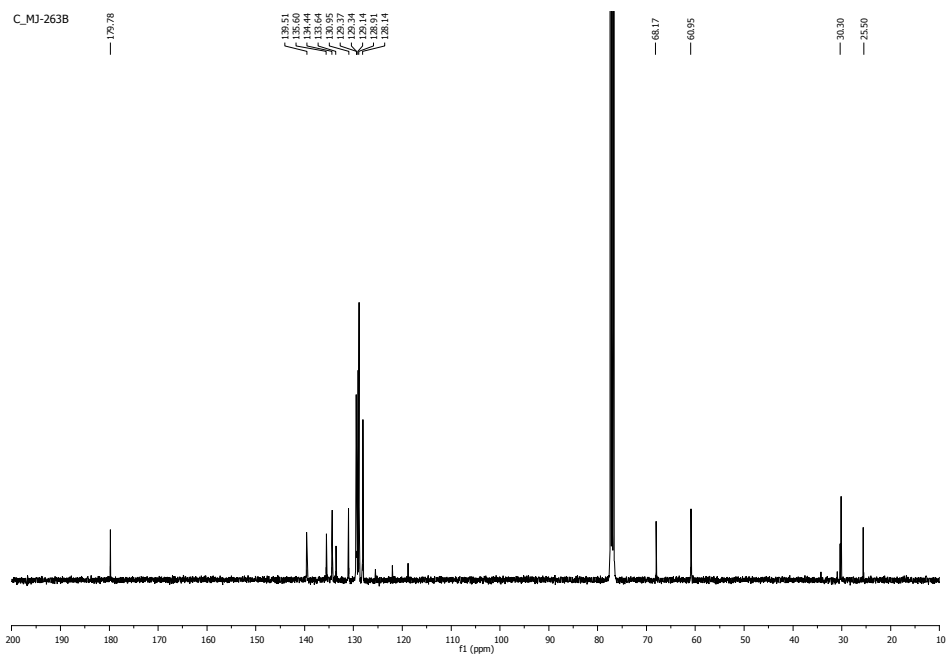
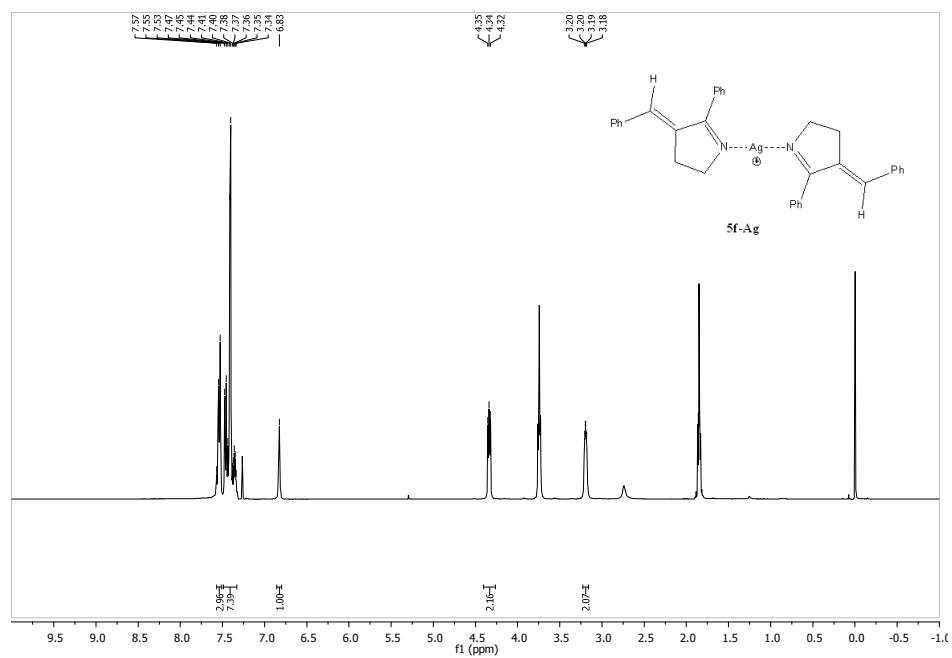


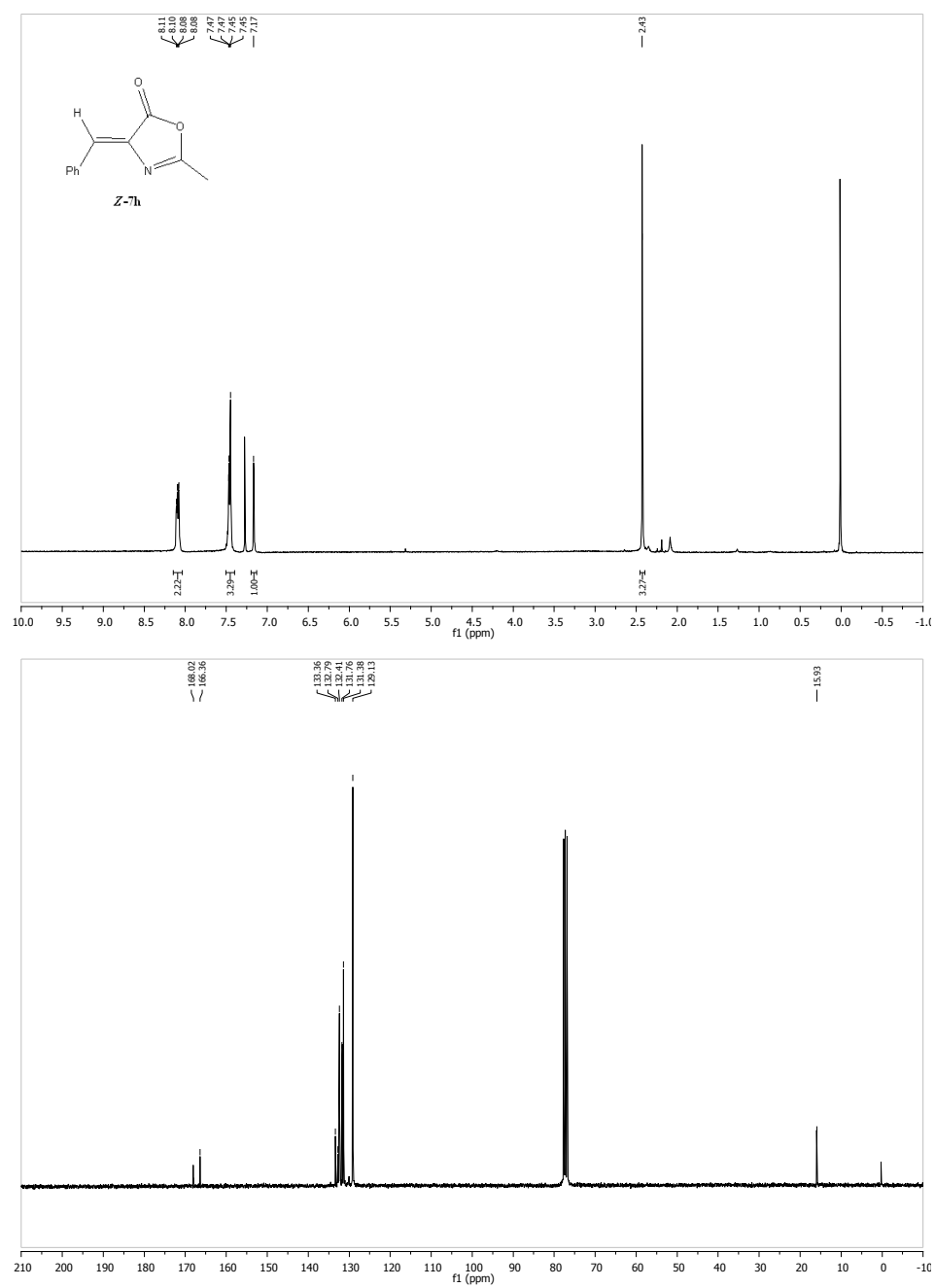


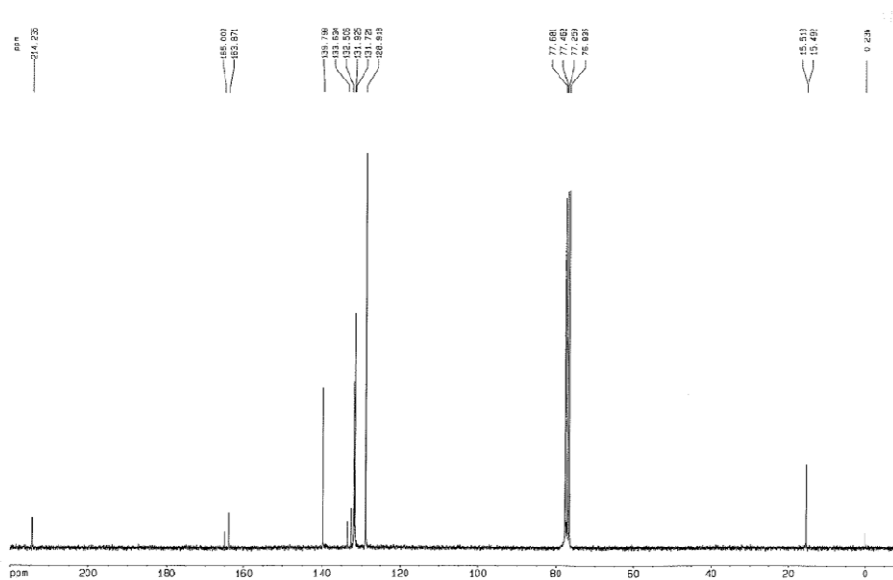
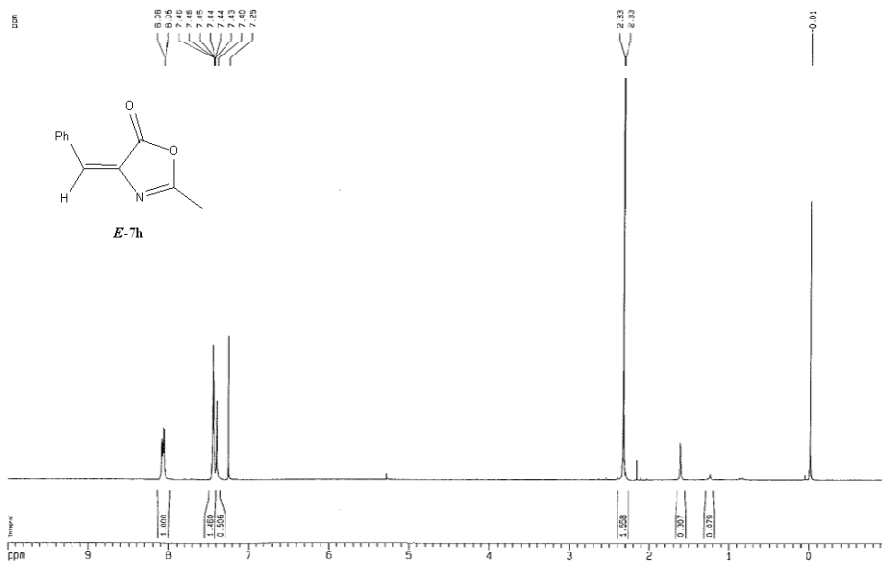


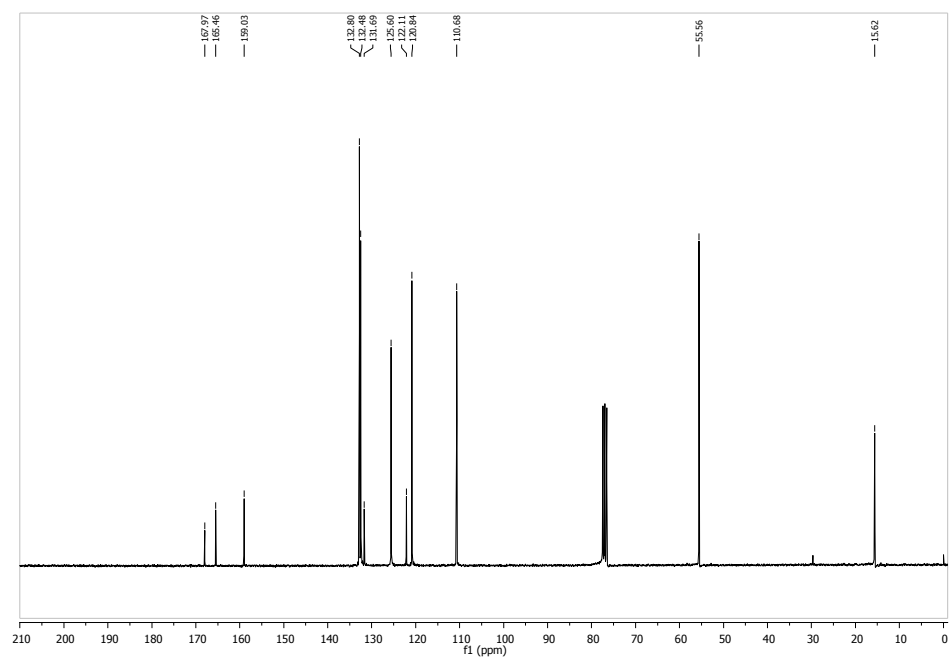
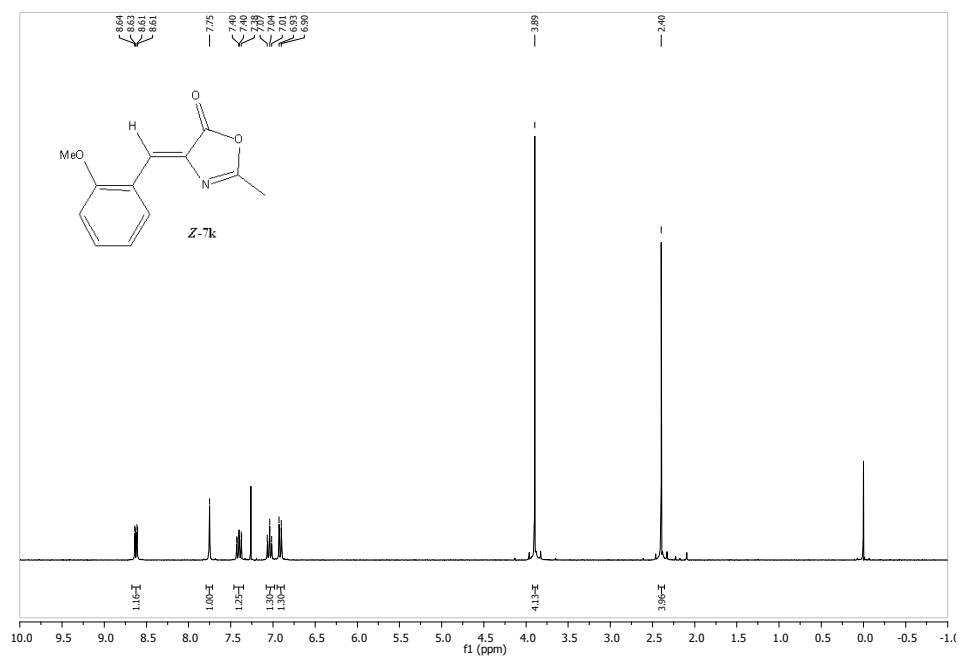


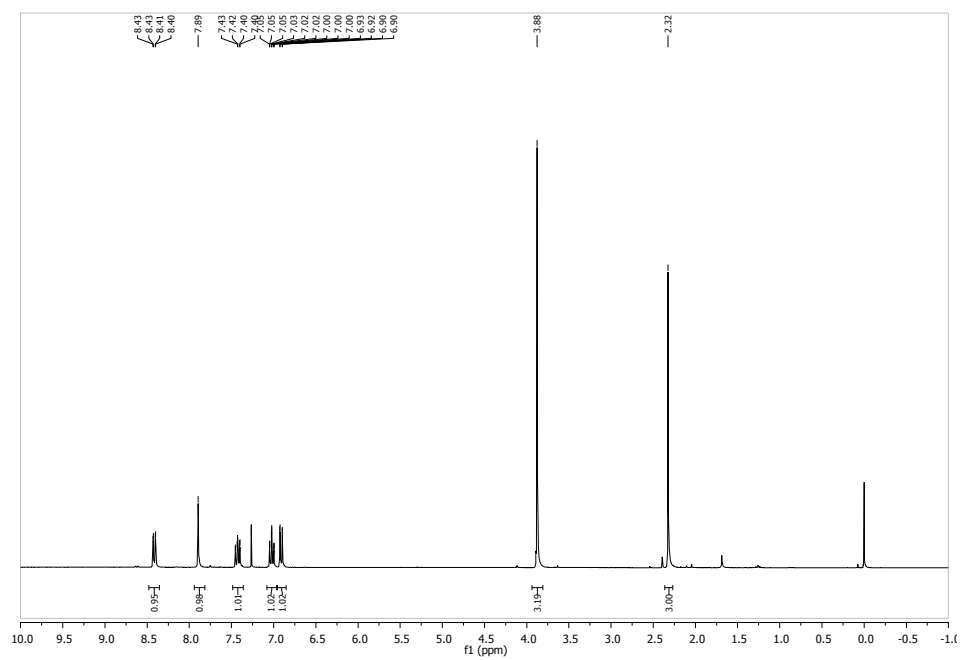
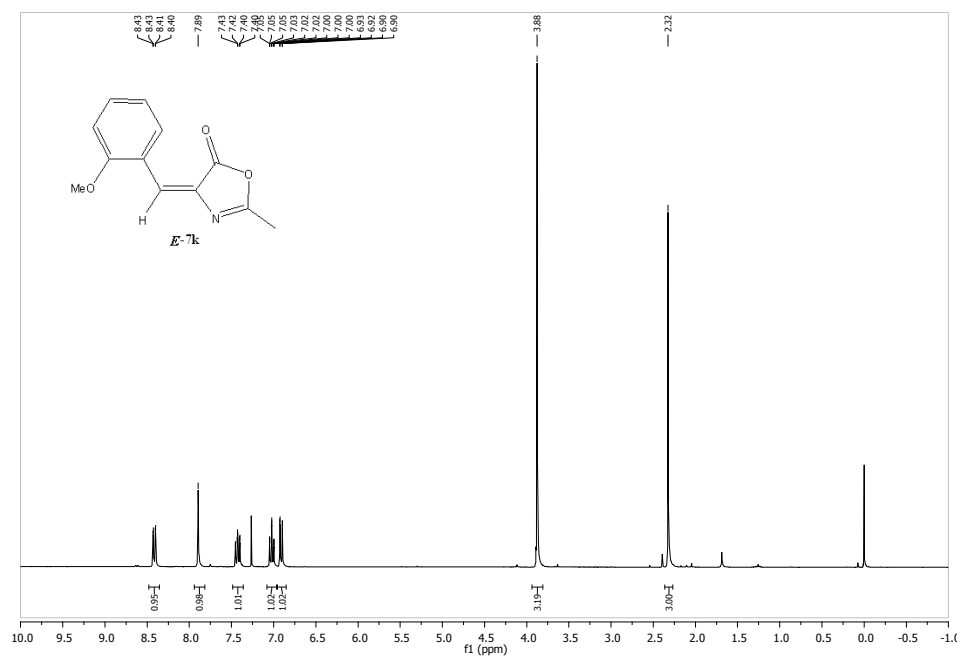


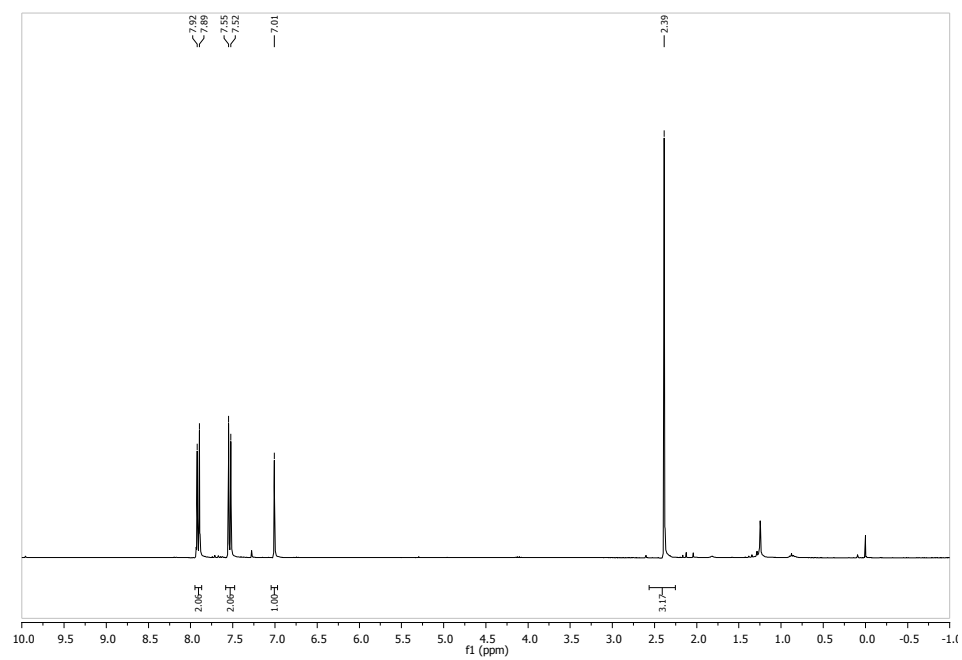
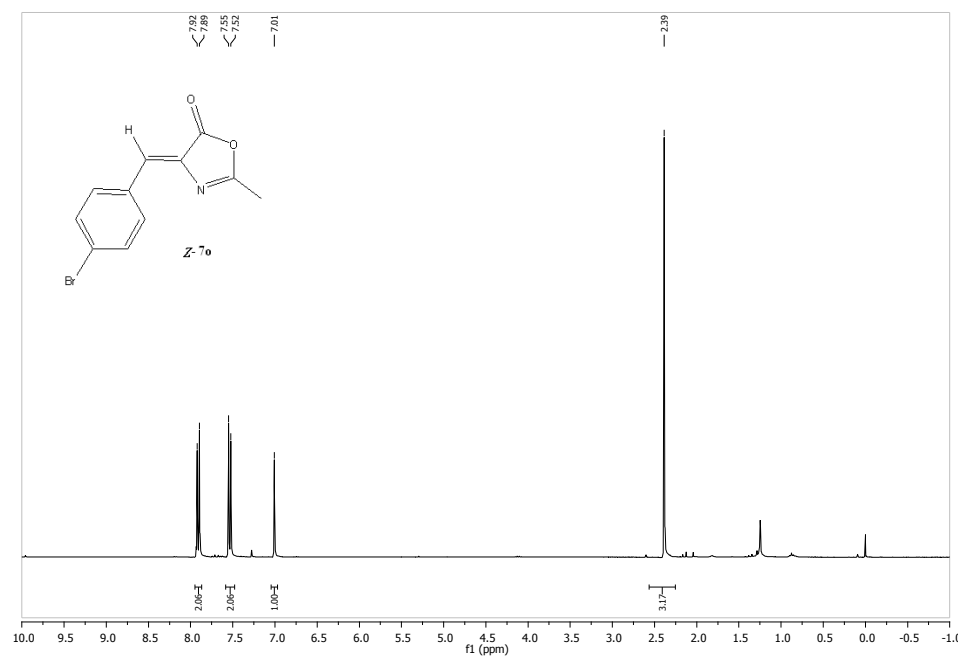


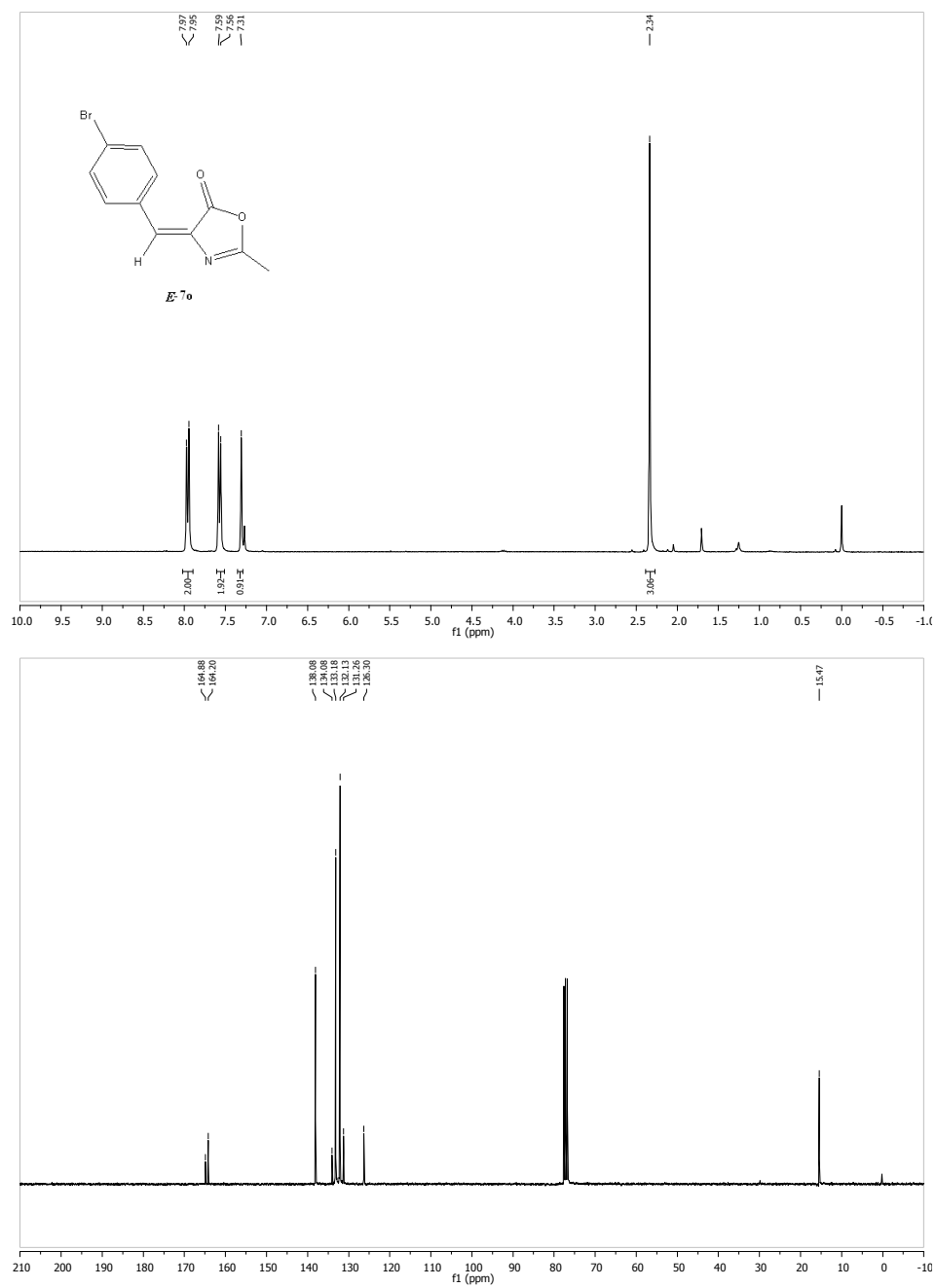


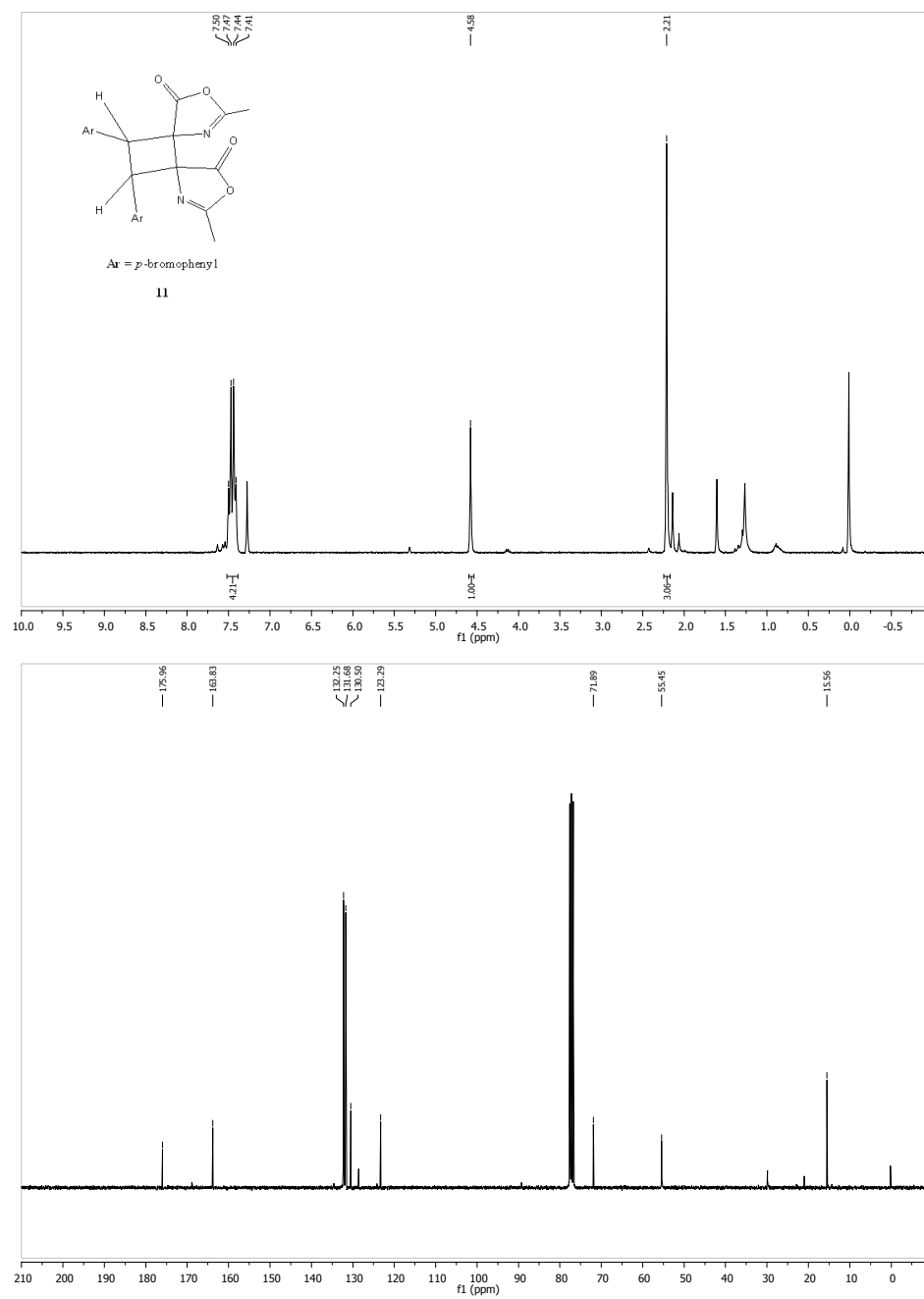










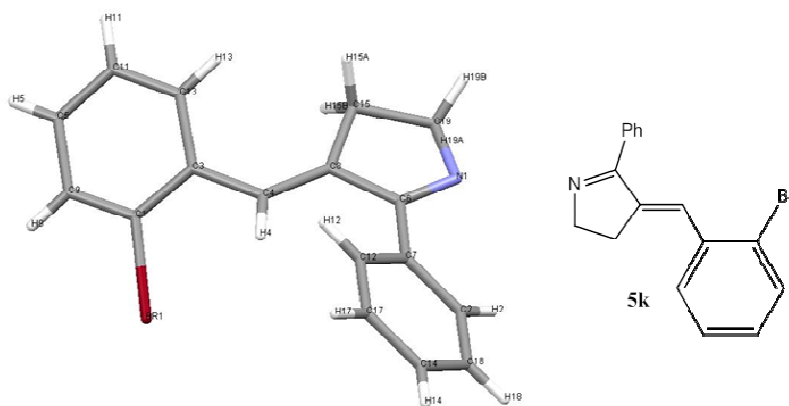


APPENDIX B

X-Ray Diffraction data

MOLECULAR SWITCHES WITH STRUCTURE BASED ON THE PSB-RETINAL CHROMOPHORE

Crystal data and structure refinement for the *E* isomer of switch 5k.



Empirical formula	$C_{17}H_{14}BrN$	
Molecular weight	312.20	
Temperature	173(1) K	
Wavelength	0.71073 Å	
Crystal system	Monoclinic	
Space group	$P 2_1/a$	
Unit cell dimensions	$a = 8.485 \text{ Å}$	$\alpha = 90^\circ$
	$b = 16.188 \text{ Å}$	$\beta = 97.19^\circ$
	$c = 10.241 \text{ Å}$	$\gamma = 90^\circ$
Volume	1395.6 Å^3	
Z	4	
Density (calculated)	1.486 Mg/m^3	
Absorption coefficient	2.930 mm^{-1}	
F(000)	632	
Crystal size	$0.4 \times 0.4 \times 0.3 \text{ mm}^3$	

θ range for data collection	2.00 to 27.42°.
Index ranges	-10 \leq h \leq 10, -20 \leq k \leq 20, -13 \leq l \leq 12
Reflections collected	15186
Independent reflections	3160 [R(int) = 0.0584]
Completeness to $\theta = 27.42^\circ$	99.6 %
Absorption correction	Semi-empirical from equivalents
Max. and min. transmission	0.4013 and 0.3140

Refinement method	Full-matrix least-squares on F ²
Data / restraints / parameters	3160 / 0 / 172
Goodness-of-fit on F ²	1.101
Final R indices [I $>$ 2 σ (I)]	R1 = 0.0362, wR2 = 0.0625
R indices (all data)	R1 = 0.0607, wR2 = 0.0810
Largest diff. peak and hole	0.376 and -0.442 e. \AA^{-3}

Data collection: Kappa CCD

Refinement: HKL Scalepack (Otwinowski & Minor, 1997)

Program used for resolving the structure: SHELXS-97 (Sheldrick, 1997)

Program used for the refinement of the structure: SHELXS-97 (Sheldrick, 1997)

Atomic coordinates ($\times 10^4$) and equivalent isotropic displacement parameters ($\text{\AA}^2 \times 10^3$) for **5k**.

U(eq) is defined as one third of the trace of the orthogonalized U^{ij} tensor.

	x	y	z	U(eq)
C(1)	5775(3)	1158(2)	1427(3)	21(1)
C(2)	8935(4)	1681(2)	7498(3)	28(1)
C(3)	5236(3)	1705(2)	2330(3)	20(1)
C(4)	5967(3)	1734(2)	3717(3)	21(1)
C(5)	3845(4)	1627(2)	-322(3)	28(1)
C(6)	7038(3)	2416(2)	5844(3)	23(1)
C(7)	7506(4)	1676(2)	6654(3)	23(1)
C(8)	6146(3)	2396(2)	4497(3)	21(1)
C(9)	5111(4)	1117(2)	121(3)	24(1)
C(11)	3268(4)	2169(2)	542(3)	33(1)
C(12)	6559(4)	973(2)	6618(3)	29(1)
C(13)	3949(4)	2209(2)	1848(3)	28(1)
C(14)	8471(4)	302(2)	8207(3)	36(1)
C(15)	5764(4)	3290(2)	4180(3)	27(1)

C(17)	7046(4)	291(2)	7380(3)	33(1)
C(18)	9395(4)	1003(2)	8268(3)	35(1)
C(19)	6839(4)	3754(2)	5254(3)	34(1)
N(1)	7434(3)	3143(2)	6263(2)	29(1)
Br(1)	7516(1)	437(1)	1964(1)	34(1)

Bond lengths [\AA] and angles [deg.].

Bond lengths (\AA)

Atom A-B	Distance
C(1)-C(9)	1.387(4)
C(1)-C(3)	1.398(4)
C(1)-Br(1)	1.909(3)
C(2)-C(18)	1.379(4)
C(2)-C(7)	1.398(4)
C(2)-H(2)	0.9300
C(3)-C(13)	1.402(4)
C(3)-C(4)	1.478(4)
C(4)-C(8)	1.334(4)
C(4)-H(4)	0.9300
C(5)-C(11)	1.379(4)
C(5)-C(9)	1.385(4)
C(5)-H(5)	0.9300
C(6)-N(1)	1.283(4)
C(6)-C(7)	1.483(4)
C(6)-C(8)	1.488(4)
C(7)-C(12)	1.391(4)
C(8)-C(15)	1.510(4)
C(9)-H(9)	0.9300
C(11)-C(13)	1.391(4)

C(11)-H(11)	0.9300
C(12)-C(17)	1.385(4)
C(12)-H(12)	0.9300
C(13)-H(13)	0.9300
C(14)-C(18)	1.376(5)
C(14)-C(17)	1.387(5)
C(14)-H(14)	0.9300
C(15)-C(19)	1.535(4)
C(15)-H(15A)	0.9700
C(15)-H(15B)	0.9700
C(17)-H(17)	0.9300
C(18)-H(18)	0.9300
C(19)-N(1)	1.473(4)
C(19)-H(19A)	0.9700
C(19)-H(19B)	0.9700

Bond angles (deg.)

Atom A-B-C	Angle
C(9)-C(1)-C(3)	122.8(3)
C(9)-C(1)-Br(1)	117.0(2)
C(3)-C(1)-Br(1)	120.2(2)
C(18)-C(2)-C(7)	120.7(3)
C(18)-C(2)-H(2)	119.7
C(7)-C(2)-H(2)	119.7
C(1)-C(3)-C(13)	116.1(3)
C(1)-C(3)-C(4)	121.5(3)
C(13)-C(3)-C(4)	122.3(3)
C(8)-C(4)-C(3)	127.1(3)

C(8)-C(4)-H(4)	116.4
C(3)-C(4)-H(4)	116.4
C(11)-C(5)-C(9)	119.5(3)
C(11)-C(5)-H(5)	120.3
C(9)-C(5)-H(5)	120.3
N(1)-C(6)-C(7)	120.9(3)
N(1)-C(6)-C(8)	114.3(3)
C(7)-C(6)-C(8)	124.8(3)
C(12)-C(7)-C(2)	118.4(3)
C(12)-C(7)-C(6)	122.2(3)
C(2)-C(7)-C(6)	119.4(3)
C(4)-C(8)-C(6)	125.4(3)
C(4)-C(8)-C(15)	129.5(3)
C(6)-C(8)-C(15)	104.5(2)
C(5)-C(9)-C(1)	119.5(3)
C(5)-C(9)-H(9)	120.3
C(1)-C(9)-H(9)	120.3
C(5)-C(11)-C(13)	120.5(3)
C(5)-C(11)-H(11)	119.7
C(13)-C(11)-H(11)	119.7
C(17)-C(12)-C(7)	120.4(3)
C(17)-C(12)-H(12)	119.8
C(7)-C(12)-H(12)	119.8
C(11)-C(13)-C(3)	121.6(3)
C(11)-C(13)-H(13)	119.2
C(3)-C(13)-H(13)	119.2
C(18)-C(14)-C(17)	119.1(3)
C(18)-C(14)-H(14)	120.4

C(17)-C(14)-H(14)	120.4
C(8)-C(15)-C(19)	102.8(2)
C(8)-C(15)-H(15A)	111.2
C(19)-C(15)-H(15A)	111.2
C(8)-C(15)-H(15B)	111.2
C(19)-C(15)-H(15B)	111.2
H(15A)-C(15)-H(15B)	109.1
C(12)-C(17)-C(14)	120.6(3)
C(12)-C(17)-H(17)	119.7
C(14)-C(17)-H(17)	119.7
C(14)-C(18)-C(2)	120.8(3)
C(14)-C(18)-H(18)	119.6
C(2)-C(18)-H(18)	119.6
N(1)-C(19)-C(15)	107.2(3)
N(1)-C(19)-H(19A)	110.3
C(15)-C(19)-H(19A)	110.3
N(1)-C(19)-H(19B)	110.3
C(15)-C(19)-H(19B)	110.3
H(19A)-C(19)-H(19B)	108.5
C(6)-N(1)-C(19)	109.2(2)

Anisotropic displacement parameters ($\text{\AA}^2 \times 10^3$) for **5k**.

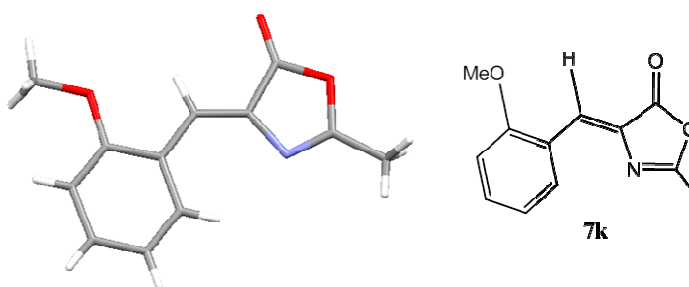
The anisotropic displacement factor exponent takes the form: $-2\pi^2 [h^2 a^{*2} U^{11} + \dots + 2 h k a^* b^* U^{12}]$

	U ¹¹	U ²²	U ³³	U ²³	U ¹³	U ¹²
C(1)	20(2)	17(2)	24(2)	1(1)	1(1)	-1(1)
C(2)	25(2)	33(2)	25(2)	-3(1)	2(1)	1(1)
C(3)	22(2)	21(2)	18(1)	-1(1)	2(1)	-3(1)

C(4)	20(2)	27(2)	17(1)	1(1)	2(1)	0(1)
C(5)	35(2)	28(2)	18(2)	-2(1)	-4(1)	-2(1)
C(6)	21(2)	31(2)	17(1)	-3(1)	4(1)	-3(1)
C(7)	26(2)	31(2)	14(1)	-2(1)	6(1)	2(1)
C(8)	19(2)	27(2)	19(2)	2(1)	3(1)	-1(1)
C(9)	31(2)	22(2)	21(2)	-5(1)	4(1)	-1(1)
C(11)	32(2)	35(2)	28(2)	-2(2)	-8(1)	8(2)
C(12)	29(2)	37(2)	20(2)	3(1)	3(1)	-4(1)
C(13)	27(2)	32(2)	25(2)	-8(1)	0(1)	7(1)
C(14)	44(2)	35(2)	29(2)	7(2)	10(2)	13(2)
C(15)	29(2)	30(2)	22(2)	-2(1)	-2(1)	1(1)
C(17)	43(2)	34(2)	25(2)	2(1)	14(1)	-6(2)
C(18)	31(2)	42(2)	29(2)	-1(2)	-2(1)	11(2)
C(19)	44(2)	28(2)	29(2)	3(1)	-5(2)	-4(2)
N(1)	33(2)	30(2)	22(1)	-2(1)	-2(1)	-3(1)
Br(1)	36(1)	31(1)	34(1)	-9(1)	-7(1)	13(1)

MOLECULAR SWITCHES WITH STRUCTURE BASED ON THE GFP CHROMOPHORE

Crystal data and structure refinement for the Z isomer of switch **7k**.



Empirical formula: $C_{12}H_{11}NO_3$
Molecular weight: 217.2

Temperature:	173(2) K
Wavelength:	0.71073 Å (Mo-K α)
Description:	yellow prism
Crystal system:	Monoclinic
Space group:	p 21/c
Unit cell dimensions:	
	a = 7.2070(5) Å α = 90 deg.
	b = 14.7670(11) Å β = 113.498(4) deg.
	c = 10.5500(5) Å γ = 90 deg.
Volume:	1029.68(12) Å ³
Z:	4
Density (calculated):	1.401 Mg/m ³
F(000):	456
Crystal size:	0.50 x 0.40 x 0.45 mm
θ range for data collection:	4.05 to 28.22 deg.
Index ranges:	-9<=h<=9, -19<=k<=19, -13<=l<=14
Reflections collected:	13912
Independent reflections:	2462 [R(int) = 0.0997]
Completeness to θ =	28.22: 96.9%
Absorption correction:	none
Refinement method:	Full-matrix least-squares on F ²
Data / restraints / parameters	2462 / 0 / 173
Goodness-of-fit on F ² :	1.039
Final R indices [I>2 σ (I)]:	R1 obs = 0.0502, wR2 obs = 0.119
R indices (all data):	R1 all = 0.073, wR2 all = 0.1339
Largest diff. Peak and hole:	0.224 and -0.265 e.A ⁻³

Data collection: Kappa CCD

Refinement: HKL Scalepack (Otwinowski & Minor, 1997)

Program used for resolving the structure: SHELXS-97 (Sheldrick, 1997)

Program used for the refinement of the structure: SHELXS-97 (Sheldrick, 1997)

Atomic coordinates ($\times 10^4$) and equivalent isotropic displacement parameters (Å² $\times 10^3$) for **7k**.

U(eq) is defined as one third of the trace of the orthogonalized U^{ij} tensor.

Atom	x	y	z	U(eq)
O(01)	0.04054(18)	0.11282(8)	-0.05773(12)	0.0393(3)
O(2)	-0.48458(18)	0.29661(8)	0.20193(11)	0.0375(3)
O(3)	-0.44184(19)	0.14953(8)	0.15764(12)	0.0421(3)
C(20)	-0.1696(2)	0.23028(11)	0.03084(16)	0.0309(4)
C(5)	-0.0345(2)	0.26489(11)	-0.02938(15)	0.0303(4)
C(6)	-0.2790(2)	0.27512(11)	0.08820(16)	0.0318(4)
N(01)	-0.2934(2)	0.36859(9)	0.10743(14)	0.0362(3)
C(08)	0.2002(2)	0.23156(11)	-0.13731(16)	0.0333(4)
H(08)	0.2693	0.1898	-0.1683	0.04
C(09)	-0.4046(2)	0.22754(11)	0.14860(16)	0.0327(4)
C(10)	0.2241(3)	0.32326(12)	-0.15192(17)	0.0367(4)
H(10)	0.3085	0.3429	-0.194	0.044
C(11)	0.0724(2)	0.20195(11)	-0.07615(16)	0.0316(4)
C(12)	-0.0047(2)	0.35698(11)	-0.04478(16)	0.0345(4)
H(12)	-0.0729	0.3994	-0.0141	0.041
C(13)	0.1241(3)	0.38656(12)	-0.10477(17)	0.0377(4)
H(13)	0.1434	0.4482	-0.1133	0.045
C(14)	0.1407(3)	0.04735(13)	-0.1082(2)	0.0430(4)
C(15)	-0.4114(3)	0.37630(12)	0.17151(17)	0.0380(4)
C(16)	-0.4757(4)	0.46006(16)	0.2184(3)	0.0546(6)
H(20)	-0.184(2)	0.1651(12)	0.0315(15)	0.028(4)
H(01)	0.095(3)	-0.0140(15)	-0.089(2)	0.053(6)
H(02)	0.289(3)	0.0540(13)	-0.0565(19)	0.049(6)
H(03)	0.100(3)	0.0572(12)	-0.208(2)	0.041(5)
H(01)	-0.616(5)	0.4603(19)	0.193(3)	0.100(10)
H(02)	-0.424(4)	0.459(2)	0.318(3)	0.111(10)
H(03)	-0.429(6)	0.509(3)	0.192(4)	0.140(13)

Bond lengths [Å] and angles [deg.].

Bond lengths (Å)

Atom A-B	Distance
O(01)-C(11)	1.3632(19)
O(01)-C(14)	1.430(2)

O(02)-C(15)	1.379(2)
O(02)-C(09)	1.3956(19)
O(03)-C(09)	1.1952(19)
C(20)-C(06)	1.344(2)
C(20)-C(05)	1.452(2)
C(20)-H(20)	0.968(17)
C(05)-C(12)	1.396(2)
C(05)-C(11)	1.416(2)
C(06)-N(01)	1.405(2)
C(06)-C(09)	1.476(2)
N(01)-C(15)	1.285(2)
C(08)-C(10)	1.382(2)
C(08)-C(11)	1.389(2)
C(08)-H(08)	0.93
C(10)-C(13)	1.388(2)
C(10)-H(10)	0.93
C(12)-C(13)	1.387(2)
C(12)-H(12)	0.93
C(13)-H(13)	0.93
C(14)-H(01)	1.01(2)
C(14)-H(02)	0.993(19)
C(14)-H(03)	0.982(19)
C(15)-C(16)	1.474(3)
C(16)-H(01)	0.94(3)
C(16)-H(02)	0.97(3)
C(16)-H(03)	0.89(4)

Bond angles (deg.)

<i>Atom A-B-C</i>	<i>Angle</i>
C(11)-O(01)-C(14)	117.43(13)
C(15)-O(02)-C(09)	105.80(12)
C(06)-C(20)-C(05)	129.79(16)
C(06)-C(20)-H(20)	113.6(10)
C(05)-C(20)-H(20)	116.6(10)
C(12)-C(05)-C(11)	117.95(14)
C(12)-C(05)-C(20)	123.71(15)
C(11)-C(05)-C(20)	118.34(15)
C(20)-C(06)-N(01)	129.73(15)

C(20)-C(06)-C(09)	122.04(15)
N(01)-C(06)-C(09)	108.19(13)
C(15)-N(01)-C(06)	105.39(14)
C(10)-C(08)-C(11)	119.73(15)
C(10)-C(08)-H(08)	120.1
C(11)-C(08)-H(08)	120.1
O(03)-C(09)-O(02)	122.02(15)
O(03)-C(09)-C(06)	133.56(16)
O(02)-C(09)-C(06)	104.42(13)
C(08)-C(10)-C(13)	120.95(15)
C(08)-C(10)-H(10)	119.5
C(13)-C(10)-H(10)	119.5
O(01)-C(11)-C(08)	123.43(14)
O(01)-C(11)-C(05)	115.98(14)
C(08)-C(11)-C(05)	120.60(15)
C(13)-C(12)-C(05)	121.45(15)
C(13)-C(12)-H(12)	119.3
C(05)-C(12)-H(12)	119.3
C(12)-C(13)-C(10)	119.31(16)
C(12)-C(13)-H(13)	120.3
C(10)-C(13)-H(13)	120.3
O(01)-C(14)-H(01)	106.2(12)
O(01)-C(14)-H(02)	108.8(11)
H(01)-C(14)-H(02)	110.1(15)
O(01)-C(14)-H(03)	108.5(11)
H(01)-C(14)-H(03)	111.4(15)
H(02)-C(14)-H(03)	111.8(16)
N(01)-C(15)-O(02)	116.20(15)
N(01)-C(15)-C(16)	127.83(18)
O(02)-C(15)-C(16)	115.96(15)
C(15)-C(16)-H(01)	110.9(17)
C(15)-C(16)-H(02)	108.3(18)
H(01)-C(16)-H(02)	102(3)
C(15)-C(16)-H(03)	112(2)
H(01)-C(16)-H(03)	114(3)
H(02)-C(16)-H(03)	109(3)

APPENDIX C

Computational study data

MOLECULAR SWITCHES WITH STRUCTURE BASED ON THE GFP CHROMOPHORE**Z-7h**

C	-2.747150	-1.411960	-0.006137
C	-3.864870	-0.570821	-0.005943
C	-3.691350	0.815037	-0.005746
C	-2.407990	1.352570	-0.005745
C	-1.270540	0.518309	-0.005940
C	-1.461690	-0.880907	-0.006133
C	0.038103	1.148900	-0.005944
C	1.274590	0.590358	-0.006075
N	1.638200	-0.764632	-0.006265
C	2.926810	-0.772688	-0.006265
O	3.548640	0.452629	-0.006147
C	2.508390	1.407740	-0.006018
O	2.718930	2.590920	-0.005916
C	3.817090	-1.968990	-0.005519
H	-2.881170	-2.490370	-0.006288
H	-4.865660	-0.994291	-0.005944
H	-4.554770	1.474520	-0.005593
H	-2.272650	2.431490	-0.005596
H	-0.594038	-1.530320	-0.006280
H	0.041647	2.237810	-0.005805
H	4.865660	-1.666670	-0.015224
H	3.625510	-2.579760	0.882870
H	3.611640	-2.590920	-0.882870

E-7h

C	-0.379253	-0.321318	-0.036486
C	0.742647	-1.094430	-0.029450
N	0.636968	-2.499850	-0.019475
C	1.840750	-2.945160	-0.014882
O	2.836530	-1.990680	-0.020518
C	2.186440	-0.750532	-0.030257
O	2.814710	0.279519	-0.036800
C	2.286780	-4.368420	-0.003858
C	-0.624804	1.111080	-0.046983
C	-1.978850	1.517600	-0.051758
C	-2.328870	2.862720	-0.061914
C	-1.330230	3.839630	-0.067481
C	0.013981	3.456720	-0.062741
C	0.371828	2.111990	-0.052623
H	-1.285810	-0.925027	-0.033517
H	3.376680	-4.427650	-0.003076
H	1.897750	-4.879400	0.882939
H	1.898220	-4.892880	-0.882939

H	-2.757370	0.758567	-0.047385
H	-3.376680	3.149850	-0.065518
H	-1.597810	4.892880	-0.075375
H	0.793099	4.214140	-0.066905
H	1.416100	1.826520	-0.048818

Z-7a

C	-3.777950	0.480447	0.000000
C	-4.783890	1.452500	0.000000
C	-4.441180	2.806620	0.000000
C	-3.101780	3.182360	0.000000
C	-2.074760	2.214750	0.000000
C	-2.437200	0.849676	0.000000
C	-0.699901	2.679530	0.000000
C	0.461549	1.974130	0.000000
N	0.663076	0.593006	0.000000
C	1.948360	0.427598	0.000000
O	2.704400	1.578260	0.000000
C	1.783410	2.643550	0.000000
O	2.128270	3.794520	0.000000
C	2.669300	-0.839382	0.000000
C	4.073480	-0.867743	0.000000
C	4.742990	-2.089300	0.000000
C	4.022190	-3.285380	0.000000
C	2.623530	-3.259910	0.000000
C	1.947050	-2.045320	0.000000
H	-4.043640	-0.573308	0.000000
H	-5.829110	1.155200	0.000000
H	-5.217110	3.567110	0.000000
H	-2.834640	4.236390	0.000000
H	-1.656290	0.098528	0.000000
H	-0.562774	3.759650	0.000000
H	4.627290	0.064747	0.000000
H	5.829110	-2.107320	0.000000
H	4.547800	-4.236390	0.000000
H	2.062120	-4.189970	0.000000
H	0.862849	-2.008320	0.000000

E-7a

C	-1.061660	1.411920	0.000000
C	-0.040332	0.506836	0.000000
N	-0.313035	-0.868769	0.000000
C	0.831721	-1.464340	0.000000
O	1.933190	-0.630882	0.000000
C	1.435460	0.675625	0.000000
O	2.181520	1.623280	0.000000
C	1.082040	-2.900520	0.000000
C	2.391890	-3.406040	0.000000
C	2.603990	-4.783110	0.000000
C	1.518230	-5.661120	0.000000
C	0.212330	-5.159450	0.000000
C	-0.008975	-3.786850	0.000000

C	-1.132020	2.862280	0.000000
C	-2.427600	3.429480	0.000000
C	-2.613060	4.806780	0.000000
C	-1.504140	5.656680	0.000000
C	-0.215808	5.114700	0.000000
C	-0.022191	3.736780	0.000000
H	-2.034490	0.922281	0.000000
H	3.231110	-2.718850	0.000000
H	3.618720	-5.170990	0.000000
H	1.687590	-6.734470	0.000000
H	-0.632929	-5.841960	0.000000
H	-1.014830	-3.380020	0.000000
H	-3.291810	2.769710	0.000000
H	-3.618720	5.217940	0.000000
H	-1.643200	6.734470	0.000000
H	0.648841	5.772840	0.000000
H	0.980439	3.328340	0.000000

Z-7v

C	-3.045790	0.393197	0.000000
C	-4.082210	1.345520	0.000000
C	-3.769310	2.715780	0.000000
C	-2.441420	3.117030	0.000000
C	-1.390810	2.174560	0.000000
C	-1.720280	0.800651	0.000000
C	-0.026099	2.669330	0.000000
C	1.142830	1.977540	0.000000
N	1.361200	0.601744	0.000000
C	2.650370	0.451610	0.000000
O	3.391760	1.611120	0.000000
C	2.459470	2.664570	0.000000
O	2.785970	3.819410	0.000000
C	3.385520	-0.805231	0.000000
C	4.790410	-0.815327	0.000000
C	5.474550	-2.028300	0.000000
C	4.767540	-3.232860	0.000000
C	3.368600	-3.225630	0.000000
C	2.677140	-2.019820	0.000000
C	-5.450030	0.919571	0.000000
N	-6.560650	0.572173	0.000000
H	-3.293180	-0.663498	0.000000
H	-4.568130	3.450090	0.000000
H	-2.203190	4.177260	0.000000
H	-0.921417	0.068964	0.000000
H	0.091966	3.751220	0.000000
H	5.332530	0.123939	0.000000
H	6.560650	-2.033570	0.000000
H	5.304780	-4.177260	0.000000
H	2.819320	-4.162690	0.000000
H	1.592660	-1.997080	0.000000

E-7v

C	-0.175117	4.351340	0.000000
C	-1.464180	4.913290	0.000000
C	-2.589130	4.070430	0.000000
C	-2.414390	2.695660	0.000000
C	-1.125640	2.112190	0.000000
C	-0.005550	2.973940	0.000000
C	-1.072770	0.660460	0.000000
C	-0.057314	-0.250054	0.000000
N	-0.333581	-1.621630	0.000000
C	0.810253	-2.222120	0.000000
O	1.914720	-1.391990	0.000000
C	1.423020	-0.086660	0.000000
O	2.168310	0.860502	0.000000
C	1.055600	-3.657270	0.000000
C	2.364550	-4.166330	0.000000
C	2.572020	-5.543690	0.000000
C	1.482910	-6.417850	0.000000
C	0.178226	-5.912750	0.000000
C	-0.039012	-4.539750	0.000000
C	-1.631520	6.336150	0.000000
N	-1.769110	7.491640	0.000000
H	0.691751	5.004230	0.000000
H	-3.585220	4.500610	0.000000
H	-3.287850	2.049300	0.000000
H	0.992759	2.555090	0.000000
H	-2.049880	0.180360	0.000000
H	3.206380	-3.482360	0.000000
H	3.585220	-5.935120	0.000000
H	1.648830	-7.491640	0.000000
H	-0.668833	-6.592810	0.000000
H	-1.043730	-4.130230	0.000000

Z-7c

C	-2.688310	0.324446	-0.000029
C	-3.743120	1.256320	-0.000021
C	-3.456630	2.628710	-0.000023
C	-2.129800	3.047120	-0.000032
C	-1.058780	2.132330	-0.000039
C	-1.373640	0.750734	-0.000037
C	0.290715	2.649960	-0.000046
C	1.481750	1.990950	-0.000053
N	1.732620	0.617335	-0.000056
C	3.022840	0.498440	-0.000061
O	3.735290	1.676310	-0.000061
C	2.774170	2.707580	-0.000056
O	3.078160	3.871260	-0.000056
C	3.789120	-0.742249	-0.000067
C	5.193300	-0.720288	-0.000072
C	5.906640	-1.916980	-0.000078
C	5.229720	-3.138400	-0.000079
C	3.831080	-3.163130	-0.000074
C	3.111270	-1.973640	-0.000068
O	-4.994130	0.727721	-0.000012

C	-6.106650	1.612590	0.000000
H	-2.936690	-0.732293	-0.000027
H	-4.250190	3.366710	-0.000018
H	-1.914020	4.112830	-0.000034
H	-0.565492	0.028955	-0.000041
H	0.385442	3.734770	-0.000046
H	5.712270	0.232027	-0.000071
H	6.992770	-1.895710	-0.000082
H	5.789330	-4.069860	-0.000084
H	3.303480	-4.112830	-0.000076
H	2.026440	-1.975730	-0.000064
H	-6.992770	0.975970	0.000010
H	-6.114210	2.247190	0.895290
H	-6.114230	2.247190	-0.895290

E-7c

C	-3.381120	-2.485680	-0.000002
C	-4.524760	-1.666900	0.000003
C	-4.376900	-0.271850	0.000016
C	-3.099560	0.275047	0.000021
C	-1.936210	-0.525768	0.000013
C	-2.113960	-1.933050	0.000003
C	-0.667210	0.166164	0.000015
C	0.639366	-0.236856	0.000005
N	1.672900	0.710513	0.000002
C	2.776050	0.040793	-0.000016
O	2.633470	-1.332830	-0.000023
C	1.256840	-1.583330	-0.000010
O	0.832641	-2.713960	-0.000012
C	4.134310	0.571164	-0.000029
C	5.245870	-0.286827	-0.000055
C	6.533670	0.245353	-0.000069
C	6.722910	1.628900	-0.000058
C	5.616850	2.485550	-0.000032
C	4.328150	1.963490	-0.000018
O	-5.715430	-2.317800	-0.000005
C	-6.912600	-1.550970	-0.000003
H	-3.519980	-3.562240	-0.000010
H	-5.239670	0.383923	0.000021
H	-2.993410	1.357140	0.000029
H	-1.245210	-2.579710	-0.000002
H	-0.754598	1.251840	0.000023
H	5.092830	-1.360620	-0.000063
H	7.391000	-0.421912	-0.000091
H	7.728760	2.039970	-0.000069
H	5.762250	3.562240	-0.000023
H	3.458950	2.612920	0.000002
H	-7.728760	-2.275000	-0.000013
H	-6.985150	-0.920763	0.895393
H	-6.985140	-0.920752	-0.895393

Z-7f-1

C	-3.724420	0.047282	0.000000
C	-4.763320	0.981042	0.000000
C	-4.470820	2.344230	0.000000
C	-3.144760	2.766470	0.000000
C	-2.066550	1.849010	0.000000
C	-2.403270	0.474451	0.000000
C	-0.688194	2.303900	0.000000
C	0.461164	1.578730	0.000000
N	0.654309	0.197177	0.000000
C	1.939210	0.021965	0.000000
O	2.703240	1.165380	0.000000
C	1.790290	2.238710	0.000000
O	2.144530	3.385540	0.000000
C	2.649400	-1.250560	0.000000
C	4.053460	-1.288910	0.000000
C	4.713940	-2.515190	0.000000
C	3.983890	-3.705740	0.000000
C	2.585410	-3.670390	0.000000
C	1.917800	-2.451010	0.000000
Br	-2.848470	4.660640	0.000000
H	-3.945590	-1.016100	0.000000
H	-5.799820	0.655772	0.000000
H	-5.266440	3.080830	0.000000
H	-1.593560	-0.245138	0.000000
H	-0.533866	3.378830	0.000000
H	4.613760	-0.360378	0.000000
H	5.799820	-2.541510	0.000000
H	4.502370	-4.660640	0.000000
H	2.017540	-4.596460	0.000000
H	0.833936	-2.406400	0.000000

E-7f-1

C	5.025850	-1.208430	-0.093243
C	5.840320	-0.075270	-0.099033
C	5.260180	1.192810	-0.080535
C	3.875600	1.319630	-0.056260
C	3.014520	0.190623	-0.049845
C	3.643120	-1.077370	-0.069262
C	1.575400	0.374290	-0.022000
C	0.511275	-0.480721	-0.019152
N	-0.792072	0.034623	0.012810
C	-1.586630	-0.981757	0.004852
O	-0.966555	-2.216640	-0.030795
C	0.405153	-1.965500	-0.047414
O	1.199800	-2.872710	-0.078465
C	-3.043440	-0.968599	0.029158
C	-3.776050	-2.166470	0.016273
C	-5.168400	-2.127800	0.039991
C	-5.836290	-0.901948	0.076525
C	-5.108170	0.292548	0.089443
C	-3.718410	0.264051	0.065953
Br	3.196580	3.115160	-0.032847

H	5.467330	-2.200590	-0.107523
H	6.922430	-0.169406	-0.117891
H	5.878120	2.083650	-0.084887
H	3.019990	-1.962610	-0.065680
H	1.253620	1.410930	0.001604
H	-3.251050	-3.115160	-0.012134
H	-5.732620	-3.056010	0.029931
H	-6.922430	-0.875733	0.094918
H	-5.627430	1.246330	0.117891
H	-3.137310	1.180290	0.075464

Z-7f-2

C	-4.184790	-0.017598	-0.006090
C	-4.969800	0.778903	0.825037
C	-4.563340	2.080070	1.126210
C	-3.366340	2.560960	0.609645
C	-2.523780	1.764610	-0.195061
C	-2.981280	0.470753	-0.515446
C	-1.264410	2.373770	-0.632827
C	-0.018170	1.849310	-0.618394
N	0.406227	0.597019	-0.180327
C	1.689700	0.590083	-0.339623
O	2.247320	1.744210	-0.856325
C	1.173490	2.625510	-1.058350
O	1.316560	3.735220	-1.493160
C	2.596730	-0.507060	-0.029648
C	3.986550	-0.358157	-0.160856
C	4.828760	-1.424040	0.147749
C	4.293130	-2.637930	0.583853
C	2.908060	-2.789030	0.710822
C	2.059390	-1.730730	0.406811
Br	-2.060280	-0.648873	-1.757000
H	-4.506970	-1.016530	-0.278404
H	-5.904030	0.387189	1.217120
H	-5.176520	2.716800	1.757000
H	-3.044660	3.572200	0.844828
H	-1.316870	3.419960	-0.930069
H	4.394280	0.587674	-0.500941
H	5.904030	-1.307290	0.047268
H	4.953240	-3.467430	0.822548
H	2.492260	-3.735220	1.045370
H	0.981870	-1.829590	0.487836

E-7f-2

C	-2.242910	4.460070	0.600977
C	-3.366020	4.742910	-0.173509
C	-3.985440	3.723410	-0.898378
C	-3.464930	2.435090	-0.853793
C	-2.304710	2.125450	-0.115678
C	-1.724080	3.166200	0.633329
C	-1.839280	0.730867	-0.146124
C	-0.608218	0.254786	-0.440484

N -0.285194 -1.106300 -0.423366
C 0.945367 -1.181480 -0.811225
O 1.552070 0.015540 -1.133170
C 0.583978 1.010470 -0.920902
O 0.795889 2.167460 -1.153120
C 1.751910 -2.389380 -0.939417
C 3.086730 -2.323310 -1.369570
C 3.837500 -3.491560 -1.480960
C 3.265440 -4.726170 -1.167000
C 1.935410 -4.794050 -0.738687
C 1.178780 -3.633370 -0.623676
Br -0.257814 2.849330 1.813390
H -1.768220 5.236050 1.190950
H -3.761130 5.754520 -0.195701
H -4.870270 3.929960 -1.493230
H -3.944180 1.638890 -1.417560
H -2.595790 -0.030732 0.038273
H 3.524040 -1.360760 -1.611660
H 4.870270 -3.437970 -1.813390
H 3.854070 -5.635300 -1.255330
H 1.490660 -5.754520 -0.494033
H 0.146431 -3.665840 -0.291456

TS-7a

C -1.892030 0.618903 -1.015280
C -0.553413 0.897192 -0.963699
N 0.459262 -0.060038 -1.063500
C 1.516790 0.472668 -0.535807
O 1.378750 1.751170 -0.050956
C 0.019338 2.073510 -0.233430
O -0.445687 3.121810 0.119295
C 2.802400 -0.184054 -0.337478
C 3.846010 0.469328 0.338486
C 5.069990 -0.173066 0.510001
C 5.260620 -1.464590 0.013779
C 4.222220 -2.117510 -0.659126
C 2.997930 -1.483580 -0.837574
C -3.123680 -0.000152 -0.486491
C -4.230290 -0.242024 -1.321280
C -5.332830 -0.936843 -0.837445
C -5.357490 -1.400290 0.482383
C -4.272120 -1.144970 1.320040
C -3.171600 -0.425735 0.853376
H -1.781430 -0.158469 -1.814740
H 3.690320 1.472320 0.720728
H 5.875830 0.334834 1.032120
H 6.216770 -1.962680 0.149537
H 4.371000 -3.121810 -1.045620
H 2.181950 -1.973760 -1.358070
H -4.212520 0.109771 -2.349010
H -6.178360 -1.120690 -1.494730
H -6.216770 -1.952660 0.851610
H -4.281400 -1.494510 2.349010

H -2.331690 -0.220863 1.509370

FC-7h

C -2.705990 -1.269160 -0.282300
C -3.813600 -0.418317 -0.264628
C -3.620720 0.961752 -0.230985
C -2.327270 1.482310 -0.214269
C -1.204790 0.638313 -0.229820
C -1.411980 -0.752345 -0.264483
C 0.119915 1.272600 -0.193527
C 1.351690 0.728546 -0.203869
N 1.724180 -0.629782 -0.252977
C 2.995740 -0.645434 -0.247412
O 3.605960 0.583001 -0.198686
C 2.614670 1.507180 -0.151680
O 2.804970 2.687290 -0.108183
C 3.922880 -1.812680 -0.219928
H -2.849780 -2.335790 -0.307133
H -4.809830 -0.825948 -0.276175
H -4.466140 1.627770 -0.214770
H -2.183190 2.549160 -0.182475
H -0.568073 -1.413980 -0.275324
H 0.118386 2.348640 -0.136320
H 4.809830 -1.594790 -0.800223
H 4.229580 -2.031270 0.800223
H 3.424500 -2.687290 -0.614827

CI S₂/S₁-7h

C -3.036610 -1.577820 -0.087738
C -4.208140 -0.734247 -0.067209
C -4.021800 0.700589 -0.021085
C -2.761460 1.243680 0.004004
C -1.551590 0.401648 -0.014845
C -1.766540 -1.050100 -0.063298
C -0.305238 1.024900 0.026451
C 1.020750 0.423107 0.037726
N 1.356130 -0.879454 -0.017622
C 2.670830 -0.929161 0.018058
O 3.258180 0.288124 0.100363
C 2.252680 1.207130 0.118000
O 2.442520 2.385790 0.176144
C 3.546220 -2.124770 -0.005757
H -3.152720 -2.644910 -0.122442
H -5.191400 -1.160270 -0.084788
H -4.875240 1.352250 -0.000866
H -2.644590 2.310710 0.044771
H -0.921286 -1.705370 -0.078156
H -0.294204 2.098820 0.070749
H 4.226860 -2.084220 -0.849597
H 4.143590 -2.173400 0.898702
H 2.936910 -3.013990 -0.079053

Min S₁-7h (planar)

C	-2.566040	-1.264690	-0.100680
C	-3.703470	-0.421635	-0.086555
C	-3.520910	0.979108	-0.030407
C	-2.204520	1.543590	0.011936
C	-1.013270	0.707046	-0.000535
C	-1.233280	-0.725788	-0.058941
C	0.247817	1.323400	0.043861
C	1.509310	0.753975	0.043073
N	1.866370	-0.592642	-0.002281
C	3.144380	-0.617522	0.019105
O	3.752470	0.599296	0.076919
C	2.755490	1.533450	0.094962
O	2.962580	2.704680	0.143711
C	4.037960	-1.804700	-0.011109
H	-2.687810	-2.330610	-0.143318
H	-4.690950	-0.840760	-0.118067
H	-4.369500	1.636730	-0.018800
H	-2.090030	2.610330	0.054191
H	-0.394103	-1.387960	-0.070974
H	0.256344	2.398740	0.085147
H	4.690950	-1.759400	-0.875672
H	4.661710	-1.825890	0.875672
H	3.441630	-2.704680	-0.055260

CI S₁/S₀-7h

C	-1.488920	-1.220220	0.559506
C	-1.339980	0.138873	-0.186317
C	-2.393280	1.198790	0.209679
C	-3.434520	0.892451	1.003210
C	-3.592200	-0.455576	1.569380
C	-2.551670	-1.463290	1.344610
C	-0.552838	0.222823	-1.288740
C	0.583540	0.070289	-0.423086
C	1.312150	1.207550	0.140476
O	2.484170	0.677058	0.605072
C	2.417930	-0.662831	0.380672
N	1.345930	-1.077210	-0.170025
O	1.019690	2.353980	0.270940
C	3.604840	-1.472180	0.756999
H	-0.762505	-1.988960	0.364013
H	-2.239030	2.211390	-0.135361
H	-4.143170	1.667930	1.258080
H	-4.424390	-0.678009	2.214310
H	-2.640300	-2.435970	1.802600
H	-0.599861	1.060670	-1.946170
H	4.462360	-1.154660	0.173390
H	3.844880	-1.340180	1.804320
H	3.400430	-2.513280	0.553818

Min S₁-7h (twisted)

N	1.697190	-0.961933	-0.336793
C	0.962475	0.094332	0.219505
C	1.785960	0.911693	0.982477
O	2.999760	0.253014	0.982319
C	2.863460	-0.827683	0.166625
C	-0.313710	0.564182	-0.367138
C	-1.600230	0.231225	0.165819
C	-1.678950	-0.589749	1.335920
C	-2.890520	-0.890424	1.878440
C	-4.066530	-0.391783	1.283330
C	-4.037460	0.397886	0.151654
C	-2.810060	0.719161	-0.419552
O	1.623990	1.958150	1.553040
C	4.071520	-1.663270	-0.052413
H	-0.312110	1.230000	-1.235790
H	-0.752049	-0.934449	1.761780
H	-2.956360	-1.500850	2.761220
H	-5.017600	-0.636123	1.730900
H	-4.952210	0.764620	-0.278343
H	-2.761300	1.333860	-1.307220
H	4.852440	-1.079760	-0.527465
H	4.462410	-2.027150	0.890654
H	3.818180	-2.501800	-0.684345

MOLECULAR SWITCHES WITH STRUCTURE BASED ON THE PSB-RETINAL CHROMOPHORE

5r-neutral

C	0.023479	0.724087	0.468006
C	0.439694	1.195576	1.724508
C	1.749878	1.023132	2.145422
C	2.716588	0.397679	1.330811
C	2.277435	-0.092557	0.085511
C	0.958669	0.052217	-0.333738
H	-0.273700	1.707698	2.365600
H	2.044801	1.398297	3.122322
C	4.082194	0.275802	1.840906
H	2.960579	-0.639760	-0.552743
H	0.650852	-0.389725	-1.274015
N	-1.326915	0.890459	0.103952
H	-1.993067	0.937956	0.867546
C	-1.946155	1.159725	-1.109840
O	-3.161495	1.281880	-1.140722
C	-1.090570	1.314298	-2.352579
H	-0.118618	1.770664	-2.147741

H	-0.918299	0.338608	-2.821696
H	-1.652510	1.929439	-3.057563
C	5.228846	0.007704	1.176336
H	4.173171	0.474509	2.906819
C	6.585255	-0.016306	1.783001
C	5.467650	-0.161825	-0.309693
N	7.551519	0.023084	0.926602
C	6.881102	-0.049789	3.234950
C	6.995067	0.073535	-0.427951
H	5.205901	-1.175927	-0.642157
H	4.876631	0.537126	-0.910703
C	6.107678	-0.786556	4.145853
C	6.449209	-0.841307	5.493059
C	7.567438	-0.145944	5.979111
C	8.332583	0.610994	5.076904
C	8.001967	0.636280	3.726771
H	5.252827	-1.355272	3.794385
H	5.856763	-1.443234	6.177708
N	7.836836	-0.198606	7.361453
H	9.169757	1.200098	5.431913
H	8.606139	1.209186	3.031025
C	9.020424	-0.247517	8.086604
H	7.036609	-0.345804	7.967075
O	8.965276	-0.319618	9.305246
C	10.340815	-0.230114	7.340962
H	7.224117	1.056719	-0.862175
H	7.499371	-0.670162	-1.055000
H	10.297069	-0.752340	6.381657
H	10.660208	0.801690	7.153733
H	11.084306	-0.697883	7.988751

5r-protonated

C	2.277435	-0.092557	0.085511
C	2.716588	0.397679	1.330811
C	1.749878	1.023132	2.145422
C	0.439694	1.195575	1.724509
C	0.023479	0.724086	0.468007
C	0.958669	0.052216	-0.333737
C	4.082194	0.275802	1.840906
C	5.228846	0.007704	1.176336
C	6.585255	-0.016306	1.783001
N	7.551519	0.023084	0.926602
C	6.995067	0.073535	-0.427951
C	5.467650	-0.161825	-0.309693
C	6.881102	-0.049789	3.234950
C	8.001967	0.636279	3.726771

C	8.332582	0.610993	5.076904
C	7.567437	-0.145944	5.979111
C	6.449208	-0.841307	5.493059
C	6.107677	-0.786556	4.145853
N	7.836835	-0.198606	7.361453
C	9.020423	-0.247517	8.086605
O	8.965274	-0.319618	9.305247
N	-1.326915	0.890458	0.103953
C	-1.946155	1.159724	-1.109839
O	-3.161495	1.281879	-1.140721
C	-1.090570	1.314297	-2.352578
C	10.340814	-0.230115	7.340963
H	-0.273700	1.707697	2.365601
H	2.044801	1.398297	3.122322
H	2.960579	-0.639760	-0.552743
H	0.650852	-0.389726	-1.274014
H	-1.993067	0.937955	0.867547
H	-0.118618	1.770663	-2.147740
H	-0.918299	0.338607	-2.821695
H	-1.652509	1.929438	-3.057562
H	4.173171	0.474509	2.906819
H	5.205901	-1.175927	-0.642157
H	4.876631	0.537126	-0.910703
H	5.252826	-1.355272	3.794385
H	5.856762	-1.443234	6.177708
H	9.169756	1.200097	5.431914
H	8.606139	1.209185	3.031025
H	7.036607	-0.345804	7.967075
H	7.224117	1.056719	-0.862175
H	7.499371	-0.670162	-1.055000
H	10.297068	-0.752341	6.381658
H	10.660207	0.801689	7.153734
H	11.084305	-0.697884	7.988752
H	8.433575	0.003393	1.414100